Untersuchungen zum Mechanismus der photosynthetischen Wasseroxidation im thermophilen Cyanobakterium *Thermosynechococcus elongatus* und Spinat

Vorgelegt von

Diplom-Biologin

Sabina Isgandarova

aus Baku, Aserbaidschan

Von der Fakultät II – Matematik- und Naturwissenschaften

Der Technischen Universität Berlin

zur Erlangung des akademischen Grades

Doktorin der Naturwissenschaften

Dr.rer.nat.

genehmigte Dissertation

Promotionsausschuss:

Vorsitzender: Prof. Dr. A.Grohmann

Berichter: Dr. Habil. J. Messinger

Berichter: Prof. Dr. G. Renger

Berichter: Prof. Dr. P. Hildebrandt

Tag der wissenschaftlichen Aussprache: 28. Januar 2004

Berlin 2004

D 83

ABSTRACT

Sabina Isgandarova

Untersuchungen zum Mechanismus der photosynthetischen Wasseroxidation im thermophilen Cyanobakterium *Thermosynechococcus elongatus* und Spinat

In Cyanobakterien und Pflanzen erfolgt die Spaltung von Wasser in molekularen Sauerstoff, vier Protonen und vier Elektronen in einem Pigment-Protein Komplex, der Teil der Thylakoidmembran ist und als Photosystem II (PS II) bezeichnet wird. Die Wasserspaltung wird von einem funktionellen Teil des PS II katalysiert, der als Sauerstoff entwickelnder Komplex („Oxygen Evolving Complex", OEC) bekannt ist und dessen katalytisches Zentrum von einem Mn_4O_xCa-Komplex gebildet wird. Der OEC durchläuft während der Wasseroxidation fünf Redoxzustände (S-Zustände). Die kürzlich veröffentlichten Kristallstrukturen von PS II aus den thermophilen Cyanobakterien *Thermosynechococcus elongatus* (*T. elongatus*) und *T. vulcanus* liefern Informationen über die komplexe Gesamtstruktur von PS II und die Anordnung vieler Kofaktoren. Bis heute existiert keine Kristallstruktur für PS II aus höherer Pflanzen. Da bisher die meisten funktionellen Untersuchungen an PS II Komplexen aus Spinat durchgeführt wurden, sind für eingehende Untersuchungen von Struktur-Funktionsbeziehungen vergleichende Funktionsstudien an PS II Komplexen aus Cyanobakterien und höheren Pflanzen erforderlich.

Ziel dieser Arbeit ist die Untersuchung von Gemeinsamkeiten und Unterschieden beim Mechanismus der Sauerstoff-Entwicklung in *T. elongatus* und Spinat. Hierfür wurden insbesondere blitzinduzierte Sauerstoff-Oszillationsmuster („Flash Induced Oxygen evolution Patterns", FIOPs) unter verschiedensten Bedingungen gemessen und im Rahmen eines erweiterten Kok-Modells analysiert. Es wurden folgende Ergebnisse erzielt:

a) Die Temperatur-Abhängigkeiten der „miss"- und „double hit"-Wahrscheinlichkeiten, sowie die Lebensdauern der S-Zustände in beiden Organismen deuten auf strukturelle Unterschiede der Akzeptorseite von PS II und in der Umgebung des Tyrosin-Radikals Y_D^{ox} hin.

b) Untersuchungen zu den Effekten von einem H/D Isotopen-Austausch auf die Reaktionen des OEC bei verschiedenen Temperaturen und pL-Werten (L = H oder D) zeigen, dass hierdurch die Reaktionen im PS II beider Organismen in vergleichbarer Weise beeinflusst werden. Im Gegensatz zu Spinat-Thylakoiden ist in Thylakoiden von *T. elongatus* aber Y_D^{ox}, das bei pH 7,0 stabil ist, bei pH 8,0 labil und wird im Dunkeln bei Raumtemperatur innerhalb einer Stunde reduziert.

c) Durch Inkubation mit den exogenen Reduktionsmitteln NH_2OH, N_2H_4 und $NO^{\bullet}$ wurde zum ersten Mal gezeigt, dass

(i) Arrhenius-Diagramme für NH_2OH induzierte $S_1 \rightarrow S_0$ and $S_0 \rightarrow S_{-1}$ Übergänge im OEC von Spinat-Thylakoiden einen Knickpunkt bei 29°C aufweisen. Unterhalb dieser Temperatur sind Aktivierungsenergie und prä-exonentielle Faktoren unabhängig von S-Zustand, wogegen oberhalb von 29°C beide Faktoren vom Redoxzustand abhängig sind.

(ii) Das S_{-2} EPR „Multiline"-Signal wurde erstmals in monomeren und dimeren PS II „core"-Komplexen von *T. elongatus* durch $NO^{\bullet}$-Inkubation erhalten. Kleine, reproduzierbare Verschiebungen einiger Tieffeld-Übergänge in den S_{-2} EPR-„Multiline"-Signalen von *T. elongatus* im Vergleich zu dem Spinat-Signal weisen auf leichte Unterschiede bei der Koordinations-Geometrie und/oder den Liganden des Mn_4O_xCa-Komplexes zwischen thermophilen Cyanobakterien und höheren Pflanzen hin.

(iii) FIOPs von N_2H_4-reduzierten Thylakoiden von *T. elongatus* zeigen eine Besetzung des S_{-3} -Zustandes von bis zu ~70% an; die Stabilität dieses Redoxzustandes macht die Existenz eines $Mn_4(II_4)$-Komplexes für diesen Zustand unwahrscheinlich. Darüber hinaus weist die numerische Analyse der FIOPs von mit Hydrazin reduziertem PS II auf die Existenz von S_{-4}- und S_{-5}-Redoxzuständen hin. Diese Ergebnisse unterstützen die Zuordnung der Mangan-Oxidationszustände $Mn_4(III_2,IV_2)$ für den S_1-Zustand.

VERÖFFENTLICHUNGEN

Wissenschaftliche Publikationen:

1. Messinger, J., Robblee, J., Bergmann, U., Fernandez, C., Glatzel, P., Isgandarova, S., Hanssum, B., Renger, G., Cramer, S., Sauer, K., & Yachandra, V. (2001) Manganese oxidation states in photosystem II, *CSIRO Publishing* (*electronic version*), S10-019, Collingwood, Australia

2. J. Sarrou, S. Isgandarova, J. Kern, A. Zouni, G. Renger, W. Lubitz & J. Messinger (2003) Nitric Oxide-induced formation of the S_{-2}-state in the OEC of PSII from *Synechococcus elongatus*, *Biochemistry* 42, 1016-1023

3. S. Isgandarova, G. Renger & J. Messinger (2003) Functional Differences of Photosystem II from *Synechococcus elongatus* and Spinach Characterized by Flash Induced Oxygen evolution Patterns, *Biochemistry* 42, 8929-8938, 2003

4. S. Isgandarova, G. Renger & J. Messinger (2004) Effect of pH 8.0 on the dark stability of the tyrosine radical Y_D^{ox} in photosystem II of *Thermosynechococcus elongatus* (zur Veröffentlichung eingereicht)

5. S. Isgandarova, G. Renger & J. Messinger (2004) Deuterium isotope effects on the reactions of the OEC in *Thermosynechococcus elongatus* and Spinach (im Vorbereitung)

Präsentationen auf wissenschaftlichen Tagungen:

1. S. Isgandarova, B. Hanssum, G. Renger & J. Messinger, Manganese oxidation states of the S_1-state in photosystem II, EURESCO Conferences: Molecular Bioenergetics of Cyanobacteria, Obernai, France, 25 – 30 May 2001, p.45 / **Abstract** & **Poster**

2. S. Isgandarova, B. Hanssum, G. Renger & J. Messinger, Manganese oxidation states of the S_1-state in photosystem II, Advanced Biophysics School on Lipid-Protein Interactions and the Organization of Membranes, Szeged, Hungary, June 23 - July 3 2001 / **Poster**

3. J. Messinger, JH. Robblee, U. Bergmann, C. Fernandez, P. Glatzel, S. Isgandarova, B. Hanssum, G. Renger, SP. Cramer, K. Sauer & VK. Yachandra, Manganese oxidation states in photosystem II, (S10-019) PS2001 Proceedings of the 12th International Congress on Photosynthesis, Brisbane, Australia, 18-23 August 2001 / **Poster**

4. Sarrou J., Isgandarova S., Kern J., Zouni A., Renger G., Lubitz W., Messinger J. Reduction of the OEC of PS II from *Synechococcus elongatus* by nitric oxide. Formation of the S_{-2}-state, XVII Pushchino Readings in Photosynthesis & International Conference on Primary Processes of Photosynthesis in Bacteria and Plant Photosystem II. Pushchino, Russia, 8-12 July 2002, p.37 / **Abstract**

5. Isgandarova S., Renger G., Messinger J. S-state transitions in the OEC of *Synechococcus elongatus,* XVII Pushchino Readings in Photosynthesis & International Conference on Primary Processes of Photosynthesis in Bacteria and Plant Photosystem II. Pushchino, Russia, 8-12 July 2002, p.13 / **Abstract**

6. S.Isgandarova, G.Renger & J.Messinger Comparison of PS II from the thermophylic cyanobacterium *Synechococcus elongatus* and from spinach, "Nordwest" Workshop on Photosynthesis of German Society for Biochemistry and Molecular Biology, Bielefeld, Germany, 11th October 2002 / **Abstract** und **Vortrag**

7. S.Isgandarova, G.Renger & J.Messinger Functional Differences of PS II from *Synechococcus elongatus* and Spinach Characterized by Flash Induced Oxygen evolution

Patterns, Gordon Research Conference on Photosynthesis, Roger Williams University, USA, 22-27 June 2003 / **Poster**

Weitere Konferenzbeiträge:

1. S. Isgandarova, R.Agalarov, R.Gasanov. Electron transfer on the donor site of Photosystem I, Proceedings of XIII International Biophysics Congress, New-Delhi, 1999, p.160 / **Abstract** & **Poster**

2. Isgandarova S.G. Monitoring of oil and its some derivative actions on microalgae by delayed light emission, Proceedings of the Second Republic Conference on Cell Biophysics, Baku, Azerbaijan, November 1999, p.55. / **Abstract** & **Poster**

3. S.G. Isgandarova, Delayed luminescence as a method for *in situ* monitoring of environmental pollution (S12-5), 6th ICPMB, Quebec Canada, 18-24 June 2000 / **Abstract**

4. S.G. Isgandarova, R.A.Gasanov The state of Delayed Luminescence characteristics of microalgae in condition of oil hydrocarbons treatment, 18th ICBMB, Birmingham, UK, 16-20 July 2000 / **Abstract**

STUDIES ON MECHANISM OF THE PHOTOSYNTHETIC WATER OXIDATION IN THERMOPHILIC CYANOBACTERIUM *THERMOSYNECHOCOCCUS ELONGATUS* AND SPINACH

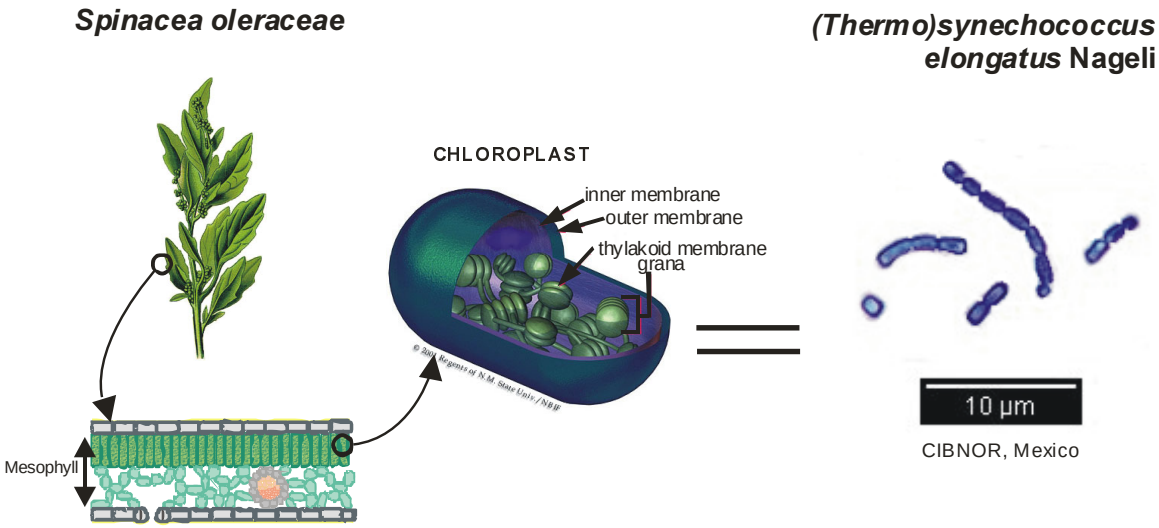

dedicated to Garabakh – the heart of Azerbaijan
recently occupied by Armenian terrorists

CONTENT

ABBREVIATIONS

α	miss probability during flash induced oxygen evolution
$\alpha_{YD\text{-}NO}$	miss probability for proposed direct oxidation of Y_D-NO by $P680^+$
APS	ammonium persulfate
β	double hit probabilities during flash induced oxygen evolution
β_1	double hit probabilities after the first flash
Chl, [Chl]	chlorophyll, concentration of Chl
Cyt	cytochrome
DCMU	3-(3,4-dichlorophenyl)-1,1-dimethylurea
DGDG	digalactosyldiacylglycerol
DMSO	dimethyl sulfoxide
FIOPs	Flash Induced Oxygen evolution Patterns
EDC	1-ethyl-3-(3-demethylaminopropyl)carbodiimide
EPR	Electron Paramagnetic Resonance
EXAFS	Extended X-ray Absorption Fine Structure
HEPES	4-(2-hydroxyethyl)-1-piperazineethanesulfonic acid
HH	hydroxylamine hydrochloride
MALDI-TOF-MS	Matrix Assisted Laser Desorption Ionization Time-of-Flight Mass Spectrometry
MGDG	monogalactosyldiacylglycerol
MES	2-(N-morpholino)ethanesulfonic acid
MQ	“Millipore Quality” distillated water
OEC	Oxygen Evolving Complex
PG	Phosphatidylglycerol
PCET	Proton Coupled Electron Transfer
PS II	Photosystem II
PS IIcc	PS II core complexes
PQ-9	Plastoquinone-9 molecule
RC	Reaction Center
SDS-PAGE	Sodium Dodecyl Sulfate Polyacrylamid Gel Electrophoresis
S_i-states,	Oxidation states of the OEC, where
i = -5,…4	i is the number of oxidizing equivalents
SQDG	Sulfoquinovosyldiacylglycerol
TRIS	2-amino-2-hydroxymethyl-1‘3-propanediol
u_p^{on}	polarization switched on
Y_D	redox active tyrosine 160 of the D2 polypeptide of PS II
Y_D-NO	nitroso tyrosine D.
Y_n	oxygen evolution yield on the n-th flash
Y_Z	redox active tyrosine 161 of the D1 polypeptide of PS II

CHAPTER 1

Introduction to Photosynthesis: from Thylakoids to Mechanism of the Water Cleavage

1.1 Why study photosynthesis?

In higher plants, algae and cyanobacteria, the photosynthetic process results in the release of molecular oxygen and the fixation of atmospheric carbon in form of carbohydrates. The carbon required for the survival of virtually all life on our planet and the molecular oxygen is necessary for the survival of oxygen consuming organisms. Photosynthetic water oxidation is therefore one of the most important biological processes on Earth. In fact, one tree of about $2 \cdot 10^5$ leaves produces $1 \cdot 10^4$ l of oxygen and 12 kg of carbohydrates in one sunny day. Cyanobacteria, for which the fossil record dates back at least three billion years, are one of the oldest oxygen-evolving organisms. Together with green unicellular algae they are the only photosynthetic organisms comprising phytoplankton and produce more than 30% of the oxygen in atmosphere [1-5]. Moreover, it is believed that an ancestor of cyanobacteria may have been introduced into a eukaryotic cell earlier in their evolution, leading to the development of the photosynthetic plant organelle, the chloroplast [6].

1.2 Structure and functional organization of thylakoid membrane

In higher plants, photosynthesis occurs in the cell organelles termed chloroplasts. These semi-autonomous organelles are comprised of two envelope membranes, an aqueous matrix known as stroma, and internal membrane referred to as thylakoids (Figure 1.1). The principal function of the envelope membranes is to control the movement of metabolites, lipids and proteins into and out of chloroplasts. Most of these transport and synthetic activities have been localized to the inner envelope membrane, while the outer membrane appears to serve primarily as a physical barrier to large molecules between the cytoplasm and the inner envelope membrane [7]. All of the light harvesting and energy-transducing functions are located in thylakoids, which form a physically continuous membrane system that encloses an aqueous compartment, the thylakoid lumen. [8]. The thylakoid network is comprised of two distinct types of membrane domains, the cylindrical stacks of appressed thylakoids, known as grana, and the interconnecting, single membranes called stroma thylakoids. Each stroma thylakoid intersects with a grana thylakoid. The two types of thylakoids are interconnected through a neckline membrane bridge.

The acyl lipid composition of the thylakoid bilayer differs significantly from that of the other plant membranes, which supports the hypothesis of the prokaryotic origin of

chloroplasts (reviewed in [9]). Besides monogalactosyldiacylglycerol (MGDG) and digalactosyldiacylglycerol (DGDG), the thylakoid membrane contains a large amount of polyunsaturated fatty acids: (i) Sulfoquinovosyldiacylglycerol (SQDG), which appears to be unique to photosynthetic membranes; (ii) Phosphatidylglycerol (PG) and possible (iii) Phosphatidylcholine (PC) [8, 10].

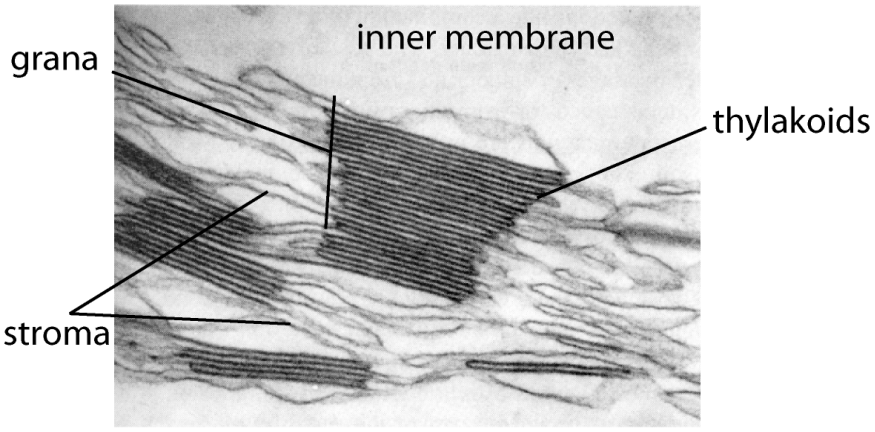

Figure 1.1. Inside of the plant cell chloroplast. [11]

The chloroplast stroma is defined as the aqueous compartment located between the inner envelope membrane and the thylakoids. The main components of the stroma include: a) multiple (about 300) copies of chloroplast DNA [12], 70 S ribosomes, m RNAs and all other elements needed for protein synthesis [13]; b) carbon reduction cycle enzymes, particularly ribulose bisphosphate carboxylase-oxygenase; c) enzymes involved in lipid, porphyrin, terpenoid, quinoid and aromatic compound synthesis [14]; and d) plastoglobuli, which contain large amount of carotenoids and plastoquinone [15, 16].

1.3 Electron transport in thylakoid membrane. The light-dependent reactions.

The overall reaction for photosynthesis is as follows:

$$6H_2O + 6CO_2 \rightarrow C_6H_{12}O_6 + 6O_2 \qquad (1.1)$$

This reaction is carried out in thylakoids by five different membrane spanning protein complexes. Photosystem I (PS I), Photosystem II (PS II) and the light-harvesting complexes II (LHC II) bind chlorophyll (Chl). PS I and PS II catalyze light-dependent

reactions while the LHC II serves as antenna system that transfers light energy to PS II. Cytochrome b_6f (Cyt b_6f) and the ATP synthase complexes do not bind Chl and catalyze reactions that are not directly depent on light (Figure 1.2).

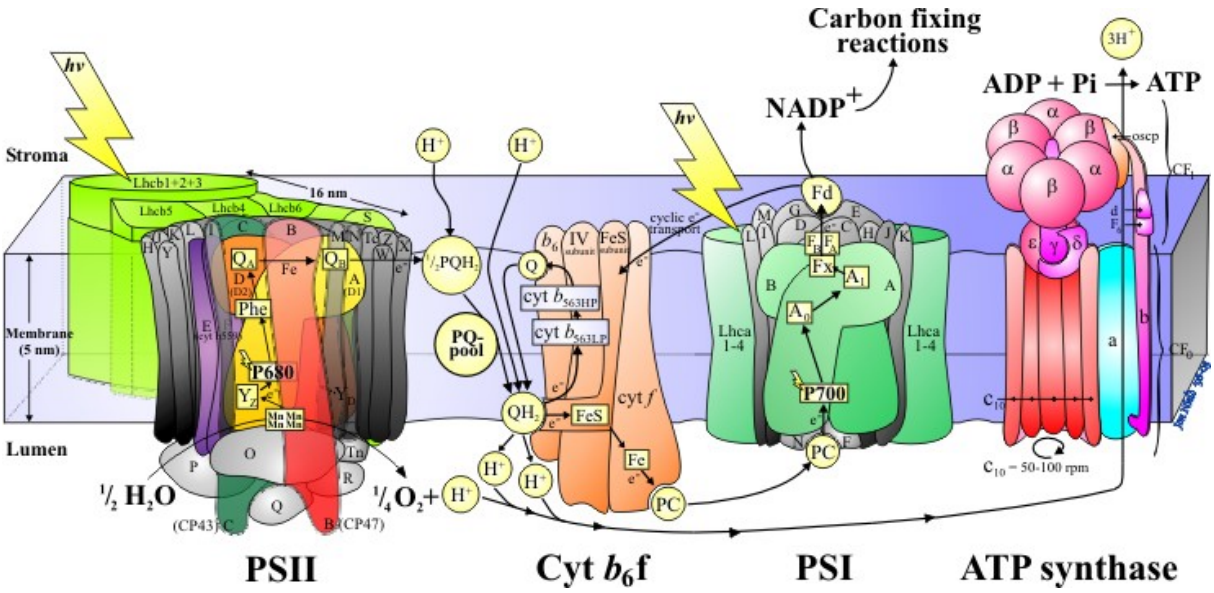

Figure 1.2. Structural and functional composition of the thylakoid membrane of chloroplasts. All protein complexes and the main light – induced reactions are presented. This Figure is adopted from [17].

The light-dependent and light-independent reactions are the two consequal stages of photosynthesis. The former convert light energy into the chemical energy, producing ATP and NADPH, while the latter reactions use these products to reduce carbon dioxide and convert the energy of the light to the chemical bond energy in carbohydrates such as glucose.

The light-dependent reactions occur in the thylakoids from the chloroplasts and can be summarized as follows:

$$2\ H_2O + 2\ NADP^+ + 3\ ADP^{3-} + 3\ HPO_4^{2-} + H_2 \xrightarrow{\text{light}} O_2 + 2\ NADPH + 3\ ATP^{4-} + 3\ H_2O \quad (1.2)$$

The first event of the light-dependent reactions is the absorption of a photon of > 1.8 eV by a Chl molecule in the LHC II antenna complex. In PS II the photon energy leadingto an electronically excited state is transferred to the photochemically active pigment P680, a special complex of Chls that constitutes the primary donor of PS II. The main electron carriers in PS II include pheophytin (Pheo), a special plastoquinone (Q_A) acting as one-electron acceptor and a dissociable plastoquinone (Q_B). The initially formed radical state – $P680^+/Pheo^-$ pair - represents the greatest electrochemical free energy gap of the system

(E_m = 1260 mV, [18]). It undergoes rapid kinetic stabilization by the transfer of an electron from $Pheo^-$ to the Q_A molecule. This forms the radical ion pair $P680^{+\bullet}PheoQ_A^{-\bullet}$ that is sufficiently stabilized for subsequent redox reactions. The above-described reaction can be summarized by the equation:

$$P680PheoQ_A \xrightarrow{k_{PC}} P680^{+\bullet}Pheo^{-\bullet}Q_A \xrightarrow{k_{stab}} P680^{+\bullet}PheoQ_A^{-\bullet}, \quad (1.3),$$

where P680 is the photoactive chlorophyll-a (Chl-a) component, Pheo is the primary acceptor, k_{PC} is the rate constant of primary radical pair formation from $P680^{+\bullet}$ and Q_A is a noncovalently bound plastoquinone-9 molecule (PQ-9) [19, 20]. This reaction is kinetically limited by k_{stab} that was found to be about $(300ps)^{-1}$ [21].

On the donor side, the primary donor $P680^+$ is reduced by redox active tyrosine residue 161 of D1 protein, Y_Z, which, in turn, oxidizes the oxygen evolving complex (OEC). The OEC is located at the luminal side of PS II and receives electrons from water oxidation to molecular oxygen and protons, which are released into the lumen (H^+_{lumen}):

$$2H_2O + 4\oplus \rightarrow O_2 + 4H^+_{lumen}, \quad (1.4)$$

where $\oplus$ represents the oxidizing redox equivalents originally generated at $P680^+$.

The resulting state $P680^{+\bullet}PheoQ_A^-$ can subsequently undergo either electron transfer to the secondary plastoquinone Q_B or recombination processes. The lipid soluble PQ molecules (~ 7 per PS II complex) serve as mobile carriers between the PS II and Cyt b_6f complexes. The Q_B –binding site acts essentially as a “loading dock” for the sequential transfer of two electrons onto the PQ, which, through the binding of two H^+, is converted to PQH_2. Formation of PQH_2 via a sequence of two one-electron transfer steps is energetically driven by $Q_A^{-\bullet}$ as reductant. This reaction can be summarized in the following equation:

$$PQ + 2Q_A^{-\bullet} + 2H^+_{stroma} \rightarrow PQH_2, \quad (1.5)$$

where PQ is a PQ-9 molecule bound to a special protein pocket (Q_B site), and H^+_{stroma} symbolizes the coupled proton uptake from the stroma side [22, 23]. The non-heme iron Fe(II), which is situated between Q_A and Q_B, appears to have mainly a structural role.

The lower affinity of PQH_2 for the Q_B site causes its replacement by another PQ molecule and transfer to Cyt *b_6f*. At Cyt *b_6f* the PQH_2 is oxidized under the release of protons into the thylakoid lumen, thereby producing a electrochemical potential that is needed for ATP-synthesis.

Cyt *b_6f* has two PQ binding sites associated with the b_6 polypeptide: the q-site that binds quinol and is located towards the lumenal surface, and the n-site, that binds quinone and is closer to the stromal surface. The first electron to be transferred from PQH_2 to Cyt *b_6f* in the q-site is immediately passed on to the Rieske iron-sulfur protein, Cyt *f* and then to plastocyanin, which carries the electrons to PS I. In contrast, the more energetic second electron is 'recycled' through the two Cyt *b_6* hemes across the membrane to the n-site where it is used to reduce another PQ molecule.

The second complex that performs light transformation into chemical free energy is the reaction center of PS I. The oxidized PS I is rereduced by an electron provided by reduced plastocyanin (PC). The electron ejected from electronically excited $^1P700^{\bullet}$ moves then through PS I across the membrane to ferredoxin (Fd), it passes through a number of prosthetic groups including a Chl known as A_0, a bound phylloquinone, A_1 and the F_X and F_A/F_B iron sulfur centers. In the electron transport chain Fd controls the flow of electrons either back to Cyt *b_6f* to increase proton transport and thereby ATP synthesis (cyclic phosphorylation), or to the NADP reductase for the synthesis of NADPH.

The protons that accumulate in the thylakoid lumen create an electrochemical potential, which is utilized by the CF_0/CF_1 complexes for the synthesis of ATP. The light reactions provide not only the reducing power in NADPH but also store the free energy in form of ATP. Both species, NADPH and ATP are essential for producing sugars from CO_2. ATP is produced through an enzyme called ATP synthase, using ADP, inorganic phosphate and the free energy from a proton motive force (pmf) across the thylakoid membrane. The pmf is composed of two components: an electrical potential across the thylakoid membrane and a proton gradient across the thylakoid membrane. The proton gradient originates from accumulation of protons (hydrogen ions) inside the lumen, giving a pH of 6.0 and proton uptake from the stroma, giving rise to a pH 8.0 outside. Protons then transferred from the thylakoid lumen through the central core of the enzyme ATP synthase (embedded in the membrane) cause conformational (rotational) changes in the enzyme, which catalyzes the phosphorylation of ADP and the release of ATP into the stromal side.

The endergonic light-independent reactions of photosynthesis use the ATP and NADPH synthesized during the exergonic light-dependent reactions to provide the energy for the synthesis of glucose and other organic molecules from inorganic carbon dioxide and water.

This is done by "fixing" carbon atoms from CO_2 to the carbon skeletons of existing organic molecules. These reactions occur in the stroma of the chloroplasts and do not require light as direct driving force [8].
These reactions can be summarized as follows:

$2NADPH + 3ATP^{4-} + CO_2 + H_2O \rightarrow -(CH_2O)- + 2NADP^+ + 3ADP^{3-} + 3HPO_4^{2-} + H_2O + H^+$ (1.6), where $-(CH_2O)-$ symbolizes generalized carbohydrate.

Most plants use the Calvin (C_3) cycle to fix carbon dioxide. C_3 refers to the importance of 3-carbon molecules in the cycle. This reaction consists from the three steps: 1) CO_2 fixation; 2) production of G3P; and 3) regeneration of RuBP. There are some plants, known as C_4 plants and CAM plants that differ in their initial carbon fixation step.

1.4 Structural organization of PS II and antenna complexes

PS II of higher plants, algae and cyanobacteria is a multimeric pigment-protein complex that is embedded into the thylakoid membrane and is comprised of almost 30 different integral subunits. Most of them are membrane, while a small number are known as extrinsic polypeptide subunits (Figures 1.3 and 1.4).
The modern crystallographic techniques allow analyzing crystal structure of PS II at high resolution. The crystal structures from different thermophilic cyanobacteria have been reported recently for *Synechococcus elongatus naegli (or Thermosynechococcus elongatus* - [24]) at resolution 3.8Å [25, 26] and *Thermosynechococcus vulcanus* at 3.7Å [27]. So far no any X-ray crystal structure have been reported for the higher plants PS II, but the RC of monomeric and dimeric PS II complexes have been structurally characterized by using electron microscopy [28-32].
The models of PS II complexes from high plants (Figure 1.3) and cyanobacteria (Figure 1.4) provide information on the overall structure and the location of many cofactors.
All cofactors required for photochemical charge separation are located in the center of PS II that is a heterodimer of the D1 and D2 proteins. These proteins are highly conserved between plant and cyanobacteria species. Both have 353 amino acids and each forming 5 membrane-spanning α-helices with their N-terminal exposed to the stromal surface of the membrane [25]. The D1 and D2 proteins are homologous in amino acid sequence to the L and M subunits of the purple bacteria RC [33-35]. This amino acid sequence homology of

the proteins and the array of the cofactors imply that PS II and bacterial RC are similar in their functional organization, especially on the reducing side. This similarity was the basis of the assumption that the structure of PS II RC is analogous to that of its purple bacteria counterpart [36, 37].

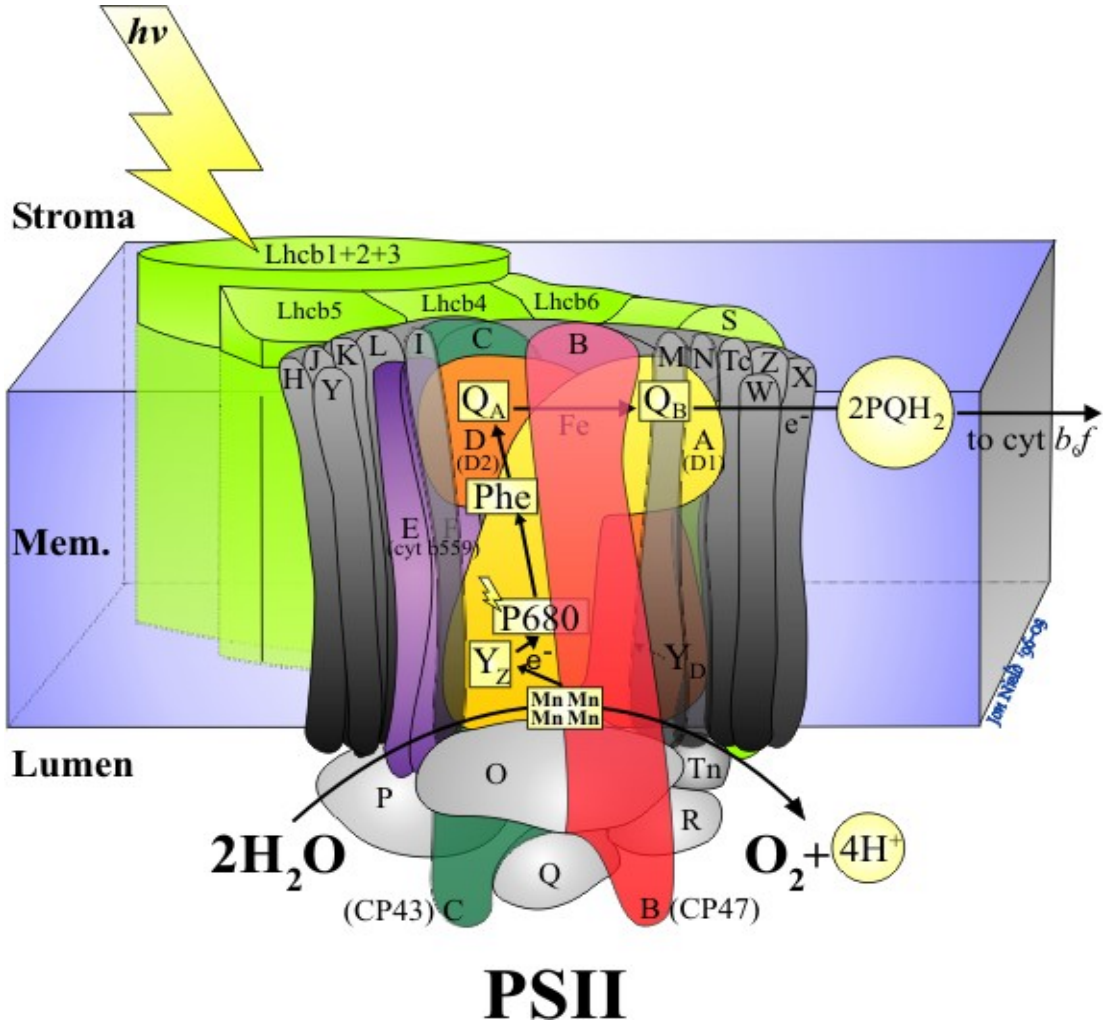

Figure 1.3. Complex of photosystem 2 (PS II) from higher plants. All electron-transport cofactors and most of the protein subunits are given [17].

It is now accepted that PS II RC preparations contain two Pheo *a* per RC [38]. Nanba and Satoh comparing the molar ratio between the chemically estimated and photochemically reduced amounts of pigments have shown that the primary photochemical reaction requires only one out of two Pheo *a* in the RC [39]. The number of Chl a and β-Car per RC varies between 2-8 and 0.5-1 respectively [40]. The isolated PS II RC complex contains virtually no PQ-9, which serves as the secondary and tertiary electron acceptor in PS II. The number of Cyt *b*-559 was estimated to be one per RC in the higher plant [41] and cyanobacteria *T.*

elongatus PS II complexes [42]. Cyt *b*-559 consist of two subunits, an α – subunit of 10 kDa (PS II – E) and β – subunit of about 4 kDa (PS II – F) [41].

Apart from the lack of Q_A, Q_B and the non-heme iron, the isolated D1/D2/Cyt *b*-559 preparations are also deproved of the manganese and the complex is completely inactive in oxygen evolution.

The D1/D2/Cyt *b*-559 complex of higher plants PS II is associated with Chl-protein complexes, which form light-harvesting antenna system. The first type is the inner antenna system, which includes CP43 and CP47 subunits (see Table 1.1). These proteins can be isolated with the RC complex and are essential for the water oxidizing activity. Biochemical characterization of the CP43 and CP47 subunits is reviewed in [43, 44]. Crosslinking studies have shown that subunits CP43 and CP47 flank both sides of the complex D1/D2/Cyt *b*-559 [45]. Furthermore, crosslinking of D1 and CP43 at the acceptor-side might prevent photoinhibition of PS II [46, 47].

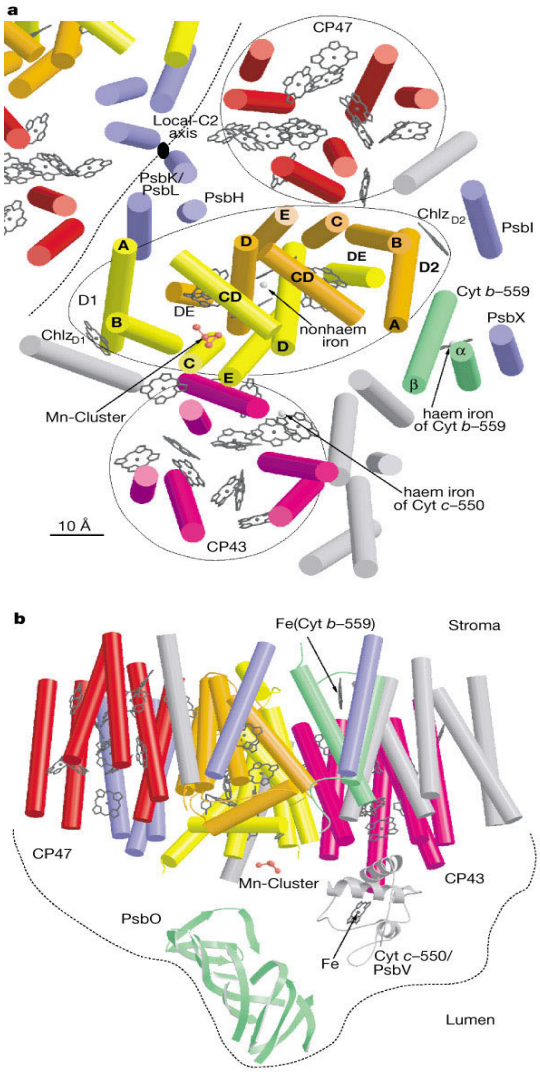

Figure 1.4. Structure of PS II from *(Thermo)Synechococcus elongatus* with assignment of protein subunits and cofactors. **a**, Arrangement of transmembrane α-helices and cofactors in PS II. One monomer of the dimer PS II complex is shown completely, with part of the second monomer related by the local-C2 axis (filled ellipse on the dotted interface). Chl *a* head groups and haems are indicated by black wire drawings. The view direction is from the luminal side, perpendicular to the membrane plane. The α-helices of D1, D2 and Cyt *b*-559 are labelled. D1/D2 are highlighted by an ellipse and of CP43 and CP47 by circles. The four prominent landmarks (three irons and the manganese (Mn) cluster) are indicated by arrows. **b**, Side view of PS II monomer looking down the long axis of the D1/D2 subunits from the right side in Fig. 1.4a, at slightly tilted membrane plane and rotated 180° so that the luminal side is bottom. PsbO (33K protein) is shown as a β-sheet structure, and Cyt *c*-550 as a helical model [25].

Another type of antenna system is the light-harvesting complex of PS II (proximal and priphiral antenna system). This part of the antenna comprises of six Chl a/b binding proteins (Lhcb1-6), which are closely associated with the PS II complex of higher plants and are encoded by the nuclear genes Lhcb 1-6 (see Table 1.1). The structure, cofactor organization and function of these subunits have been reviewed in detail [48-56]. The structure of a trimeric form of LHC II Lhcb 1-3 subunits in different ratios from pea has been determined to a resolution of 3.4 Å [57] by electron crystallography.

Lhcb1-3 have, correspondingly, apparent molecular masses of 25, 27 and 28 kDa. Lhcb4-6 are often referred to as CP24, CP26 and CP29, respectively, and have been shown to be more closely associated with PS II than Lhcb1-3 as they remain bound to the core complex under conditions that result in LHC II dissociation [58]. Several pieces of evidence point to Lhcb4-6 being involved in the transfer of excitation energy from LHC II to the PS II reaction center via CP43 and CP47. LHC II binds 50-65% of the total chlorophyll while the Lhc4-6 proteins together only bind about 20% of this pigment [50, 58]. Although it is likely that the Lhcb4-6 proteins can harvest light energy as well, their major role is thought to be one of facilitating and controlling excitation energy transfer from LHC II to PS II [17]. In some alga (*Rhodophyta*) and all cyanobacteria the role of the light-harvesting antenna belongs to the phycobilisomes, large multiprotein organelles, that are located on the stromal side of thylakoids (reviewed in [9, 59]).

Composition and functions of nearly all known PS II and LHC II subunits is presented in Table 1.1. The majority of the PS II proteins have already been characterized. But the role of the some low-molecular mass polypeptides in the range of 3-10 kDa is still not clear. At present there are about 30 genes, which have been identified as encoding proteins for the PS II core and are referred to as *psb* (photosystem b) genes. In higher plants and algae, most of these genes are located in the chloroplast genome, but some are in the nucleus. In some cases these components are restricted to a particular class of organism. In addition there are the genes that encode the proteins of the outer antenna systems; cab genes in higher plants and green algae give rise to a series of chl *a* / chl *b* binding proteins (Lhcb1-6) [50, 53, 60] while the *apc* and *cpc* genes encode the protein of the phycobilisomes of cyanobacteria and red algae [61].

Components	**Size (kDa)**	**Gene**	**Connection with co-factors and main functional aspects**
D1 (M)	32	psbA (C)	RC core, Q_B, Pheo, Chl special pair
D2 (M)	34	psbD (C)	RC core, Q_A, Pheo, Chl special pair

Cyt b_{559} α (M)	9.2	psbE (C)	RC core, heme b, photoprotection, involved in electron transport [62]
Cyt b_{559} β (M)	4.4	psbF (C)	RC core, heme b, photoprotection, involved in electron transport [62]
CP47 (M)	47-51	psbB (C)	Inner antenna, Chl a; interaction psbO
CP43 (M)	43-47	psbC (C)	Inner antenna, Chl a; interaction psbO
PS II-H (M)	7.7	psbH (C)	Phosphoprotein, photoprotection [63]; effect on the structure of the Q_B-site [64]
PS II-I (M)	4.2	psbI (C)	PC core, optimizes PS II function [65]
PS II-J (M)	4.1	psbJ (C)	Controls the amount of functionally assembled PS II [66]; regulates ET processes [67]; control of PS I accumulation [68]
PS II-K (M)	4.3	psbK (C)	Optimizes PS II function [65]; assembly and stability of PS II [69]
PS II-L (M)	4.5	psbL (C)	Donor side [70] and acceptor side function [71, 72]
PS II-M (M)	3.7	psbM (C)	Unknown function
PS II-N(M)	4.7	psbN (C)	Unknown function
PS II – O (L)	33	psbO (N)	Mn^{++} - stabilizing extrinsic protein
PS II – P (L)	24	psbP (N)	Absent in cyanobacteria, stabilizes oxygen activity; regulatory function (Cl^-, Ca^{2+})
PS II – Q (L)	18	psbQ (N)	Absent in cyanobacteria, stabilizes oxygen activity; regulatory function (Cl^-, Ca^{2+})
PS II-R (M)	10.2	psbR (N)	Absent in cyanobacteria [73]; donor and acceptor side function [30]
PS II – Tc (Ycf8 protein)	3.3	psbT (C)	Unknown function
PS II - Tn	3	psbT (N)	Absent in cyanobacteria, nuclear-encoded lumen protein; function unknown [74]
PS II - U	12	psbU	Absent in high plants [73], optimizes the OEC [75]
PS II – V (Cyt c550)	15	psbV	Absent in high plants [73], binds heme, donor side stability OEC [76]
PS II – W	6.1	psbW (N)*	Absent in cyanobacteria, nuclear-encoded protein closely associated with the reaction center [77]; function unknown
PS II - X	4.1	psbX (N)	Optimizes PS II [73]
PS II - Y	6 and 7	psbY	Tandem protein [78], involved in Mn binding [79], no essential PS II function, possibly difference between cyanobacteria and plants [80]
PS II - Z	6.5	psbZ (ycf9) (C)	controls the interaction of PSII cores with the light-harvesting antenna [81, 82]
Chl a/b antenna			
LHC II – Type I (M)	25	Lhcb1 (N); 8 genes	LHC II binds 6-8 Chl a and 6 Chl b,

LHC II – Type II (M)	25	Lhcb2 (N); 2 genes	2 luteins, one neoxanthin; DGDC and PG; PG is necessary for the trimerization of LHC II. [50, 83, 84]
LHC II – Type III (M)	24	Lhcb3 (N); 4 genes	
CP29 (M)	28	Lhcb4 (N); 2 genes	Binds Chl a and b, lutein, neoxanthin, violaxanthin
CP26 (M)	27	Lhcb5 (N)	Binds Chl a and b, lutein, neoxanthin, violaxanthin
CP24 (M)	23	Lhcb6 (N); 2 genes	Binds Chl a and b, lutein, neoxanthin (?), violaxanthin
CP22 (M)	21.7	PsbS (N)	Binds Chl a and b

Table 1.1. Protein composition of PS II. The proteins, forming the inner core complex, are shown in bold letters. The location denotes whether this protein is membrane-spanning (M) or associated with membrane at the stromal (S) or lumen (L) surface. Proteins that constitute the PS II complex are products of the *psbA* to *psbY* genes, which occur in all types of oxygenic organisms. In eukaryotic organisms the *psb* genes are located in either the chloroplast (C) or the nuclear (N) genomes. This Table is modified from [8, 73].

The proteins of the reaction center complex are similar in plants and cyanobacteria, while the surrounding proteins of the core complex and especially the antenna complexes vary between these organisms.

1.4.1 Extrinsic proteins

Extrinsic proteins play an important role, particularly, the 33kDa (PS II - O protein). Higher plants and alga contain additionally to the 33kDa polypeptide the subunits PS II – P (24 kDa) and PS II – Q (18kDa). In cyanobacteria, these two proteins are replaced by analogous polypeptides PS II – V (Cyt *c*550, 15kDa) and PS II – U (12kDa) [85]. Extrinsic proteins bind to PS II on the lumenal side of the thylakoid membrane. The main function of the extrinsic proteins is the stabilization of the Mn_4-cluster and hence the oxygen activity. Several research groups have independently shown by targeted mutagenesis that the 33kDa protein is not absolutely essential for oxygen evolving activity, although 33kDa less mutants are more sensitive to photoinhibition [86]. But if 33kDa deactivated, an apparent increase in generation of H_2O_2 as a water oxidation side product appears [87-89]. *Synechocystis* sp. PCC6803 mutant with deactivated 33kDa encoding gene *psbO* still grow photoautotrophically [90-92], but combined loss of the 33 kDa and the Cyt *c*550 results in a photoheterotrophic strain [93]. Crosslinking of extrinsic proteins to the CP47 and CP43 prevents release of these polypeptides from the PS II complex and conserves near to 100% of oxygen evolving activity.

1.5 Oxygen evolving complex

The oxidative water splitting to molecular oxygen and protons is catalysed by the Mn_4O_xCa complex. The Mn_4O_xCa complex together with Y_Z and Y_D tyrosine residues, Cl^- and possibly NO_3^- constitutes water-oxidizing complex (WOC) or oxygen-evolving complex (OEC).

1.5.1 Flash – Induced Oxygen Evolution Pattern Studies

Based on measurements of the oxygen yield induced by a sequence of flashes in dark-adapted samples, Kok and collaborators [94] proposed a model, by which each OEC functions independently and cycles during water oxidation through 5 different steps. These steps were indicated as S_i-sates, where i = 0, 1, ..4 is the number of oxidizing equivalents stored by OEC (Figure 1.5).

The storage capability of the OEC for oxidizing equivalents was first discovered by Joliot et al. [95]. Illuminating dark-adapted alga and chloroplasts by a train of the short, saturating flashes, he found that the oxygen was evolved with a characteristic periodicity of four. A typical pattern of dark-adapted thylakoids is given in Figure 1.5. One of the main characteristics of this pattern is the first maximum on the 3rd flash with repetition on every forth flash thereafter. An explanation for this is that in the dark, S_2 and S_3 states are reduced to the dark-stable S_1 state, which, in FIOP, refers to the first maximum on the 3rd flash. The decay of S_2 and S_3 states is biphasic and has fast and slow phases. The fast decay has a halftime of up to 10 seconds and is due to reduction by Y_D^{red} [96-100]. The slow decay is due the recombination with the electrons from the acceptor side ($Q_B^{-/2-}$) and has halftimes in the order of few minutes [23, 101-103]. The S_0 state is slowly oxidized in the dark to the S_1 state by Y_D^{ox} [96, 104]. The halftimes of the different S_i states transitions are strongly dependent on temperature and pH [100, 105-109]. The S_4-state is a transient state, in which molecular oxygen is formed and released, whereby the center returns to S_0-state.

Two other important features of the FIOPs are (i) the damping of the oscillation with increasing flash number (ii) the small oxygen yield on the second flash. To explain these characteristics Kok et al. introduced the “miss” (α) and “double hit” (β) probabilities [94, 110]. The miss probability gives the percentage of OECs that are in the same S state before and after flash excitation. Renger & Hanssum proposed that the occurrence of misses is

depended on redox equilibria on the donor ($Y_ZP680^+ \leftrightarrow Y_Z^{ox}P680$) and the acceptor side ($Q_A^-Q_B \leftrightarrow Q_AQ_B$) of PS II [111, 112].

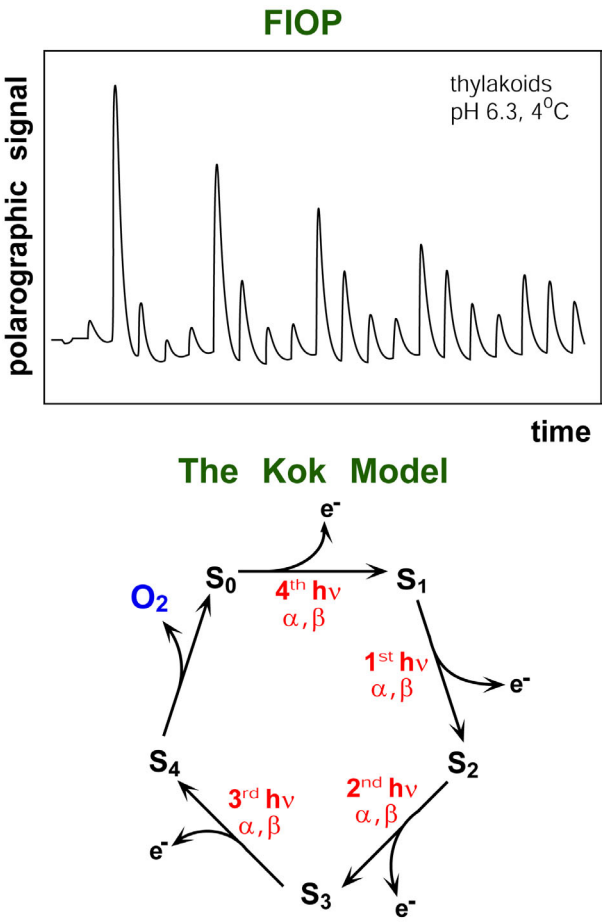

Figure 1.5. Flash-induced oxygen evolution pattern (FIOP) and the Kok-model [113].

The double hit probability equals the percentage of centers that have been excited twice in a single flash. The double hit probability depends on the flash profile, which in case of Xe-flashes usually includes a “tail” of residual intensity, which extends over a time range of more than 100 μs [94, 110, 114]. Double hits are essentially absent if illumination with tailless ns laser flashes is used (see also Chapter 7.3.6 of this work). For spinach thylakoids, typical Kok parameters for miss probabilities are 6-10% and for double hit probabilities 3-5% with Xe-flashes, and when laser excitation used only the miss probability remains.

The miss and double hit probabilities are strongly temperature and pH dependent [100, 108, 109, 113].

All characteristics of the FIOP remain essentially unchanged after inactivating of about 90% of the PS II centers [94].

The classic Kok model includes S_i-states, (i = 0,1…4) and the miss and double hit parameters. This model is more precise if extended by taking into account back reactions

of S states. The back reactions of S states mainly happen due to (i) reactions of S_2 and S_3 states with Y_D during the dark-time between flashes [100, 106, 108, 115, 116] and (ii) reduction of different S states by exogenous donors [115-120] and ADRY substances [121].

1.5.2 Y_Z and Y_D

The D1 protein has a tyrosine residue at position 161 also known as Y_Z. Y_Z is an intermediate electron carrier between the Mn_4 cluster and $P680^+$ and responsible for EPR signal II (signal II very fast (vf) (fast (f))) [122]. [25] reported distances of ~7Å between Mn_4 and Y_Z and ~12Å between Y_Z and P680. Recently it was considered that Y_Z might be directly involved in the chemistry of water oxidation either by direct hydrogen atom transfer or by facilitating proton coupled electron transfer (PCET) between substrate water and Y_Z (for review see [123, 124]). A second tyrosine residue, Y_D, is found at homologous position to Y_Z in the D2 protein. Y_D is located at about the same distance to P680 as Y_Z, but its distance to the Mn_4 cluster is ~30Å. Therefore, Y_D is not part of the main electron transport pathway. However, Y_D undergoes slow redox reactions with certain oxidation states of WOC (as described in 1.5.1). Y_D can form a stable radical, Y_D^{ox}, which is responsible for EPR signal II slow (s) [122]. Faller et al. have shown that Y_D is oxidized by $P680^+$ in Y_Z-deletion mutants with a similar rate constant as Y_Z in Mn-depleted samples [125, 126]. The function of Y_D/Y_D^{ox} is still unknown, but it has been speculated that Y_D^{ox} enhances the redox potential of the primary donor [127]. Ananyev et al. proposed that Y_D^{ox} has a functional role in photoactivation of PS II. Y_D and Y_Z are highly conserved in all species so far reported [128].

1.5.3 Cofactors of the OEC

Several cofactors like Ca^{2+}, Cl^- and possible HCO_3^- have been found to be essential for optimal oxygen evolution activity [129-131]. It was demonstrated that Ca^{2+} ions restore O_2 evolving activity after various treatments, which release the functionally important Ca^{2+} ions from the OEC. There are two Ca^{2+} ions in PS II, which are stoichemetrically bound to it. One of these Ca^{2+} ions is suggested to be located in the LCH II antenna, while the second is believed to be associated directly with the OEC [132, 133].

It has been found, that Sr^{2+} ions can functionally replace Ca^{2+} ions with a partial restoration of total oxygen activity [134]. The precise functional role of the Ca^{2+} ion in the OEC

remains unclear at the moment, although it does appear to be a prerequisite for the proper photoassembly of the Mn_4O_xCa complex [135, 136]. It has also been proposed that ions of Ca^{2+} may have a structural role [137], or to function as gatekeeper, which regulates the access of water [138-140] and as a binding site for chloride [141, 142], or a water binding site [141, 143]. In a theoretical study, it was concluded that Ca^{2+} ions might be required for the formation and stabilization of a Mn(IV)-$O^{\bullet}$ radical in the S_3 state [144].

Chloride has also been suggested to be a catalytic cofactor for the OEC based on treatments that reduce oxygen activity and are subsequently restored after addition of Cl^- ions. The reconstitution of activity, however, is not limited to Cl^- and can be replaced by $Br^- > I^- > NO_3^-$ in their decreasing order of effectiveness [145-147]. It was concluded that Cl^- is required for S state transitions $S_2 \rightarrow S_3$ and $S_3 \rightarrow S_0$, but not for the $S_0 \rightarrow S_1$ and $S_1 \rightarrow S_2$ transitions [148, 149]. Treatments with alkaline pH and/or addition of high sulfate concentrations have been used to displace Cl^- from its binding site in PS II. However, the possibility of side effects that create the observed Cl^- requirement of PS II have to be taken into consideration [150-152]. It was shown that the treatments for Cl^- depletion remove some of the extrinsic polypeptides [152]. Oxygen measurements at various light intensities show that after complete release of Cl^- all PS II centers are still active, but evolve oxygen at reduced rate due to slow S state turnover. Lindberg and Andreasson have concluded that Cl^- is not a cofactor for oxygen evolution [153] and that it does not bind directly to Mn [152]. In contrast, they suggest that Cl^- is an important part in a proton-relay network that helps to shuttle protons from the OEC to the lumen. Other research groups have suggested that charge neutralization may be achieved through direct binding to the Mn_4O_xCa complex [154, 155].

The main effect of bicarbonate on the electron transfer in PS II is due to binding at the acceptor side of PS II, where it is involved in the protonation of Q_B^{2-} [156]. However, several recent reports conclude that bicarbonate also affects the PS II donor side. For example, Baranov et al. have suggested that bicarbonate promotes the assembly of the Mn_4O_xCa complex during photoactivation ([157] and references therein). The functional role of bicarbonate on water-oxidizing chemistry is still unclear.

1.5.4 Current state of research on chemistry of water oxidation

Until the recent crystal structure determination of PS II at 3.8 Å resolution, most of the information about the structure of the Mn_4O_xCa complex has come from electron paramagnetic resonance (EPR) and X-ray absorption spectroscopy studies of the S_1 and S_2

states. Extended X-ray absorption fine structure (EXAFS) measurements have firmly established that the OEC comprises di-µ-oxo-bridged Mn_2 motifs which show Mn–Mn scattering at a distances of about 2.7 Å. In addition, a single Mn–Mn and 1-2 Mn–Ca interactions at 3.3–3.4 Å have been fit to the data [158, 159]. With these EXAFS-derived structural building blocks many different models can be proposed for the Mn_4O_xCa complex. For a long time a so-called "dimer of dimers" model of the OEC (Figure 1.6 **A**) was favored because of its simplicity and consistency with most EXAFS data [124, 159]. However, on the basis of simulations of EPR spectra from the S_2 state structures **B** or **C** have been supported because these structures provide better rationales for the strong exchange coupling between two di-µ-oxo bridged Mn–Mn moieties.

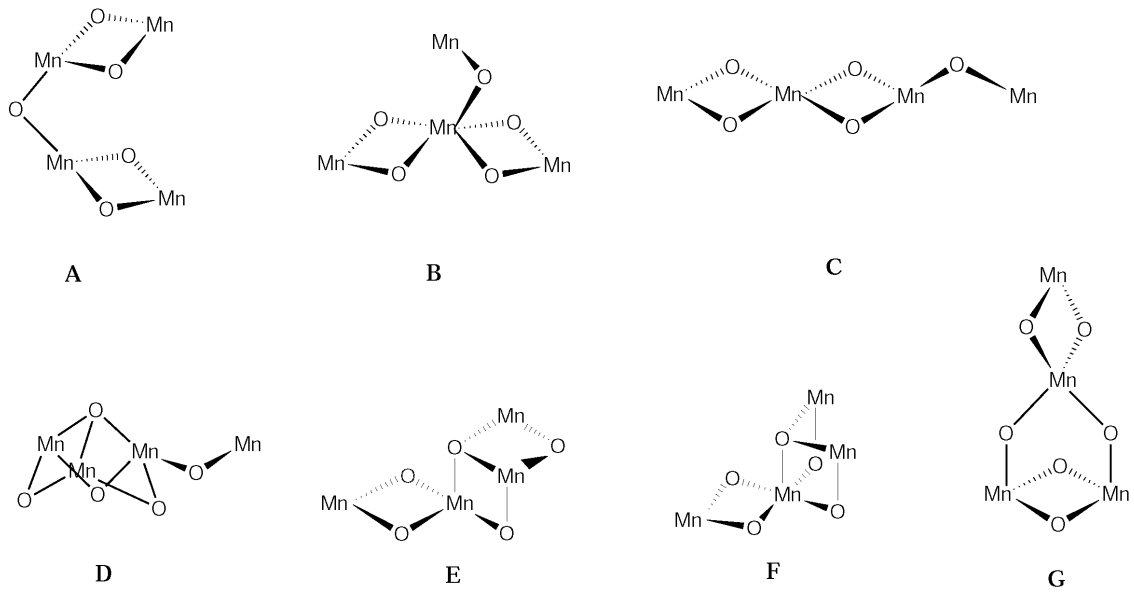

Figure 1.6. Different models proposed for the Mn_4-cluster. Explanations for each model are given in text. This Figure is adopted from [124].

Models **A**, **B** and **C** contain two 2.7 Å distances and one 3.3 Å Mn-Mn distance. However, the EXAFS analysis of most groups is consistent with two or three 2.7 Å Mn-Mn distances. Models **D, E** and **F** (Figure 1.6) are among the few possible structures for the OEC that contain three di-µ-oxo type Mn–Mn moieties and one 3.3 Å Mn-Mn distance. These structures are now favored by the Berkeley group based on a detailed analysis of EXAFS data of the S_0 state [124]. A structure similar to **D** was also suggested based on simulations of EPR spectra from the S_2 state obtained by Kusunoki and co-workers [160]. Interestingly, the S_{-2} EPR signal has great similarities with the EPR signal of the Mn_2(II, III) form of di-Mn-catalase [161, 162]. This may indicate structural analogies between parts of the Mn_4O_xCa complex of PS II and the dimeric catalytic site of Mn catalase [116, 161].

From the structures displayed in Figure 1.6, models **D**, **E** and **F** appear to offer the best geometry for containment within the electron density envelope ascribed to the 3.8 Å X-ray structure of the Mn cluster in PS II (Figure 1.7, [25]). However, as suggested by the Mn and Sr EXAFS studies [163], the OEC is most accurately described as a Mn_4O_xCa heteronuclear complex; therefore, Ca should be incorporated into each of the proposed structures in Figure 1.6 so that 1-2 Mn-Ca vectors exist which are oriented close to the membrane normal [164]. Structures like **G** also correspond well with the data of the PS II crystal structure (Figure 1.7, [25]).

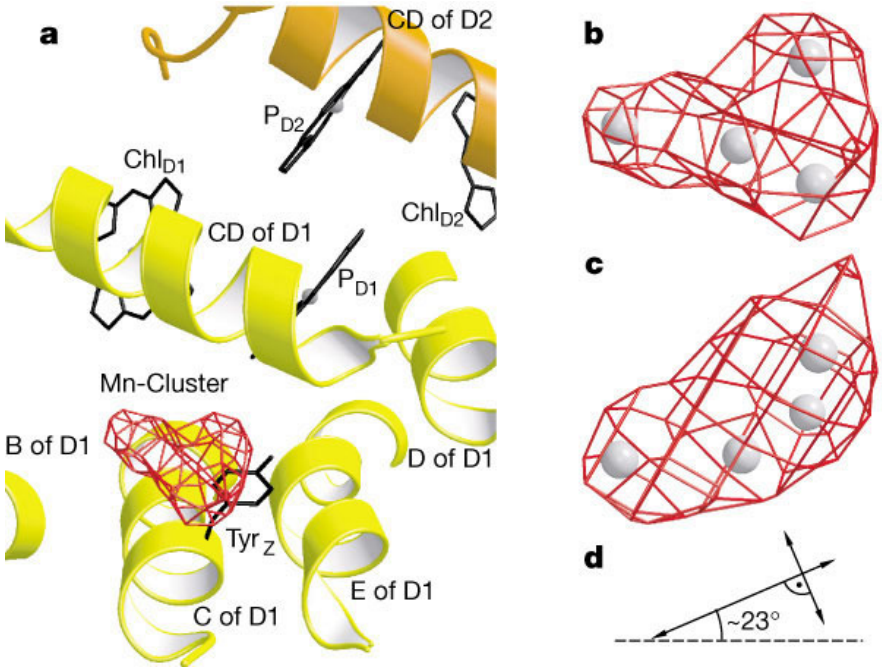

Figure 1.7. Location and orientation of manganese cluster in PS II crystal from (*Thermo)Synechococcus elongatus*. **a**, Close-up view of the reaction center, with the electron density of the manganese cluster contoured at 5 σ. The view is from the luminal side onto the membrane plane, as in Figure 1.4a. **b**, Enlarged view of the electron density of the manganese cluster; **c**, 90° rotated around the horizontal axis (view along the membrane with the luminal side on top). **d**, Orientation of the short and long axes of **c**. The latter is tilted 23° against the luminal side of the membrane plane (hatched line) [25].

Although a unique structure determination of a multi-nuclear center like the Mn_4O_xCa complex is complicated using EXAFS alone, structural changes of the Mn_4O_xCa complex upon S state transitions should be detectable by this technique. Based on EXAFS spectroscopy the Mn_4O_xCa complex has essentially the same structure in the S_1 and S_2 states [165]. However, in the S_0 state one of the 2.7 Å distances is longer by ~ 0.15 Å [166]. This increase is consistent with the protonation of one bis-μ-oxo bridge and/or the presence of one Mn(II) center in the S_0 state.

1.5.5 Mn Ligands and Role of Proteins

Depending on the number of Mn-Mn μ -oxo bridges and assuming 6 ligands per Mn center, 13 to 14 monodentate protein ligands should exist for the Mn_4O_xCa complex. This number may be reduced by 1-2 ligands if oxo bridges exist between Mn and Ca. Furthermore, 1-2 substrate water (see below), one Cl^- and/or HCO_3^- may be bound to Mn. This leaves about 6-10 protein ligands to the Mn_4O_xCa complex. Based on site directed mutagenesis, possible ligands are Asp170, Glu 189, His190, His332, Glu333, His337, Asp342 and Ala344 of the D1 protein [167, 168]. ESEEM measurements provide evidence for at least one histidine ligand [169, 170] in the S_2 state.

The protein-secluded position of the Mn_4O_xCa complex within the PS II structure suggests that the protein matrix is important for the proper function of the OEC. In absence of the extrinsic proteins, for example, unphysiologically high Ca^{2+} and Cl^- concentrations are required to restore oxygen evolution activity. Similarly, small deletions in the extrinsic loops of CP43 and CP47 can inactivate the OEC. Possible functions of the protein include: a) to prevent unregulated access of water and other molecules to the Mn_4O_xCa complex by providing specific channels for substrate water entry and oxygen release [171], b) to form specific H-bonding networks or proton release chains (proton wires) involved in releasing protons into the lumen, c) to induce or support structural changes of the Mn_4O_xCa complex during water oxidation, d) position and 'concentrate' required co-factors and e) tuning of the energetics of the S state transitions.

1.5.6 Mn oxidation states of the S_1 and S_2 states

The knowledge of the Mn oxidation states of each S state is of great importance for the understanding of water oxidation in PS II. Many different techniques like flash induced UV-absorption changes, EPR, X-ray absorption near edge structure (XANES) and Kβ X-ray emission spectroscopy (Kβ XES) have been employed to analyze this question. A straightforward interpretation of the data is complicated by the fact that maximally one out of four Mn ions changes its redox state on each S state transition. In the following, this question is split into two parts: 1) what are the Mn oxidation states in the S_1 and S_2 states, and 2) do Mn oxidation state changes occur during all S state transitions?

Because it is relatively easy to prepare concentrated PS II samples with nearly 100% S_1 or S_2 state population, these two S states have been studied in detail by EPR and XANES spectroscopy. A comparison of XANES Mn K-edges of PS II in the S_1 state and S_2 states

with spectra of relevant Mn model compounds shows that (i) a Mn-centered oxidation occurs on this transition and (ii) that the Mn oxidation states of the S_1 state are $Mn_4(III_2, IV_2)$ [172-174]. This finding is corroborated by recent Kβ XES data of the S_1 and S_{-1} states [175] and by ^{55}Mn ENDOR of the S_2 state [176]. Most simulations of the S_2 EPR multiline signal are consistent with Mn_4(III, IV, IV, IV), which is in line with the above proposal for the S_1 state, but some groups argue for Mn_4(III, III, III, IV) in S_2, which would indicate Mn_4(III, III, III, III) in the S_1 state [177].

In agreement with the relatively high Mn oxidation states in the above two proposals, several studies show that (i) additional S states exist below the S_0 state that can be generated by reduction of the OEC with molecules like hydrazine, hydroxylamine or NO$^{\bullet}$, and (ii) that light induced oxidation of free Mn^{2+} by Mn-depleted PS II preparations (apo-PS II) is required for the assembly of a functional Mn_4O_xCa complex in PS II.

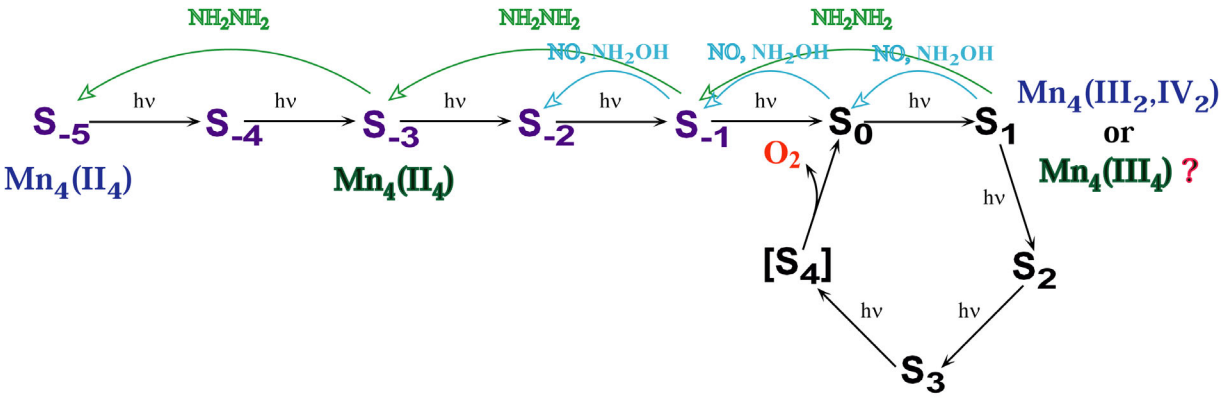

Figure 1.8. The Kok Model extended to the S_{-i} states (i = 1,..5). This Figure shows pathways of the reduction of the OEC by exogenous electron donors used in the present study: one-electron reductants NH_2OH (Chapter 6) and NO (Chapter 8) and two-electron reductant NH_2NH_2 (Chapter 7).

The photoactivation process in PS II is a low quantum yield process requiring several hundred flashes. Several intermediate states have been identified. The reduction of the Mn_4O_xCa complex below the redox level of the S_0 state may be viewed as a reversal of the photoactivation process (Figure 1.8). Using hydrazine as a reductant it has been clearly shown that relatively stable (hours) S_{-1}, S_{-2} and S_{-3} state populations of more than 60 % can be generated in PS II [119, 120]. In addition, first indications for the existence of the S_{-4} and the S_{-5} states have been obtained from the analysis of the oxygen oscillation patterns (Chapter 7 of present work), but they appear to be (i) significantly less stable then the other S states, and (ii) the maximum population observed was about 20 % of S_{-4} or S_{-5} [120]. Therefore, the S_{-3} state is the lowest long-term stable redox state of the OEC that can be generated in PS II by reduction.

Taken together, these data indicate that the lowest long term stable state of the OEC, i.e. the S_{-3} state, has the same redox level as the first long-lived photo-activated state, i.e. Mn_4(II, II, III, III). Since the $NO^{\bullet}$ induced formation of the S_{-2} state EPR multiline signal [161, 178, 179] and XAS measurements on reduced S states [180, 181] prove that Mn centered reductions occur down to at least the level of the S_{-2} state, these considerations strongly support the idea that the Mn oxidation states in S_1 state, which is four steps more oxidized, are Mn_4(III, III, IV, IV) (for review see [124]).

1.6 The thesis goals

The research work of this thesis addresses two main goals.

1) To investigate functional differences and similarities of the PS II from higher plants and thermophilic cyanobacteria, from which the PS II crystal structure was reported recently [25, 26]. This included flash-induced oxygen evolution studies (FIOPs) to unravel the temperature dependencies of the miss and the double hit probabilities as well as the S states lifetime in both organisms. The most interesting results of this research are outlined in the Chapter 3 of this thesis. In Chapter 4 the effects of the H/D isotope exchange and pH- (or pD-) dependencies on the above described processes are summarized. As an outcome of these results, the effect of the alkaline pH on the dark stabilization of the tyrosine D in *T. elongatus* is studied separately and described in Chapter 5. The discussions of these results are given in the end of each chapter and present possible mechanisms of the novel effects.

2) To understand the mechanism of the water oxidation in higher plants and cyanobacteria. This involved characterization of the "super-reduced" S_{-i} states in *T. elongatus*. Thus, nitric oxide induced formation of the "S_{-2}" state obtained for the first time in PS II core complexes from *T. elongatus* is characterized in Chapter 8. The results of Chapter 7 reveal that hydrazine-induced reduction of the Mn_4O_xCa complex to the "S_{-3}" state is more successful in thylakoids from *T. elongatus* than in spinach (compared to [119]. Moreover, these results improve the work of [119] by (i) stabilization of the OEC activity with different protectors of the oxygen evolution prior to hydrazine incubation; (ii) taking into account in numeric analysis the possible effect of (a) reduced form of tyrosine D and (b) the double hit probability on the calculated percentage of the S_{-i} states. The results of the

Chapters 7 and 8 are discussed within the framework of the possible oxidation state of Mn_4O_xCa-complex in S_1 state.

The results presented in Chapter 6 improve the work of [182] by determination of the rate constants for the $S_1 \rightarrow S_0 \rightarrow S_{-1}$ transition also at higher temperatures.

CHAPTER 2

Materials and Methods

2.1 Reagents

All reagents used in this work had analytical or high purity grade (99.97% - 99.999%). The reagents were provided from Sigma, Aldrich, Fluka, Pharmacia, etc.

2.2 Biological samples

Samples from two organisms were used in this work: thermophilic cyanobacterium *Thermosynechococcus elongatus* (*T. elongatus*) and higher plant *Spinacia oleracea* (spinach).

The culture of *T. elongatus* (another name is *Synechococcus elongatus naegli*) was grown in two 30 *l* glass columns at 56°C. The cells were harvested at their mid to late logarithmic phase as it is described in [183].

Fresh spinach was bought from the market and sample preparations were done at the same day. All isolation procedures were done in cold room, on ice and at very dim green light.

2.3 Preparative procedures

2.3.1 Thylakoid membranes

The thylakoids from *T. elongatus* were provided by the group of Dr. A. Zouni (details will be published elsewhere).

The spinach thylakoid membrane was isolated as described in [184] with slight modifications given in [185]. This preparation procedure consists from following steps:

- Grinding of leaves in P-1 buffer using a standard blender
- Filtration of homogenate through two layers of mira-cloth separated by one layer of cotton wool
- Immediate centrifugation (Beckman, GSA rotor, 5000 rpm / 10 min)
- Careful resuspension of pellets in the P-1 buffer with followed centrifugation (Beckman, GSA rotor, 7500 rpm / 10 min)
- Resuspension of pellets in the P-1 buffer, thorough homogenisation with followed centrifugation (Beckman, SS34 rotor, 7500 rpm / 10 min)
- Resuspension of pellets in the P-1 buffer, followed by centrifugation (Beckman, GSA rotor, 7500 rpm / 10 min)

- Careful resuspension of pellets in the P-1 buffer to [Chl] ~ 3 mM
- Storage at –80°C as small aliquots in liquid nitrogen.

2.3.2 Photosynthetic membrane fragments

Photosynthetic membrane fragments (BBY type) with high oxygen evolving activity were prepared from the market spinach leaves according to the method of [186] with modifications from [187]. The isolation of BBY fragments included following steps:

- Homogenisation of refined spinach leaves in P-2 buffer
- Filtration of homogenate through 4 layers cheesecloth
- Immediate centrifugation (Sorvall, GS-3 rotor, 6000 rpm / 10 min)
- Quickly resuspension of chloroplast pellets in P-3 buffer
- Centrifugation (Sorvall, GS-3 rotor, 6000 rpm / 10 min)
- Resuspension and homogenisation of pellets in P-4 buffer
- Triton treatment: incubation in P-5 buffer for 5 min at 4°C
- Centrifugation ((Sorvall, SS-34 rotor, 17500 rpm / 15 min)
- Resuspension of the PS II enriched membranes in P-4 buffer with following centrifugation (Sorvall, SS-34 rotor, 2000 rpm / 2 min)
- Centrifugation of the supernatant (Sorvall, SS-34 rotor, 17500 rpm / 15 min)
- Washing of pellets in P-6 buffer and centrifugation (Sorvall, SS-34 rotor, 17500 rpm / 30 min)
- Two additional washings in P-6 buffer and centrifugation (Sorvall, SS-34 rotor, 17500 rpm / 30 min)
- Final resuspension in P-6 buffer, homogenisation and storage at –80°C as small aliquots in liquid nitrogen.

2.3.3 PS II core complexes from T. elongatus

The PS II core complexes (PS IIcc) from *T. elongatus* were extracted from the membranes using β-dodecyl maltoside as detergent and purified by weak anion exchange chromatography as described [188]. Monomeric and dimeric PS IIcc were separated chromatographically (details will be published elsewhere). Both forms of the PS IIcc were fully active in water oxidation and show the same subunit composition as tested by

MALDI-TOF-MS and SDS-PAGE. The dimeric PS IIcc are similar to the material used to grow single crystals suitable for x-ray structure analysis [188].

2.3.4 Depletion of Extrinsic Proteins

Depletion of all extrinsic proteins was performed according to [189-191] with modifications. For this procedure, the BBY fragments were diluted 1:5 with B-1 medium and incubated for 30 min. After this treatment the sample was spun down (Biofuge, 8500 g / 20 min / 4°C) and the supernatant, contained extrinsic subunits, was dialyzed overnight against B-4 buffer. Next day the sample was concentrated by centrifugation using microconcentrators (Centricon-10, Amicon, Inc) and frozen until used. All procedures were done on ice and at very dim green light.
Depletion of 24 kDa and 18 kDa was performed as described in [191] with modifications. The whole procedure is the same as described in above case, but the samples were incubated in B-2 buffer for 30 min at room light, on ice.

2.3.5 Crosslinking experiments

Crosslinking experiments were done with BBY fragments and both types of thylakoid membranes. EDC was used according to [191] as an effective crosslinker (SS-4), which itself does not inhibit oxygen evolution activity [191]. Stock solution SS-4 was prepared fresh before experiments. Samples were incubated with different concentrations of EDC for 10 min at room temperature or 20 min on ice. Afterwards the samples were washed at least twice (dilution 1:10) in MMCH or SMCH buffers (Biofuge, 8500 g / 20 min / 4°C).

2.4 Sodium Dodecyl Sulphate Polyacrylamid Gel Electrophoresis

SDS-Urea-PAGE was performed by a standard procedure described in [192]. 12-14% and 4-6% of acrylamide : bis-acrylamide solution (50:1.33) with 6 M Urea were used for the resolving and stacking gels, respectively. The gels were pre-electrophoresed for 30 min at 20 mA and 6°C using Hoefer® mini *VE* and EPS 301 units (Amersham Pharmacia Biotech). The samples were incubated with Laemmli sample buffer (1:1) for 40 min with 2 – 3 intermediate vortexes and then loaded to the gels. In case of *T. elongatus* thylakoids, samples with sample-buffer were heated for 3 min at 60°C and spun down (Minifuge, 10 000 x g / 3min). After that procedure samples were ready to load. The “Mark 12™ protein

unstained medium standard marker (Invitrogen), which has a range from 99 to 14 kDa was used. The continuous current of 120 V / 350 mA was given for 5-6 hours at 6°C. Gels were fixed in SS-5 overnight; afterwards stained with CB R-250 (SS-6) for 1 hour and destained in the SS-5 (3 x 30 min).

2.5 Chlorophyll determination

Determination of the chlorophyll content in spinach thylakoids and BBY fragments was done according to [193] with small modifications.

The chlorophyll from different spinach preparations was extracted in 80% buffered acetone solution (C-1 buffer) together with other pigments and lipids. After stirring and quick centrifugation (Minifuge, 10000 g / 1 min), which removes the absorption spectra of the supernatant were measured against 80% buffered acetone solution at 646.6 nm, 663.6 nm and 750 nm using a Thermo Spectronic Vision 32 spectrophotometer.

Obtained values of absorption (A) were analysed in mM using following equations:

For total [Chl] $[17.75(A_{646.6} - A_{750}) + 7.34(A_{663.6} - A_{750})]\ k$ (2.5.1)

For [Chl **a**] $[12.25(A_{663.6} - A_{750}) - 2.55(A_{646.6} - A_{750})]\ k$ (2.5.2)

For [Chl **b**] $[20{,}31(A_{646.6} - A_{750}) - 4{,}91(A_{663.6} - A_{750})]\ k$ (2.5.3),

where k is a dilution factor (k = µl C-1/μl_{sample})

Additionally, the ratio of Chl **a** to Chl **b** was calculated.

The chlorophyll concentration of *T. elongatus* thylakoids was determined according to the following procedure: 5 µl of thylakoids were resuspended in 195 µl of C-2 buffer and 800 µl 100% acetone was added. After stirring, incubation for 10 min and one more stirring, the sample was centrifuged (Minifuge, 10000 g / 1 min). The absorption spectrum (A) was measured at 664 nm and 700 nm using Cary spectrophotometer and c = [Chl] was calculated in mM according to equation:

$\Delta A = c \cdot \varepsilon \cdot d \cdot k$, (2.5.4)

where $\Delta A = A_{664} - A_{700}$; ε molar extinction coefficient, ε = 76780 (l mol^{-1} cm^{-1}) and d is length of the cuvette (cm).

2.6 Buffers and solutions

2.6.1 Buffers used in preparation procedures (P)

All P- buffers were prepared before experiments in distilled water (Millipore Quality, MQ). pH of these solutions was always adjusted at the temperature specified in the procedures.

P-1	400 mM Sucrose / 50 mM HEPES / 5 mM $MgCl_2$ / 15 mM NaCl	pH 7
P-2	1 mM EDTA / 50 mM HEPES / 4 mM $MgCl_2$ / 400 mM NaCl / 5 mM Sodium Ascorbate / 2 mM BSA *	pH 7.5
P-3	50 mM MES / 8 mM $MgCl_2$ / 150 mM NaCl	pH 6.0
P-4	50 mM MES / 5 mM $CaCl_2$ / 10 mM $MgCl_2$/ 15 mM NaCl	pH 6.0
P-5	25% Triton X-100 in P-4	
P-6	P-4 + 400 mM Sucrose	pH 6.0

* 5 mM Sodium Ascorbate / 2 mM BSA were added to P-2 buffer shortly before grinding.

2.6.2 Buffers and solutions used in depletion of extrinsic proteins, crosslinking and SDS-PAGE experiments (B)

B-1	25 mM MES/NaOH / 200 mM NaCl / 2.6 M Urea	pH 6.5
B-2	25 mM MES/NaOH / 1 M NaCl	pH 6.55
B-3	25 mM MES/NaOH / 10 mM NaCl / 300 mM Sucrose	pH 6.5
B-4	10 mM Tris/HCl / 10 mM NaCl **– buffer for dialysis**	pH 7.2
B-5	12% AA:bisAA (50:1.33) / 1.5 M Tris/HCl / 6 M Urea / MQ / 20% SDS / 10% APS / 0.025% v/v TEMED **– 12% resolving gel**	pH 8.8
B-6	4% AA:bisAA (50:1.33) / 0.3 M Tris/HCl / 6 M Urea / MQ / 20% SDS / 10% APS / 0.025% v/v TEMED **– 4% stacking gel**	pH 6.8
B-7	0.0625 M Tris/HCl / 2% SDS / 10% Glycerol / 5% 2-mercaptoethanol / 0.001% bromphenol blue **- Laemmli**	pH 6.8

	sample buffer	
B-8	0.025 M Tris/ HCl / 0.192 M Glycine / 0.1% SDS – **running buffer**	pH 8.3

2.6.3 Buffers used in chlorophyll determination (C)

C-1	80% Acetone in 2.5 mM $H_2NaPO_4 \cdot 2H_2O$	pH 7.8
C-2	20 mM MES / 50 mM Mg_2SO_4	pH 6.4

2.6.4 Buffers used in oxygen evolution measurements

Buffers used in oxygen evolution measurements were prepared either in MQ (M) water or in D_2O (D). In the latter case, the buffer solutions were adjusted by using a glass electrode with corrections according to [194].

M-1, D-1	20 mM HEPES/NaOH / 10 mM NaCl	pH 7.2
MMCH	0.4 M Mannitol / 10 mM $MgCl_2$ / 20 mM $CaCl_2$ / 50 mM	pH 6.8
M-2, D-2	HEPES	
M-3	0.4 M Sucrose / 5 mM $MgCl_2$/ 15 mM NaCl / 40 mM MES	pH 6.5
SMCH	0.4 M Sucrose / 10 mM $MgCl_2$ / 20 mM $CaCl_2$ / 50 mM	pH 6.5
M-4, D-4	HEPES	
MMCM	0.4 M Mannitol / 10 mM $MgCl_2$ / 20 mM $CaCl_2$ / 50 mM	pH 6.0
M-5, D-5	MES	
MMCT	0.4 M Mannitol / 10 mM $MgCl_2$ / 20 mM $CaCl_2$ / 50 mM	pH 8.0 or 9.0
M-6, D-6	Tricine	
MCH	10 mM $MgCl_2$ / 20 mM $CaCl_2$ / 50 mM HEPES	pH 6.8
M-7, D-7		
MCM	10 mM $MgCl_2$ / 20 mM $CaCl_2$ / 50 mM MES	pH 6.0
M-8, D-8		
MCT	10 mM $MgCl_2$ / 20 mM $CaCl_2$ / 50 mM Tricine	pH 8.0 or 9.0
M-9, D-9		

Stock solutions (SS) were prepared as it is described below and kept until used.

SS-1	50 mM $K_3Fe(CN)_6$ in MQ water	-20°C
SS-2	20 mM *p* – phenyl – benzoquinone (PPBQ) dissolved in dimethylsulfoxid	-20°C
SS-3	1 M NH_4Cl in MQ water	0°C
SS-4	1% EDC in different buffers	Immediately used
SS-5	Acetic Acid : Ethanol : MQ = 1:3:6 – solution for fixing and destaining of gels	0°C
SS-6	Coomassie brilliant blue R250 (**CB R250**) dissolved in SS-5 –solution for staining of gels	0°C

2.7 Oxygen evolution measurements

2.7.1 Clark electrode

The rate of the oxygen evolution was measured with a Hansatech oxygen electrode at 20°C using a saturating light. Measurements were performed with 10 – 20 μM of Chl in 1 ml of M-1 buffer with 500 μM of $K_3Fe(CN)_6$ and 200 μM PPBQ as artificial electron acceptors. In case of the spinach thylakoids 100 μM of the SS-3 were added.

The oxygen evolution rate (**v**) was calculated in $\{\mu mol \cdot mg^{-1} \cdot h^{-1}\}$ using following equation:

$$v = k \times \frac{S(O_2)}{[Chl]} \times \frac{S}{c} \times \frac{mV_m}{mV_c} \times 3600 \qquad (2.7.1.1)$$

where ***k*** is slope; ***S(O₂)*** is solubility of oxygen in air saturated water at 20°C and standard atmospheric pressure (0.276 nmol/ml) [195]; **[*Chl*]** is the chlorophyll concentration (μg/ml); **S** is speed of the chart recorder (mm/s); ***c*** is calibration (mm), *mV* is a unit of voltage during measurements (***mV_m***) and calibration (***mV_c***).

2.7.2 Joliot electrode

FIOPs of *T. elongatus* thylakoids and PS II membranes were obtained in the absence of exogenous electron donors with an unmodulated Ag/Pt home-build Joliot type (bare platinum) electrode [113, 196], which keeps the temperature of the electrode constant within 0.3°C. Samples were transferred to the electrode in very dim green light. To insure complete sedimentation and temperature equilibration 10μL aliquots of thylakoids from *T.*

elongatus and spinach were kept for 5 min and 3 min, respectively, on the electrode at the given temperature.

For flash excitation a xenon flash lamp (EG&G, model PS 302, light pack FY-604) was used that was trigged from a personal computer. Data were recorded with a sampling rate of 3 ms/point and the flash rate was 2 Hz.

For all FIOP measurements the polarization of – 750 mV was switched on 40s before the flash train and the pH of the flow buffer was adjusted to pH 6.8 at the indicated temperatures. All measurements were repeated at least 2 times.

2.7.3 Numeric analysis

The first 16 flashes of each FIOP were analyzed using an Excel spreadsheet that was based on an extended Kok model, which includes the reduced S_{-1}-state and an activity parameter *d* that compensates changes in the number of active PS II centers during the flash train [119]. This extended Kok model is summarized by equation 2.7.3.1:

$$\begin{bmatrix} S_{-1} \\ S_0 \\ S_1 \\ S_2 \\ S_3 \end{bmatrix}_n = \begin{bmatrix} \alpha & 0 & 0 & 0 & 0 \\ \gamma & \alpha & 0 & \beta & \gamma \\ \beta & \gamma & \alpha & 0 & \beta \\ 0 & \beta & \gamma & \alpha & 0 \\ 0 & 0 & \beta & \gamma & \alpha \end{bmatrix} * \begin{bmatrix} S_{-1} \\ S_0 \\ S_1 \\ S_2 \\ S_3 \end{bmatrix}_{n-1} * d \qquad (2.7.3.1),$$

where $\gamma = 1-\alpha-\beta$ is the single hit probability, *n* is the flash number and *d* is an activity parameter that compensates for changes in the number of active PS II centers during the flash train [119].

Equation 2.7.3.1 implies the assumption of equal miss and double hit probabilities for all S state transitions. For some fits of Tables 3.3.2 and 5.3.1 S state dependent miss or double hit parameters were used under special constraints, which are outlined in the result section:

$$\begin{bmatrix} S_{-1} \\ S_0 \\ S_1 \\ S_2 \\ S_3 \end{bmatrix}_n = \begin{bmatrix} \alpha_{-10} & 0 & 0 & 0 & 0 \\ \gamma_{-10} & \alpha_{01} & 0 & \beta_{20} & \gamma_{30} \\ \beta_{-11} & \gamma_{01} & \alpha_{12} & 0 & \beta_{30} \\ 0 & \beta_{02} & \gamma_{12} & \alpha_{23} & 0 \\ 0 & 0 & \beta_{13} & \gamma_{23} & \alpha_{30} \end{bmatrix} * \begin{bmatrix} S_{-1} \\ S_0 \\ S_1 \\ S_2 \\ S_3 \end{bmatrix}_{n-1} * d \qquad (2.7.3.2),$$

where, for example, $\gamma_{12} = 1-\alpha_{12}-\beta_{13}$.

The oxygen yield of the *n*th flash, Y_n^f, was fit using equation 2.7.3.3:

$$Y_n^f = (1-\alpha)[S_3]_{n-1} + \beta[S_2]_{n-1} \qquad (2.7.3.3)$$

for the equal miss case and equation 2.7.3.4 if the S state dependent misses or double hits were considered:

$$Y_n^f = (1-\alpha_{30})[S_3]_{n-1} + \beta_{20}[S_2]_{n-1} \qquad (2.7.3.4)$$

The program is minimizing the expression

$$dx_n^2 = \sum_{n=1}^{F}\left(Y_n^{\exp} - Y_n^f \cdot \sum_{n=1}^{F} Y_n^{\exp} \Big/ \sum_{n=1}^{F} Y_n^f \right)^2 \qquad (2.7.3.5),$$

where Y_n^{exp} is the relative oxygen yield of the *n*th-flash and *F* is the number of analyzed flashes.

The normalization is given by

$$\sum_{i=-1}^{3}[S_i] = 1 \qquad (2.7.3.6)$$

The fit quality is calculated according to equation 2.7.3.7:

$$fq = \frac{dx_n^2}{(F-P)} \qquad (2.7.3.7),$$

where *P* is the number of free parameters used.

For the calculation of the S_{-i} states (i = -1…-5), the data were analyzed using the extended Kok model, which in addition to the S_0, S_1, S_2 and S_3 states also includes the S_{-5}, S_{-4}, S_{-3}, S_{-2} and S_{-1} states. PS II can be found in these redox states after reduction with exogenous electron donors or during photoactivation [119, 182], (see also Chapters 6 – 8).

Within the equal miss model the S state populations $[S_i]$, i = -5…3, after the *n*th-flash are given by:

$$\begin{bmatrix} [S_{-5}]_n \\ [S_{-4}]_n \\ [S_{-3}]_n \\ [S_{-2}]_n \\ [S_{-1}]_n \\ [S_0]_n \\ [S_1]_n \\ [S_2]_n \\ [S_3]_n \end{bmatrix} = \begin{bmatrix} \alpha & 0 & 0 & 0 & 0 & 0 & 0 & 0 & 0 \\ \gamma & \alpha & 0 & 0 & 0 & 0 & 0 & 0 & 0 \\ \beta & \gamma & \alpha & 0 & 0 & 0 & 0 & 0 & 0 \\ 0 & \beta & \gamma & \alpha & 0 & 0 & 0 & 0 & 0 \\ 0 & 0 & \beta & \gamma & \alpha & 0 & 0 & 0 & 0 \\ 0 & 0 & 0 & \beta & \gamma & \alpha & 0 & \beta & \gamma \\ 0 & 0 & 0 & 0 & \beta & \gamma & \alpha & 0 & \beta \\ 0 & 0 & 0 & 0 & 0 & \beta & \gamma & \alpha & 0 \\ 0 & 0 & 0 & 0 & 0 & 0 & \beta & \gamma & \alpha \end{bmatrix} \cdot \begin{bmatrix} [S_{-5}]_{n-1} \\ [S_{-4}]_{n-1} \\ [S_{-3}]_{n-1} \\ [S_{-2}]_{n-1} \\ [S_{-1}]_{n-1} \\ [S_0]_{n-1} \\ [S_1]_{n-1} \\ [S_2]_{n-1} \\ [S_3]_{n-1} \end{bmatrix} \cdot d \qquad (2.7.3.8)$$

2.8 Other technical applications

2.8.1 MALDI-TOF-Mass Spectrometry

The protein compositions of the samples was analysed with a mass spectrometer Voyager-DE PRO 6164.
The Sinapinic acid was used as a calibration matrix. Other conditions: Laser repetition rate - 5.3 Hz, Acceleration voltage – 25000V, Grid voltage – 94%, Vertical scale - 1000 mV and number of recorded data points was 68049.

2.8.2 EPR

CW EPR spectra were recorded at liquid helium temperatures on a Bruker ESP 300E instrument fitted with a liquid helium cryostat (Oxford ESR 9) and a standard Bruker TE102 cavity.

CHAPTER 3

Functional Differences of PS II from *Thermosynechococcus elongatus* and Spinach

3.1 Introduction

Since the crystal structure of PS II is available only for the thermophilic cyanobacteria *T. elongatus*, [25, 26] and *T. vulcanus* [27], which grow at about 55°C, it is important to investigate whether functional and structural differences exist between *T. elongatus* and the until now functionally better characterized plant PS II from spinach. Earlier studies have shown that the kinetics of S state transitions and their activation energies are surprisingly similar in these different organisms [197, 198]. Likewise, on the basis of EPR and EXAFS studies the structure of the Mn_4O_xCa clusters are very similar in the two systems [116, 199-201]. On the other hand also some differences have been reported: (i) a greater stability of the S_2 and S_3 states in whole cells of *T. elongatus* [202, 203], (ii) differences in the effects of various cations and anions [204], (iii) the absence of the g = 4.1 signal in cyanobacteria [205]. It is unknown if some of these functional differences relate to reported deviations in the protein composition of PS II complexes from the different organisms. Of special interest in this regard might be that the 12 kDa and the cytochrome c550 extrinsic regulatory subunits of PS II in cyanobacteria have been replaced by proteins with apparent molecular weights of 17 kDa and 23 kDa [206]. Furthermore, the intrinsic psbW protein is probably absent in cyanobacteria [31].

For the studies of the present Chapter FIOPs were measured in order to compare the temperature dependencies of the miss and double hit probabilities and of the S state lifetimes in *T. elongatus* and spinach. This study reveals clear differences on the acceptor side of PS II, which are most likely related to the elevated growth temperature of *T. elongatus*. Furthermore, slight differences in the redox potential of Y_D/Y_D^{ox} have been found.

3.2 Experiments and analysis

3.2.1 Sample preparation

For oxygen evolution measurements two kinds of samples were used: i) *$S_1Y_D^{red}$-samples* containing a high percentage of the reduced form of tyrosine D, Y_D^{red}, due to long term storage at –70°C [97, 105, 106, 113, 207] and ii) *$S_1Y_D^{ox}$-samples* with Y_D oxidized in about 90% of the centers. In case of spinach thylakoids $S_1Y_D^{ox}$ samples were obtained by excitation of $S_1Y_D^{red}$ thylakoids with one saturating flash directly on the Joliot type electrode and 5 min of dark adaptation before the FIOPs were recorded. Because of the very slow S_2-state decay in *T. elongatus* thylakoids (see results), these samples had to be flashed and dark-adapted in glass vials. To ensure oxidation of most Y_D^{red} in the *T. elongatus* thylakoids under these conditions, the *T. elongatus* samples were flashed twice in 50 µL aliquots ([Chl] = 0.15 mM) by a frequency doubled Nd:YAG Laser (532 nm, 800 mJ/Puls), with an intermediate dark-adaptation of 15 min at room temperature. Afterwards, the samples were kept in the dark at room temperature for one hour and then stored on ice until the FIOP measurements were performed.

For the final measurements the thylakoid beads were thawed in the dark on ice and diluted to [Chl] = 0.15 mM (*T. elongatus*) or 0.8 mM (spinach) with MCMH buffer (400mM Mannitol, 20 mM $CaCl_2$, 10 mM $MgCl_2$ and 50 mM HEPES/NaOH at pH 6.8/4°C).

3.2.2 Lifetime measurements

For S_2 and S_3 lifetime measurements the thylakoids were first sedimented and temperature equilibrated on the Joliot electrode for 3 min or 5 min as indicated above. Then the samples were excited with 1 or 2 preflashes, respectively, followed by a flash train of 2 Hz that was started after various dark-adaptation times ranging between 0.5 – 600 s. To observe the $S_0Y_D^{ox} \rightarrow S_1Y_D^{red}$ reaction the sedimented samples were illuminated on the Joliot electrode with three flashes and after dark-times varying between 1 s and 120 min FIOPs were measured (Scheme 3.2.1).

For all FIOP measurements the polarization of – 750 mV was switched on 40s before the flash train and the pH of the flow buffer was adjusted to pH 6.8 at the indicated temperatures. All measurements were repeated at least twice.

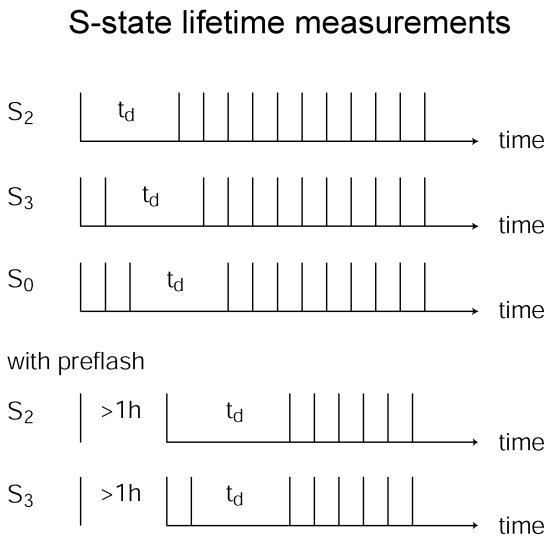

Scheme 3.2.1. The S states lifetime measurements protocol used in the present study.

3.2.3 Data analysis

The first 16 flashes of each FIOP were analyzed using an Excel spreadsheet that was based on an extended Kok model, which includes the reduced S_{-1}-state and an activity parameter *d* that compensates changes in the number of active PS II centers during the flash train [119] (Eq. 2.7.2.1 of Chapter 2.7.3).

Effects arising from fast reductions of S_2 and S_3 by Y_D between flashes (see e.g. Figure 3.3.1) have been taken into account by further extending the Kok model according to Scheme 3.2.2 (see also [105, 108]).

Such corrections are of special relevance for *T. elongatus* thylakoids at high temperatures. The required first order rate constants (k_2^f, k_3^f) and the percentage of reduced tyrosine in the samples were determined from lifetime measurements in an iterative process that is described below. Only minor corrections for the miss and double hit probabilities resulted from this process for preflashed ($S_1Y_D^{ox}$) samples. In Scheme 3.2.2 it is assumed that the miss and double hit probabilities are independent of the redox state of tyrosine D. The validity of this approximation is analyzed in the Results part of this Chapter (see Table 3.3.2).

In order to cope with effects arising from the fast S_2 and S_3 state reductions by Y_D^{red} the S state lifetime data were analyzed in three cycles. In the first step the data of the flash train were deconvoluted into S state populations ignoring back reactions of S_2 and S_3 with Y_D and using the miss and double hit probabilities determined from the preflashed samples at the respective temperatures. The semi-logarithmic plot of these values versus time was used as a first estimate of the rate constants for fast and slow decay. In the second step

these estimates were used to improve the fits by including Y_D back reactions between flashes, as described above. In the third step these improved rate constants were used to obtain the final rate constants given in the text and tables. Only very small changes were obtained by applying the third step of fitting.

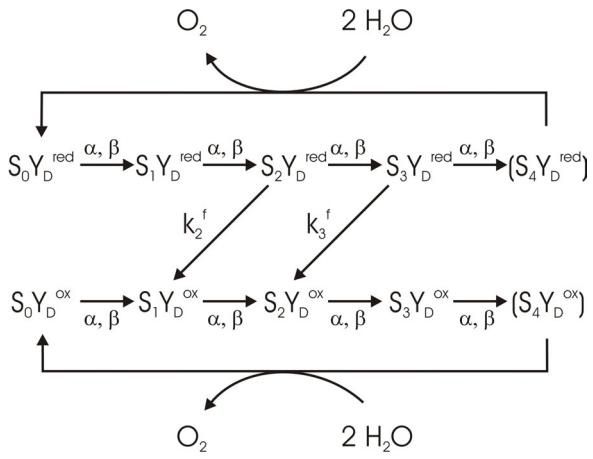

Scheme 3.2.2. Extended Kok model that takes into account S state redistributions resulting from the fast reductions of the S_2 and S_3 states by Y_D^{red} during a flash train (see text for details).

The rate constants for the fast (k_i^f) and slow (k_i^s) S_2 and S_3 decay were calculated based on equation 3.2.1:

$$S_i(t) = A_i \cdot e^{-k_i^f \cdot t} + B_i \cdot e^{-k_i^s \cdot t} \qquad (3.2.1)$$

where i = 2, 3 and t is the dark-time between the last preflash and the flash train. A_i and B_i are the relative amplitudes of fast and slow decay, respectively.

For the S_0 oxidation to S_1 a simple one exponential decay was assumed:

$$S_0(t) = S_0(t=0) \cdot e^{-k_0 \cdot t} \qquad (3.2.2)$$

Half-times were calculated according to:

$$t_{1/2} = (\ln 2)/k \qquad (3.2.3)$$

Activation energies were determined from the slope of Arrhenius-type plots (ln k vs. T^{-1}).

3.3 Results

3.3.1 $S_1Y_D^{red}$ and $S_1Y_D^{ox}$ thylakoids from T. elongatus

In this study two types of samples were used: i) long time dark-adapted thylakoids with a high percentage of reduced tyrosine D (*$S_1Y_D^{red}$-samples*) and ii) thylakoids, in which tyrosine D was largely oxidized due to a combination of a preflash treatment and subsequent dark-adaptation (*$S_1Y_D^{ox}$-samples*, for details see part 3.2.1). Figure 3.3.1 shows normalized flash-induced oxygen evolution patterns (FIOPs) measured at 20°C in *T. elongatus* thylakoids with high populations of states $S_1Y_D^{ox}$ (filled symbols) and $S_1Y_D^{red}$ (open symbols). In both cases the typical period four oscillations are observed with maxima in the 3rd and 7th flashes. However, the $S_1Y_D^{ox}$ sample gives rise to a clearly more pronounced oscillation, than the $S_1Y_D^{red}$ thylakoids.

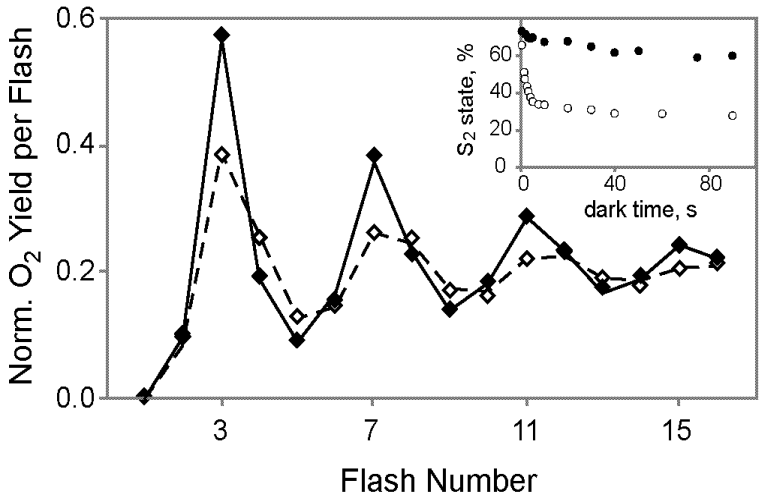

Figure 3.3.1. Normalized FIOPs of $S_1Y_D^{ox}$ (filled symbols) and $S_1Y_D^{red}$ (open symbols) thylakoids from *T. elongatus* at 20°C and pH 6.8. Lines are fits C and I of Table 3.2.2. Inset: $S_2 \rightarrow S_1$ decay of $S_1Y_D^{ox}$ (filled symbols) and $S_1Y_D^{red}$ (open symbols) thylakoids from *T. elongatus* under the same conditions.

A detailed analysis (Table 3.3.2 and last section of the results) within the framework of an extended Kok model, which takes into account partial reductions of redox states S_2 and S_3 by Y_D during the dark-time between the flashes (see Chapter 2.7.2 - 2.7.3 and Scheme 3.2.2), showed that the observed differences between these two sample types can be mostly accounted for by **i)** a somewhat increased S_0 population in $S_1Y_D^{red}$ thylakoids and **ii)** a larger extent of $Y_D^{red}S_2$ and $Y_D^{red}S_3$ recombination during the flash train in the $S_1Y_D^{red}$ compared to the $S_1Y_D^{ox}$ thylakoids. The percentage of reduced tyrosine D used in the fits

as fixed parameter was determined from the relative amplitude of fast S_2 state decay, which yielded values of 55% and 11% for $S_1Y_D^{red}$ and $S_1Y_D^{ox}$ samples, respectively (see inset Figure 3.3.1).

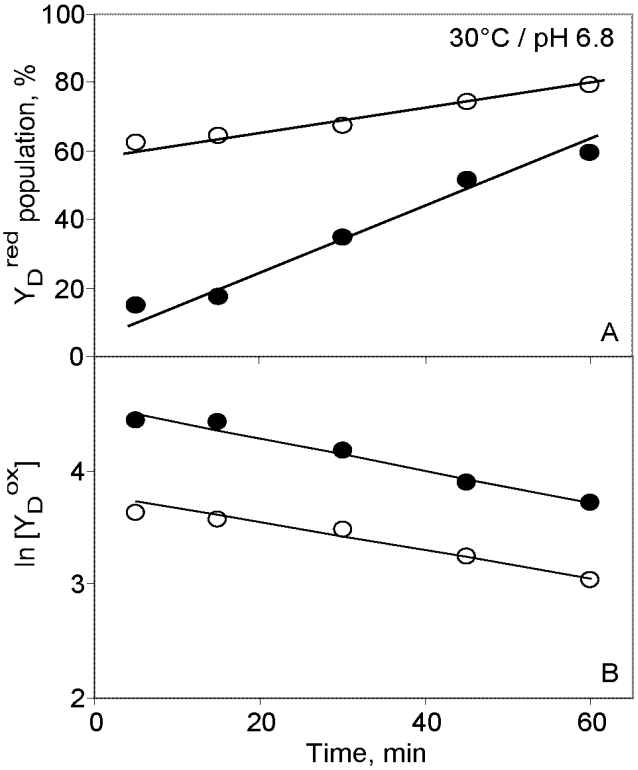

Figure 3.3.2. **A**: Percentage of the reduced form of tyrosine D (Y_D^{red}) and **B**: Semilogarithmic plots of the relative Y_D^{ox} populations as a function of the dark adaptation time on the electrode. The $S_1Y_D^{red}$ (open symbols) and $S_1Y_D^{ox}$ (filled symbols) thylakoids from *T. elongatus* were used, which were resuspended in MMCH buffer adjusted to pH 6.8 at 30°C.

Furthermore, the stability of the Y_D^{ox} population as a function of the dark time on the electrode was investigated at 30°C in $S_1Y_D^{red}$ and $S_1Y_D^{ox}$ thylakoids from *T. elongatus* (Figure 3.3.2 **A**). While the percentage of Y_D^{red} in $S_1Y_D^{red}$ thylakoids increases by ~ 20% during the one hour dark adaptation time, Y_D^{red} population in $S_1Y_D^{ox}$ thylakoids enhances from 15% at 5 min up to 60% after 60 min dark incubation on the electrode. The rate constants for the decay of Y_D^{ox}, which were determined from the semilogarithmic plots presented in Figure 3.3.2 **B**, are very similar in both cases with half-times of 56 s and 48 s for $S_1Y_D^{red}$ and $S_1Y_D^{ox}$ samples, respectively.

3.3.2 Temperature dependence of the miss and double hit probabilities in thylakoids from T. elongatus and spinach

For the following comparison of the temperature dependencies of the miss and double hit parameters of spinach and *T. elongatus* PS II the $S_1Y_D^{ox}$ thylakoids were used, since these

samples allow a determination of parameters α and β essentially without interference by the fast back reactions caused by Y_D^{red}. Figure 3.3.2 shows three original FIOP traces of *T. elongatus* thylakoids at 3°C (top), 20°C (middle) and 40°C (bottom). In $S_1Y_D^{ox}$ thylakoids the ratio of the 4th to 3rd flashes, Y_4/Y_3, (or 8th to 7th flashes and so on) is a suitable qualitative measure for the miss parameter, while the relative amplitude of the second flash is representative for the double hit probability.

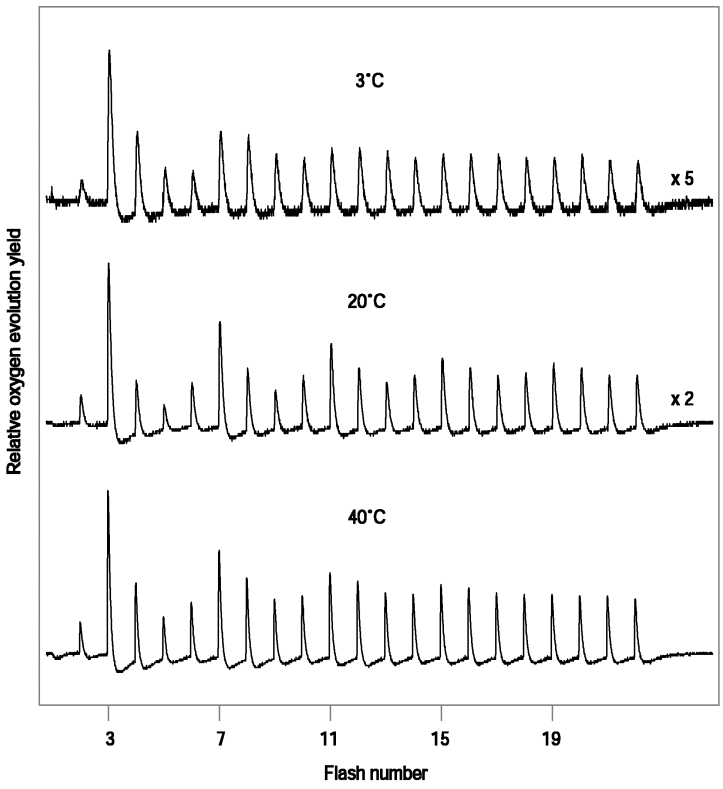

Figure 3.3.3. Original FIOPs of $S_1Y_D^{ox}$ thylakoids from *T. elongatus* measured at 3°C, 20°C or 40°C and pH 6.8.

The FIOPs of *T. elongatus* thylakoids monitored at different amplification factors show that the relative amplitude of the second flash (double hit probability) increases with increasing temperature. In contrast, the Y_4/Y_3 ratio (misses) attains its minimum at 20°C and increases at lower and higher temperatures. While the double hit probability of *T. elongatus* thylakoids follows the trend observed earlier for spinach samples [208, 209], the temperature dependence of the miss parameters appears to differ significantly from the known trend. With spinach thylakoids it was observed that the Y_4/Y_3 ratio increases continuously with increasing temperature [208].

In order to better characterize this difference, the FIOPs of spinach and *T. elongatus* thylakoids were measured at various temperatures between 3°C and 35°C and analyzed then with an extended Kok model (Eq. 2.7.2.1 of Chapter 2.7.2 - 2.7.3). The obtained

values for the miss parameter α and the double hit probability β are depicted in Figure 3.3.4 as a function of temperature. For spinach thylakoids these data agree with those of a previous report, although the absolute value at low temperature is about 2% higher [119]. In case of *T. elongatus* thylakoids this quantitative analysis confirms the very different temperature dependence of the miss probability in this organism and shows that the lowest values for the α parameter are obtained at 25°C under our conditions.

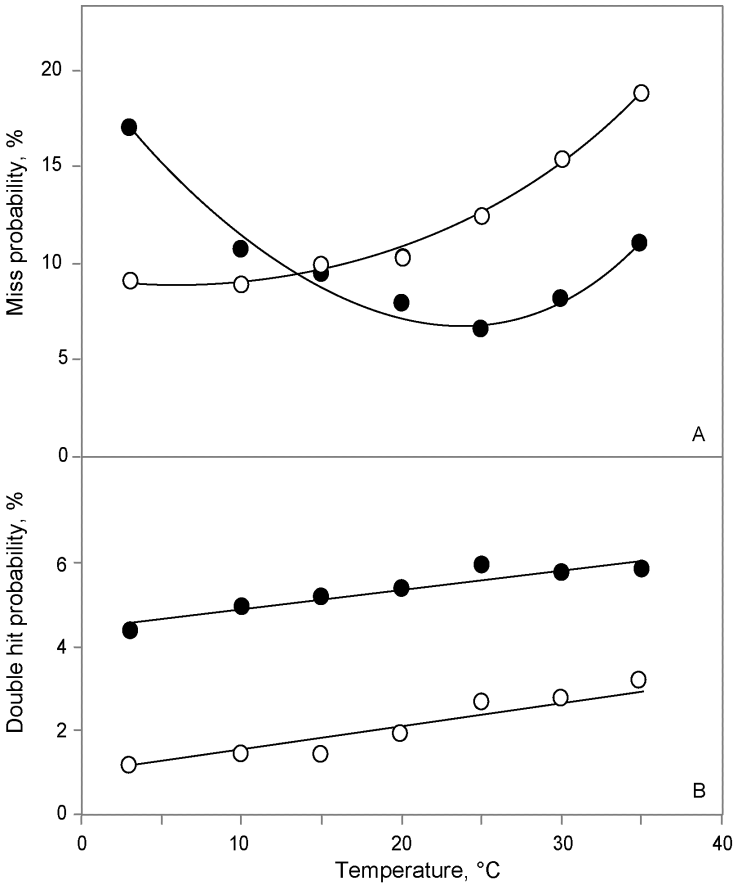

Figure 3.3.4. Temperature dependence of the miss (**A**) and double hit (**B**) probabilities of $S_1Y_D^{ox}$ thylakoids from *T. elongatus* (filled symbols) and spinach (open symbols). The pH was adjusted to 6.8 at the given temperatures. S state independent miss (α) and double hit (β) probabilities were calculated from FIOPs using the extended Kok model (described in Chapter 2.7.2 - 2.7.3) and in fit C of Table 3.3.2.

A comparison of the α values between the two species shows that at temperatures below 10°C a clearly lower probability for misses is found in spinach, while at temperatures between 20°C-35°C this parameter is lower in *T. elongatus*. Above 35°C the OEC of spinach starts to lose its functional/structural integrity and therefore a comparison is impossible. The double hits increase in both spinach and *T. elongatus* almost linearly with temperature, but the β values are generally higher in *T. elongatus* by an increment Δβ of about 3%.

The high miss parameter at low temperatures in *T. elongatus* could be either caused by temperature dependent shifts of redox equilibria between PS II cofactors or by a kinetic limitation. To address this problem, the dark-time between all flashes of the illuminating flash train were varied between 500 ms (2 Hz) and 3 seconds (0.33 Hz) at a measuring temperature of 3°C.

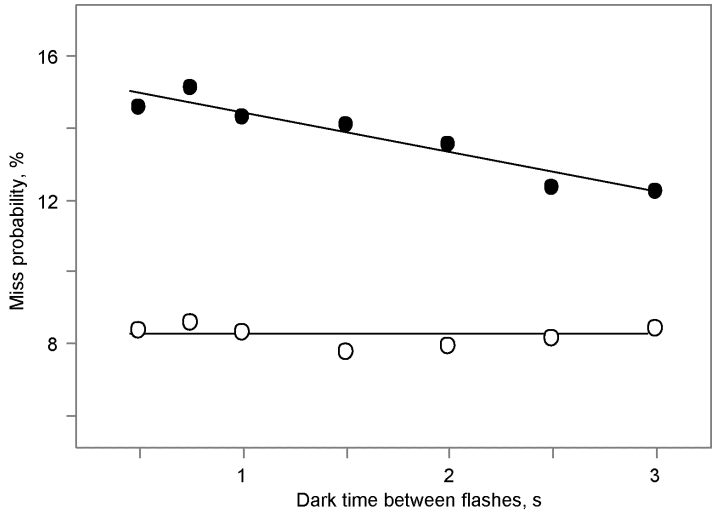

Figure 3.3.5. Dependence of the miss probability α on the dark time between all flashes of a train in $S_1Y_D^{ox}$ thylakoids from *T. elongatus* (filled symbols) and spinach (open symbols). The measurements were recorded at 3°C/pH6.8. The S state independent miss parameters were calculated from FIOPs using the extended Kok model (described in Chapter 2.7.2 - 2.7.3) and in fit C of Table 3.3.2.

As expected for these conditions (Figure 3.3.5), essentially no change is observed for miss parameter with spinach samples. In contrast, a clear decline of the miss parameter from 15% at t_d = 500 ms down to about 12% at t_d = 3 s is observed for *T. elongatus* thylakoids. These data support the idea that a rate-limiting step contributes in *T. elongatus* to the increase of the miss parameter at temperatures below 15°C.

3.3.3 S states lifetimes in thylakoids from T. elongatus

A further characteristic property of the OEC is the lifetime of the S states. While the S state lifetimes were thoroughly characterized with spinach thylakoids, only few information was available for the intact cyanobacterial PS II. Thus, in the present study lifetime measurements were performed with $S_1Y_D^{red}$ and $S_1Y_D^{ox}$ thylakoids from *T. elongatus* in a temperature range from 5°C to 38°C.

Figure 3.3.6 shows a comparison of the decays of the S_2 and S_3 states in Y_D^{red} thylakoids at 10°C (A and C) and 25°C (B and D). To determine the fast phases, which represent the reactions $S_2Y_D^{red} \rightarrow S_1Y_D^{ox}$ and $S_3Y_D^{red} \rightarrow S_2Y_D^{ox}$, the slow phases were subtracted from the row data and the resulting pure fast decays are shown in the Figure 3.3.7. The fast reductions of the S_2 and S_3

states are found to occur with very similar rate constants ($t_{1/2}$ = 0.8s) at 25°C (B and D). At 10°C the S_3 state decays slightly faster (C) with a half-time of 2.9s compared to 3.4s for the S_2 state (A).

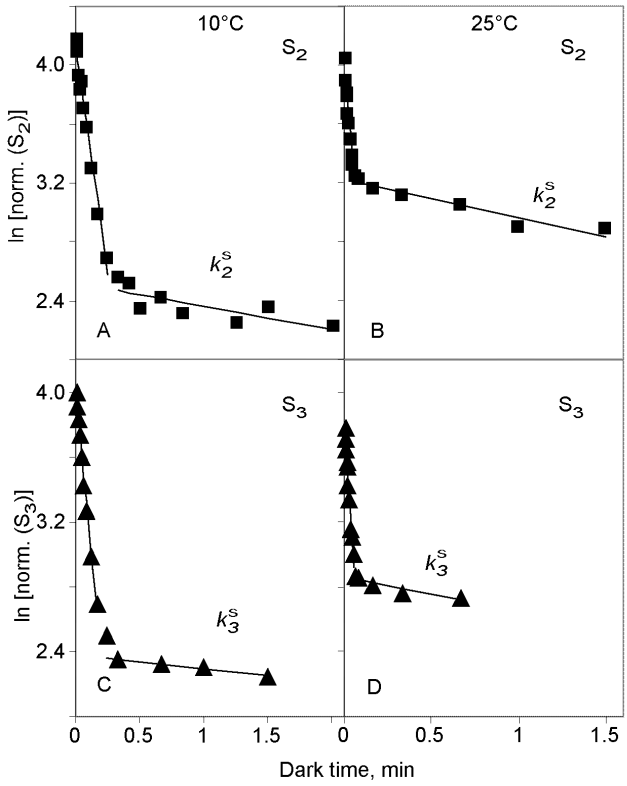

Figure 3.3.6. Semilogarithmic plot of the relative S_2 (A, B; squares) and S_3 (C, D; triangles) population in Y_D^{red} thylakoids from *T. elongatus* as a function of the dark time between first and second (S_2) or second and third (S_3) flashes in the train of saturating single turnover flashes. The thylakoids were resuspended in MMCH buffer adjusted to pH 6.8 at 10°C (A, C) or 25°C (B, D).

The $S_1Y_D^{ox}$ thylakoids were used to determine more precisely the slow decay of the S_2 and S_3 states via acceptor side (Figure 3.3.8). Indeed, while the slow relaxations of the S_2 and S_3 states was observed to decay in $S_1Y_D^{red}$ thylakoids only up to 1.5 min (Figure 3.3.6), in $S_1Y_D^{ox}$ thylakoids these relaxations could be monitored up to 10 min. Slow reductions of the S_2 and S_3 states at 10°C were determined to have half-times of about 1500 s and 3000 s, respectively (Figure 3.3.7 A and C). At 30°C these numbers are 300 s and 221 s for the S_2 and S_3 states, respectively.

The activation energies and the pre-exponential factors for the S_2 and S_3 fast and slow decays and S_0 decay to S_1 state were calculated from the Arrhenius plots presented in Figure 3.3.9. These parameters and the values of the rate constants for the above described reactions are listed in the Appendix (Tables 1-3).

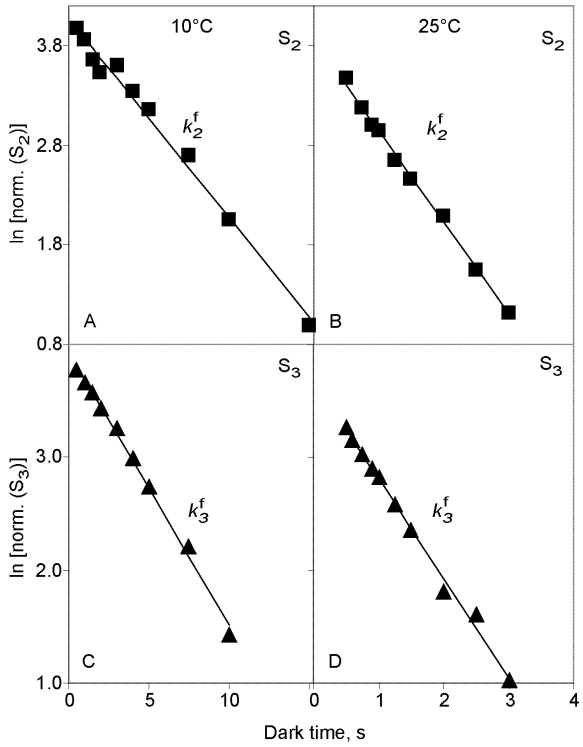

Figure 3.3.7. Semilogarithmic plot of the relative S_2 (A, B; squares) and S_3 (C, D; triangles) population in $S_1Y_D^{red}$ thylakoids from *T. elongatus* as a function of the dark time between first and second (S_2) or second and third (S_3) flashes in a train of saturating single turnover flashes. Only the fast decay is shown, which was obtained by subtraction of the slow decay (compare with Figure 3.3.6). The thylakoids were resuspended in MMCH buffer adjusted to pH 6.8 at 10°C (A, C) or 25°C (B, D).

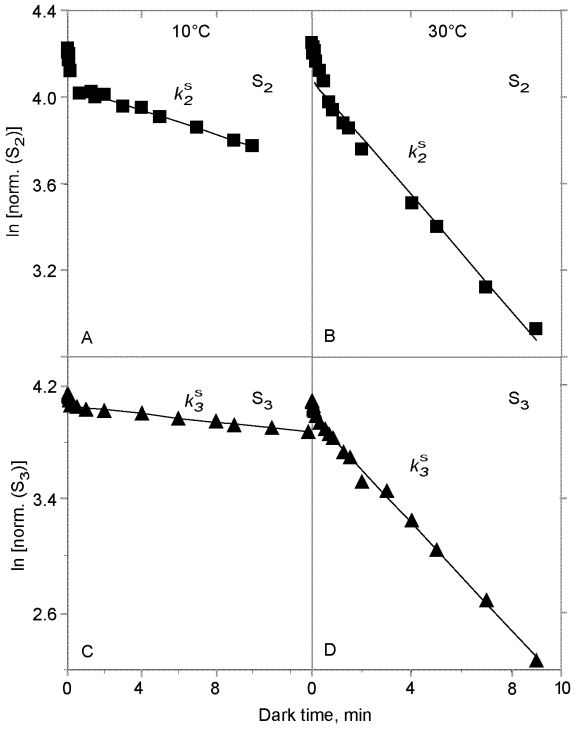

Figure 3.3.8. Semilogarithmic plot of the relative S_2 (A, B; squares) and S_3 (C, D; triangles) population in $S_1Y_D^{ox}$ thylakoids from *T. elongatus* as a function of the dark time between first and second (S_2) or second and third (S_3) flashes in a train of saturating single turnover flashes. The thylakoids were resuspended in MMCH buffer adjusted to pH 6.8 at 10°C (A, C) or 30°C (B, D).

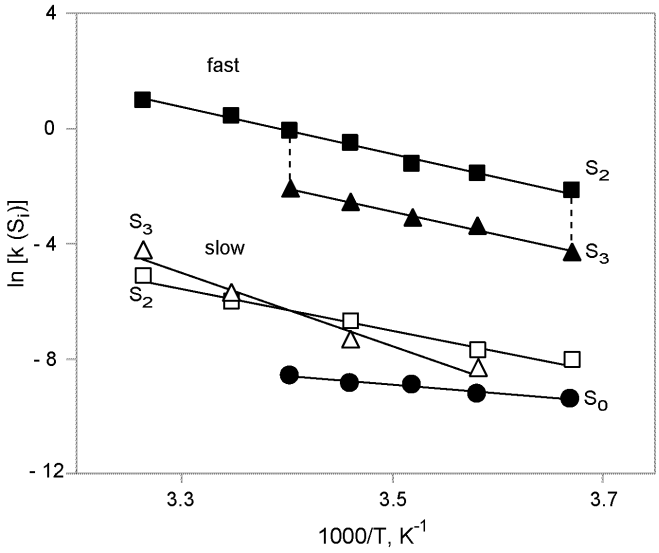

Figure 3.3.9. Arrhenius-type plot of the rate constants of the S_2 (squares), S_3 (triangles) and S_0 (circles) decay in *T. elongatus* thylakoids. Filled symbols, fast S_2 and S_3 decay through reduction by Y_D; open squares and triangles, slow S_2 and S_3 decay by other electron donors (e.g. Q_B^-); circles, S_0 oxidation to S_1 by Y_D^{ox}. For the sake of clarity the data for the fast S_3 decay are displaced by a constant down shift indicated by broken lines. The obtained activation energies are presented in Table 3.3.1.

The S – states decay in $S_1Y_D^{ox}$ thylakoids from *T. elongatus* were additionally simulated for the consecutive reaction $S_3 \rightarrow S_2 \rightarrow S_1$. In this reaction, the equations for the formation and decay of the S_3, S_2 and S_1 states were used to fit the data. The initial concentration of S_3 state was indicated as $[S_3]_0$, etc. In this approach the S_3 state simply decays according to Eq. 3.3.1, while the intermediate S_2 state increases due to the decay of the S_3 state, but it also decreases by decaying into the "product", S_1 state (Eq. 3.3.2). The S_1 state is assumed to be formed by the first order decay of the S_2 state (Eq. 3.3.3). The $[S_3]_0$, $[S_2]_0$ and $[S_1]_0$ parameters, the rate constants ($k_{3,2}$ and $k_{2,1}$) were freely varied using "Solver" routine to minimize the fit error ($dx^2 \rightarrow 0$), which was defined as the square of the difference of measured and calculated S – states populations.

$$[S_3]_t = [S_3]_0 e^{-k_{3,2}t} \tag{3.3.1}$$

$$[S_2]_t = \frac{k_{3,2}[S_3]_0\left(e^{-k_{3,2}t} - e^{-k_{2,1}t}\right)}{\left(k_{2,1} - k_{3,2}\right)} + [S_2]_0 e^{-k_{2,1}t} \tag{3.3.2}$$

$$[S_1]_t = \left([S_3]_0 + [S_2]_0 + [S_1]_0\right) - [S_3]_t - [S_2]_t \tag{3.3.3}$$

The fits (lines) obtained for the S - state (symbols) decays are presented in the Figure 3.3.10. The rate constants obtained at different temperatures are presented in a Arrhenius type plots and are compared to those obtained before (Figure 3.3.9).

This comparison shows very similar rates for the S_3 state decay at all temperatures, while in case of the S_2 decay small differences are present, which may be explainable if one takes into account that in the $S_3 \rightarrow S_2 \rightarrow S_1$ reaction, the S_2 state is an intermediate. The activation energies for the S_3 decay depicted from the Arrhenius plots are very similar to those obtained before (105 kJmol^{-1} in both cases) and show small deviation for the S_2 slow decay (75 kJmol^{-1} compared to 60 kJmol^{-1}, see Figure 3.3.11 and Table 3.3.1).

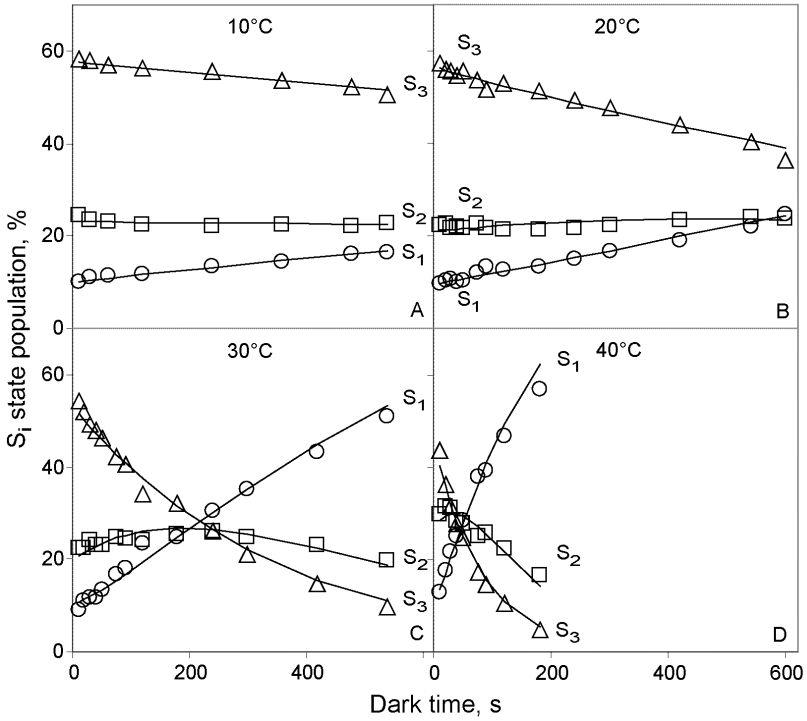

Figure 3.3.10. S – states population as a function of the dark time between second and third flashes in the train of saturating single turnover flashes. For that the $S_1Y_D^{ox}$ thylakoids from *T. elongatus* were resuspended in MMCH buffer adjusted to pH 6.8 at 10°C (A), 20°C, 30°C (C) and 40°C (D). The lines represent fits for the S_3 (triangles), S_2 (squares) and S_1 (circles) states in the consecutive reaction $S_3 \rightarrow S_2 \rightarrow S_1$ (described in text).

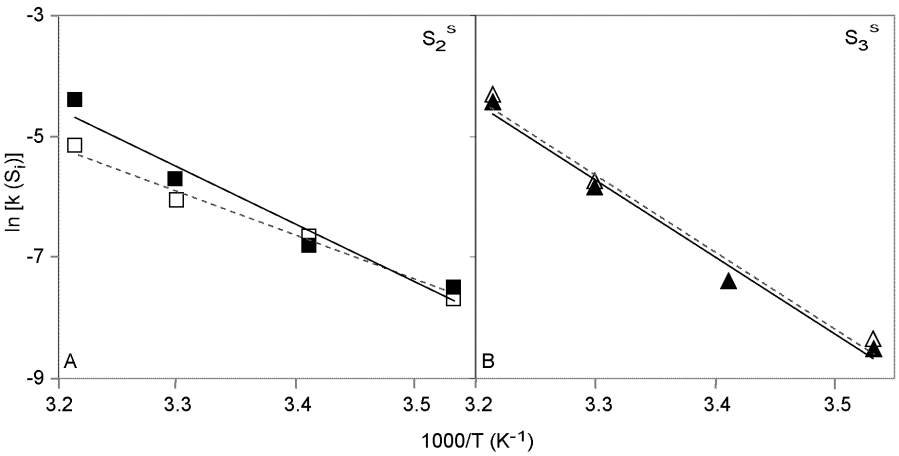

Figure 3.3.11. Arrhenius type plot for the S_2 (A) and S_3 (B) slow relaxation as a function of reciprocal temperature in $S_1Y_D^{ox}$ thylakoids from *T. elongatus*. The filled symbols represent the rate constants obtained through simulations in consecutive reaction $S_3 \rightarrow S_2 \rightarrow S_1$. For comparison the Arrhenius plots for the S_2 and S_3 slow decays are given (open symbols), which also presented in the Figure 3.3.9.

3.3.4 Comparison of the S states lifetime in thylakoids from spinach and T. elongatus

Figure 3.3.12 shows a semi- logarithmic plot of the S_2 and S_3 decay at 20°C in $S_1Y_D^{ox}$ thylakoids from spinach (open symbols) and *T. elongatus* (filled symbols). Since in these samples most tyrosine D was oxidized by a preflash treatment, the S_2 and S_3 decay is dominated by the slow reduction with electron donors. On the basis of thermoluminescence experiments the dominant donor for this slow reaction should be Q_B^- [103, 203], but Q_BH_2 or even other electron donors may contribute as well. Only a small percentage of fast recombination with Y_D is discernable, which confirms the effectiveness of the preflash treatment. The data of Figure 3.3.12 reveal that the slow relaxations of S_2 and S_3 are 15 times and 30 times slower, respectively, in *T. elongatus* than in spinach. This is in qualitative agreement with earlier data gathered from measurements of thermoluminescence and FIOPs in whole cells of *T. vulcanus* [202], where retardations by factors of four and seven were observed.

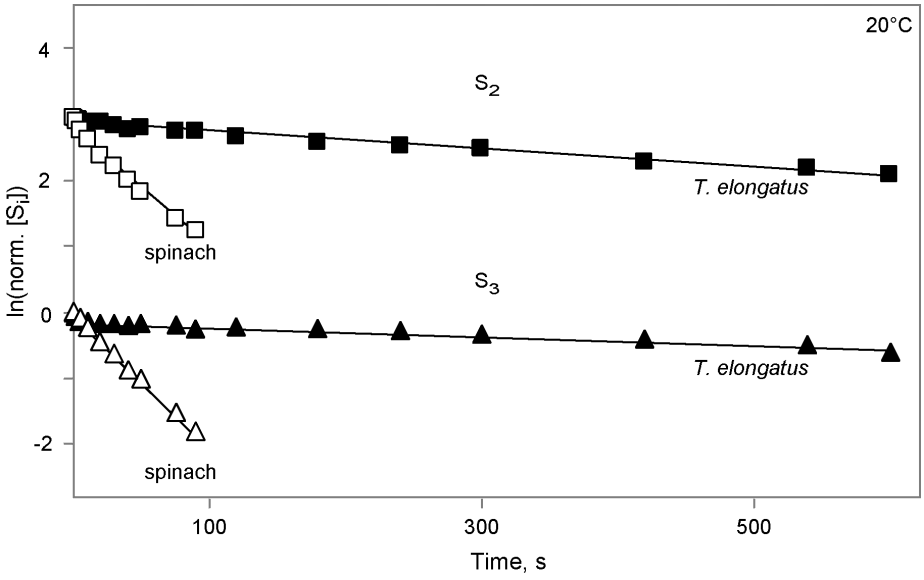

Figure 3.3.12. Semilogarithmic plot of the S_2 (squares) and S_3 (triangles) state decay in Y_D^{ox} thylakoids from *T. elongatus* (filled symbols) and spinach (open symbols). The lifetime measurements were performed at 20°C and pH 6.8. For details of data deconvolution see part 3.2. of this Chapter.

It seems unlikely that the differences in the slow relaxation rates between *T. elongatus* and spinach thylakoids are due to changes of distance between Q_B and the Mn_4-cluster (or between other intermediate cofactors) in the two species. Therefore, the results of Figure 3.3.12 raise questions about redox-potential shifts either on the donor and/or the acceptor side of PS II (see also [203]).

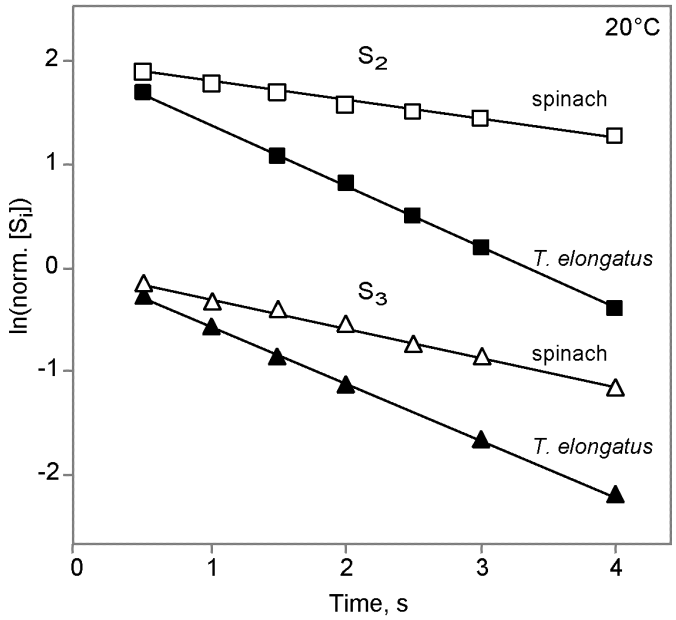

Figure 3.3.13. Semilogarithmic plot of the fast phase of S_2 (squares) and S_3 (triangles) state decay in Y_D thylakoids from *T. elongatus* (filled symbols) and spinach (open symbols). The lifetime measurements were performed at 20°C and pH 6.8. For details of data deconvolution see part 3.2. of this Chapter. The pure fast phase was isolated through subtraction of the slow component from the original data.

In the case of donor side effects the rates of the fast S_2 and S_3 reductions by Y_D are expected to change in a similar way as the slow relaxation rates. This was tested using S_1Y_D thylakoids and the results are displayed in Figure 3.3.13. It is obvious that for these reactions the differences are much less pronounced than for the slow phase of S_2 and S_3 decay. Remarkably, in this case the S_2 and S_3 states are more stable by a factor of 2 to 3 in spinach than in *T. elongatus* thylakoids. Based on these findings it seems unlikely that donor side effects are the dominating factor for the large differences shown in Figure 3.3.12. In line with the S_2 and S_3 reduction by Y_D also the oxidation of S_0 to S_1 by Y_D^{ox} proceeds at 20°C with a rate that differs only slightly from that of the spinach samples. However, in contrast to the fast S_2 and S_3 reductions by Y_D, the S_0 oxidation by Y_D^{ox} is four times *slower* in *T. elongatus* than in spinach as illustrated in Figure 3.3.14.

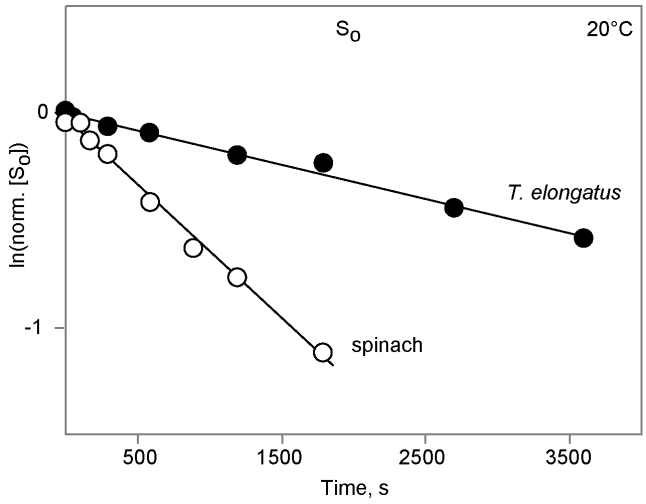

Figure 3.3.14. Semilogarithmic plot of the S_0 state population as a function of dark-adaptation time at 20°C and pH 6.8. The measurements were performed with Y_D^{ox} thylakoids from *T. elongatus* (filled symbols) and spinach (open symbols). For details of data deconvolution see Chapter 3.2.

	T. elongatus	Spinach		
	thylakoids pH 6.8 E_a, kJmol^{-1}	BBY pH 6.5 E_a, kJmol^{-1}	thylakoids pH 7.0 E_a, kJmol^{-1}	thylakoids pH 7.5 E_a, kJmol^{-1}
S_2 fast	68±3	60±10	55	44
S_3 fast	69±3	55±10	50	47
S_2 slow	60±3	80±5	85	63
S_3 slow	106±6	75±5	75	73
S_0	28±3	-	30	-
Reference	This study	[209]	[208]	[105]

Table 3.3.1. Comparison of activation energies for S state decay in *T. elongatus* and spinach.

The comparative lifetime measurements presented in Figures 3.3.12 – 3.3.14 reflect the properties of the S states at 20°C. Since the relaxations of S_2 and S_3 were shown to be reactions with comparatively high activation energies in spinach samples [105, 208, 209] some of the observed differences might originate from the species dependent characteristics of thermal activation. Therefore, the activation energies calculated for *T. elongatus* (see part 3.3.3) are compiled in Table 3.3.1 and are compared with those previously reported data for spinach samples. An inspection of these values reveals that for a given S - state all activation energies of *T. elongatus* deviate from those previously reported for spinach by not more than a factor of 1.5 [105, 208, 209]. Interestingly, the differences between the slow S_2 and S_3 decay is larger in *T. elongatus* (factor 1.8) than in spinach (0.9 to 1.2).

3.3.5 Numeric analysis of FIOPs of T. elongatus thylakoids

On the basis of the obtained rate constants for the fast S_2 and S_3 decay detailed analyses of the FIOPs of S_1Y_D and $S_1Y_D^{ox}$ thylakoids were performed in order to address two relevant problems: a) the validity of the approximation of S state independent probabilities of misses and double hits and b) possible effects of the redox state of Y_D on the energetics of $P680^{+\bullet}$.

The values in rows A-F in Table 3.3.2 are the results of a systematic fit approach for the $S_1Y_D^{ox}$ sample. In fit A we start with the assumption of 100% S_1 state population and only the two S state independent parameters α and β were free running. The damping parameter *d*, which accounts for possible changes of the number of active PS II centers during the

flash train, was found to be $0.99 \leq d \leq 1.0$ for all analyzed patterns of this study and is therefore not shown in Table 3.3.2. Fit A also accounts for the fast relaxation reactions of S_2 and S_3 by using the above determined values of Y_D population and the rate constants of the fast S_2 and S_3 decay measured at 20°C (Y_D= 11%, $k_3^f = 0.54\ s^{-1}$, $k_2^f = 0.60\ s^{-1}$).

With this procedure, a good overall description of the data could be achieved. However, a closer inspection revealed some small systematic deviations after the 5th and following flashes. As expected from this feature, the inclusion of S_2 and S_0 as free parameters (fit B) gives rise to a fit of only a slightly (10%) higher quality. However, if also the redox state S_{-1} is included as a free running parameter a drastic improvement by a factor of 3 (fit C) is obtained and the data are almost perfectly simulated as illustrated in Figure 3.3.1, where fit C is shown as a solid line. Fit D shows that setting Y_D to zero has only a minor effect on the deconvolution of the FIOP of this preflashed sample (the α and S_0 parameters are only slightly larger).

Sample	Fit	Fit Parameters, %									Goodness of Fit	
		α	α_{23}	α_{30}	β	S_2	S_1	S_0	S_{-1}	Y_D	dx^2 ($\times 10^{-6}$)	Fq ($\times 10^{-6}$)
	A	9.5			6.4		100*			11*	115	8.9
	B	8.5			6.2	1.2	92.6	6.2		11*	80	8.0
	C	8.1			5.4	2.1	87.9	3.8	6.2	11*	25	2.8
$S_1Y_D^{ox}$	D	8.6			5.4	2.5	85.3	6.2	6.3		24	2.7
	E		15.8	15.8	5.9		100*			11*	55	4.3
	F		30.0		5.2		100*			11*	21	1.6
	G	13.2			7.7		100*			55*	217	16.7
	H	8.4			5.8	5.6	72.5	15.5	6.4	55*	5	0.6
	I	9.0			7.6		79.0	17.1	3.9	55*	51	5.1
S_1Y_D	J	12.5			7.4		68.4	27.8	3.8		110	11.0
	K		17.5	17.5	7.2		87.9	12.1		55*	45	4.1
	L		30.3		6.4		84.0	16.0		55*	52	4.7

Table 3.3.2. Fits of the flash induced oxygen evolution patterns (FIOPs) of long-term dark-adapted S_1Y_D thylakoids and of preflashed $S_1Y_D^{ox}$ thylakoids from *T. elongatus*. The FIOPs of S_1Y_D and $S_1Y_D^{ox}$ obtained at 20°C and pH 6.8 (open and filled symbols in Figure 1, respectively) were fit using different approaches, which are outlined in the text. For fits A-D and G-J a Kok model with S state independent miss and double hit parameters was used. In fits E and K the miss parameters of the $S_2 \rightarrow S_3$ and $S_3 \rightarrow S_0$ transitions (α_{23} and α_{30}, respectively) were forced to be equal, while those for the $S_0 \rightarrow S_1$ and $S_1 \rightarrow S_2$ transitions (α_{01} and α_{12}, respectively) were fixed to 0. In Fits F and L only α_{23} was varied freely, while those of the other S state transitions were fixed to 0. If no values are given for a parameter it was excluded from the fit. Stars indicate that the parameter was fixed to the specified value. The values of 11% and 55% Y_D population for the $S_1Y_D^{ox}$ and S_1Y_D samples, respectively, and the rate constants for the fast S_3 and S_2 decay ($k_3^f = 0.54\ s^{-1}$, $k_2^f = 0.60\ s^{-1}$) were obtained from S_2 and S_3 state lifetime measurements (see Figures 3.3.1 and 3.3.13). The goodness of fit parameters was calculated as outlined in Chapter 3.2.

The above fit result that suggests the existence of S_{-1} in the preflashed $S_1Y_D^{ox}$ is not easily understandable and requires additional assumptions (e. g. small S_{-2} population or fast reduction in a small fraction of PS II) that are difficult to rationalize. However, we consistently find also for spinach samples an improvement of fit quality for dark adapted samples if a small percentage of S_{-1} is included in the fits of FIOPs [208]. In this respect it is very important to note that a quite similar apparent S_{-1} population (and no S_{-2} population) is required for the best fit of the FIOP of the non-preflashed sample (fit H).

Therefore it seems more likely that the apparent S_{-1} population is a parameter that simply compensates for imperfections of the Kok model used to describe the data. One important approximation of the applied Kok scheme is the assumption of equal misses for each S state transition (see Chapter 1.5.1). To check whether this approximation can possibly account for the described differences between 'normal' fits and the data, fits were performed assuming various unequal miss models. With S state dependent misses no unique solution can be found [210] and only two special cases shall be discussed below (fits E and F).

On the basis of recent studies on a correlation between the extent of μs components in the $P680^{+\bullet}$ reduction kinetics and the α -values [211, 212] and taking into account the period four oscillation of these reactions [213, 214] the miss probabilities for oxidation of S_0 and S_1 are assumed to be small compared with those of the oxidation of S_2 and S_3. Therefore we assumed for the sake of simplicity in fit E that the miss parameters for the $S_0 \rightarrow S_1$ and $S_1 \rightarrow S_2$ transitions (α_{01} and α_{12}, respectively) are zero and those of the $S_2 \rightarrow S_3$ and $S_3 \rightarrow S_0$ transitions (α_{23} and α_{30}) are identical. The fit quality of this unequal miss fit is twice as good as that of fit A, which assumes equal misses for all S state transitions. Even better fits are obtained when only one miss parameter is varied and the three others are set to zero. This is shown for α_{23} in Table 3.3.2 (fit F), but very similar results are obtained for α_{12} and α_{30}. In contrast, no reasonable fits are possible if only α_{01} is varied (data not shown). It is remarkable that the fit quality of fit F is of similar quality (or even better) as that of fit C without the need to include any S_2, S_0 or S_{-1} population as fit parameters. In this context it should be noted that similar unequal miss fits of S_2 EPR multiline oscillation patterns such as that published in [174] show, that more than half of the misses have to occur in the $S_1 \rightarrow S_2$ and / or the $S_2 \rightarrow S_3$ transitions (fits not shown), which is at slight variance to the conclusions in [212], where the S_3 oxidation was inferred to account for more than 50 % of the misses.

The rate constants of the $S_2 \rightarrow S_3$ and $S_3 \rightarrow S_0$ transitions are similar or even smaller than that of the electron transfer from Q_A^- to Q_B. It is therefore reasonable to assume that in

these transitions no double hits occur [94]. In addition, a period two oscillation for the double hits might be expected, which reflects the redox state of Q_B [215]. Therefore, also the effect of S state dependent double hit parameters on the fits of FIOPs was tested using various models. However, in no tested case this kind of extension was able to account for the 5^{th} flash deviation discussed above (fits not shown). These results show that the assumption of unequal misses is one possible way for a better description of the obtained FIOPs. However, the present data do neither provide an unambiguous proof for unequal misses, nor permit an identification of the S state transition with the highest miss factor.

In the following we analyze whether the redox state of Y_D affects the miss parameter. The rationale for this analysis provides recent reports that the redox potential of P680 may be modulated by the redox state of Y_D [126, 127, 216]. A change of $E_m(P680/P680^+)$ should affect its reduction kinetics and may thereby also change the value of α [212, 214]. In addition, the redox state of Y_D could change the miss parameter via more indirect effects, for example through changes in the H-bonding network. Therefore, FIOPs measured in *T. elongatus* thylakoids either preflashed ($S_1Y_D^{ox}$) or extensively dark-adapted (S_1Y_D) were analyzed in order to show whether the probability of misses depends on the redox state of Y_D. Since the rate constants for the reactions of Y_D with S_2 and S_3 and the percentage of reduced tyrosine D were determined by independent measurements, we can use the extended Kok model described in the Chapter 2.7.2 - 2.7.3 to separate the known fast back reactions of Y_D with S_2 and S_3 from possible effects on the 'real' miss parameter. For the sake of simplicity, the parameters α and β were initially assumed to be independent of the S state (fits G-J). Fit approach H in Table 3.3.2 shows that an excellent fit quality is obtained for S_1Y_D thylakoids by using the Y_D level of 55% gathered from the S_2 lifetime experiments. In this fit miss and double hit probabilities are only slightly higher than for the preflashed sample (fit C). An increase of the percentage of Y_D to about 60% leads to an identical miss parameter as in fit C (data not shown). At a first glance these kinds of fits seem to indicate that Y_D has a vanishingly small (if any) effect on the miss factor. However, a closer inspection of the resulting S state populations reveals that about 6% of S_2-state population is required to obtain the excellent fit quality of fit H. This result is puzzling, because this value is two to three times higher than that obtained from fits of the preflashed sample (see B to D). Furthermore, it should be expected that the S_2 population in the extremely long term dark-adapted S_1Y_D samples is zero and in any case cannot exceed the level of the preflashed sample. Therefore, in fit I we have fixed the S_2 population to zero. Under this constrain miss and double hit probabilities are calculated for the S_1Y_D sample, which are significantly higher than for the $S_1Y_D^{ox}$ sample (fit C). Taking

into account that the S_1Y_D sample contains only about 55% Y_D, the result of fit G suggest that for a sample where all PS II complexes have tyrosine D in its reduced form, the miss parameter might be higher by an increment of about 2% compared to a sample where all tyrosine D is oxidized. To test whether this result is specific for the extended Kok model used in fits C and I, the S_1Y_D data were also analyzed using the 100% S_1 state approach of fit A (see fit G) and by excluding the fast back reactions of Y_D (compare fit J with fit D). Also in these two cases a significantly higher miss parameter was found for the S_1Y_D sample compared with that for the $S_1Y_D^{ox}$ sample. Similarly, using the $\alpha_{23} \neq \alpha_{30}$ unequal miss approach in fit K results in a clearly higher miss for the S_1Y_D sample (compared to fit E). One exception appears to be fit L, where only α_{23} was varied. In this case the miss parameter is almost identical to that of fit F. However, for this fit only a shallow minimum exists, where the values of the miss parameter and the S_0 population are highly dependent on each other. Constraining the S_0 population for example to 12% as seen in fit K, results in α_{23} of about 32% without a significant effect on the fit quality (data not shown).

3.4 Discussion

The present study compares in detail the period four oscillations of FIOPs of dark-adapted thylakoids from thermophilic cyanobacteria (*T. elongatus*) and higher plants (spinach). The aim was to address the following three problems concerning the mechanism of water oxidation in PS II: **a**) Do evolutionary changes exist at the level of the water oxidation between thermophilic cyanobacteria and higher plants? **b**) Is the miss parameter α - dependent on the S state? **c**) Does the redox state of Y_D affect the miss parameter through mechanisms other than the fast back reactions with S_2 and S_3?

3.4.1 Differences between PS II from spinach and T. elongatus

In this paper several functional differences between PS II from spinach and *T. elongatus* have been described: **i**) double hits are generally higher in *T. elongatus* than in spinach thylakoids, **ii**) at 20°C the slow reduction of S_2 and S_3 by electron donors other than Q_A^- and Y_D is more than one order of magnitude slower in *T. elongatus*, **iii**) in contrast, the reduction of S_2 and S_3 by Y_D is 2-3 times faster in *T. elongatus*, whereas the rate of S_0 oxidation by Y_D^{ox} is 4 times slower and **iv**) the temperature dependence of the miss parameter is strikingly different in *T. elongatus* compared to that known for spinach, with a surprisingly high value at temperatures close to 0°C.

The generally higher double hit parameter is a clear indication for a faster electron transfer from Q_A^- to Q_B (Q_B^-) in *T. elongatus*, since at least for the S_0 and S_1 states the rate of Q_A^- reoxidation by Q_B (Q_B^-) is the rate limiting step for a second "stable" turnover of PS II, which can be caused by the residual light intensity ('tail') of µs xenon flashes [94, 114]. In a former study the double hit probability was inferred to be almost linearly related to the rate constant of the Q_A^- reoxidation (see Appendix of Ref. [208]). Based on this approximation the data of this study suggest that the reoxidation of Q_A^- is 2-4 times faster in *T. elongatus* than in spinach thylakoids. This reaction depends also on the conformational flexibility of the protein matrix [217, 218]. Accordingly, the difference in the kinetics between both sample types could be explained (i) by changes in redox potentials of Q_A or Q_B, (ii) a slightly shorter distance between Q_A^- and Q_B (Q_B^-) or (iii) by

faster protein dynamics in *T. elongatus*. This phenomenon has to be clarified in further detailed investigations that are beyond the scope of the present study.

An independent line of evidence in support of the idea that the acceptor sides of *T. elongatus* and spinach are different is the significant retardation of the slow S_2 and S_3 decay in *T. elongatus* in marked contrast to the much smaller change in the opposite direction of the fast reduction by Y_D. The most straightforward interpretation is that in *T. elongatus* the reduced forms of Q_B are better stabilized than in spinach. This interpretation is in line with thermoluminescence measurements on intact *T. elongatus* cells, in which a stabilization of states $S_2Q_B^-$ and $S_3Q_B^-$ was found [202]. However, a similar increase in lifetime and temperature was also seen for the thermoluminescence bands of the states $S_2Q_A^-$ and $S_3Q_A^-$. Therefore, on the basis of these thermoluminescence experiments it was not possible to separate donor and acceptor side effects. At temperatures close to 0°C the proposed stabilization of reduced plastoquinone in its pocket at the acceptor side might imply a slow exchange of plastoquinol by plastoquinone from the pool in the thylakoid membrane. The different lipid composition of the thylakoid membranes of the thermophilic *T. elongatus* and mesophilic spinach may contribute to this effect. A slow quinol/quinone exchange, would explain the high miss parameter at low temperatures in *T. elongatus* and its frequency dependency.

When considering a possible physiological role for drastic retardation of the rates of the slow S_2 and S_3 decay of *T. elongatus* at 20°C, it is interesting to extrapolate the data to the growth temperature of these cyanobacteria by using the activation energies gathered from the Arrhenius plot (Figure 3.3.9). It turns out that at 55°C the rates for the slow S_2 and S_3 decay are only slightly faster in *T. elongatus* than those measured for spinach at 20°C. It therefore appears that the acceptor side of *T. elongatus* PS II has been modified in a way that prevents too fast S_2 and S_3 recombinations with electrons from the acceptor side at its growth temperature. Such fast recombinations would significantly reduce the efficiency of oxygen evolution, especially under low light conditions (see also [203]).

Differences between *T. elongatus* and spinach thylakoids on the donor side of PS II are less significant as reflected by comparatively small factors of 2-3 for the fast rates of S_2 and S_3 reduction by Y_D and of about 4 for the oxidation of S_0 by Y_D^{ox}. The opposite trend of both reactions could be explained by a minor change in the redox potential of the Y_D/Y_D^{ox} couple. Changes of the redox potential of the S states of the Mn_4 cluster itself are less likely, because of the similarities in the EPR and EXAFS properties (outlined in Chapter 1.5.4). Likewise former studies clearly showed that the activation energies of the stepwise oxidation of the WOC are very similar in the thermophilic cyanobacterium *Synechococcus*

vulcanus [197] and PS II membrane fragments from spinach [198]. Therefore this study demonstrates for the first time that the stabilization of the $S_2Q_B^-$ and $S_3Q_B^-$ states in thermophilic cyanobacteria compared to spinach is predominantly due to changes in the redox potentials of the acceptor side quinones rather than the S states.

3.4.2 Effect of tyrosine D on the miss parameter

The detailed FIOP measurements and their analyses within the framework of an extended Kok model that takes the fast $S_2Y_D \rightarrow S_1Y_D^{ox}$ and $S_3Y_D \rightarrow S_2Y_D^{ox}$ reactions into account were used to address the question of a possible direct effect of the redox state of Y_D on the miss parameter. It has been suggested that the positive charge in form of a proton trapped in the microenvironment of Y_D^{ox} enhances the midpoint potential of P680/P680$^{+\bullet}$ via electrostatic interactions [126, 127, 216]. This effect could reduce the extent of µs kinetics in the multiphasic pattern of P680$^{+\bullet}$ reduction by Y_Z thus giving rise to a decrease of the probability of misses [219]. Based on the reasonable assumption that after the very long dark adaptation the S_2 population in S_1Y_D samples is practically zero, our detailed analyses of FIOPs suggest that the probabilities of misses is somewhat smaller in $S_1Y_D^{ox}$ samples than in S_1Y_D samples. This suggests that the positive charge in the vicinity of Y_D^{ox} affects the redox equilibria and/or electron transfer kinetics between PS II cofactors. However, the precise mechanism for this effect cannot be deduced from FIOP measurements and for most practical applications this effect is small enough to be ignored. A consistent explanation for these fit results is the above discussed concept of an E_m(P680/P680$^{+\bullet}$) modulation by Y_D^{ox}, but the fits cannot proof this mechanism. In another recent publication on PS II complexes from *Chlamydomonas* mutants it was concluded that the substitution of Y_D by phenylalanine affects the hydrogen bond network, which regulates the kinetics of P680$^{+\bullet}$ reduction [220]. It therefore appears also possible that Y_D^{ox} affects the miss parameter via this latter mechanism.

3.4.3 Unequal misses

The detailed fits of Table 3.3.2 show that the Kok models assuming S state independent miss and double hit parameters lead to a small, systematic under-estimation of the oxygen yield in the 5th flash of FIOPs of dark-adapted thylakoids. This problem can be numerically 'solved' by either including the S_{-1} state in the fits or alternatively by the assumption of S state dependent misses. If only the fit quality is considered, the data of this study neither

permit a distinction between these two options, nor exclude further possibilities. However, the finding that preflashing hardly effects the apparent S_{-1} population appears to be a strong argument against a real S_{-1} population in these dark-adapted samples and favor the idea of S state dependent misses, which have already been discussed in previous reports [94, 111, 112, 212, 221].

Our fits to the FIOPs only exclude the option that most of the misses occur on the $S_0 \rightarrow S_1$ transition, but do not allow a further distinction between other possibilities. Therefore we need to refer to independent data for a further discussion. The known fact that under optimized conditions about the same S_2 EPR multiline signal amplitude can be generated with a single flash excitation of a PS II sample as by continuous illumination at 200 K argues for a fairly small miss parameter for the $S_1 \rightarrow S_2$ transition. On the other hand our above mentioned S state dependent miss fits to S_2 EPR multiline patterns reveal that at least half of the misses have to occur during the $S_1 \rightarrow S_2$ and $S_2 \rightarrow S_3$ transitions, because otherwise the S_2 multiline amplitude after the 2^{nd} flash cannot be fit with reasonable assumptions. Therefore, the above data indicate that $\alpha_{23} \geq \alpha_{12} \geq \alpha_{01}$ and $\alpha_{12} + \alpha_{23} \geq \alpha_{30} + \alpha_{01}$.

Earlier reports have indeed suggested a high α_{23} [111, 221] on the basis of the finding that it is very difficult to achieve light saturation for this transition, while a large α_{30} was proposed based on the high extend of µs component for $P680^+$ reduction for this transition [212]. Therefore, at present it appears to be possible that the $S_2 \rightarrow S_3$ and the $S_3 \rightarrow S_0$ transitions are coupled to higher miss parameters than the other two transitions. However, further studies following simultaneously markers for several S states in one set of samples are required to solve this fundamental question of the Kok cycle. Only with precise numbers at hand it will then be possible to assess possible impacts of S state dependent misses and double hits on the interpretation of many data concerning the kinetics and redox states within the OEC.

CHAPTER 4

Effect of the H/D Isotope Exchange on the Reactions of the OEC in Thylakoids from *Thermosynechococcus elongatus* and Spinach as a Function of pL and Temperature

4.1 Introduction

The effect of the H/D isotope exchange on the reactions of PS II was studied mostly on spinach samples using flash – inducing fluorescence absorption and FIOPs [207, 214, 219]. Both methods have led to similar results, which reveal that replacement of the exchangeable protons by deuterons affects the microsecond kinetics of the reduction of $P680^{+}$ by Y_Z [214, 219]. Additionally, a possible coupling of relaxation processes in the microsecond time domain with the proton movement in the environment of Y_Z^{ox} was proposed. It was suggested that $P680^{+\bullet}$ is reduced via ns kinetics, when the base of His 190 stays unprotonated and hydrogen bridged with Y_Z. The extent of the ns kinetics depends on the protonation state of His 190. The pH value of His in solution is around 6.0 and hence the extent of ns kinetics is expected to decrease at acidic pH without significant effect on oxygen evolution as long as the relaxation processes are not blocked and the probability of the misses does not increase drastically [214, 219]. Measurements of laser flash induced absorption changes at 820 nm and 355 nm revealed that H/D isotope exchange is virtually without effect on the ns kinetics of $P680^{+\bullet}$ reduction by Y_z in PS II core complexes from spinach [207]. This study also showed the reaction between Y_Z^{ox} and the WOC in S_3 exhibits a kinetic H/D isotope exchange effect of similar magnitude as that recently observed in PS II membrane fragments [222].

In this Chapter, extensive studies on the effect of H/D isotope exchange on the S states reactions of the OEC from thylakoids from *T. elongatus* and spinach have been performed. Particularly, the temperature dependencies of the miss and double hit probabilities and of the steady state oxygen yields are compared at different pH and pD values in both organisms. Furthermore, the lifetime measurements of the S_2 and S_3 reduction by Y_D at pH and pD values in acidic, neutral and alkaline regions present a clear picture of the effect of H/D isotope exchange on the reduction of the S states with tyrosine D.

4.2 Experiments and analysis

4.2.1 Sample preparation

For the H_2O/D_2O exchange experiments the $S_1Y_D^{ox}$ thylakoids from spinach and *T. elongatus* were prepared as described below at different pL values (6.0, 6.8, 7.0, 7.6, 8.0 and 8.9).

After thawing on ice in the dark the samples were diluted (1:12) with buffers M,D-2; M,D-5-9 (see Chapter 2.6.4) adjusted to the corresponding pL at 5°C and incubated for 3 minutes in the dark and on ice. The samples were then centrifuged in a minifuge ("Micro 7", Fisher Scientific inst.) at 9 000 rpm/5min/4°C and resuspended to the initial volume with the same buffer. Finally the thylakoids were diluted to [Chl] = 0.15 mM (*T. elongatus*) or 1 mM (spinach) with the same buffer at the corresponding pL value adjusted at measuring temperatures.

For FIOPs measurements samples were transferred to the Joliot-type electrode (for description see Chapter 2) in very dim green light. To insure complete sedimentation and temperature equilibration 10 µL aliquots of thylakoids from *T. elongatus* and spinach were kept for 5 min and 3 min, respectively, on the electrode at the given temperature. No exogenous electron acceptors were added.

The $S_1Y_D^{red}$ thylakoids from spinach and *T. elongatus* were used for the lifetime measurements to determine the fast decays of the S_2 and S_3 states. For the H_2O/D_2O exchange experiments only $S_1Y_D^{ox}$ – thylakoids from spinach and *T. elongatus* were used. Additionally, $S_1Y_D^{ox}$ – thylakoids from *T. elongatus* were used to obtain the rate constants for the S_2 and S_3 slow relaxations via acceptor side at 20°C and pD 7.6.

While $S_1Y_D^{ox}$ spinach thylakoids were obtained by preflashing and subsequent dark adaptation directly on the electrode (see for details part 3.2, p. 42), $S_1Y_D^{ox}$ thylakoids from *T. elongatus* were prepared by preflashing twice in 50 µL aliquots ([Chl] = 0.15 mM) by a frequency doubled Nd:YAG Laser (532 nm, 800 mJ/Puls), which were separated by a dark adaptation time of 15 min at room temperature. Afterwards, the samples were kept in the dark at room temperature for one hour and then stored on ice until the FIOP measurements were performed. This protocol was found to oxidize most tyrosine D in PS II of *T. elongatus* (see Figure 3.3.1).

To test if this procedure affects the determination of the miss and double hit probabilities in the H_2O/D_2O exchange experiments, the $S_1Y_D^{ox}$ thylakoids from *T. elongatus* were preflashed in a separate experiment directly on the electrode. This latter experiment was performed in the temperature range from 5°C – 40°C and pD 6.8. The results were then compared to those data obtained by the laser preflash protocol. Miss (circles) and double hit (triangles) probabilities determined from these FIOPs are presented in the Figure 4.2.1.

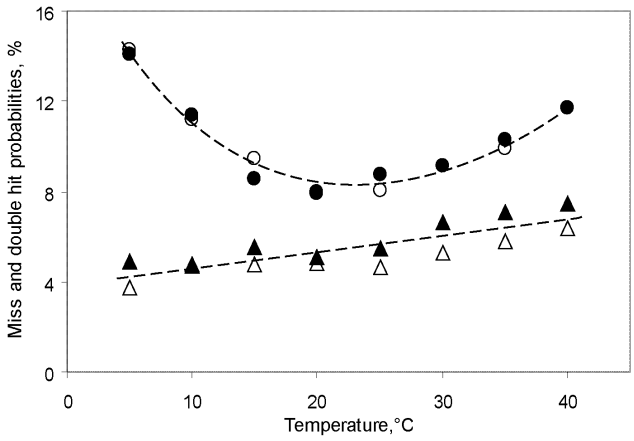

Figure 4.2.1. Dependence of the miss (circles) and double hit (triangles) probabilities from temperature in D_2O-washed $S_1Y_D^{ox}$ thylakoids from *T. elongatus* obtained by preflashing with Nd: YAG laser in glass vial (open symbols) or direct on the Joliot electrode with a Xenon flash lamp (filled symbols). Both data sets were obtained at pD 6.8.

Essentially no differences were found in the miss and double hit probabilities using the two independent preflash protocols (Figure 4.2.1). Thus, it was decided to use the laser preflashing protocol was used bacause this procedure is much less time consuming.

4.2.2 Data analysis

Data analysis was performed as described in Chapter 2 and using an extended Kok model (Scheme 3.2.2), which includes $S_2Y_D^{red} \rightarrow S_1Y_D^{ox}$ and $S_3Y_D^{red} \rightarrow S_2Y_D^{ox}$.

Initially numerical analysis on the $S_1Y_D^{ox}$ thylakoids from spinach was done using different fit approaches, as it was found that spinach FIOPs do not need to have $Y_D^{red/ox}$ included to minimize the fit error. Table 4.2.1 shows an example of such kind of analysis performed on spinach FIOPs at different temperatures. A good fit is already obtained with fit approach A, where only the fit parameters α, β are varied at an initial S_1 state population is fixed to 100%.

However, the fit quality slightly improves in fit B, where the S_2 state (that accounts for the possible S_2 state remained after the preflashes) is also included as a free parameter.

Sample	Fit approa-ches	Fit Parameters, %							Goodness of fit	
		α	β	S_2	S_1	S_0	S_{-1}	Y_D	dx^2 (1×10^6)	Fq (1×10^6)
5°C	**A**	6.9	2.8		100*				452	37.6
	B°	6.9	2.0	4.9	95.1				345	31.4
	C	6.3	1.5	6.5	86.2	1.8	5.4		184	20.1
	D	7.0	3.2		100*			0	452	41.1
10°C	**A**	7.4	2.9		100*				426	35.5
	B°	7.4	2.0	3.1	96.9				267	24.3
	C	7.0	1.5	5.0	89.1	0	5.8		117	13.0
	D	7.5	2.9		100*			0.3	426	38.8
15°C	**A**	7.9	2.9		100*				399	33.2
	B°	7.8	2.0	3.1	96.9				242	22.0
	C	7.4	1.5	5.0	89.0	0	6.0		94	10.4
	D	7.9	2.9		100*			0.9	398	36.2
20°C	**A**	8.8	4.2		100*				405	33.8
	B°	8.7	3.0	3.4	96.6				182	16.5
	C	7.9	2.4		85.7	1.8	6.3		39	4.3
	D	7.2	3.7		100*			34.2	236	21.5
25°C	**A**	10.5	5.2		100*				492	41.0
	B°	10.3	3.7	4.1	95.9				212	19.3
	C	9.0	2.7	7.3	81.4	3.6	7.8		30	3.3
	D	8.1	5.2		100*			31.4	434	39.4
30°C	**A**	12.9	6.0		100*				471	39.2
	B°	12.6	4.3	3.0	97.0				244	22.1
	C	10.9	2.9	7.1	79.7	3.6	9.7		47	5.3
	D	10.5	5.8		100*			20.2	387	35.2
35°C	**A**	18.2	7.5		100*				264	22
	B°	17.7	5.4	0	100*				236	21.4
	C	14.9	3.7	4.9	78.2	5.9	11		35	3.9
	D	14.9	6.9		100*			19.2	173	15.7
40°C	**A**	30.0	7.1		100*				537	44.8
	B°	29.2	4.3	0	100*				749	68
	C	16.8	5.2	0	57	28.2	14.2		25	2.8
	D	19.6	7.5		100*			41.2	146	13.3

Table 4.2.1. Different fit approaches of $S_1Y_D^{ox}$ thylakoids from spinach obtained at temperatures 5°C-40°C and pH 6.8. The assumed population of 100% for S_1 state is indicated with asterisk. In fit approach D the Y_D^{red} population was included and freely varied based on the fixed rate constants for the $S_2Y_D^{red} \rightarrow S_1Y_D^{ox}$ and $S_3Y_D^{red} \rightarrow S_2Y_D^{ox}$ fast decays obtained at corresponding temperature and pH 6.8. The goodness of the fit was determined as described in the Chapter 2.7.2 - 2.7.3.

Fit approach C, which includes the "S_0 state" and "S_{-1} state" shows the best fit, but including these additional parameters in the fit is not easily explained in terms of the classic Kok model (discussed in Chapter 3). Fit D is similar to Fit A, but the percentage of Y_D is an additional free running parameter. The fit results at the various temperatures give largely different percentages of Y_D^{red}. At low temperatures the back reactions are too slow to contribute significantly to the damping, while at higher temperatures an intermediate

range is reached, where the parameter is interdependent with the miss parameter (at even higher rates Y_D^{red} is correlated with the initial S_0 population). This way fit minima become possible, which indicate for higher levels of Y_D^{red} than actually present. In our case of $S_1Y_D^{ox}$ samples, the percentage of Y_D^{red} should actually be 5% to 15%. Under these conditions it is therefore not possible to have both parameters free running. Thus, fit approach B is applied to all FIOP measurements of spinach samples in this chapter.

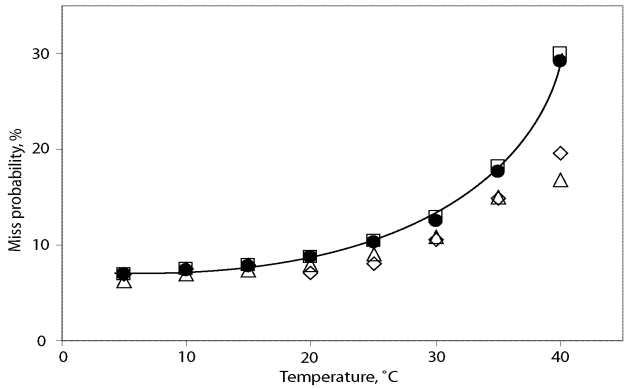

Figure 4.2.2. Miss probability as a function of temperature calculated in the framework of the Kok-model using fit approaches A (squares), B (filled circles), C (triangles) and D (diamonds) of the Table 4.2.1 in $S_1Y_D^{ox}$ thylakoids from spinach obtained at pH 6.8.

Independent of the difference in the S states distribution and value of the fit error, the miss and double hit probabilities, which are the focus of this Chapter, were found to be largely independent in all fit approaches up to 20°C. Above 20°C the miss probabilities determined by using fit approaches A and B are higher than those obtained from the fits C and D (Figure 4.2.2), which is caused by the factors mentioned above.

The $S_1Y_D^{ox}$ thylakoids from *T. elongatus* were analyzed as described in the Chapter 3 using the classic approach of equal miss and double hit probabilities for all S states transitions. To analyze the FIOPs obtained at pL 6.0 and 7.0 introduction of the β_1 parameter was found to be required, which is the double hit probability in the first flash (see *Results* of this Chapter).

4.3 Results

In the present study the effect of H/D isotope exchange on the S states transition is analysed in FIOPs measured at various pL values and temperatures in thylakoids from spinach and *T. elongatus*.

Figure 4.3.1 **a** and **c** shows FIOPs of spinach thylakoids recorded at 10°C and 30°C and pH 6.8. Pattern **a** confirms previously reported observations on the relatively high ratio of the oxygen yields on the third and forth flashes Y_3/Y_4 in FIOPs of spinach at low temperature, which in this case is equal to 4.4. The smaller Y_3/Y_4 ratio at 30°C (2.8; Fig. 4.3.1 **c**) reflects the higher miss parameter under these conditions. FIOPs of spinach thylakoids washed in D_2O buffer are shown in the Figure 4.3.1 **b** and **d**. No big differences are observed between spinach thylakoids washed in H_2O/D_2O at pL 6.8 (L = H or D), but the Y_3/Y_4 ratios are somewhat smaller in pD samples: 3.7 and 2.3 at 10°C and 30°C, respectively.

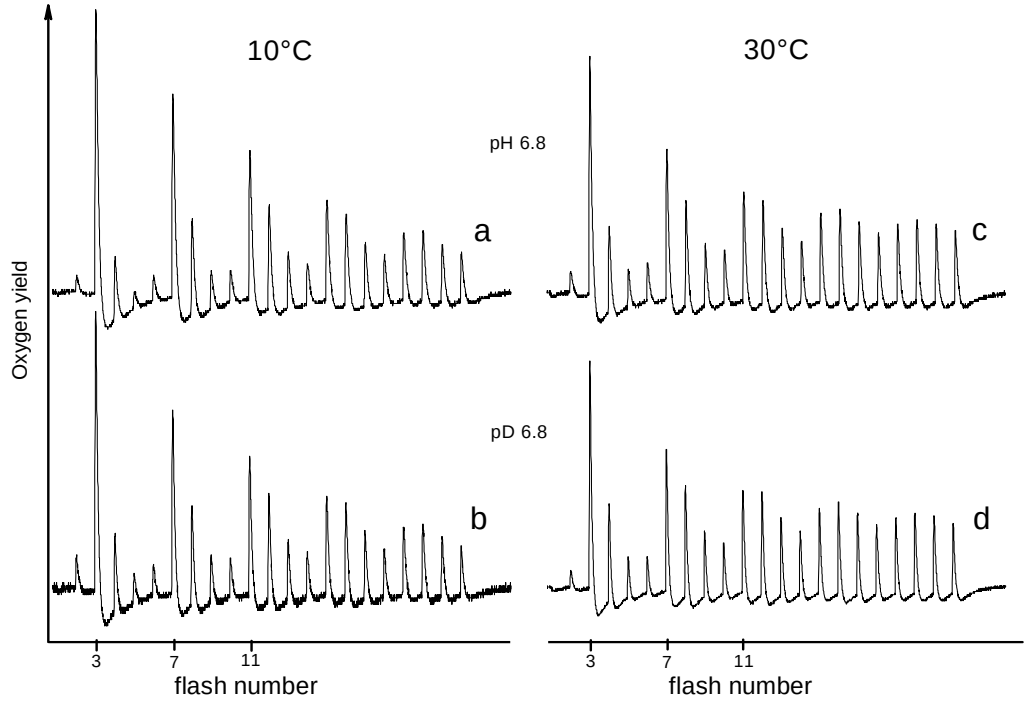

Figure 4.3.1. FIOPs of $S_1Y_D^{ox}$ spinach thylakoids obtained at 10°C (**a** and **b**) and 30°C (**c** and **d**). Samples **a** and **c** are control measurements in MCMH buffer adjusted to pH 6.8 at given temperatures, while samples **b** and **d** were washed in buffer of the same composition, where H_2O was replaced with D_2O.

The FIOPs obtained under the same conditions for $S_1Y_D^{ox}$ thylakoids from *T. elongatus* are displayed in Figure 4.3.2. The Y_3/Y_4 ratio of the pattern obtained at 10°C/pH 6.8 (Figure 4.3.2 **a**) is 2.4. This reflects a fairly high miss probability at 10°C, which is in agreement with data presented in the Chapter 3. At 30°C and pH 6.8 the ratios Y_3/Y_4 are 2.8 and 2.0 for samples suspended in H_2O and D_2O (Figure 4.3.2 **c** and **d**, respectively).

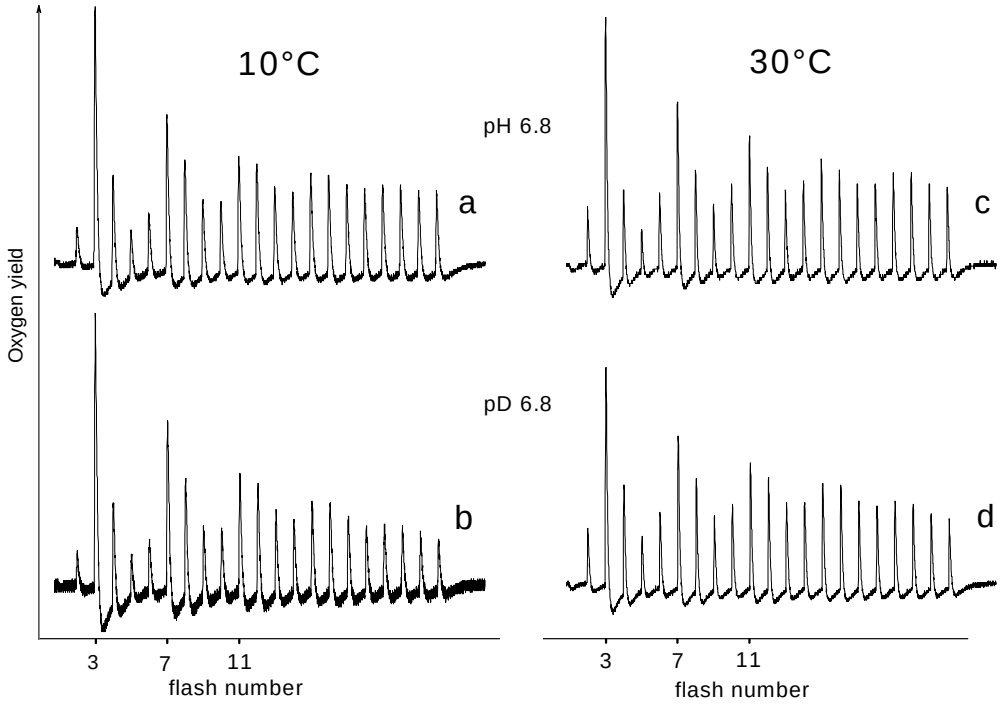

Figure 4.3.2. FIOPs of $S_1Y_D^{ox}$ thylakoids from *T. elongatus* obtained at 10°C (**a** and **b**) and 30°C (**c** and **d**). Samples **a** and **c** present control measurements in MCMH buffer adjusted to pH 6.8 at given temperatures, while samples **b** and **d** were washed in buffer of the same composition, where H_2O was replaced with D_2O.

Using numeric analysis within the framework of the Kok model, the miss and double hit probabilities were determined at different temperatures and pL values in spinach FIOPs and compared to those obtained from *T. elongatus*.

4.3.1 Temperature dependence of the miss probability in thylakoids from spinach

The temperature dependence of the miss parameters of the $S_1Y_D^{ox}$ thylakoids from spinach at different pL values is presented in Figure 4.3.3.

The filled circles symbolizing the miss probability of the H_2O-samples at pH 7, exhibit minimal values of about 7% at 5°C to 8.7% at 20°C (Fig. 4.3.3 B). At higher temperatures

the miss probability of H_2O-samples increases noticeably and reaches 29% at 40°C and pH 7. In contrast to the pH 7 data, the miss probabilities obtained at pH 6 are slightly higher at low temperatures (about 10%), but the increase of misses with temperature is significantly smaller (20% at 40°C) (Fig 4.3.3 B, filled diamonds). An even more pronounced temperature sensitivity of the PS II samples is observed at pH 8.0 (filled triangles). At this pH it was not possible to determine the miss parameter at temperatures above 30°C since the sample became inactivated.

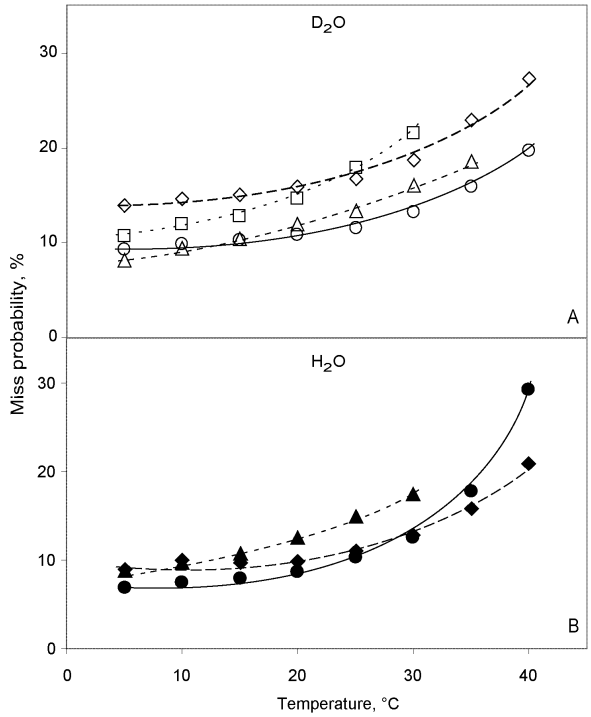

Figure 4.3.3. Miss probability as a function of temperature determined from FIOPs of $S_1Y_D^{ox}$ thylakoids from spinach after incubation in D_2O buffer (A) or H_2O buffer (B) at pL 6.0 (diamonds), 7.0 (circles), 8.0 (triangles) and 9.0 (squares). The corresponding buffers are listed in Chapter 2.6.4. The numeric analysis was done as described in part 4.2.2 of this chapter.

The miss probabilities determined from the FIOPs of D_2O-samples are shown in Figure 4.3.3 A. pD 7.0 samples (open circles) have a slightly higher miss parameter at low temperature (9% / 5°C) compared to pH 7.0 samples (7% / 5°C). This confirms the qualitative analysis on the basis of Y_3/Y_4 ratio of the FIOPs in Figure 4.3.1. This comparison also shows that PS II samples are clearly less sensitive to a temperature rise at pL 7.0 in D_2O compared to H_2O. The same observation is made at pL 8.0, where measurements up to 35°C were possible in D_2O buffer. In addition, it is even possible to record FIOPs at pD 9.0 up to 30°C. In contrast to pL 7.0, where the miss parameter varied only slightly in H_2O vs. D_2O, a significantly larger miss parameter is observed at all temperatures at pL 6.0 in D_2O (open diamonds) (14% at 5°C) compared to H_2O (9% at

5°C). The comparison of the pH/pD samples of spinach is shown more clearly for pL 6 (A) and 7 (B) in Figure 4.3.4.

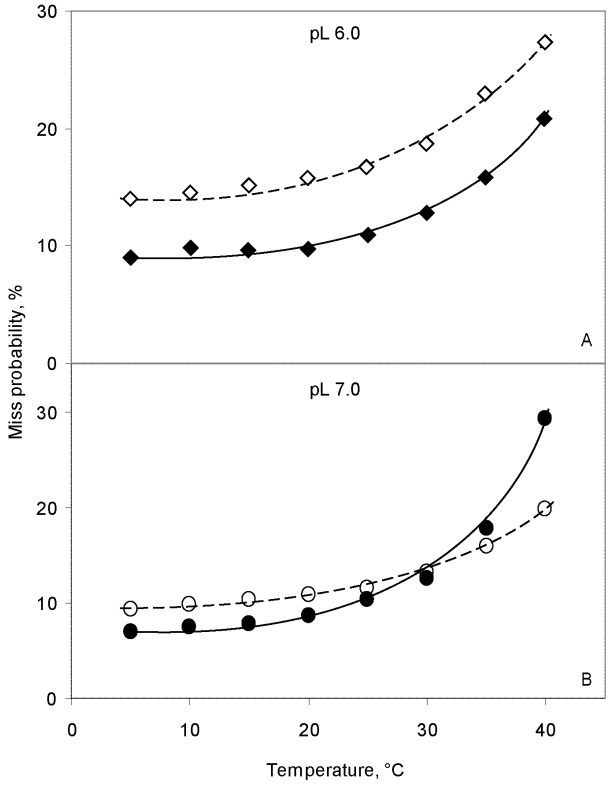

Figure 4.3.4. Comparison of the miss probabilities as a function of temperature in $S_1Y_D^{ox}$ thylakoids from spinach after incubation in D_2O buffer (open symbols) or H_2O buffer (filled symbols) at pL 6.0 (A) and 7.0 (B). All other conditions are as described in Figure 4.3.3.

4.3.2 Temperature dependence of the miss probability in thylakoids from T. elongatus

The miss probabilities determined for the $S_1Y_D^{ox}$ FIOPs from *T. elongatus* incubated at pL 6.0 (diamonds), 7.0 (circles), 8.0 (triangles) and pD 9.0 (squares) as a function of temperature are shown on Figure 4.3.5. At all temperatures the miss parameter of H_2O samples obtained at pH 6.0 is slightly higher than in samples incubated at pH 7.0 with minima of ~10% (pH 6.0) and 8% (pH 7.0) at temperatures of about 30°C and 25°C, respectively. Furthermore, in contrast to the spinach samples, the H_2O samples of *T. elongatus* obtained at pH 8.0 have a high miss probability at all temperatures with its minimum of ~20% at ~20°C. Thus, the minimum of the miss parameter is shifted to lower temperatures when the pH of the medium increases.

The miss probabilities in D_2O samples are slightly higher at 5°C and pD 7.0 (16%) compared to pH 7.0 (14%) and show a minimum of 8% at 30°C (Figure 4.3.5 A, open circles). The samples incubated at pD 6.0 have generally higher miss parameters with a

minimum of 13% at 30°C. In contrast to H_2O, the miss parameters of the D_2O samples at pD 8.0 are very similar to those obtained at pD 7.0. Interestingly, that all values of the miss parameter at pD 9.0 resemble those of pH 8.0. In contrast to the measurements in H_2O-buffer the minima of the miss parameter in D_2O samples always appear to occur at 30°C irrespective of the pD value.

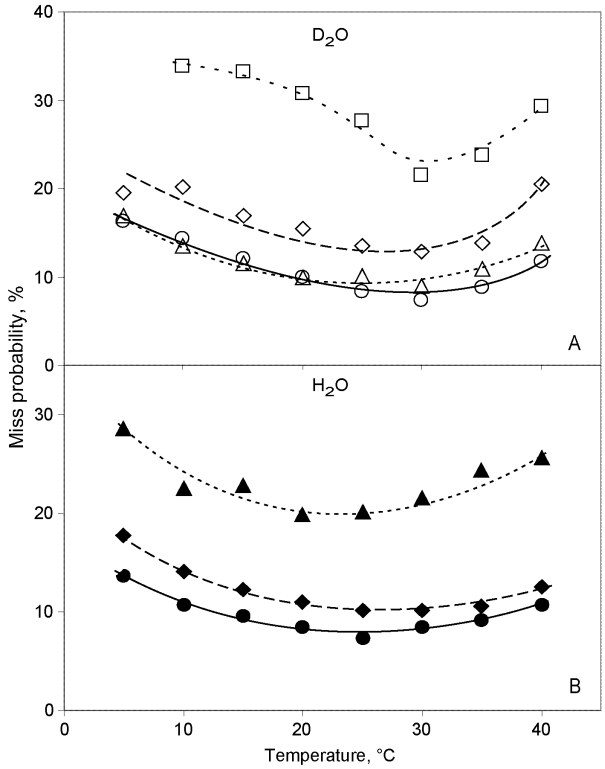

Figure 4.3.5. Miss probability as a function of temperature determined from FIOPs of $S_1Y_D^{ox}$ thylakoids from *T. elongatus* after incubation in D_2O buffer (A) or H_2O buffer (B) at pL 6.0 (diamonds), 7.0 (circles), 8.0 (triangles) and 9.0 (squares). The corresponding buffers are listed in Chapter 2.6.4. The numeric analysis was done as described in the Chapter 3.3.5 and in part 4.2 of this chapter.

Figure 4.3.6 shows a comparison of H_2O and D_2O samples at pL 6.0 (A) and pL 7.0 (B) in *T. elongatus*. It is analogues to Figure 4.3.4, where the data for spinach are presented.

Despite the different temperature dependence of the miss parameters in samples obtained from spinach and *T. elongatus*, the relative changes induced by H_2O/D_2O are very similar at pL 6.0 and pL 7.0: (i) the miss parameter obtained at pL 6.0 is higher in D_2O compared to H_2O samples; (ii) samples incubated at pL 7.0 are not sensitive to H_2O/D_2O exchange at temperatures between 25°C and 35°C; (iii) the samples become less temperature sensitive after H/D exchange, especially at high pL values.

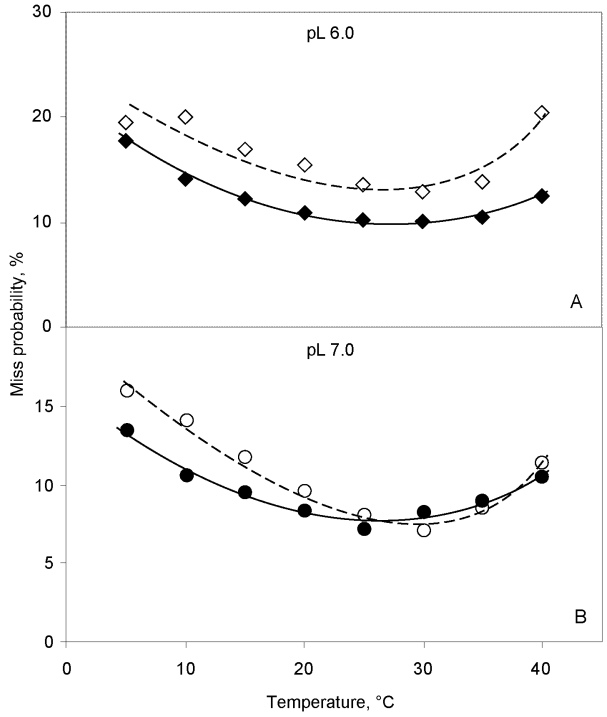

Figure 4.3.6. Comparison of the miss probabilities as a function of temperature in $S_1Y_D^{ox}$ thylakoids from *T. elongatus* after incubation in D_2O buffer (open symbols) or H_2O buffer (filled symbols) at pL 6.0 (A) and 7.0 (B). All other conditions are as described in Figure 4.3.5.

4.3.3 Dependence of the double hit probability on temperature in thylakoids from spinach and T. elongatus

The double hit probabilities of $S_1Y_D^{ox}$ spinach thylakoids increase slowly with temperature at all pL values with the minimum of about 2% at 5°C.

However, two different types of temperature dependence are observed: (1) at pL 6.0 and 7.0 a non-linear increase is observed with relatively small changes between 5°C and 20°C and a pronounced enhancement with temperature rising up to 40°C, (2) at high pL (pL 8.0 and pD 9.0) a linear dependence of double hits on temperature is measured. The only significant difference caused by the D_2O/H_2O exchange appears to be the significantly larger double hit probability at pD 6.0 compared to pH 6.0 (Figure 4.3.7).

At first glance the temperature dependence of the double hit probability is very different in *T. elongatus* (Figure 4.3.8) compared to spinach (Figure 4.3.7). However, despite the differences in the general trends, there are surprising similarities between the two organisms: (1) the double hit probabilities are very similar at pH 6.0 and pH 7.0, while they are higher at pH 8.0; (2) the double hits are clearly higher at pD 6.0 that at pD 7.0, while the values of pD 7.0 and 8.0 are similar over a large temperature range.

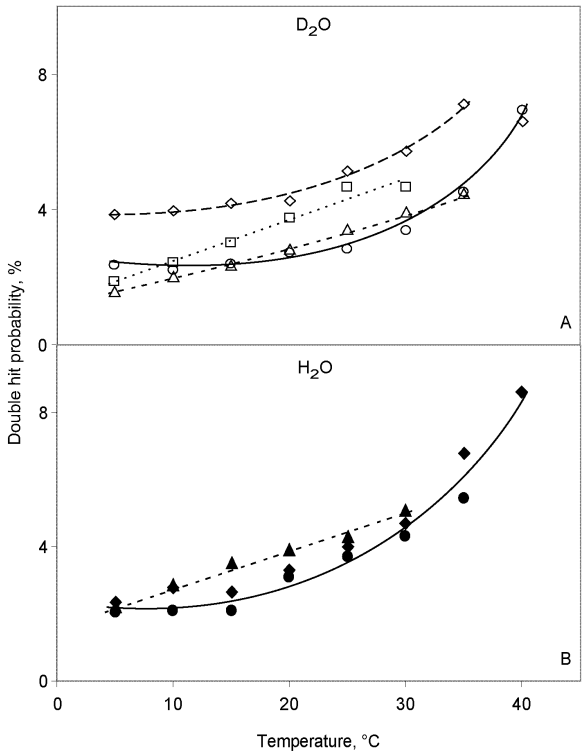

Figure 4.3.7. The double hit probability as a function of temperature determined from FIOPs of $S_1Y_D^{ox}$ thylakoids from spinach after incubation in D_2O buffer (A) or H_2O buffer (B) at pL 6.0 (diamonds), 7.0 (circles), 8.0 (triangles) and 9.0 (squares). The corresponding to each pL buffers are listed in Chapter 2.6.4. All other conditions are as described the legends to Figure 4.3.3.

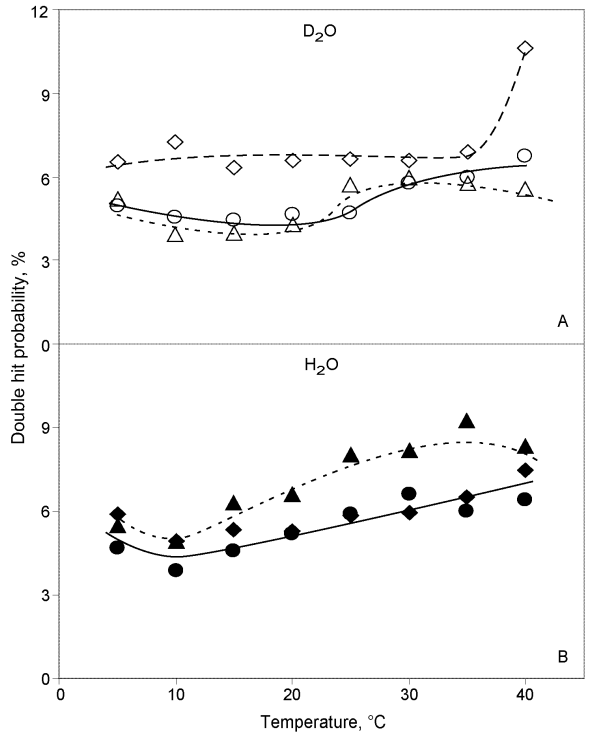

Figure 4.3.8. The double hit probability as a function of temperature determined from FIOPs of $S_1Y_D^{ox}$ thylakoids from *T. elongatus* after incubation in D_2O buffer (B) or H_2O buffer (A) at pL 6.0 (diamonds), 7.0 (circles) and 8.0 (triangles). The corresponding to each pL buffers are listed in Chapter 2.6.4. All other conditions are as described the legends to Figure 4.3.3. The data were obtained by taking β_1 into account (see text and Figure 4.3.9).

The numerical analysis of FIOPs of *T. elongatus* incubated at pL 6.0 – 7.0 shows that the high oxygen yield after the second flash cannot be fit by a general increase of the double hit parameter, but only by a higher double hit probability for the first flash (β_1). This higher double hit probability on the first flash is believed to be caused by a fraction of PS II centers in *T. elongatus* that contains oxidized non-heme Fe^{3+}. The electron transfer from Q_A^- to Fe^{3+} occurs in the μs range, which opens the reaction center to a second charge separation within the same flash. Thus, the β_1 parameter depends on 1) population of the Fe^{3+}; 2) the rates of $Q_A^-Fe^{3+} \rightarrow Q_AFe^{2+}$ reduction and 3) the flash profile. The origin of the oxidation of the Fe^{2+} to Fe^{3+} is unknown. The present study shows that the β_1 parameter increases with temperature (Figure 4.3.9). The traces at pL 7.0 (circles) and pD 6 (open diamonds) reveal similar temperature dependence of the β_1 parameter, which saturates at 30°C-40°C. In contrast, the β_1 values are higher at all temperatures at pH 6.0 and no saturation is observed.

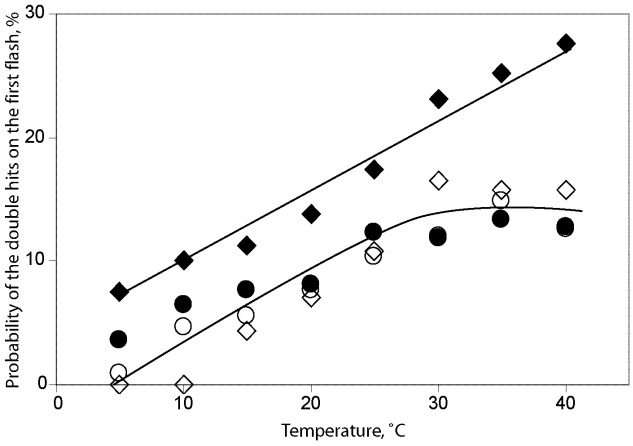

Figure 4.3.9. The double hit probability on the first flash as a function of temperature in $S_1Y_D^{ox}$ thylakoids from *T. elongatus* after incubation either in D_2O buffer at pD 6.0 (open diamonds) and 7.0 (open circles) or in H_2O buffer at pH 6.0 (filled diamonds) and 7.0 (filled circles). All other conditions are as described in Figure 4.3.5.

Numerical analysis of the FIOPs of *T. elongatus* obtained at pD 9.0 (data are not shown) and pH 8.0 revealed that also these samples had a deviation on the calculated and measured oxygen yield on the second flash. However, in these cases the measured oxygen yields of the second flash are smaller than predicted on the basis of classical Kok model. Thus, the introduction of the β_1 parameter could not improve the fit quality. The only possibility found in this study to decrease this deviation was the use of S state dependent miss probabilities. For the FIOPs of *T. elongatus* obtained at pH 8.0 this approach is discussed in the Chapter 5.

4.3.4 pL dependence of the miss and double hit parameters in spinach

The miss (A) and double hit (B) probabilities of $S_1Y_D^{ox}$ thylakoids from spinach resuspended in D_2O (open symbols) and H_2O (filled symbols) are shown for 10°C (diamonds), 20°C (circles) and 30°C (squares) in Figures 4.3.10 and 4.3.11, as a function of pD or pH. These data reveal that the miss parameter of pD-samples is more pronounced at acidic pD but becomes smaller at alkaline pD compared to pH-samples. Furthermore, a shift of the minimal miss probability, α_{min}, to more acidic pL with increasing temperature is observed for thylakoids in H_2O and D_2O. Figure 4.3.10 A reveals the shift of the α_{min} in D_2O samples from pD 7.5 ± 0.3 with average misses 9% at 10°C via pD 7.2 ± 0.3 with 10.5% misses at 20°C to pD 7.1 ± 0.3 with 13.5% average misses at 30°C. The small shift of α_{min} to acidic pL with temperature rise is also observable in the H_2O-samples (Figure 4.3.11 A). The values of the α_{min} in this case are 7.5% at pH 7.0 ± 0.3, 9% at pH 6.7 ± 0.3 and 12% at pH 6.6 ± 0.2 for 10°C, 20°C and 30°C, respectively.

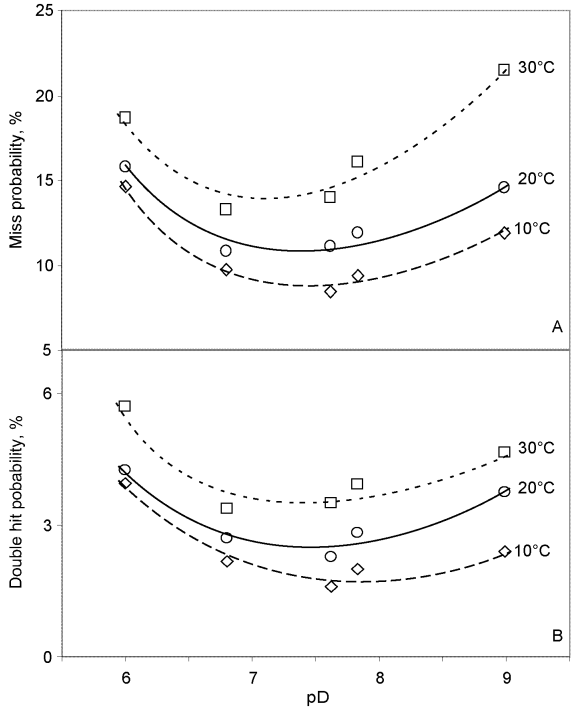

Figure 4.3.10. Miss (A) and double hit (B) probabilities as a function of pD in $S_1Y_D^{ox}$ thylakoids from spinach after incubation in D_2O buffer at 10°C (diamonds and dashed line), 20°C (circles and straight line) and 30°C (squares and dotted line). All other conditions are as described in Figure 4.3.3.

Similar to the miss parameter described above, the double hit probability is higher in D_2O at low pL values, but lower at high pL values compared to H_2O samples. The double hit parameters are about 4% at pD 6.0 and 10°C (Figure 4.3.10 B). This value increases with

temperature and is about 6% at 30°C (dotted line) and pD 6.0. The minimum of double hits β_{min} is at pD 7.9 ± 0.4 at 10°C (~2%) and shifts down to pD 7.3 ± 0.5 at 20°C (~2.7%) and 30°C (~3.7%). For pH-samples β_{min} is found at pH 6.9 ± 0.4 at all temperatures. Its value is ~2% at 10°C and increases by an increment of about 1% for every 10°C temperature rise (Figure 4.3.11 B). Comparison of the dependence of the beta parameter on alkaline pL reveals that pD samples show lower values at pD 8.0 (1.8%/10°C, 2.7%/20°C and 3.6%/30°C) than pH samples (~3%/10°C, ~4%/20°C and 4.5%/30°C).

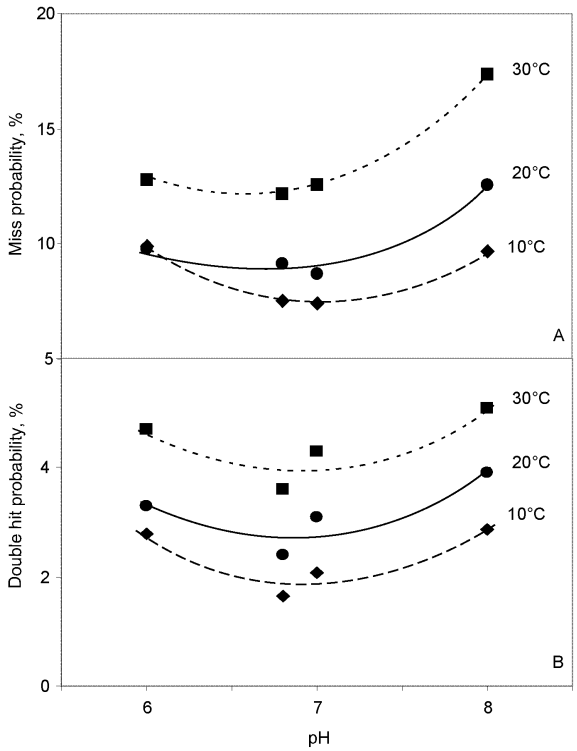

Figure 4.3.11. Miss (A) and double hit (B) probabilities as a function of pH in $S_1Y_D^{ox}$ thylakoids from spinach after incubation in H_2O buffer at 10°C (diamonds and dashed line), 20°C (circles and straight line) and 30°C (squares and dotted line). All other conditions are as described in Figure 4.3.3.

A direct comparison of the miss (A) and double hit (B) probability in pD (open circles) and pH (filled circles) samples measured at 20°C is shown in Figure 4.3.12. The intersection point for misses in pD and pH samples is observed to be around pL 7.8 (Figure 4.3.12 A). Below this number miss probabilities of pD samples are much higher in D_2O, while above pL 7.8 the samples in H_2O exhibit higher misses. The intersection point for the double hit probabilities is ~ 2.7% at pL 6.9.

4.3.5 pL dependence of the miss and double hit parameters of T. elongatus

The miss and double hit probabilities as a function of pL at 10°C, 20°C and 30°C show a quite different dependence in *T. elongatus* samples compared to spinach thylakoids

(Figures 4.3.13 and 4.3.14). The high miss probability at 10°C and pH 6.8 compared to 20°C and 30°C in thylakoids from *T. elongatus* was discussed already in Chapter 3. Figure 4.3.13 A and Figure 4.3.14 A show that the miss probability at 10°C (diamonds) is higher at all analysed pL values (6.0 → 8.9) compared to 20°C and 30°C. The miss probabilities are minimal near neutral pL and increase towards acidic and alkaline pL. In contrast to spinach samples, the traces at 20°C and 30°C in *T. elongatus* exhibit equal miss probabilities at all pH values and up to pD 8.0. At pH 6.8 ± 0.3 α_{min} of *T. elongatus* is found to be ~ 8% at 20°C and 30°C and ~12% at 10°C. In D_2O-samples at pD 7.2 ± 0.4 the α_{min} are ~12.5% at 10°C and ~ 10% at 20°C and 30°C.

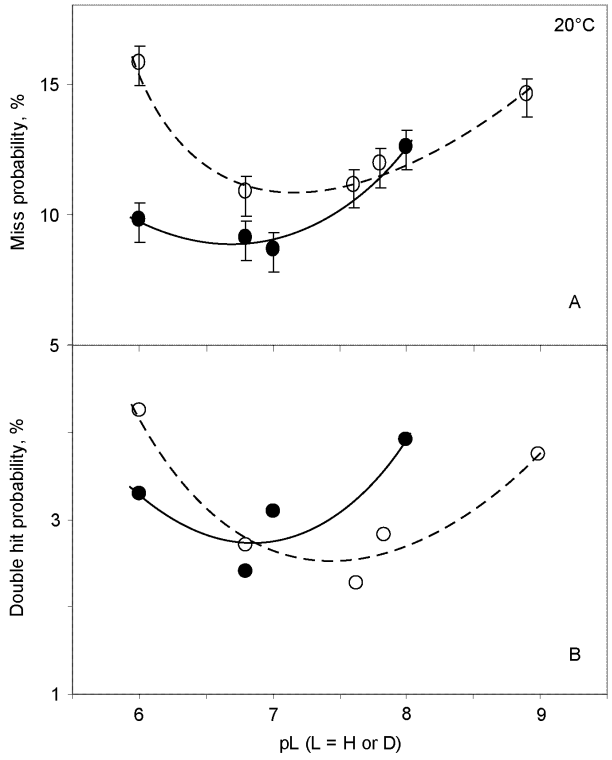

Figure 4.3.12. Comparison of the miss (A) and double hit (B) probabilities as a function of pL (L = H (filled symbols) or D (open symbols)) in $S_1Y_D^{ox}$ thylakoids from spinach at 20°C. All other conditions are as described in Figure 4.3.3.

The double hit probability, which is generally higher in *T. elongatus*, than in spinach, exhibits an almost linear dependence on pH at 10°C, 20°C and 30°C with higher values at alkaline pH (Figure 4.3.14 B). The dependence of the double hits on pD is very similar at 10°C and 20°C (Figure 4.3.13 B). In these cases, in contrast to the H_2O measurements, the double hits decrease towards to alkaline pD, while at 30°C double hits are steeply increasing between pD 7.5 and 8.7.

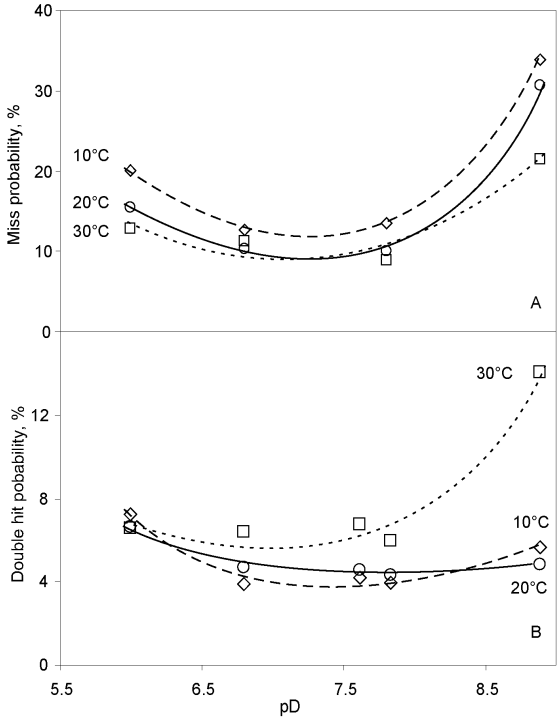

Figure 4.3.13. Miss (A) and double hit (B) probabilities as a function of pD in $S_1Y_D^{ox}$ thylakoids from *T. elongatus* after incubation in D_2O buffer at 10°C (diamonds), 20°C (circles) and 30°C (squares). All other conditions are as described in Figure 4.3.5.

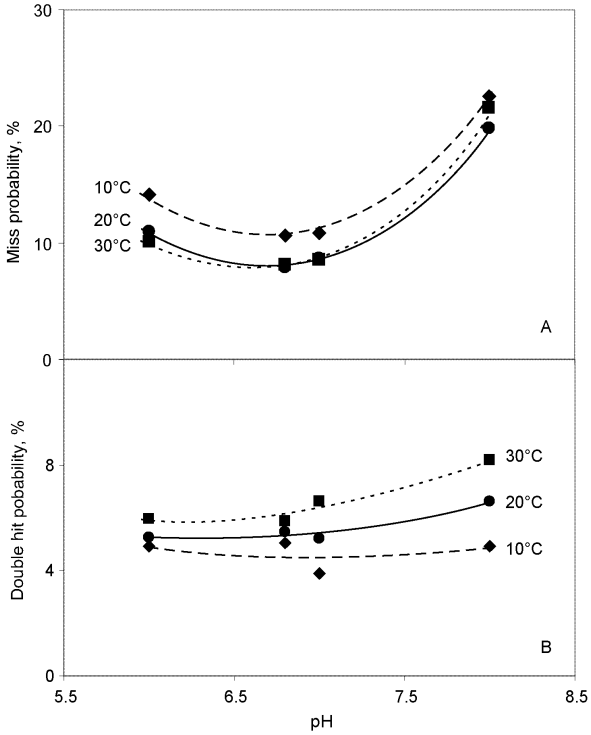

Figure 4.3.14. Miss (A) and double hit (B) probabilities as a function of pH in $S_1Y_D^{ox}$ thylakoids from *T. elongatus* after incubation in H_2O buffer at 10°C (diamonds), 20°C (circles) and 30°C (squares). All other conditions are as described in Figure 4.3.5.

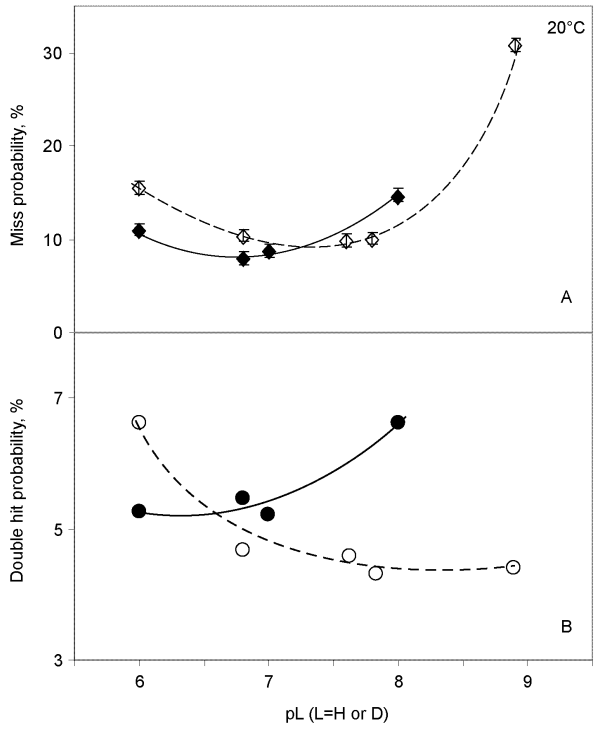

Figure 4.3.15. Miss (A) and double hit (B) probabilities as a function of pL (L = H or D) in $S_1Y_D^{ox}$ thylakoids from *T. elongatus* after incubation in either D_2O (open symbols) or H_2O (filled symbols) buffer at 20°C. All other conditions are as described in Figure 4.3.5.

Figure 4.3.15 presents a comparison of the misses (A) and double hits (B) extracted from the FIOPs of H_2O (filled symbols) and D_2O (open symbols) samples of *T. elongatus* obtained at 20°C at different pL values. These data are comparable with spinach data presented in Figure 4.3.12. The intersection points are 10% at pL 7.2 for the miss probability and ~ 5% at pL 6.6 for the double hit probability. The miss probability of the pH-sample is lower at acidic pL, while after the intersection it increases faster than in the D_2O sample. At alkaline pL the miss parameter in *T. elongatus* is twice as big as that in spinach. This interesting phenomenon is further analysed in the next chapter.

4.3.6 Steady state oxygen yield as a function of temperature

To further characterize the effect of H/D isotope exchange on PS II, the temperature dependence of the steady state oxygen yield was investigated at different pL values in spinach and *T. elongatus*.

Figure 4.3.16 shows the comparison of the absolute oxygen yields in the H_2O and D_2O FIOPs of spinach thylakoids at pL 6.0 (A) and pL 7.0 (B) as a function of temperature. These measurements reveal that the steady state oxygen yield increases with temperature up to 35°C. Above this temperature the absolute oxygen yield drops in H_2O samples incubated at pH 6.0 (filled diamonds) and 7.0 (filled circles). This finding is in agreement with the known inactivation of spinach PS II at high temperatures. In contrast to the H_2O samples, the steady state of D_2O FIOPs is stable at least up to 40°C (open symbols), which shows a significant stabilizing effect of D_2O against the thermoinactivation of OEC. This is in line with earlier data obtained with a Clark-type oxygen electrode in spinach PS II membrane fragments [223].

Overall, the absolute oxygen yield in D_2O samples is found to be much smaller at pL 6.0 compare to H_2O samples (Figure 4.3.16 A). However, the pD/pH ratios show that the temperature dependencies are very similar in H_2O and D_2O. At pL 7.0 the steady state oxygen yields are unaffected by H/D exchange up to 35°C. The absolute oxygen yield in thylakoids from *T. elongatus* is shown in Figure 4.3.17 (A and B). As in case of spinach thylakoids the steady state oxygen yield in D_2O and H_2O samples increases with temperature. But in contrast to spinach, the OEC of *T. elongatus* does not undergo the thermoinactivation at 40°C, since the native growth temperature of this cyanobacteria is 56°C. Another interesting factor is that the dependence of the steady state oxygen yield on

temperature in FIOPs of *T. elongatus* is clearly different in the D_2O (open symbols) and H_2O samples.

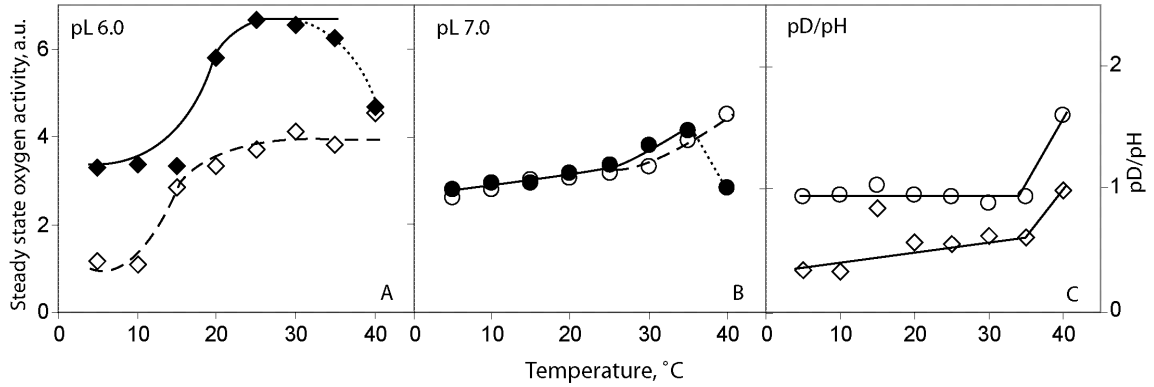

Figure 4.3.16. Comparison of the absolute oxygen yield as a function of temperature obtained from the FIOPs of the $S_1Y_D^{ox}$ thylakoids from spinach after incubation in either D_2O (A, B, open symbols) or H_2O (A, B, filled symbols) buffers at pL 6.0 (A) and pL 7.0 (B). The steady state oxygen yield (A, B) was determined by averaging the relative oxygen yields of the last eight flashes in the train of the 16 flashes. In Figure 4.3.16 C the ratios of the D_2O and H_2O steady state values obtained at pL 6.0 (open diamonds) and pL 7.0 (open circles) are given. All other conditions are as described in Figure 4.3.3.

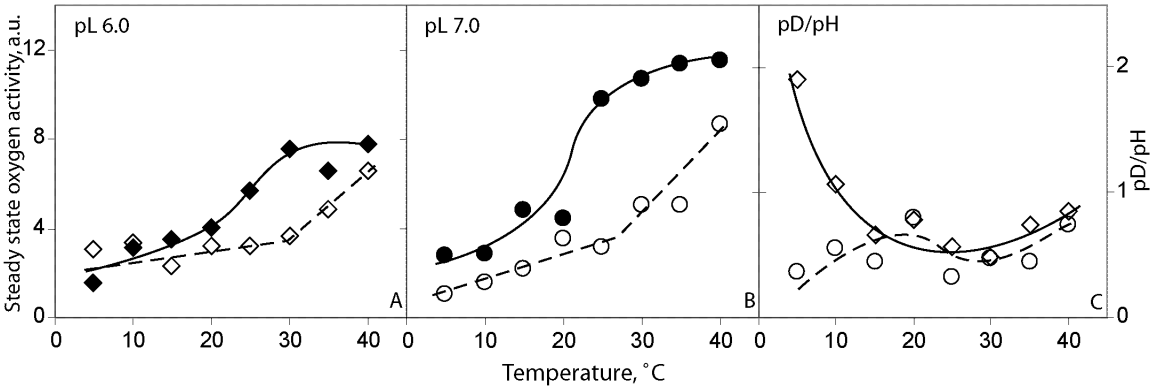

Figure 4.3.17. Comparison of the absolute oxygen yield as a function of temperature obtained from the FIOPs of the $S_1Y_D^{ox}$ thylakoids from T. elongatus after incubation in either D_2O (A, B, open symbols) or H_2O (A, B, filled symbols) buffers at pL 6.0 (A) and pL 7.0 (B). The steady state oxygen yield was determined by averaging the relative oxygen yields of the last eight flashes in the train of the 16 flashes. In Figure 4.3.17 C the ratios of the D_2O and H_2O steady state values obtained at pL 6.0 (open diamonds) and pL 7.0 (open circles), which presented in A and B, respectively, are given. All other conditions are as described in Figure 4.3.5.

The steady state oxygen evolution increases in both samples very similarly up to 20°C, while after 20°C the absolute oxygen yield of H_2O samples (filled symbols) visibly increases and at 30°C to 40°C it stays constant at nearly the same value. Contrary to H_2O samples, the steady state yield in D_2O samples is nearly invariant up to 30°C, but then increases significantly at both pD 6.0 and pD 7.0. The same can be observed in the absolute oxygen yield of the spinach FIOPs at pD 7.0 (Figure 4.3.17 B, open symbols), but the overall increase of the oxygen steady state yield with temperature in spinach is visibly

smaller (from 2.6 a.u. at 5°C to 4.5 a.u. at 40°C), than in *T. elongatus* (from 1.0 a.u. at 5°C to 8.3 a.u. at 40°C). The ratio pD/pH varies more strongly at pL 6.0 and, particularly, at low temperatures (open diamonds, Figure 4.3.17 C). For pL 7.0 the average of pD/pH ratio is 0.5, which, if compare to spinach, is two times smaller.

4.3.7 Effect of the H/D isotope exchange on the lifetimes of the S_2 and S_3 states in the OEC of spinach

Figure 4.3.18 shows semilogarithmic plots of the fast phases of the reactions $S_2Y_D^{red} \rightarrow S_1Y_D^{ox}$ (Figure 4.3.16 A and B) and $S_3Y_D^{red} \rightarrow S_2Y_D^{ox}$ (C and D) at 10°C (A and C) and 25°C (B and D) in $S_1Y_D^{red}$ thylakoids from spinach resuspended in H_2O – buffer at pH 6.8 (filled squares and triangles), or D_2O – buffer at pD 6.8 (open squares and triangles) and pD 7.6 (double squares and triangles). The fast phases shown were obtained by subtraction of slow phase (see below).

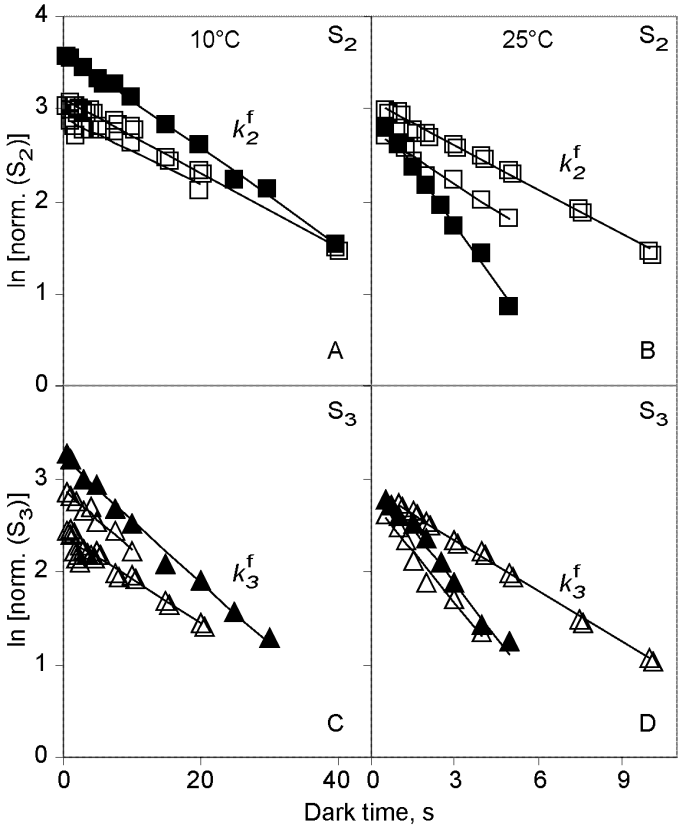

Figure 4.3.18. Semilogarithmic plot of the relative S_2 (A, B; squares) and S_3 (C, D; triangles) population in S_1Y_D thylakoids from spinach as a function of the dark time between first and second (S_2) or second and third (S_3) flashes in the train of saturating single turnover flashes. The samples were incubated either in D_2O at pD 6.8 (open symbols) and pD 7.6 (open double symbols) or H_2O buffer at pH 6.8 (filled symbols) at 10°C (A, C) and 25°C (B, D). The buffers of the corresponding pL are given in Chapter 2.6.4.

At 10°C (Figure 4.3.18 A and C) the S_2 decay was found to have similar half-times of 19.7s and 17.7s for pD 7.6 and 6.8, respectively. In H_2O at pH 6.8 the fast S_2 decay is faster, than in D_2O at the same pL with a half-time of 13s (Figure 4.3.18 A). This feature is even more pronounced at 25°C, where the S_2 decay is more than two times faster at pH 6.8 ($t_{1/2}$ = 1.7s), than at pD 6.8 ($t_{1/2}$ = 3.6s) and pD 7.6 ($t_{1/2}$ = 4.4s). The half-times for the reduction of the S_3 state by Y_D are 10.4s, 10.7s and 15s at 10°C and 1.8s, 1.9s and 3.8s at 25°C and pH 6.8, pD 6.8 and pD 7.6, respectively. Therefore, in contrast to the S_2 decay, the fast S_3 decay is virtually invariant towards a H_2O/D_2O exchange, but significantly slows down with increasing pD.

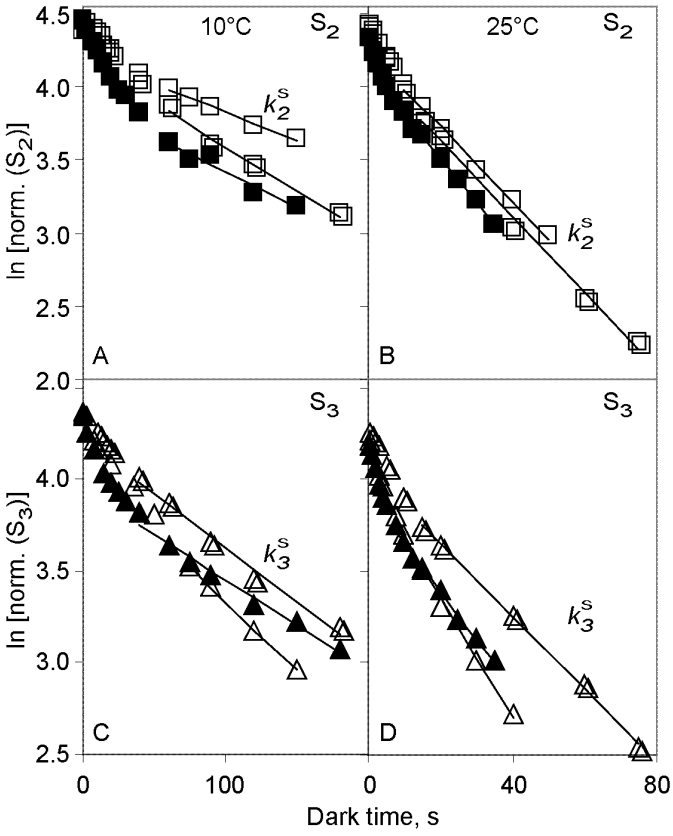

Figure 4.3.19. Semilogarithmic plot of the relative S_2 (A, B; squares) and S_3 (C, D; triangles) population in S_1Y_D thylakoids from spinach as a function of the dark time between first and second (S_2) or second and third (S_3) flashes in the train of saturating single turnover flashes (slow phase). The samples were incubated either in D_2O at pD 6.8 (open symbols) and pD 7.6 (open double symbols) or H_2O buffer at pH 6.8 (filled symbols) at 10°C (A, C) and 25°C (B, D). The buffers of the corresponding pL are given in Chapter 2.6.4.

The slow phases of the S states decay at 10°C (A and C) and 25°C (B and D) in spinach thylakoids are presented in Figure 4.3.19. The slow reduction of the S_2 state was determined to have half-times of $t_{1/2}$ = 141s (pH 6.8), 176s (pD 6.8) and 115s (pD 7.6) at 10°C. The half-time at 25°C is 23-27s for all pL values. For the relaxation of the S_3 state the half-times are 140s (pH 6.8), 91s (pD 6.8) and 119s (pD 7.6) at 10°C and 26s (pH 6.8), 21s (pD 6.8) and 35s (pD 7.6) at 25°C. A comparison of the fast and slow phases in D_2O

and H_2O samples shows that the S_2 decay in D_2O seems to be generally slower than in H_2O, while fast and slow decays of the S_3 state are largely unaffected by an H_2O/D_2O exchange at pL 6.8, but slow down at pD 7.6. One exception of this general trend is the slow decay of the S_3 state at 10°C, where the slowest half time is at pH 6.8.

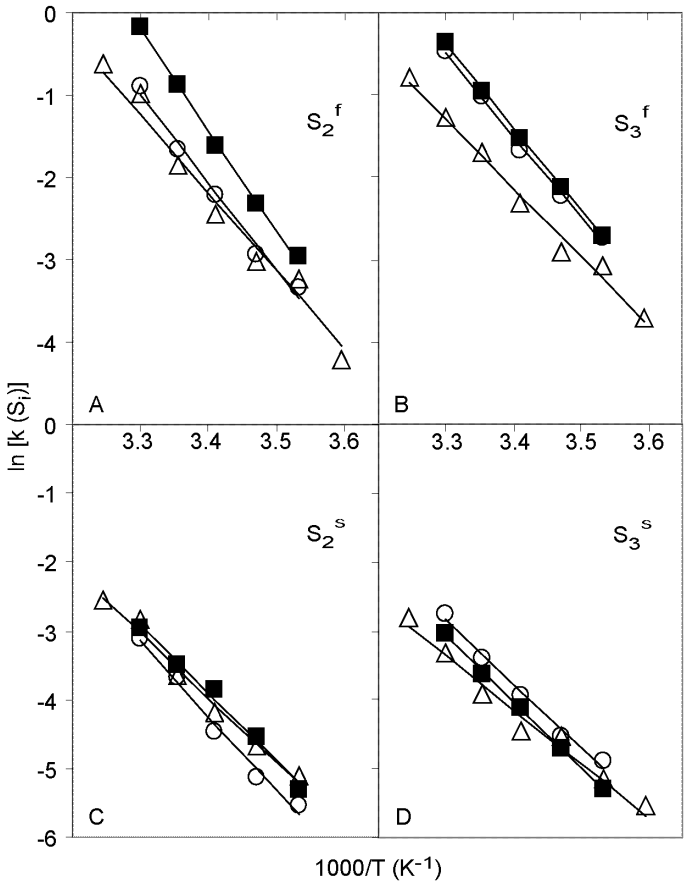

Figure 4.3.20. Semilogarithmic plots of the rate constants of the fast (A, B) and slow (C, D) S_2 (A, C) and S_3 (B, D) state decay as a function of the inverse temperature (Arrhenius type plot) determined with the S_1Y_D thylakoids from spinach incubated either in D_2O at pD 6.8 (circles) and pD 7.6 (triangles) or H_2O buffer at pH 6.8 (squares). The buffers of the corresponding pL values are given in Chapter 2.6.4.

Similar lifetime measurements were performed in the temperature range from 5°C to 35°C for D_2O samples at pD 6.8 and 7.6 and compared to those obtained in H_2O at pH 6.8. The Arrhenius type plots of the rate constants for the fast and slow S_2 and S_3 decays in $S_1Y_D^{red}$ thylakoids from spinach are presented in Figure 4.3.20. The activation energies and pre-exponential factors were determined from the Arrhenius type plots are listed in Table 4.3.1. Comparison of these parameters calculated for D_2O and H_2O samples reveal that the activation energy for the reaction $S_2Y_D^{red} \rightarrow S_1Y_D^{ox}$ is larger by 12 kJmol^{-1} (14%) at pH 6.8 than at pD 6.8, but that the pre-exponential factor is 450 times smaller in the D_2O sample. The differences for the slow S_2 decay are not so pronounced. The pre-exponential factor is found to be 20 times and the activation energy 8 kJmol^{-1} larger at pD 6.8

compared to pH 6.8. In contrast, the activation energies and pre-exponential factors for the fast and slow reduction of the S_3 state are very similar in D_2O and H_2O samples.

pL of the Sample	Reaction	Decay	A, s^{-1}	Ea, $kJmol^{-1}$
pH 6.8	$S_2Y_D^{red} \rightarrow S_1Y_D^{ox}$	fast	$2.70 \cdot 10^{17}$	100
	$S_3Y_D^{red} \rightarrow S_2Y_D^{ox}$	fast	$1.44 \cdot 10^{14}$	83
	$S_2Q_B^- \rightarrow S_1Q_B$	slow	$7.99 \cdot 10^{12}$	82
	$S_3Q_B^- \rightarrow S_2Q_B$	slow	$2.88 \cdot 10^{12}$	80
pD 6.8	$S_2Y_D^{red} \rightarrow S_1Y_D^{ox}$	fast	$5.95 \cdot 10^{14}$	88
	$S_3Y_D^{red} \rightarrow S_2Y_D^{ox}$	fast	$8.27 \cdot 10^{13}$	82
	$S_2Q_B^- \rightarrow S_1Q_B$	slow	$1.48 \cdot 10^{14}$	90
	$S_3Q_B^- \rightarrow S_2Q_B$	slow	$9.55 \cdot 10^{11}$	77
pD 7.6	$S_2Y_D^{red} \rightarrow S_1Y_D^{ox}$	fast	$9.36 \cdot 10^{12}$	78
	$S_3Y_D^{red} \rightarrow S_2Y_D^{ox}$	fast	$2.12 \cdot 10^{11}$	69
	$S_2Q_B^- \rightarrow S_1Q_B$	slow	$1.53 \cdot 10^{12}$	78
	$S_3Q_B^- \rightarrow S_2Q_B$	slow	$6.81 \cdot 10^{9}$	66

Table 4.3.1. Comparison of the activation energy (Ea, $kJmol^{-1}$) and pre-exponential factor (A, s^{-1}) calculated for S_2 and S_3 fast and slow decay in thylakoids from spinach obtained at pH 6.8, pD 6.8 and pD 7.6.

4.3.8 Effect of the H/D isotope exchange on the lifetimes of the S_2 and S_3 states in the OEC of T. elongatus

A similar set of the lifetime measurements was performed on the Y_D^{red} thylakoids from *T. elongatus*.

The rates for the slow relaxation of S_2 and S_3 states through reduction by the acceptor side obtained at pD 7.6 and 20°C are shown on the Figure 4.3.21 (slopes a and b). For this experiment the PS II samples were preflashed twice with Nd:YAG laser with intermediate dark adaptation of 15 min, after which $S_1Y_D^{ox}$ samples were dark adapted for 1 hour at room temperature and then transferred on ice before measurements (slopes a). Slopes b of the Figure 4.3.19 represent the S_2 (diamonds) and S_3 (circles) decays of the $S_1Y_D^{ox}$ thylakoids obtained by illumination under non-saturated conditions and long dark adaptation on ice. As expected, both types of the preflashed thylakoids ($S_1Y_D^{ox}$ thylakoids) exhibited virtually the same rate constants for the slow S_2 and S_3 decay, which are 0.0018 s^{-1} and 0.0014 s^{-1} (slopes a) and 0.0019 s^{-1} and 0.0014 s^{-1} (slopes b), respectively. This confirms our deconvolution procedure for the determination of the rate constants for the slow S - state reduction. Slopes c represent the data obtained with Y_D^{red} samples, i.e. without any preflash procedure. The comparison of the slopes c with a and b clearly

demonstrates that the real slow phase in $S_1Y_D^{red}$ thylakoids from *T. elongatus* cannot be determined in these samples, because it is essentially fully dominated by the fast S state decay through Y_D^{red} (~90% for S_2 and S_3).

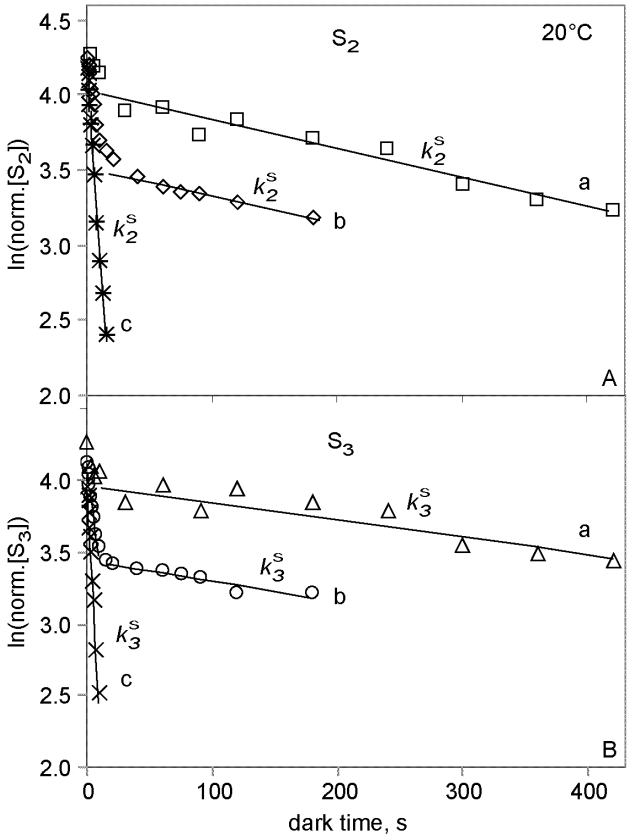

Figure 4.3.21. Semilogarithmic plot of the relative S_2 (A) and S_3 (B) population in $S_1Y_D^{red}$ (c) and $S_1Y_D^{ox}$ (a, b) thylakoids from *T. elongatus* as a function of the dark time between first and second (S_2) or second and third (S_3) flashes in the train of saturating single turnover flashes (slow phase). The samples a and b were pre-illuminated either by Nd:YAG laser (a) or under non-saturated conditions. The samples were incubated in D_2O buffer at pD 7.6 and 20°C.

A similar population of the reduced tyrosine D in the $S_1Y_D^{red}$ thylakoids from *T. elongatus* was also estimated at pH 6.8 (discussed in Chapter 3). Based on this estimation and on the low amount of the slow phase and because rates for the slow decay at pD 7.6 and 20°C is very similar to the previously obtained rate at pH 6.8, (e.g. for S_2 decay 0.0018 s^{-1} and 0.0013 s^{-1}, respectively), the rates for the slow S_2 and S_3 decays obtained at pH 6.8 at the respective temperatures were used for the subtraction of the small fraction of the slow decay in the $S_1Y_D^{red}$ thylakoids from *T. elongatus*.

Figure 4.3.22 shows the semilogarithmic plots of the fast S_2 (A, B) and S_3 (C, D) decays in *T. elongatus* at 10°C and 25°C. In contrast to spinach, the fast S_2 and S_3 decays in *T. elongatus* are both significantly slower in D_2O compared to H_2O. The fast decays of the S_2 (9s/10°C and 1.9s/25°C) and S_3 (8s/10°C and 1.8s/25°C) states are more than two times

slower at pD 7.6 compared to pH 6.8 (3.4s/10°C and 0.8s/25°C for S_2 and 3s/10°C and 0.8s/25°C for S_3). The half-times for the fast S_2 and S_3 decays at pD 6.8 are even slower than at pD 7.6. This is consistent through out the lifetime measurements at all temperatures and half-times of 47s (10°C) and 4s (25°C) for S_2 decay and 38s (10°C) and 4s (25°C) for the S_3 decay were determined from the data shown in Figure 4.3.22.

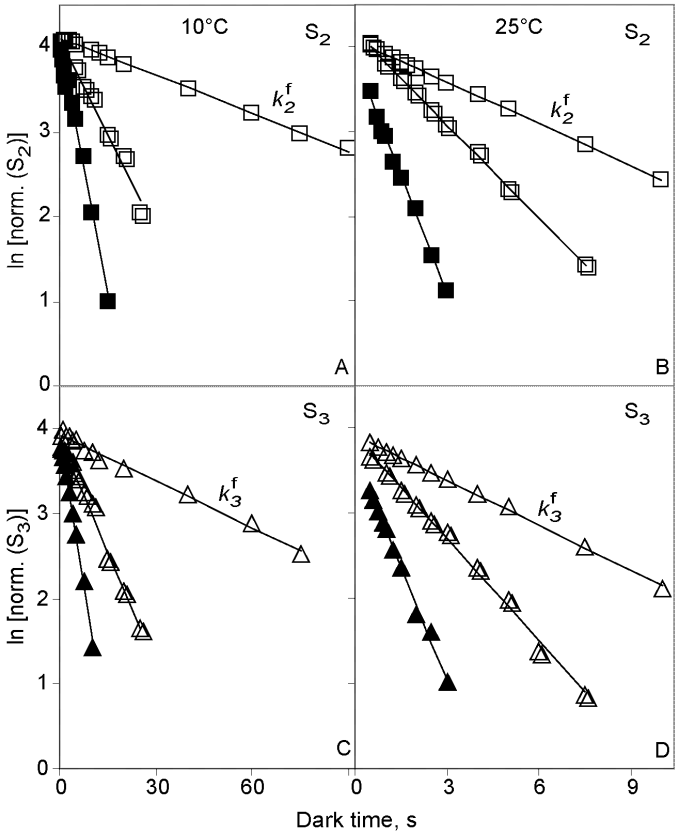

Figure 4.3.22. Semilogarithmic plot of the relative S_2 (A, B; squares) and S_3 (C, D; triangles) population in S_1Y_D thylakoids from *T. elongatus* as a function of the dark time between first and second (S_2) or second and third (S_3) flashes in the train of saturating single turnover flashes. The fast phase obtained after subtraction of the slow phase as described in the text. The samples were incubated either in D_2O at pD 6.8 (open symbols) and pD 7.6 (open double symbols) or H_2O buffer at pH 6.8 (filled symbols) at 10°C (A, C) and 25°C (B, D). The buffers of the corresponding pL are given in Chapter 2.6.4.

pL of the Sample	Reaction	Decay	A, s^{-1}	Ea, $kJmol^{-1}$
pH 6.8	$S_2Y_D^{red} \rightarrow S_1Y_D^{ox}$	fast	$8.23 \cdot 10^{11}$	68
	$S_3Y_D^{red} \rightarrow S_2Y_D^{ox}$	fast	$9.92 \cdot 10^{11}$	68
pD 6.8	$S_2Y_D^{red} \rightarrow S_1Y_D^{ox}$	fast	$3.71 \cdot 10^{16}$	100
	$S_3Y_D^{red} \rightarrow S_2Y_D^{ox}$	fast	$4.83 \cdot 10^{15}$	95
pD 7.6	$S_2Y_D^{red} \rightarrow S_1Y_D^{ox}$	fast	$4.27 \cdot 10^{12}$	75
	$S_3Y_D^{red} \rightarrow S_2Y_D^{ox}$	fast	$3.79 \cdot 10^{12}$	74

Table 4.3.2. Comparison of the activation energy (Ea, $kJmol^{-1}$) and pre-exponential factor (A, s^{-1}) calculated for S_2 and S_3 fast decay in Y_D^{red} thylakoids from *T. elongatus* obtained at pH 6.8, pD 6.8 and pD 7.6.

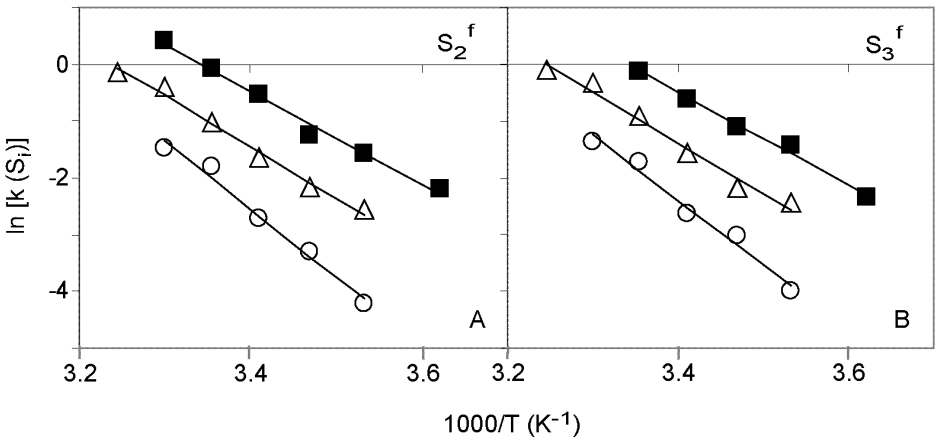

Figure 4.3.23. Semilogarithmic plots of the rate constants of the fast S_2 (A) and S_3 (B) states (Arrhenius type plot) as a function of inverse temperature determined from the S_1Y_D thylakoids from *T. elongatus* incubated either in D_2O at pD 6.8 (circles) and pD 7.6 (triangles) or H_2O buffer at pH 6.8 (squares). The buffers of the corresponding pL are given in Chapter 2.6.4.

The Arrhenius type plots for the $S_2Y_D^{red} \rightarrow S_1Y_D^{ox}$ and $S_3Y_D^{red} \rightarrow S_2Y_D^{ox}$ decays of the S_1Y_D thylakoids from *T. elongatus* incubated at pH 6.8 (control), pD 6.8 and pD 7.6 are presented in Figure 4.3.23. The Arrhenius plots for the D_2O and H_2O samples incubated at pL 6.8 differ significantly between each other and compared to spinach. In contrast to spinach, the activation energies for the fast decay of the S_2 and S_3 states are higher by 40-50% in D_2O. Similarly, the pre-exponential factor is 3-5 orders of magnitude larger in D_2O for both reactions. Interestingly, the activation energies and pre-exponential factors calculated for the fast S_2 and S_3 decays are found to be very similar in D_2O samples at pD 7.6 and H_2O samples at pH 6.8 (Table 4.3.2)

4.4 Discussion

In this Chapter the effect of the H/D isotope exchange on the reactions of OEC at different temperatures and pL values in thylakoids from spinach and *T. elongatus* was studied by measurements and analysis of FIOPs. Two questions were addressed to this study: i) Does H/D isotope exchange affect reactions on the donor and acceptor side of PS II? ii) Are there differences in the effect of H/D isotope exchange on the OEC reactions in thylakoids from spinach and *T. elongatus*?

The effect of the H/D exchange on the acceptor side of PS II can be characterized by the miss and double hit parameters of OEC as well as with the lifetime of slow reduction of the S_2 and S_3 states by the acceptor side. For this purpose the temperature and pL dependence of the slow decay of the S_2 and S_3 states and of the miss and double hit probabilities were studied in thylakoids from spinach and *T. elongatus*.

The results obtained reveal that the miss parameter is larger at pD 6.0 than at pH 6.0, while at pL 7.0 there is virtually no difference observed and at pH 8.0 an opposite feature emerges, i.e. the misses are markedly larger in H_2O compared to D_2O samples. Furthermore, in the alkaline region the miss parameter increases in any case, regardless of H/D exchange. In general, it seems as if the pH dependence of the miss probability in thylakoids is shifted to the alkaline region in D_2O compared to H_2O samples with a more pronounced feature in the acidic region of D_2O samples. These data are in line with a former study [214], where it was also proposed that the enhanced miss parameters in the acidic and alkaline regions are of different origin. In acidic region the increased probability of misses is explained by an increase of the fraction of PS II complex, where $P680^{+\bullet}$ undergoes the recombination with $Q_A^{-\bullet}$ leading to dissipation of oxidizing redox equivalents. On the other hand, in the alkaline region the higher S states seem to be destabilized. It has been suggested that the $P680^{+\bullet}$ reduction by Y_Z in the short nanosecond time domain occurs via a “rocket-type” mechanism where the electron transfer is coupled with a proton shift within a hydrogen bridge between the OH group of Y_Z and a nearby base [224]. The latter group is most likely the imidazole ring of His 190 (His 189 in cyanobacteria) in polypeptide D1 [225-231]. The extent of $P680^{+\bullet}$ reduction by Y_Z further increases in the microsecond time domain by relaxation processes, which give rise to a shift of the equilibrium $P680^{+\bullet}Y_Z \leftrightarrow P680Y_Z^{ox}$ toward the right side [211, 213, 214]. Based

on H/D isotope exchange effects, the relaxation processes were inferred to be coupled with local proton movements [213, 219, 232].

Different mechanisms were discussed in [214] for the interpretation of the pH and pD effects described above. One of them is assumption that extent of ns kinetics of $P680^{+\bullet}$ reduction decrease when the hydrogen bridge between Y_Z and His 190 becomes interrupted owing to the protonation of the imidazole moiety in the moderate acidic region. As a consequence the extent of ns kinetics and concomitantly the probability of dissipative back reaction increases. This idea implies that the pH dependence of the extent of the ns kinetics in the moderate acidic region reflects the pK-value of the imidazole group of His 190. Accordingly, a pK value of about 5 emerges for the imidazolium ↔ imidazole equilibrium that is markedly lower than that (pK = 6) known for the formation of the imidazolium state of His in solution. It is conceivable that the protonation of a hydrogen bonded imidazole ring is more difficult and therefore pK shifted toward lower values. Additionally, depending on the strength of the hydrogen bonding also the pK value of Y_Z is expected to decrease [233], where the pK value of hydrogen-bonded Y_Z was estimated to be 8.0-8.3. Although [233] used samples, which do not contain Mn cluster, the general tendency of a shift toward lower values of the pK of Y_Z and His 190 in can be also expected for the native state of PS II [214].

Alternative interpretation of pH effect on the extent of ns kinetics of $P680^{+}$ reduction is an allosteric interruption of the hydrogen bridge with Y_Z by proton – induced release of Ca^{2+}. A detachment of Ca^{2+} from its binding sites due to protonation of ligands in the acidic region has been discussed recently and a pK value of ~4.7 was estimated from measurements of pH-dependent Ca^{2+} release from PS II membrane fragments [234]. This effect could lead to conformational changes, which disturb the H-bonding geometry between Y_Z and His 190 and thereby block the “rocket-type” mechanism of $P680^{+\bullet}$. Accordingly, pH-induced Ca^{2+} release would lead to interruption of this chain and/or conformational changes, which disturb the interaction between Y_Z and His 190 [214].

The pH dependent regulation of $P680^{+\bullet}$ reduction in the moderately acidic range is probably of physiological relevance because the thylakoid lumen becomes acidified under strong light and attains pH values of about 5 or even lower [214]. Therefore, the pH region between 5 and 8 is the most relevant when considering in vivo conditions [214].

A different mechanism has to be responsible for an increase of the miss parameter in the moderate alkaline region. The previously published results of [214] and [235] clearly show, that the contribution of nanosecond kinetics to the overall $P680^{+\bullet}$ reduction remains almost insensitive to a pH shift from 6.5 to 8.0. Furthermore, the results of this Chapter

show that the H/D kinetic exchange effects on the miss parameter becomes reversed at around 7.0, which is in line with [214]. These authors also showed that the period-four-oscillation patterns of the amplitudes of nanosecond kinetics exhibit almost the same damping at 5.0 and 8.0 for H_2O samples and at pD 6.5 for D_2O samples. The corresponding miss parameters gathered from FIOPs are markedly larger than those of the control (this work and [214]). Therefore, it is clear, that the general dependence of the $P680^{+\bullet}$ reduction by Y_Z on the redox state S_i of the OEC that are reflected by the period-four-oscillation of the extent ns kinetics remain almost the same at different types of modulation induced either by pH shift (to 5.0 or 8.0) or by H/D isotope exchange at pH 6.5. The conclusion that the average extent of the very fast electron transfer from Y_Z to $P680^{+\bullet}$ via the rocket-type mechanism is affected only in the acidic region leads to the conclusion that in the near alkaline region the increase of the miss parameter can be caused either by retardation of the slower relaxation processes in a similar way as recently shown for replacement of exchangeable protons by deuterons at pL 6.5 [213, 214] or due to an alternative mechanism [214].

However, it should be mentioned that there are some differences in the H/D effect observed in thylakoids from spinach and *T. elongatus*. In particular, the increase of the miss parameter in thylakoids from *T. elongatus* is much more pronounced in the alkaline region than that of spinach. Although basically the same mechanism can be proposed for the both organisms, additional effects seem exist in case of *T. elongatus* (for further discussion see Chapter 5).

The tyrosine D had been reported to act extremely slowly under H/D isotope exchange [127], which is in line with results presented in this Chapter. One of the possible mechanisms for such kind of slow kinetics can be related to the exchangeable proton coupling in the vicinity of Y_D.

CHAPTER 5

Effect of pH 8.0 on the Dark Stability of the Tyrosine Radical Y_D^{ox} in PS II of *Thermosynechococcus elongatus*

5.1 Introduction

pH induced changes in spinach PS II have been studied previously by several groups. It is well known that pH values above pH 8.5 – 9.0 cause irreversible damage in PS II [236, 237], however, no significant changes have been observed up to pH 7.8 [107]. These results were recently further extended by determining of pK values for the individual S state transitions [237]. These authors report that the $S_1 \rightarrow S_2$ transition is essentially pH independent, while all other transitions are blocked with apparent pK's of 4.0 – 4.7 and $\geq$ 8.0. On the basis of the analysis of FIOPs and S states lifetime measurements obtained at various pH values it was concluded that spinach PS II undergoes structural changes with characteristic pH values of 5.0 – 5.5 and 6.5 – 7.0 [109]. These results were further extended by studying the pH dependence of the reaction rates of the S_1 state by hydrazine or hydroxylamine. Based on the results obtained three transitions were identified with characteristic pH values of 5.3 – 5.5, 6.2 – 6.5 and above 7.4 [238].

Based on the measurements of flash induced absorption changes in the UV it was inferred that in the alkaline pH the S_1 state of the OEC becomes highly destabilized and reduces to S_0 in PS II membrane fragments from spinach. This idea was later questioned by measurements of FIOPs and the effect ascribed to a fast S_2 and/or S_3 decay by Y_D^{red} during the time between the first flashes [111]. However, so far it is not clear whether or not the stability of S_1 and /or Y_D^{ox} at alkaline pH is a general property of PS II in all oxygen evolving organisms, i.e. cyanobacteria and plants. In order to clarify this problems flash induced oxygen evolution patterns (FIOPs) were measured at pH 7.0 and 8.0 by using thylakoids isolated from *T. elongatus* and spinach. Data analysis within the framework of an extended Kok model reveal that Y_D^{ox} in *T. elongatus* is significantly less stable at pH 8.0 than at pH 7.0 and also compared to spinach thylakoids at pH 8.0. No indications were found for a destabilizing of the S_1 state.

5.2 Experiments and analysis

5.2.1 Sample preparation

For control experiments at neutral pH the samples were diluted to [Chl] = 0.15 mM (*T. elongatus*) or 1 mM (spinach) with MCMH buffer (400mM Mannitol, 20 mM $CaCl_2$, 10 mM $MgCl_2$ and 50 mM Hepes/NaOH) and adjusted to pH 7.0 at the temperatures given in the text. For experiments at pH 8.0 samples were first washed (1:12 dilution) with MCMT buffer (400mM Mannitol, 20 mM $CaCl_2$, 10 mM $MgCl_2$ and 50 mM Tricine/NaOH at pH 8.0/5°C) or MCMH buffer (pH 8.0/20°C) and incubated for 3 minutes in the dark and on ice. Then samples were centrifuged in minifuge ("Micro 7", Fisher Scientific inst.) at 9 000 rpm/5min/4°C and resuspended to the initial volume with the same pH 8.0 buffer. Thereafter thylakoids were diluted to [Chl] = 0.15 mM (*T. elongatus*) or 1 mM (spinach) with MCMT or MCMH buffer, which had been adjusted to pH 8.0 at the measuring temperature of the FIOPs.

For oxygen evolution measurements two kinds of samples were used: i) $S_1Y_D^{red}$*-samples* containing a high percentage of the reduced form of tyrosine D, Y_D^{red}, due to long term storage at –70°C [97, 105, 106, 113, 207] and ii) $S_1Y_D^{ox}$*-samples* which were preflashed and dark-adapted to oxidize Y_D in most centers. Because of the very slow S_2-state decay in *T. elongatus* thylakoids (Chapter 3, [100]), these samples had to be preflashed and dark-adapted in glass vials. To ensure oxidation of most Y_D in the *T. elongatus* thylakoids under these conditions, the *T. elongatus* samples were flashed twice in 50 µL aliquots ([Chl] = 0.15 mM) by a frequency doubled Nd:YAG Laser (532 nm, 800 mJ/pulse). These two pre-flashes were separated by a dark-adaptation time of 15 min at room temperature. Afterwards, the samples were kept in the dark at room temperature for one hour and then stored on ice until the FIOP measurements were performed. For all FIOP measurements the polarization of – 750 mV was switched on 40s before the flash train.

5.2.2 Data analysis

The first 16 flashes of each FIOP were analyzed using an Excel spreadsheet that was based on an extended Kok model, which includes $S_2Y_D^{red} \rightarrow S_1Y_D^{ox}$ and $S_3Y_D^{red} \rightarrow S_2Y_D^{ox}$ reactions (discussed in Chapter 3.2.4).

For graphical representation all data and fits were normalized to one quarter of the sum of the 1^{st} to the 16^{th} flashes of the FIOPs, which corresponds to the release of one oxygen molecule per OEC.

5.3 Results

Figure 5.3.1 shows normalized FIOPs of $S_1Y_D^{ox}$ thylakoids from *T. elongatus* recorded after 5 minutes of dark adaptation on the Joliot-type electrode at 10°C (A) and 30°C (B). The open symbols show data of $S_1Y_D^{ox}$ thylakoids at pH 7.0, while the filled symbols represent measurements with similarly pre-treated samples at pH 8.0. At 10°C and pH 7.0 a typical flash induced oxygen evolution pattern (FIOP) is observed with maxima after the 3rd, 7th and so forth flashes. This damped period four oscillations is well understood within the framework of the conventional Kok – model, where miss (α) and double hit (β) probabilities lead to a dephasing of the S - state populations (see Chapter 1.5.1).

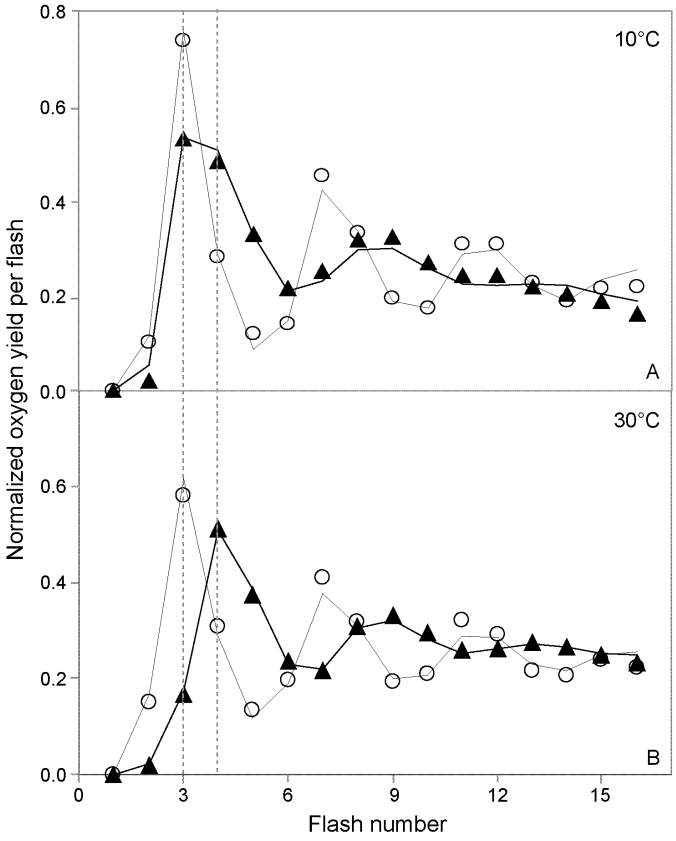

Figure 5.3.1. Normalized oxygen yield per flash from $S_1Y_D^{ox}$ thylakoids from *T. elongatus* as a function of flash number in a train of saturating single turnover flashes at 10°C (A) or 30°C (B) at pH 7.0 (dashed line and open circles) or pH 8.0 (solid line and filled triangles). The symbols represent measured data while the lines are calculated by fit approach C (see Chapter 5.2 and Table 5.3.1).

A simple phenomenological parameter for the characterization of these oscillations is the ratio of the oxygen yields due to the 3rd and 4th flash (Y_3/Y_4). In case of a low miss parameter and high initial S_1 population the Y_3/Y_4 ratio is about 4 - 5 for spinach PS II

thylakoids and up to 4 for *T. elongatus* [100, 108]. At pH 7.0 (open symbols) the period-four-oscillation with its first maximum after the 3rd flash is largely retained at 30°C. The small differences in the Y_3/Y_4 ratio between the FIOPs measured at 10°C and 30°C (pH 7.0) are consistent with our recently published data [100] and can be explained by a small increase of the miss parameter and the same contribution of Y_D. In marked contrast, the changing of pH from 7.0 to 8.0 has a much more dramatic effect on *T. elongatus* thylakoids than the described temperature rise at pH 7.0 (filled triangles). At 10°C the Y_3/Y_4 ratio is drastically reduced at pH 8.0, but the first maximum still occurs after the 3rd flash. This reduction of Y_3/Y_4 ratio is even more pronounced at 30°C, where the first maximum is clearly shifted to the 4th flash. Such a change cannot be explained by a simple increase of the miss parameter, but additional factors need to be taken into account.

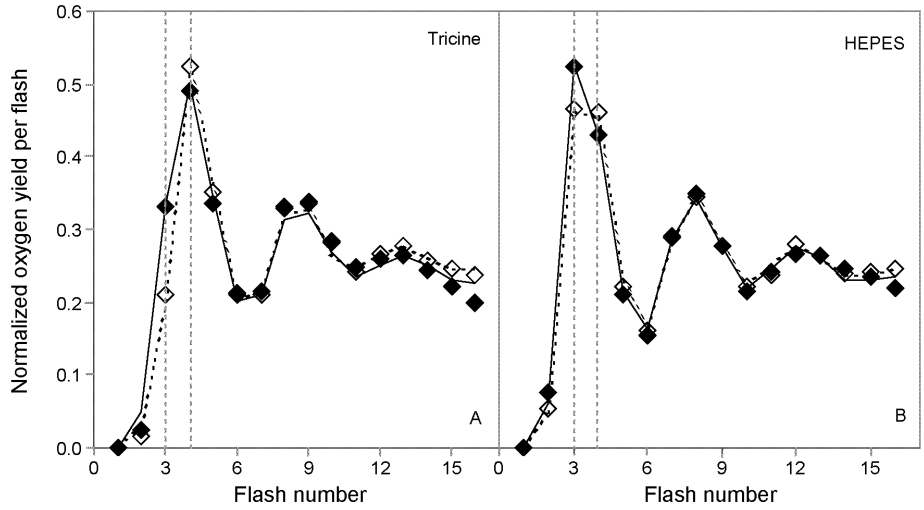

Figure 5.3.2. Normalized oxygen yield per flash of $S_1Y_D^{ox}$ thylakoids from *T. elongatus* as a function of the flash number in a train of saturating single turnover flashes at 20°C and pH 8.0. The measurements were performed either in MCMT buffer (Tricine buffer, A) or MCMH buffer (HEPES buffer, B) and at flash frequencies of 2Hz (solid lines, filled symbols) or 1 Hz (dashed line, open symbols). The symbols represent the data, while the lines are fits calculated by approach C of Table 5.3.1. For details see Chapter 5.2 and Table 5.3.1.

At a first glance two different effects may account for this shift of the first maximum: a) a reduction of S_1 to S_0 in the dark time before the flash train or b) a fast reduction of the S_2 state by a one-electron donor such as Y_D during the dark time between the first flashes of the flash train. In the former case no significant changes in the FIOPs should occur if the flash frequency or measuring temperature is varied, while the 2nd mechanism predicts clear changes in the Y_3/Y_4 ratio as a function of these parameters. In an attempt to distinguish between these two alternatives, FIOPs were measured at different dark times between the flashes of the train. Figure 5.3.2 **A** shows for 20°C/pH 8.0 that at a frequency of 1Hz (open

symbols) the ratio of Y_3/Y_4 (0.4) is markedly smaller than that measured at 2Hz (filled symbols) with $Y_3/Y_4 = 0.7$.

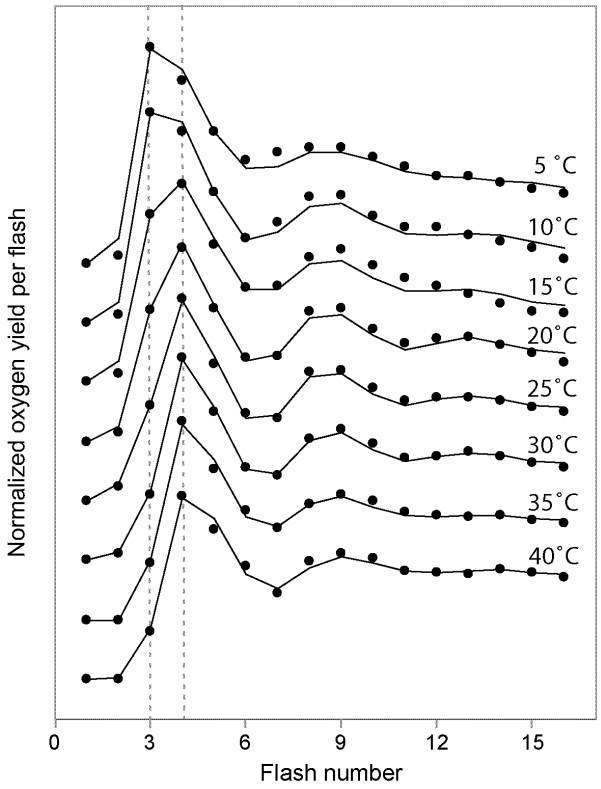

Figure 5.3.3. Normalized oxygen yield per flash of $S_1Y_D^{ox}$ thylakoids from *T. elongatus* as a function of flash number in a train of saturating single turnover flashes (2Hz) at pH 8.0. The symbols represent measured data, while the lines are calculated by fit approach C data. For details see Chapter 5.2 and Table 5.3.1.

This effect can be even better illustrated when the measuring temperature is varied at 2 Hz flash frequency. Figure 5.3.4 shows that the Y_3/Y_4 ratio continuously decreases with measuring temperature and that an almost complete shift by one flash number occurs between the 5°C and the 40°C patterns. This feature cannot be explained by a drastic increase of the misses because this parameter was recently shown to exhibit nearly the same value at 10°C and 35°C in thylakoids from *T. elongatus* [100]. Therefore, a one-electron reduction of the S_2 and/or S_3 states between the first flashes of the flash train provides the most plausible explanation for our observations.

On the basis of a comparison with earlier data obtained with spinach thylakoids after incubation with chaotropic agents [208], it appears possible that at pH 8.0 Y_D^{ox} becomes reduced during the one hour dark time after the preflashes and can then act as the one-electron reductant. This idea is strongly supported by our finding of virtually identical FIOPs for $S_1Y_D^{red}$ and $S_1Y_D^{ox}$ thylakoids at pH 8.0, while at pH 7.0 the FIOPs are clearly different for these sample types (data not shown).

The experiments reported so far in this study were performed in 50mM HEPES buffer at pH 7.0 and in 50mM Tricine at pH 8.0. To check whether or not also the chemical nature of the buffer contributes to the observed pH effects, we also measured FIOPs of preflashed *T. elongatus* in HEPES buffer at pH 8.0. Figure 5.3.2 **B** shows that in spite of the fact that the Y_3/Y_4 ratio is somewhat higher in HEPES buffer compared to that measured with samples suspended in Tricine buffer (Figure 5.3.2 **A**) it is still small and remains dependent on the flash frequency (compare open and filled symbols in Figure 5.3.2 **B**).

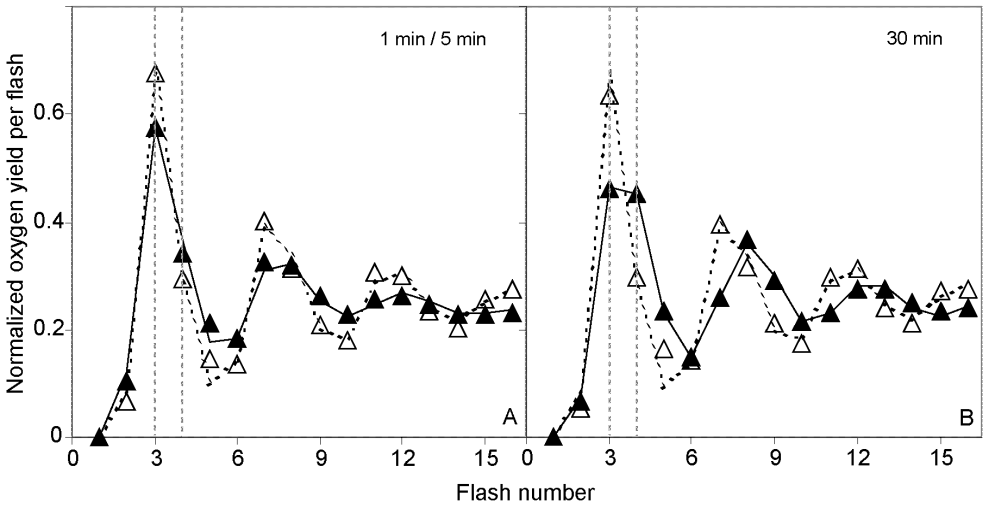

Figure 5.3.4. Normalized oxygen yield per flash as a function of the flash number in a train of saturating single turnover flashes in $S_1Y_D^{ox}$ thylakoids from spinach (dashed line, open symbols) and *T. elongatus* (solid line, filled symbols). The data were obtained at 20°C and pH 8.0 after (A) 1 min (*T. elongatus*) or 5 min (spinach) and (B) 30 min of the dark adaptation time on the electrode. Polarization was always switched on 40s prior to the flash train. For further details see Chapter 2.7.2 - 2.7.3 and Table 5.3.1.

To further test the Y_D^{red} hypothesis and to quantify these observations we analyzed our data in the framework of the extended Kok model described in Chapter 2.7.2 - 2.7.3. This model takes into account the fast back reactions of Y_D^{red} with the S_2 and S_3 states. Fit 1 of Table 5.3.1 shows that a reasonable fit quality can be obtained for the FIOPs of *T. elongatus* at pH 7.0 and 20°C if one only uses the miss (α) and double hit probabilities (β), the damping parameter (not shown on the Table 5.3.1, but always 0.97 ± 0.01) and the S_1 population as free parameters. As expected, a similar fit is not possible for the FIOP of *T. elongatus* obtained at pH 8.0/20°C (fit 2 in Table 5.3.1 and Figures 5.3.2 **A**, filled symbols). Fit 3 shows that the pattern at pH 8.0 can in principle be fit by including S_0, but as explained above, this option can be excluded on the basis of the dependencies of the FIOPs on flash frequency and temperature. Fit approaches C and D both include the fast reactions of Y_D^{red} with the S_2 and S_3 states. For the sake of simplicity and because these rates are usually found to be very similar at pH ≥ 6.5 (see [109]; also Table 5.3.2 for values at pH 6.8), they are set to be identical for all fits, i.e. $k_3^f = k_2^f$.

Fit number	Sample description	Fit approach	Fit Parameters						Goodness of fit	
			α %	β %	S_1 %	S_0 %	Y_D^{red} %	$k_{2,3}^f$ s^{-1}	dy_n^2 ($\times 10^{-6}$)	fq ($\times 10^{-6}$)
1	*T. elongatus* pH 7.0, 20 °C	A	13.1	5.7	100				438	36.5
2	T. elongatus	A	39.5	3.5	100				1531	117.7
3	pH 8.0 in:	B	22.2	4.2	40.7	59.3			192	17.5
4	Tricine / 2Hz	C	19.8	6.6	100*		100*	1.1	170	14.2
5		D	52.7	2.4	100*		100*	1.0	99	8.2
6	Tricine / 1Hz	C	19.8*	6.6*	100*		100*	1.1*	193	
7		D	52.7*	2.4*	100*		100*	1.0*	410	
8	HEPES / 2Hz	C’	15.3	6.7	100*		57.4	1.1*	74	6.1
9		D’	40.9	4.6	100*		63.4	1.0*	187	15.6
10	HEPES / 1Hz	C’	15.3*	6.7*	100*		51.9	1.1*	19	
11		D’	40.9*	4.6*	100*		54.3	1.0*	109	

Table 5.3.1. Different fit approaches of the FIOPs of $S_1Y_D^{ox}$ thylakoids *T. elongatus* measured at 20°C and pH 7.0 or pH 8.0 (see Fig. 5.3.1). For fit approaches A-C a Kok model with S state independent miss and double hit probabilities was used. In fit approach D only the miss parameter (α) for $S_2 \rightarrow S_3$ transition was varied, while the miss parameters for all other transitions were fixed to 0. If no values are given for a parameter, it was excluded from the fit. Stars indicate that a parameter was fixed to the specified value. The goodness of fit parameters was calculated as described in Chapter 2.7.2 - 2.7.3.

The precise percentage of reduced Y_D in the presented samples is unknown, but the shift of the FIOP by one flash number observed in Figure 5.3.4 is clearly indicative for a virtually full dark reduction of Y_D at pH 8.0, regardless of the preflash treatment. Therefore, in the following Y_D^{red} was fixed to 100%. Similarly, also the S_1 population was fixed to 100% because of the applied preflash protocol. The only difference in approaches C and D is that for C we assume an S – state independent miss parameter, while for D we consider an S – state dependent miss parameter.

As an extreme example of an S state dependent miss parameter, all misses occur during the $S_2 \rightarrow S_3$ transition [100, 111]. Fit 4 applies approach C and achieves a very good fit quality with a rate constant $k_2^f = 1.1\ s^{-1}$. A very similar result ($k_2^f = 1.0\ s^{-1}$) is also obtained in fit 5 using approach D. Fit 5 has a smaller fit error (dx^2), mainly because approach D describes the oxygen yield of the second flash better than approach C. In a good approximation both the miss and double hit parameters are independent of the flash frequency. Similarly, the percentage of Y_D^{red} and the rate constants for the reactions $S_2Y_D^{red} \rightarrow S_1Y_D^{ox}$ and $S_3Y_D^{red}$

→ $S_2Y_D^{ox}$ are sample properties and therefore unaffected by the frequency of the flash train. Therefore, if the above fits 4 and 5 are "correct", then it should be possible to describe the flash patterns obtained at 1 Hz (Figure 5.3.2 **A**, open symbols) by simply changing the dark time between flashes in the fit program. The moderate increase of the fit errors (dx_i^2) of fit 7 compared with fit 5 and especially the almost vanishing difference of dx_i^2 between fits 4 and 6 clearly shows that this is indeed possible. The only parameter that was optimized in fits 6 and 7 is the damping factor, which can be expected to be somewhat larger (closer to 1.0) at lower flash frequencies, since there is more time to reoxidize the plastoquinone pool between the flashes. This "frequency check" strongly supports fits 4 and 5 and allows us to apply fit approaches C and D also to the data of Figures 5.3.2 **B** and 5.3.3.

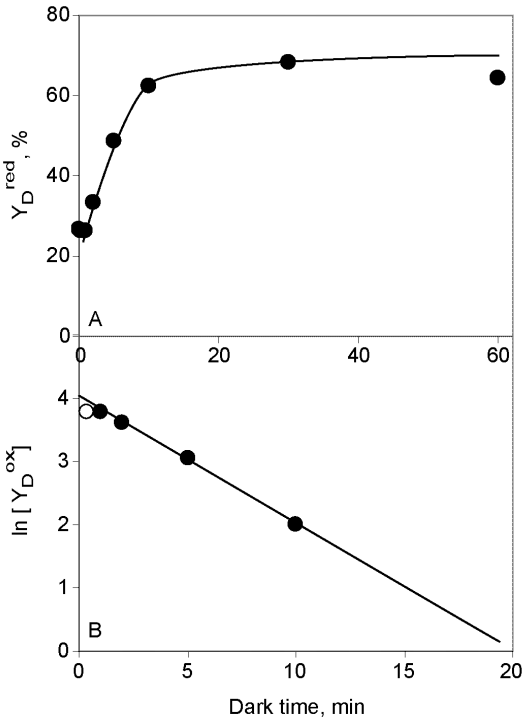

Figure 5.3.5. **A** – Percentage of Y_D^{red} as a function of the dark adaptation time on the electrode after a preflash used to generate $S_1Y_D^{ox}$ thylakoids from *T. elongatus* at 20°C and pH 8.0; **B** – Semilogarithmic plot of the fast decay of Y_D^{ox} as a function of the dark adaptation time on the electrode. These data were calculated from Figure 5.3.5 **A** by subtraction of the slow phase of Y_D^{ox} reduction.

The FIOPs measured in the presence of HEPES buffer exhibit a somewhat larger Y_3/Y_4 ratio than in Tricine buffer at the same pH (Figure 5.3.2 **A** and **B**). Fits 8 and 10 reveal that this is due to a lower miss parameter (15.3% vs. 19.8%) and a lower percentage of reduced Y_D in the sample, which was found to be between 50-65% in HEPES instead of 100% in Tricine buffer. For fits 8 and 10 the rate constant k_2^f was fixed to the value determined for the Tricine samples.

Temperature, °C	pH 8.0		pH 6.8	
	fit C $k_3^f = k_2^f$, s^{-1}	fit D $k_3^f = k_2^f$, s^{-1}	fit C k_3^f, s^{-1}	fit C k_2^f, s^{-1}
5	0.32	0.40	0.10	0.110
10	0.51	0.56	0.24	0.20
15	0.82	0.79	0.33	0.28
20	1.10	1.00	0.54	0.59
25	1.68	1.45	0.88	0.92
30	2.73	1.91	1.43	1.50
35	(9.43)	2.34	2.22	2.21
E_A, $kJmol^{-1}$	58	42	69	68
A, s^{-1}	3.2×10^{10}	4.0×10^{7}	9.9×10^{11}	8.2×10^{11}

Table 5.3.2. Comparison of the rate constants of the fast S_2 and S_3 reduction by Y_D in thylakoids from *T. elongatus* measured at pH 8.0 and pH 6.8. Values for the rate constants at pH 8.0 were calculated from the temperature dependence of FIOPs measured at pH 8.0 (Figure 5.3.3). These fits were performed by using approaches C (equal misses) and D (all misses zero except for the $S_2 \rightarrow S_3$ transition). In both cases we set $k_3^f = k_2^f$. Rate constants, activation energies (E_A) and pre-exponential factors (A) for the fast S_2 and S_3 decays at pH 6.8 were gathered from S_2 and S_3 lifetime measurements reported in [100] and Chapter 3.3.3.

This assumption is justified by the very similar levels of reduced Y_D obtained in the fits of the FIOPs measured at 1 Hz and 2 Hz (compare fits 8 and 9 with 10 and 11, respectively). Based on the above described finding, the temperature dependent changes in the FIOPs depicted in Figure 5.3.4 can now be used to determine the 'average' rate constant for the fast decays of the S_2 and S_3 states between 5°C and 40°. The values obtained are compiled in Table 5.3.2 and in the Arrhenius type plot of Figure 5.3.6.

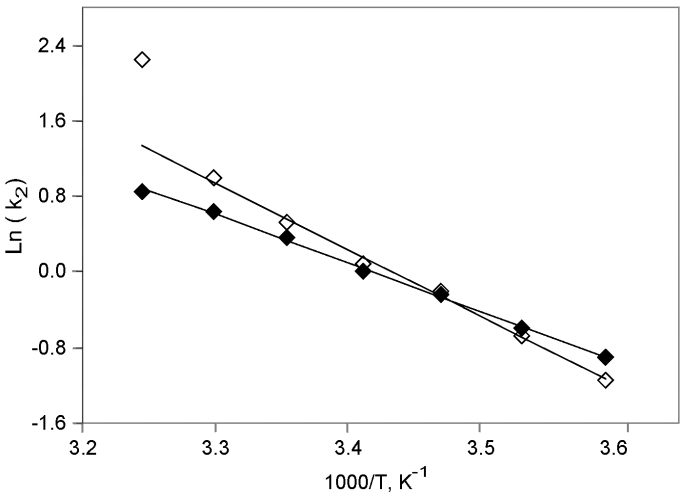

Figure 5.3.6. Arrhenius type plot of rate constants calculated by fit approaches C (open symbols) and D (filled symbols) for the fast S_2 and S_3 decay through reduction by Y_D measured at pH 8.0. For both fit approaches the restriction $k_2^f = k_3^f$ was used. For details see text.

The above data clearly show that in *T. elongatus* the tyrosine radical Y_D^{ox} is significantly less stable at pH 8.0 than at pH 7.0. In order to obtain an estimate on the rate of the Y_D^{ox} reduction we preflashed $S_1Y_D^{red}$ thylakoids from *T. elongatus* and spinach on the electrode and measured FIOPs after various dark times ranging between 2s and 60 minutes. Because the $S_1Y_D^{red}$ thylakoids from *T. elongatus* have a population of Y_D^{red} at pH 8.0 close to 100%, about 90% of the S state had decayed back to S_1 state already after 2s and 100% S_1 population was reached after 1 minute. For spinach thylakoids a dark time of 5 min was required for complete decay of the S_2 state. Figure 5.3.4 **A** shows that under these conditions quite similar FIOPs are obtained for spinach and *T. elongatus* thylakoids even at pH 8.0. While the spinach FIOP is hardly effected by a 30 min dark time compared to 5 min, a significant decrease in the Y_3/Y_4 ratio is seen for *T. elongatus*. These data are fully consistent with a rapid reduction of Y_D^{ox} in *T. elongatus*, while Y_D^{ox} appears to be more stable in spinach. The latter result is in line with a $t_{1/2}$ of 200 min at pH 8.0 and 20°C obtained with EPR experiments for Y_D^{ox} PS II membrane fragments [107].

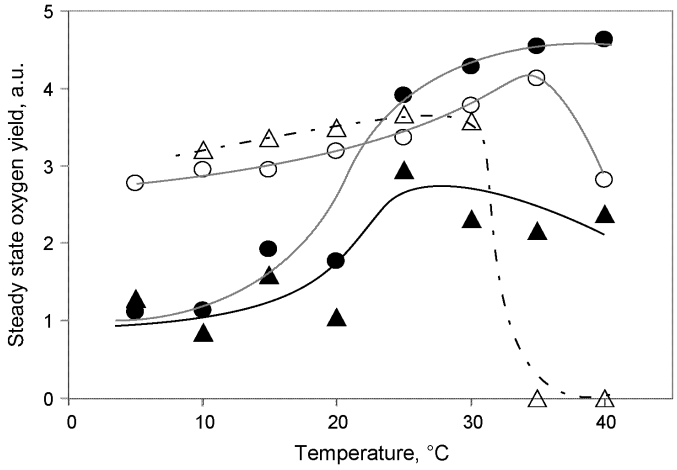

Figure 5.3.7. Steady state oxygen yields of *T. elongatus* (filled symbols) and spinach (open symbols) thylakoids at pH 7.0 (circles) and pH 8.0 (triangles) as a function of temperature. The steady state oxygen yields were calculated as the average of the oxygen yields induced by flashes 9 to 16. The samples were incubated on the Joliot-type electrode for 3 min (spinach) or 5 min (*T. elongatus*) at the indicated temperatures. The pH was adjusted to the given values at measuring temperatures.

The analysis of these FIOPs with the extended Kok model yields Y_D^{red} populations that are given in Figure 5.3.5 **A**. It can be seen that under these conditions ~70% of Y_D^{ox} are reduced within 10 min, while the remaining ~30% are reduced with significantly slower lifetimes. From the semilogarithmic plot on Figure 5.3.5 **B** a halftime of 3-4 min can be extracted. The instability of Y_D^{ox} raises questions on possible structural changes occur in thylakoids from *T. elongatus* at pH 8.0 that could also affect the oxygen evolving capacity of the PS II complexes. To address this point the steady state oxygen yields were

determined, which were calculated as the average of the oxygen yields of the flashes 9 to 16, as a function of measuring temperature at pH 7.0 and pH 8.0. The results obtained are depicted in Figure 5.3.7. At both pH values *T. elongatus* thylakoids (filled symbols) exhibit a pronounced increase of their steady state oxygen yields around 20°C. However, while the values are very similar for pH 7.0 and pH 8.0 between 5°C and 15°C, the rise is smaller by a about a factor of two at pH 8.0. Furthermore, the value of the steady state yields even starts to decline between 30°C and 40°C. As a consequence of these findings it is concluded that at pH 8.0 the optimal performance of PS II in *T. elongatus* thylakoids is diminished, especially at temperatures above 15-20 °C. For comparison also data for spinach thylakoids are shown (open symbols). Although the absolute values cannot be compared between the two species because of i) different chlorophyll concentrations and ii) different sedimentation properties, the relative temperature dependencies should not be affected by these parameters. In the temperature range of 5°C to 30°C spinach thylakoids show only a weak increase of the steady state yields at pH 7.0 and pH 8.0 (a more pronounced temperature dependence was observed at pH 6.0; data not shown). In this temperature range also very similar steady state oxygen yields are observed at both pH values. However, at higher temperatures a steep drop of the O_2 yields occurs, which is caused by the known destruction of the OEC that is coupled with the release of Mn^{2+}. Interestingly, the susceptibility to alkaline OEC impairment is S state dependent. The half-inhibition temperature for a 3 min incubation at the indicated temperatures is > 40°C at pH 7.0 and ~32°C at pH 8.0. For a comparison with the thermophilic cyanobacterium the corresponding value for thermal degradation after 3 min incubation was found to be 40°C in spinach thylakoids at pH 7.0 [239].

5.4 Discussion

The data of this study reveal that the flash induced oxygen patterns (FIOPs) of *T. elongatus* drastically differ at pH 7.0 and 8.0. The fits of the FIOPs with an extended Kok model show that all data gathered at pH 8.0 can be consistently described when taking into account the possibility of fast reductions of the S_2 and S_3 states by a single one-electron donor in PS II that cannot recover during a sequence of 16 saturating Xe-flashes with a dark time of 0.5s between each flash (Figures 5.3.1 – 5.3.3 and Table 5.3.1). This behavior is the typical fingerprint for the reduction of the S_2 and S_3 states by the reduced form of tyrosine D, Y_D^{red}. This assignment is further supported by a) the similarity of rate constants for the fast decay at pH 7.0 and pH 8.0 (depending on temperature two to four times faster rates are observed at pH 8.0 than at pH 7.0; see Table 5.3.2) and b) the finding that, in contrast to pH 7.0, the FIOPs of preflashed and non-preflashed samples exhibit only small differences after a one hour dark-adaptation of *T. elongatus* thylakoids at room temperature in a pH 8.0 buffer. Taken together, these data unequivocally show that Y_D^{ox}, which is normally stable for several hours at room temperature [107], becomes largely reduced within an one hour dark incubation at pH 8.0.in *T. elongatus* thylakoids

In a previous study with spinach thylakoids [109] such a rapid reduction of Y_D^{ox} as in the present experiments was not observed. The data in Figure 4 support this idea and suggests that at pH 8.0 Y_D^{ox} is more stable in spinach thylakoids than in *T. elongatus* thylakoids. This phenomenon could be a consequence of the environmental differences of Y_D^{ox} between cyanobacteria and higher plants, i.e. Y_D^{ox} seems to form two hydrogen bonds in *Synechocystis* but only one in spinach [233]. The conclusion of destabilization of Y_D^{ox} at alkaline pH is in line with former EPR data (signal IIa), where Y_D^{ox} was shown to be reduced with a halftime of about 200 min at pH 8.0 and 20°C in spinach PS II membranes [107]. The EPR experiments also revealed a significant destabilization of Y_D^{ox} in the alkaline compared to the pH range of 4.7 – 7.2, where the half-time is 9 – 10h. On the basis of these findings, this faster reduction was inferred to originate from a destruction of the OEC owing to the loss of Mn and extrinsic proteins, which concomitantly destroys the hydrophobic pocket around Y_D^{ox} that is normally responsible for extreme stability of this radical. Although this explanation cannot be ruled out for the EPR data on PS II membranes, for two reasons the even faster Y_D^{ox} reduction observed in this study in *T. elongatus* thylakoids is clearly not correlated with a loss of the functional Mn: i) our

oxygen measurements detect only the properties of PS II with an intact OEC and ii) the data of Figure 7 indicate that no irreversible damage of the oxygen evolving capacity occurs at pH 8.0 in the time domain, where the fast ($t_{1/2}$ = ~ 4min) Y_D^{ox} reduction is observed. Alternative explanations could imply the loss of specific extrinsic proteins or the deprotonation of a group in the vicinity of Y_D^{ox}. In the latter case His-H^+-190 of the D2 protein would be a possible candidate since His-190 of polypeptide D2 (His-189 in cyanobacteria) is postulated to form a hydrogen bond with the OH group of Y_D and likely accepts its proton upon oxidation. The pK value for the structural change or specific deprotonation can be roughly estimated to be 7.5 since at pH 7.0 mostly slow reduction occurs, while at pH 8.0 about 70% of the centers display the fast reaction. The idea of conformational changes at the PS II donor side is supported by several findings indicating higher susceptibility to exogenous reductants [238], trypsin attack [240], Cl^- binding [241] in thylakoids or PS II membrane fragments from higher plants. The present results suggest that this might be a general feature of PS II that also occurs in cyanobacteria.

In some of our fits a model was used, where only the $S_2 \rightarrow S_3$ transition is affected by misses, while all other S – state transitions proceed with 100% efficiency. This is a very extreme case of the S state dependent misses and an over simplification of the real situation. Nevertheless, in many cases a better fit is reached with this kind of approach. It is worth mentioning that a similar phenomenon has been observed in former studies on the effect of alkaline pH on the FIOP of PS II membrane fragments [111].

In summary, we have shown that the drastically different pattern of the FIOPs at pH 8.0 does not reflect a significant dark population of redox state S_0 of the OEC but rather indicates that the tyrosine radical Y_D^{ox} becomes very unstable in PS II from *T. elongatus* in the alkaline pH. This phenomenon may be caused by a structural modification of PS II that does not affect the functional integrity of the OEC or may originate from a specific deprotonation near Y_D^{ox} that occurs with an apparent pK_a of about 7.5. In contrast to previous conclusions [242], the results of this Chapter do not support the idea that alkaline pH destabilizes S_1 in favor of S_0.

CHAPTER 6

Temperature Dependence of the S_1 Reduction by Hydroxylamine Hydrochloride in Spinach Thylakoids

6.1 Introduction

The S_{-1} redox state, which is not part of the Kok cycle, was first described by [243]. She discovered that exogenous reductants like hydroxylamine can induce a two-electron shift of the first maximum of oxygen evolution from the 3rd to 5th flash.

It is now widely accepted, that exogenous reductants like hydrazine and hydroxylamine can reduce the Mn ions of the water oxidase during dark incubation [47, 244, 245]. This view is supported by: (i) the slow reactions that lead to the shift [118, 246], (ii) the fact that the two-electron shift cannot be reversed by removal of hydroxylamine or hydrazine from the sample [108, 245, 247], (iii) the finding that S_{-1} can be oxidized by Y_D^{ox} to S_0 [108], and (iv) Mn K-edge shifts toward lower energy observed after incubation of the dark-adapted PS II core particles with hydroxylamine [180, 181].

The aim of this study was to characterize the $S_1 \rightarrow S_{-1}$ reaction and determine the activation energy for reduction of the S_1 state by NH_2OH. For that the FIOPs of non-preflashed spinach thylakoids were characterized after reduction with various concentrations of the hydroxylamine hydrochloride at different temperatures.

6.2 Experiments and Analysis

6.2.1 Sample preparation

The $S_1Y_D^{red}$ thylakoids from spinach were diluted with MMCH buffer (pH 6.8) to a final concentration of 1mM and incubated for 5 minutes in 1.5 ml - Eppendorf tubes in the water bath adjusted to 5°C, 10°C, 15°C, 20°C, 23°C, 26°C, 29°C, 32°C or 37°C.

For the S_1 reduction the unpreflashed thylakoids from spinach were treated with various concentrations of exogenous electron donor $NH_2OH{\cdot}HCl$ (Hydroxylamine Hydrochloride - HH) to give final concentration of 0, 2.5, 5, 10, 20, 30, 40 and 50 µM. All HH stock solutions in MMCH buffer were prepared fresh and adjusted to pH 6.8 at 10°C prior to use.

After the incubation in the water bath samples were transferred to the Joliot electrode in very dim green light and measured at 10°C after 40s of polarisation at –750 mV.

Miss and double hit probabilities were determined for each incubation temperature from the 0 µM HH control sample.

6.2.2 Data analysis

The first 16 flashes of the FIOPs were analysed with the extended Kok model, which takes into account super-reduced S_{-i} states (described in Chapter 2.7.2 - 2.7.3).

A fit approach, which included the miss and double hit probabilities, damping factor and S_1 and S_0 states as free parameters, was used for the deconvolution of the control FIOPs. In all other FIOPs the S_{-1} state was additionally included. The S_{-2} and S_{-3} states were included in samples with higher concentration of hydroxylamine to avoid visible deviation between measured and calculated oxygen yield at higher flash numbers.

The resulting S_1 populations were plotted against the HH concentration to determine the rate constants for the S_1 reduction at various temperatures (Equation 6.2.1 and approach A of Table 6.3.1).

As an alternative approach, the second order rate constants k_{10} and, additionally, $k_{0\text{-}1}$ were also determined based on Equations (6.2.1 - 6.2.4) for the consecutive reaction $S_1 \rightarrow S_0 \rightarrow S\text{-}_1$ listed below (approach B of Table 6.3.1).

$$[S_1]_c = [S_1]_0 e^{-k'_{10}c} \qquad (6.2.1)$$

$$[S_0]_c = \frac{k'_{10}[S_1]_0\left(e^{-k'_{10}c} - e^{-k'_{0-1}c}\right)}{\left(k'_{0-1} - k'_{10}\right)} + [S_0]_0 e^{-k'_{0-1}c} \quad (6.2.2)$$

$$[S_{-1}]_c = \left([S_1]_0 + [S_0]_0 + [S_{-1}]_0\right) - [S_1]_c - [S_0]_c \quad (6.2.3)$$

$k_{10} = k'_{10}/300$ and

$k_{0\text{-}1} = k'_{0\text{-}1}/300$ (6.2.4)

Where the $[S_1]_0$, $[S_0]_0$ and $[S_{-1}]_0$ are initial concentrations of the S_1, S_0 and S_{-1} state, respectively. The $[S_1]_0$, $[S_0]_0$ and $[S_{-1}]_0$ parameters, the rate constants (k'_{10} and $k'_{0\text{-}1}$) were freely varied using "Solver" routine to minimize the fit error ($dx^2 \rightarrow 0$), which was defined as the square of the difference of measured and calculated S – states populations.

Although Equations (6.2.1- 6.2.3) are valid for the pseudo-first order reactions, they can be used to calculate the second-order rate constants for the consecutive reaction $S_1 \rightarrow S_0 \rightarrow S_{-1}$ if take into account that the concentration of the hydroxylamine hydrochloride does not change during the incubation time and, hence, may considered as a constant.

The final rate constants k_{10} and $k_{0\text{-}1}$ ($M^{-1}s^{-1}$) were then calculated by dividing k'_{10} and $k'_{0\text{-}1}$ by the constant incubation time (300s).

The values for activation energy and pre-exponential factors were extracted from Arrhenius type plots.

6.3 Results

In the present study the rates of the S_1 reduction were studied as a function of the hydroxylamine hydrochloride (HH) concentration at different temperatures.

Figure 6.3.1 shows normalized FIOPs of spinach thylakoids treated for constant time of 5 minutes with various concentrations of HH at 5°C and pH 6.8. The one-electron shift from S_1 to S_0 state by hydroxylamine is already observable at 5 µM HH concentration, based on a decrease of the oxygen yield on the third flash (Y_3) and corresponding increase in the fourth (Y_4) flash. This shift is clearer in the patterns where the HH concentration is increased up to 30µM and a further shift to the fifth flash, which corresponds to the S_{-1} state, is seen.

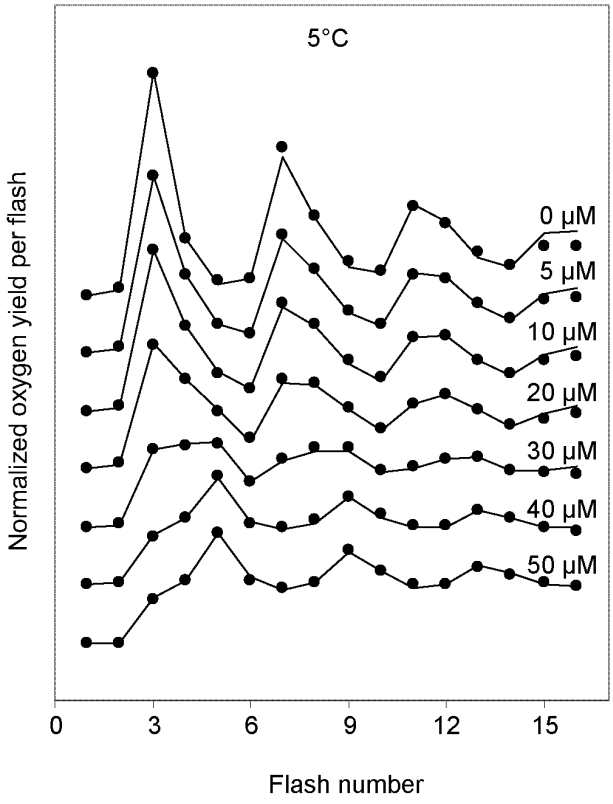

Figure 6.3.1. Normalized FIOPs of spinach thylakoids incubated with various concentrations of Hydroxylamine Hydrochloride (HH) in MMCH buffer at 5°C and pH 6.8.

In the latter FIOP the populations of the S_1, S_0 and S_{-1} states are virtually equal, while at 40µM and 50µM HH patterns the S_{-1} state is already dominant. These data confirm that NH_2OH reacts as a one-electron reductant inducing a sequential reduction of the form: $S_1 \rightarrow S_0 \rightarrow S_{-1}$ [182].

A further shift of the first maximum to the S_{-2} state can be observed either by increasing the concentration of HH, or by longer dark incubation at given concentrations [182]. As the aim of this study was to analyse the decay of the S_1 state, those experiments have not been done. Figure 6.3.1 clearly shows that the reduction of the S_1 state can be studied by varying the concentration of the one-electron donor hydroxylamine and simultaneously keeping the incubation time constant. Indeed, the population of the S_1 state was calculated to be ~18% at 50µM HH and 5°C and only 9% at 10°C.

Figure 3.6.2. shows the temperature dependence of the S_1, S_0 and S_{-1} populations obtained after 5 minutes incubation with the 5µM (A) and 30µM (B) of HH. Under incubation with 5µM of HH the S_1, S_0 and S_{-1} states vary almost linearly and appear to have only small changes in their populations (open symbols) with temperature.

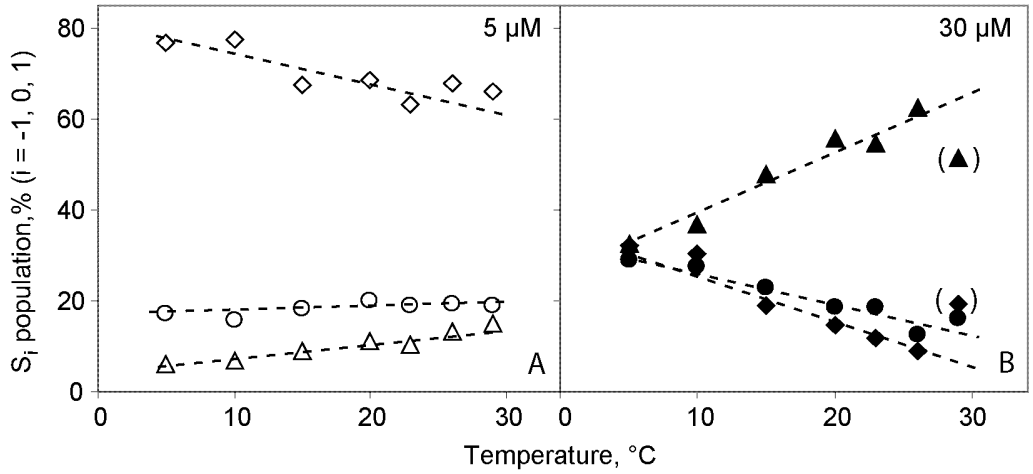

Figure 6.3.2. Temperature dependence of the populations in S_1 (diamonds), S_0 (circles) and S_{-1} (triangles) states after 5 minutes of incubation with 5µM (A) or 30µM (B) Hydroxylamine Hydrochloride (HH) in MMCH buffer (pH 6.8).

A quite different temperature dependence of the S state distribution is observed after incubation with 30 µM HH (Figure 6.3.2 B). Here there is already at 5°C a nearly equal distribution in the S_1, S_0 and S_{-1} states (see also 30 µM trace of Figure 6.3.1). With a further temperature rise the S_{-1} state markedly increases (triangles), while S_0 and S_1 states decay with similar populations. The decay of the S_0 population induced by 30 µM HH is in line with the previously reported fast rates for $S_0 \rightarrow S_{-1}$ transition [182].

Figure 6.3.3 shows the S state decay as a function of HH concentration at constant reaction time of 5 minutes. As expected, the S_1 state decreases when the concentration of NH_2OH is increased. At the same time an increase of the S_{-1} state can be observed. The dependence of the S_0 state population on the NH_2OH concentration is not monoexponential: at small concentrations the population of the S_0 state increases slightly, but it decays at higher concentrations.

The second order rate constants k_{10} and $k_{0\text{-}1}$ calculated from the Figure 6.3.3 on the basis of equations 6.2.1 - 6.2.4 are k_{10} = 110 $M^{-1}s^{-1}$ and $k_{0\text{-}1}$ = 150 $M^{-1}s^{-1}$ at 5°C and pH 6.8 (Approach **B** of Table 6.3.1). These data are comparable with previously reported studies on the dependence of the S state populations on the concentration of NH_2OH [182]. Keeping an incubation time of 1 minute constant, these authors calculated in a similar way the second order rates at ice temperature and pH 7.2 to be 76 $M^{-1}s^{-1}$, 120 $M^{-1}s^{-1}$ and 17 $M^{-1}s^{-1}$ for S_1, S_0 and S_{-1} states, respectively. Although the experimental conditions are slightly different, the ratio k_0/k_1 is about 1.5 in both cases.

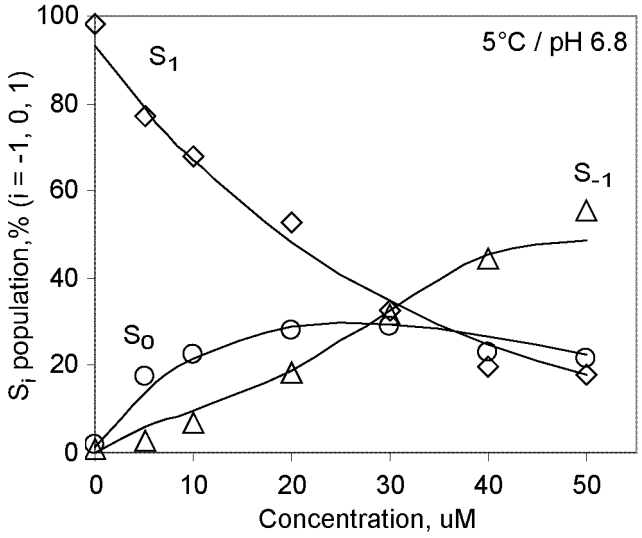

Figure 6.3.3. S_1 (diamonds), S_0 (circles) and S_{-1} (triangles) state populations as a function of Hydroxylamine Hydrochloride concentrations of in MMCH buffer at fixed incubation time (5 min) 5°C and pH 6.8. The lines are fits, from which the rate constants k_{10} and $k_{0\text{-}1}$ were determined based on equations 6.2.1 – 6.2.4.

To check the accuracy of the obtained data, another possibility to determine the rate constants for the NH_2OH induced decay of the S_1 state was used. In this alternative approach, the rate constant k_{10} was extracted from the slope of the semilogarithmic plot of the S_1 populations plotted as a function of NH_2OH concentration for each temperature individually (Approach **A** of the Table 6.3.1). These plots of the k_{10} are presented in the Figure 6.3.4 for selected temperatures. Additionally, from this figure the temperature dependence of the HH induced S_1 decay rates can be deduced.

The rate constants obtained by different approached are listed in Table 6.3.1.

The Arrhenius plot of the rates of the S_1 decay obtained at different temperatures is presented in Figure 6.3.5. Surprisingly, the Arrhenius plot shows a break point around 30°C.

A comparison of the rates for the decay of S_1 state shows that they vary only slightly between 5°C and 26°C (119 $M^{-1}s^{-1}$ vs. 248 $M^{-1}s^{-1}$) and much stronger between 29°C and 37°C (Figure 6.3.5 A and Table 6.3.1 A).

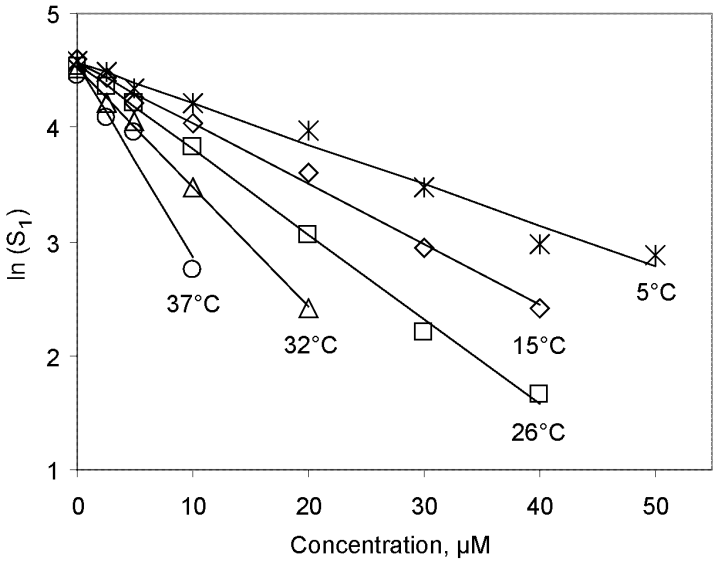

Figure 6.3.4. Semilogarithmic plot of the S_1 state population as a function of concentration of hydroxylamine hydrochloride dissolved in MMCH buffer at pH 6.8.

T, °C	*Approach A*			*Approach B*					
	k_{10}, $M^{-1}s^{-1}$	A, $M^{-1}s^{-1}$	E_a, $kJmol^{-1}$	k_{10}, $M^{-1}s^{-1}$	A, $M^{-1}s^{-1}$	E_a, $kJmol^{-1}$	$k_{0\text{-}1}$, $M^{-1}s^{-1}$	A, $M^{-1}s^{-1}$	E_a, $kJmol^{-1}$
5	119			110			150		
10	150			124			173		
15	178			157			206		
20	207	$2.7 \cdot 10^6$	23	173	$6.5 \cdot 10^5$	20	263	$6.2 \cdot 10^6$	25
23	219			176			244		
26	248			207			339		
29	279			190			283		
32	348	$2.3 \cdot$	69	299	$7.4 \cdot$	60	543	$2.2 \cdot$	90
37	563	10^{14}		441	10^{12}		973	10^{18}	

Table 6.3.1. Rate constants, activation energies and pre-exponential factors determined for the $S_1 \rightarrow S_0 \rightarrow S\text{-}_1$ transition. In approach *A* – calculation was performed as described in the figure legends to Figure 6.3.4 (see also Figure 6.3.5 A); *B* – calculation was performed as described in the legends to Figure 6.3.3 (see also Figure 6.3.5 B and C).

This difference is more clearly seen if one compares the pre-exponential factors determined for both regions: this value is about 10^8 times higher at temperatures above 30°C. The activation energy is 3 times higher in the corresponding temperature range. If the last point, which corresponds to the k_1 obtained at 37°C is excluded (see Figure 6.3.5

A), it is possible to fit the data without a break point. The value E_a is then 26 kJmol^{-1} and the pre-exponential factor is calculated to be $7.2 \cdot 10^6$ M^{-1}s^{-1}.

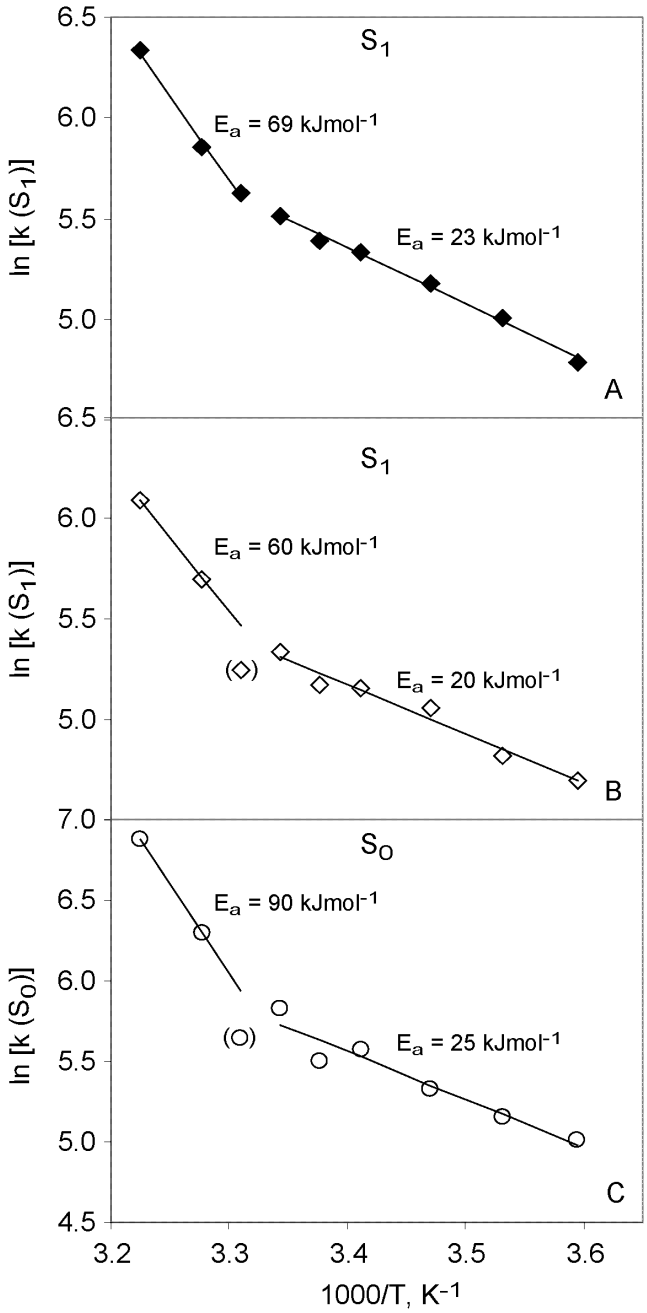

Figure 6.3.5. Arrhenius type plot of the rate constants obtained for the decay of S_1 state in $S_1 \rightarrow S_0 \rightarrow S_{-1}$ transition. **A** – obtained by approach *A* (described in the legends to Figure 6.3.4); **B** and **C** – obtained by approach *B* (described in the legends to Figure 6.3.3).

In Figure 6.3.5 B and C the Arrhenius type plots are given for the k_{10} and $k_{0\text{-}1}$ values listed in Table 6.3.1 (approach B). Although there are small differences in values of k_{10} obtained by different approaches, the break point around 29°C is observed in both cases. Moreover, the values of activation energies and pre-exponential factors found to be very similar before and after the break point. Interestingly, the Arrhenius plot for the $S_0 \rightarrow S_{-1}$ transition also shows a break point around 29°C (Figure 6.3.5 C). The activation energy at

temperatures between 5°C and 26°C is 25 $kJmol^{-1}$, which is very similar to those values obtained for $S_1 \rightarrow S_0$ decay, but at temperatures above 29°C the activation energy is higher (90 $kJmol^{-1}$) than $S_1 \rightarrow S_0$ transition (60-70 $kJmol^{-1}$). Based on this finding and on comparison of the activation energies and pre-exponential factors obtained before and after the break point for S_1 and S_0 decays it can be concluded that there are two reaction pathways, which are located on different temperature regions. One, which is in a temperature range of 0°C - 29°C and where activation energy is the S state independent, while at temperatures above 29°C the S state dependent activation energies can be observed.

6.4 Discussion

The present work was undertaken to further investigate the interaction of the exogenous reductant NH_2OH with the OEC of spinach thylakoids.

The first part of the results presented in this study confirms previously published work [182]: a) NH_2OH acts as one-electron reductant, b) in $S_1 \rightarrow S_0 \rightarrow S_{-1}$ transition, the rates of S_0 decay to S_{-1} are faster, than the rates obtained for the decay of the S_1 state and c) the presence of the S_{-2} state induced by NH_2OH treatment.

As outlined in the results section, also the second order rate constants for the S_1 and S_0 reductions at 0°C – 5°C are very similar in both studies, while that of Beck and Brudwig is lower with 45.6 ± 10 $M^{-1}s^{-1}$, but in the latter report no pH value is given, [248].

In present study a possible break point at ~29°C in the Arrhenius plot was discussed for the first time. Consequently, activation energies were calculated to be 69 $kJmol^{-1}$ and 23 $kJmol^{-1}$ above and below 29°C, respectively. In a previous work an estimate of 50 $kJmol^{-1}$ was given for the temperature range 0°C – 20°C based on three data points [182]. Since many more points over a wider temperature range are analysed in this study, the current values are considered to be more accurate. Other possible factors for the deviation could be the constant incubation time of 5 minute in this study compared to 1 minute in the work of [182] and the slightly different pH values of the samples used (pH 6.8 vs. pH 7.2).

The break point in activation energy at 30°C could originate from a double effect of the NH_2OH treatment and elevated temperatures, which both induce changes in the protein environment and even assist the release of extrinsic proteins of PS II to the lumen. The low activation energy at temperatures up to 29°C may indicate that the activation energy is determined by the diffusion of NH_2OH to the Mn_4-cluster. Above 29°C some of extrinsic proteins may fall off and the rate of S_1 reduction is then limited by electron transfer from NH_2OH to the Mn_4-cluster. This would also explain why at temperatures below 29°C the activation energy is essentially S state independent, while above 29°C a clear difference is seen between values of activation energies for the reduction of S_1 and S_0 by NH_2OH.

Further studies analysing 1) the protein composition after incubation at various temperatures; 2) the activation energy of S_1 reduction in salt-washed PS II membranes and 3) more data points above 29°C are required to test this hypothesis.

CHAPTER 7

Characterization of the "Super"- Reduced S_{-i} states of the OEC of *Thermosynechococcus elongatus*

7.1 Introduction

The redox states of the four Mn ions of the water oxidase in the dark stable S_1 state are still a matter of controversial debate. From the simulations of the EPR multiline signal of the S_2 state [177] a redox state of four Mn(III) is favored for S_1, while Mn K-edge XANES measurements strongly suggest a configuration of two Mn(III) and two Mn(IV) [120, 172, 173, 180, 249]. In case of S_1 being four Mn(III), the lowest S_i state would be S_{-3}, and in the latter case, it could even be S_{-5}, providing that all four Mn ions of the water oxidase can be reduced to Mn(II) without leaving their binding sites.

The existence of an unstable S_{-3} state has been discussed before [137, 245, 250, 251], but was discounted by [252]. On the basis of the numerical analysis of the FIOPs incubated either with 50-250 µM hydroxylamine or 100 mM hydrazine, first evidence for S_{-3} state had been reported [182, 238]. In these studies, the maximal S_{-3} population never exceeded 20% and, therefore, no firm conclusions could be drawn. Later, the evidence was provided not only for the existence of a discrete and relatively stable S_{-3} state but also indications obtained for unstable S_{-4} and S_{-5} states in spinach thylakoids. This progress was achieved by treatment of thylakoids with higher concentration of hydrazine (100 mM) and longer dark-incubation time [119].

Here evidence for the dark stable S_{-3} state obtained via two electron reduction by hydrazine is reported for the first time for the OEC of *T. elongatus*. It is shown that inclusion of the S_{-4} and S_{-5} states in the data analysis significantly improves the goodness of the fits. Additionally, the dependence of the S_{-i} state formation on (i) the double hit probability and (ii) Y_D^{red} is analysed. Moreover, the stability of thylakoids from *T. elongatus* under hydrazine treatment is studied under various conditions and effects of EDC as a crosslinker are investigated by protein analysis of the PS II after hydrazine incubation.

7.2 Experiments and analysis

7.2.1 Sample preparation

For control experiments the samples were diluted to [Chl] = 0.15 mM (*T. elongatus*) or 1 mM (spinach) with MMCH buffer (400mM Mannitol, 10 mM $MgCl_2$, 20 mM $CaCl_2$ and 50 mM Hepes/NaOH) and adjusted to pH 6.8 at 4°C.

For various experiments several additional compounds ($CaCl_2$, $MnCl_2$, glycinebetaine) were added to MMCH buffer. In all cases the same modified buffers were used for hydrazine stock solutions, the incubation medium and flow buffer (pH 6.8 at 4°C). Additional information is described in the figure legends results.

In this studies hydrazine sulfate ($H_6N_2S0_4$) of the "Merck" was used (for the sake of simplicity, in the following only the word "hydrazine" is used). The hydrazine stock solutions were freshly prepared prior to the experiments and adjusted to pH 6.8 at 4°C.

In order to reduce percentage of Y_D^{red}, prior to experiments thylakoids from *T. elongatus* were preflashed twice with a frequency doubled Nd/YAG-laser (9 ns pulse width) and with an intermediate dark - time of 15 min. Afterwards these samples were dark-adapted at room temperature for one hour and then transferred on ice ($S_1Y_D^{ox}$-samples).

For experiments with laser flash excitation (Results 7.3.5) the home-built Joliot-type electrode was connected to the Nd/YAG laser (532 nm). The laser beam was first reduced in intensity by means of a quarter wave plate and a beam splitter cube and then focused onto a fiber optic. The final intensity of the flashes was about 5-10 mJ/Puls. The flash frequency for the FIOPs was 1 Hz, which was achieved by selecting pulses with a shutter from the laser running at 10 Hz. Polarographic signals were stored on a computer and flash artefacts and O_2 uptake signals were measured separately and then subtracted from the original traces within Excel.

For protein analysis samples were prepared essentially as described in Chapter 2.4. SDS-PAGE was performed according to [192]. Prior loading to the gels thylakoids and BBY fragments from spinach at [Chl] = 1 mM or thylakoids from *T. elongatus* at [Chl] = 0.15 mM were incubated with Laemmli sample buffer (1:1).

7.2.2 Data analysis

The first 16 flashes of each FIOP were analyzed using an Excel spreadsheet that was based on an extended Kok model (Chapter 2.7.2 - 2.7.3), which includes S_{-i} states, (i = -5 …4) and $S_2Y_D^{red} \rightarrow S_1Y_D^{ox}$ and $S_3Y_D^{red} \rightarrow S_2Y_D^{ox}$ reactions (described in Chapter 3.2.2 – 3.2.3). For graphical representation, where applicable, data and fits were normalized to one quarter of the sum of the 1^{st} to the 16^{th} flashes of the FIOPs, which corresponds to the release of one oxygen molecule per OEC.

7.3 Results

7.3.1 Formation of the S_{-3} state and the S_{-5} state in thylakoids from T. elongatus

In FIOPs, a hydrazine induced two electron shift of the oxygen yield from the first maximum on the third flash, Y_3, (S_1 state), to the fifth flash, Y_5, (S_{-1} state) and further to the seventh flash, Y_7, (S_{-3} state) is a direct indication for redox changes in the OEC (Figure 1.8). The population of the S_{-i} states, i.e. the number of OEC reduced to the corresponding redox state, is dependent on the hydrazine concentration and dark incubation time. Thus, the aim of the present study was to improve conditions, under which the S_{-3} and lower states can be studied in more detail. Figure 7.3.1 shows FIOPs of *T. elongatus* thylakoids treated for 10 minutes on ice with various concentrations of hydrazine.

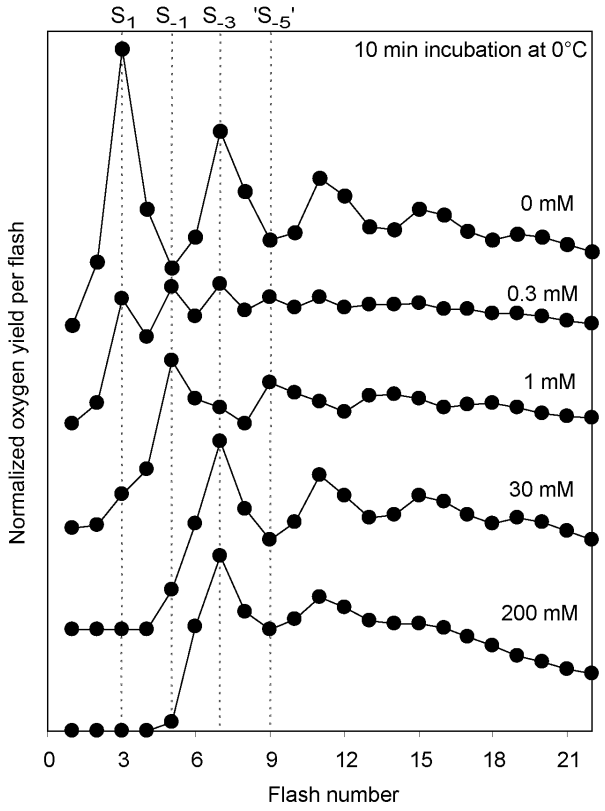

Figure 7.3.1. Normalized FIOPs of *T. elongatus* thylakoids measured after 10 minutes dark incubation on ice with various hydrazine concentrations. The MMCH buffer (pH 6.8 / 4°C) was used for hydrazine stock solutions and as flow and incubation buffer. FIOPs were measured after 5 minutes of dark stabilization time on the Joliot electrode; polarization (–750 mV) was switched on 40 s before the measurements.

The FIOP incubated with 0.3 mM hydrazine shows a two-electron transition of the oxygen yield from Y_3 to Y_5 (Figure 7.3.1). The period-two-oscillation indicates that for an incubation time of 10 min and a concentration of 0.3 mM about half of the PS II centers are reduced from the S_1 to the S_{-1} state. Already at 1 mM the first maximum shifts to Y_5, while after 10 min incubation with 30mM hydrazine the S_{-3} state is prominent. A first maximum on the 9th flash, which would be correlated with the S_{-5} state, has not been achieved so far. The main reason for this is that a further increase of the hydrazine concentration, which seems to be necessary to see a two-electron shift to Y_9, induces a destruction of the OEC and, hence, loss of oxygen activity.

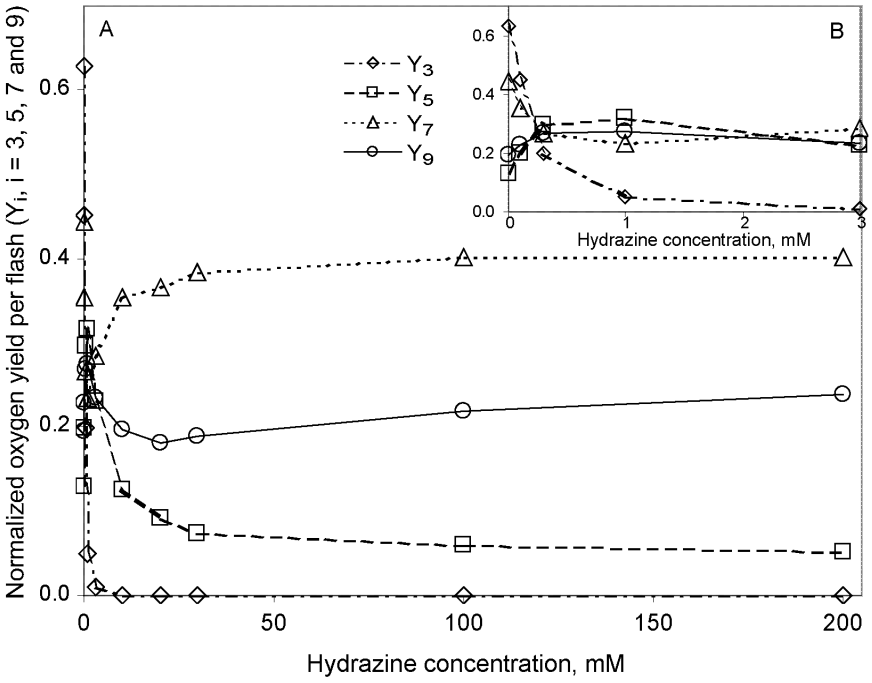

Figure 7.3.2. Normalized oxygen yield of Y_3 (diamonds), Y_5 (squares), Y_7 (triangles) and Y_9 (circles) flashes as a function of hydrazine concentration in *T. elongatus* thylakoids. For the sake of clarity insert B presents the normalized oxygen yield as a function of hydrazine concentrations from 0 mM to 3 mM. The MMCH buffer (pH 6.8 / 4°C) was used for hydrazine stock solutions and as flow and incubation buffer. FIOPs were measured after 20 min dark incubation time with hydrazine and 5 min of dark stabilization time on the Joliot electrode and polarized (–750 mV) last 40 s before the measurements.

However, at least 15 - 20% of the S_{-5} state accompany the S_{-3} state at hydrazine concentration of 20 mM and higher (described below). This observation is supported by the data of Figure 7.3.2, which shows normalized oxygen yield of flashes 3, 5, 7 and 9 (Y_3, Y_5, Y_7 and Y_9) as a function of hydrazine concentration at a constant dark incubation time of 20 min. It can be seen that Y_7 is larger than the other oxygen yields already at 5 mM hydrazine. It stays dominant up to 200 mM hydrazine (last point of this experiment), which is indicative for the high stability of the S_{-3} state in *T. elongatus*. The oxygen yield Y_9,

which partly corresponds to the S_{-5} state, is smaller than Y_7, but larger than Y_3 and Y_5. A visible increase of Y_9 between 20 mM and 200 mM hydrazine concentration is consistent with formation of some S_{-5} state at higher hydrazine concentrations.

To check the stability of the S_{-3} and S_{-5} states in an absence of hydrazine, thylakoids from *T. elongatus* were incubated for 10 minutes either with 10 mM or 100 mM hydrazine and then washed in hydrazine-free MMCH buffer (dilution 1:10), centrifuged and resuspended to the initial chlorophyll concentration (Figure 7.3.3). This procedure leads to a decrease of the hydrazine concentration to ~0.1 mM and ~1mM respectively.

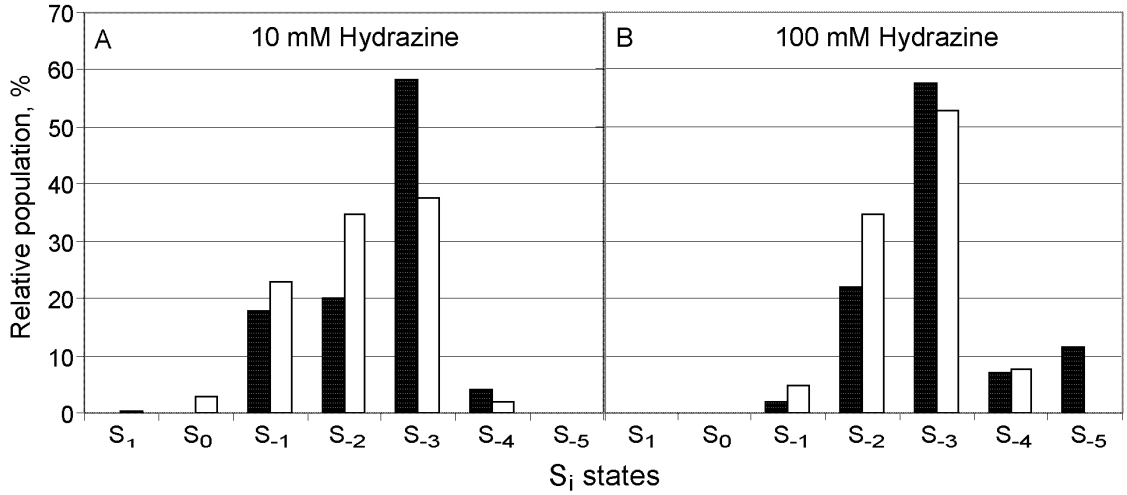

Figure 7.3.3. S state population in *T. elongatus* thylakoids after 10 min of incubation with 10 mM (A) or 100 mM (B) hydrazine (black columns). Afterwards, samples were diluted with MMCH buffer (1:10), centrifuged (4000g / 5min / 20°C) and resuspended to initial concentration (1mM) (white columns). FIOPs were measured after 5 min of dark stabilization time on the Joliot electrode and polarization (–750 mV) was switched on 40 s before the measurements.

Figure 7.3.3 shows that about 60% S_{-3} state can be obtained by incubation of thylakoids with 10 mM and 100 mM hydrazine in MMCH buffer (black columns). However, after the washing procedure there is a clear decrease of the S_{-3} state and an increase of the S_{-2} state population. This decrease is smaller in case of 100 mM compared to 10 mM hydrazine, possibly because some of the lost S_{-3} state is reformed from S_{-4} and S_{-5} states. Additionally, 10 mM hydrazine seems to be not high enough to reduce the OEC beyond the S_{-3} state. Samples incubated with 100 mM hydrazine show complete reduction of the S_1, S_0 states and only a few centers still remained in the S_{-1} state. Moreover, about 8% of centers are in the S_{-4} and 12% in the S_{-5} states. However, the S_{-5} state is unstable and disappears after a washing protocol, while the S_{-4} state appears to be more stable.

The stability of the steady state photosynthesis in the *T. elongatus* thylakoids incubated with various concentrations of hydrazine is presented in Figure 7.3.4. This figure shows

that the steady state oxygen yield significantly drops already at small concentrations of hydrazine (0.3 mM - 1 mM). Although a further decrease of the steady state slows down with higher hydrazine concentrations, there is only about 20 - 25% of the initial oxygen activity remaining after incubation of thylakoids with 200 mM hydrazine. Moreover, two different incubation times, 10 min (filled circles) and 20 min (open circles), which have been chosen to monitor the steady state photosynthesis under hydrazine treatment, show very similar results. This observation suggests that the most dramatic changes in the activity of the OEC induced by hydrazine treatment happen already during the first 5 – 10 min of incubation and only small changes thereafter.

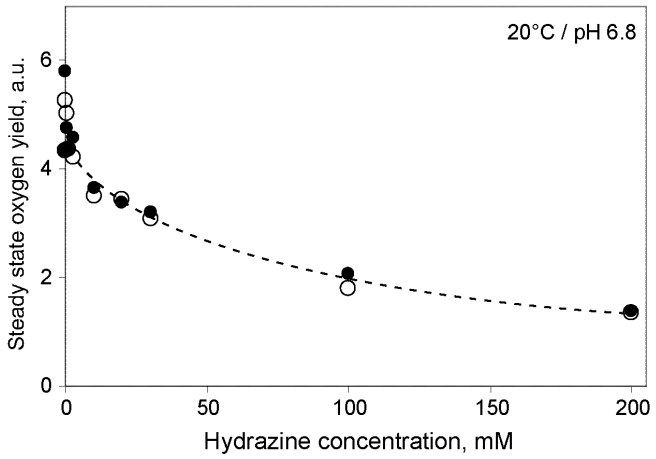

Figure 7.3.4. Steady state photosynthesis in *T. elongatus* thylakoids as a function of 10 min (filled circles) or 20 min (open circles) dark incubation with various hydrazine concentrations. The MMCH (pH 6.8 / 4°C) buffer was used for stock solutions and as flow and incubation buffer. FIOPs were measured after 5 min of dark stabilization time on the Joliot electrode (20°C) and polarization (–750 mV) was switched on 40 s before the measurements.

The above presented data show that with 30 - 200 mM of hydrazine the Mn_4O_xCa complex of PS II of *T. elongatus* can be reduced down to a stable S_{-3} state (Mn (II_2, III_2) or Mn (II_4)). Consequently, if a further reduction to S_{-5} state is possible, it can be achieved only with higher hydrazine concentrations. On other hand, hydrazine is known as a reagent, which induces the release of Mn ions from the OEC and, as a result of it, leads to the loss of the oxygen evolving capacity. Thus, already after 30 min incubation with 10 mM hydrazine, the spinach OEC loses ~60% of its activity (Figure 7.3.5). A stabilization of the OEC during a hydrazine treatment is, therefore, an important point in this study. To check whether or not a hydrazine reduction of the Mn_4-cluster below S_{-3} state is possible, various “protectors” of the oxygen evolving capacity were used prior to hydrazine treatment.

7.3.2 Effect of Ca ions on the formation of the S_{-3} and S_{-5} states

A number of studies have reported on stabilizing effects of Ca ions on the PS II activity under environmental changes of different nature, especially, if part of the extrinsic proteins are lost [132, 134, 135, 253-257]. Thus, in the present study it was decided to use calcium chloride as a possible protector of the oxygen activity under hydrazine treatment. For this proposal, a concentration of calcium chloride in the buffer was varied from 0 mM up to 100 mM (Figure 7.3.5). Two different concentrations of hydrazine were chosen to monitor changes in the oxygen evolving activity at different incubation times.

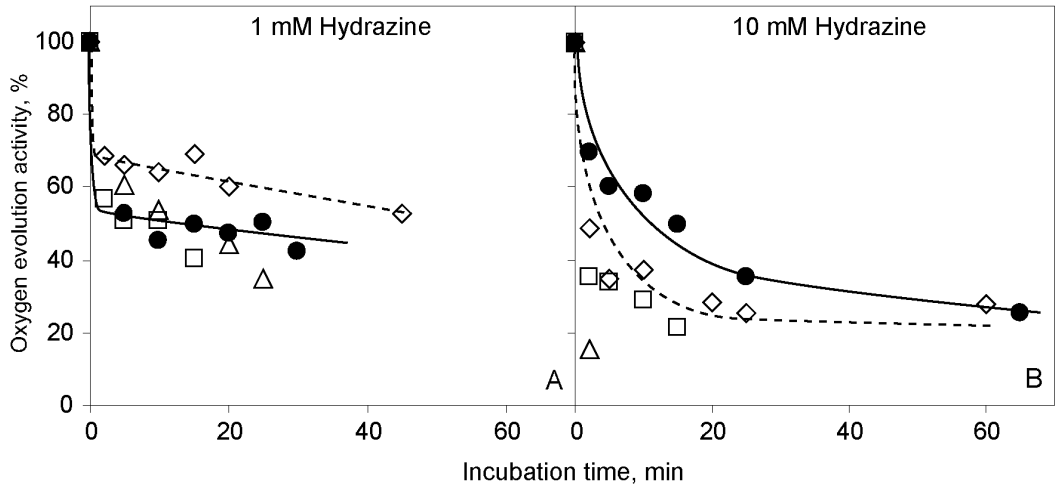

Figure 7.3.5. Normalized oxygen evolving capacity in spinach thylakoids as a function of the dark incubation time with either 1 mM (A) or 10 mM hydrazine (B) in the medium. The MMCH buffer with 0 mM (squares), 20 mM (diamonds), 50 mM (filled circles) or 100 mM (triangles) of $CaCl_2$ was used as a flow and incubation buffer and for hydrazine stock solutions. FIOPs were measured after 2 min of dark stabilization time on the Joliot electrode (10°C); polarization (–750 mV) was switched on 40 s before the measurements.

Figure 7.3.5 A shows that during the first 5 min of incubation with 1 mM hydrazine the OEC of spinach drastically loses 30-50% of its activity. However, during subsequent dark incubation time, the oxygen evolving activity is stabilized in the samples incubated with 50 mM $CaCl_2$ (~50%), while in the samples incubated with 20 mM $CaCl_2$ it slightly decays from ~70% at 10 min to ~50% after 50 minutes incubation with 1 mM hydrazine. Based on this finding, the stabilizing effect of 20 mM $CaCl_2$ especially at short incubation time and 50 mM $CaCl_2$ during a long incubation time with 1 mM hydrazine can be proposed. In those samples, which were incubated in buffer containing either 100 mM $CaCl_2$ (triangles) or 0 mM $CaCl_2$ (squares), the oxygen evolving capacity significantly breaks down with incubation time. This observation leads to the suggestion that only intermediate Ca concentrations (20 – 50 mM) protect the OEC, while both absence of Ca ions in the buffer and too high Ca concentration (100 mM) cannot prevent hydrazine induced loss of oxygen

activity. This is also observed in Figure 7.3.5 B, where 10 mM hydrazine is used to monitor the stabilization of the oxygen evolving activity by various concentrations of $CaCl_2$ in medium. As in previous case, the OEC loses ~ 50% of its activity mostly during the first 5 min of incubation. But at 10 mM hydrazine only those samples have relative higher oxygen capacity left, which were resuspended in MMCH buffer with 50 mM $CaCl_2$. Particularly, during the first 15 min of incubation these samples preserve at least 50% of the oxygen evolving activity.

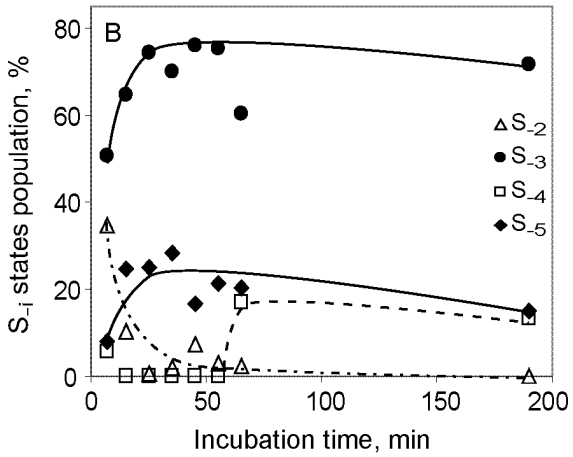

Figure 7.3.6. S state population in *T. elongatus* thylakoids as a function of incubation time with 30 mM hydrazine. All incubations were done in dark on ice. The MMCH buffer with 50 mM $CaCl_2$ was used as a flow and incubation buffer and also for hydrazine stock solutions. FIOPs were measured after 5 min of dark stabilization time on the Joliot electrode (20°C) and polarization (–750 mV) was switched on 40 s before the measurements. FIOPs were analyzed by fit approach C described in the legends and text to Figure 7.3.9.

Based on this finding, thylakoids from *T. elongatus* were incubated with 30 mM of hydrazine and in presence of 50 mM $CaCl_2$ in the medium. The FIOPs obtained in this experiment at different incubation time were calculated based on a Kok model, which is extended to include the S_{-5} state and also takes the back reactions of the reduced S_{-i} states with Y_D^{red} into account. The resulting populations of the S_{-i} states are presented in Figure 7.3.6. This Figure shows that about 75% of the PS II centers attain the S_{-3} state already after 20 min incubation of thylakoids with 30 mM hydrazine in the presence of 50 mM $CaCl_2$ in the medium. At the same time almost 25% of the S_{-5} state is generated. However, the S_{-5} state is less stable in the time course compared to the S_{-3} state. Interestingly, an increase in S_{-4} state after about 60 min incubation with hydrazine was observed. This maybe correlated to the oxidation of the S_{-5} state by Y_D^{ox} to the $S_{-4}Y_D^{red}$ as previously described for $S_{-2}Y_D^{ox} \rightarrow S_{-1}Y_D^{red}$ [182]. However, the nature of the S_{-3}, S_{-4} and S_{-5} states interaction with Y_D^{ox} is not clear and a subject for further investigations.

7.3.3 Effect of glycinebetaine on the formation of the S_{-3} and S_{-5} states

There are several reports on the protective effect of betaine (or glycinebetaine) on PS II activity under salt and temperature stress [258-260]. It was concluded that betaine (i) has a stabilizing effect on binding of the extrinsic proteins to thylakoid membrane and (ii) prevents release of Mn atoms from the cluster during thermoinactivation. Despite these data, there are no reports on the effects of betaine during the reduction of PS II by hydrazine or hydroxylamine.

In this work betaine was used as a possible protector of the oxygen evolving activity during hydrazine-induced redox shifts in the OEC of *T. elongatus* thylakoids.

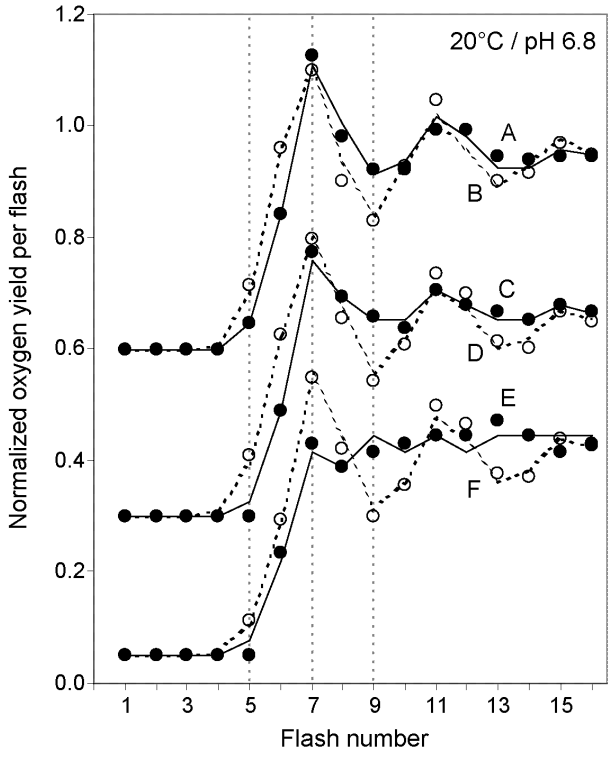

Figure 7.3.7. Normalized FIOPs of *T. elongatus* thylakoids incubated with 100 mM hydrazine under different conditions. *Sample A* was incubated for 10 min with 100 mM hydrazine, then measured at 2 Hz with polarization (u_p^{on} –750 mV) switched on all 5 minutes of the dark stabilization time on the electrode. *Sample B* was incubated for 10 min with 100 mM of hydrazine, then resuspended with MMCH buffer (1:10), centrifuged (Biofuge, 4000 g / 5 min / 20°C), resuspended to initial volume and then measured at 2 Hz after polarization for 40s. *Sample C* - like *A*, but measured at 1 Hz; *Sample D* – like *B*, but measured at 1 Hz; *Sample E* – like *A*, but measured at 0.5 Hz of the flash frequency and *Sample F* – like *E*, but polarized for 40s. MMCH buffer with 0.5 M Betaine (pH 6.8 / 20°C) was used as a flow and incubation buffer and for hydrazine stock solutions. All FIOPs were measured after 5 min of dark stabilization time on the Joliot electrode (20°C). The S state populations for all samples are listed in Table 7.3.1.

Figure 7.3.7 represents FIOPs of samples incubated with 100 mM hydrazine in the presence of 0.5 M betaine in medium. As this concentration of hydrazine is high enough to suppress significantly the oxygen evolving activity even at short incubation time (can be

suggested based on data presented in Figures 7.3.4 and 7.3.5), it was decided to (i) remove or (ii) destroy hydrazine from/in the medium after 10 min of incubation to prevent its further action on the OEC activity. To remove hydrazine samples *B* and *D* were diluted (1:10), spun down, resuspended to initial volume and then measured at usual conditions (see legends to Figure 7.3.7). In contrast, samples *A*, *C* and *E* were measured directly after incubation with hydrazine, but polarized all 5 minutes of the dark stabilization time on the Joliot electrode. This was done to destroy hydrazine electrochemically and by dialysis into the flow buffer. Additionally, the flash frequency was varied in those samples to monitor whether or not (i) the back reactions of S_{-i} states with Y_D^{red} or NH_2NH_2 affect the FIOPs or (ii) additional time for the completion of the light induced $S_{-4} \rightarrow S_{-3}$ and $S_{-5} \rightarrow S_{-4}$ transitions is required.

Control FIOPs	Fit Parameters, %								FQ (10^{-6})
	α	β	d	S_3	S_2	S_1	S_0	Y_D^{red}	
2 Hz	8.6	6.7	99.4	0	2.5	97.5	0	45.5	16.8
1 Hz	8.6*	6.7*	99.4*	0	2.5*	97.5*	0	37.8	13.9
0.5 Hz	8.6*	6.7*	99.4*	0	2.5*	97.5*	0	36.4	14.0

Sample	S_1	S_0	S_{-1}	S_{-2}	S_{-3}	S_{-4}	S_{-5}	Y_D^{red}	FQ (10^{-6})
A: 100mM, u_p^{on}(5')/2Hz	0	0	0.8	3	74.6	0	21.6	49.3	13.4
B: 100mM, u_p^{on}(40s)/2Hz/w	0	0	0	32.7	67.3	0	0	47.2	20.2
G: 10mM, u_p^{on}(40s)/2Hz	1.5	0.1	22.6	29	46.8	0	0	17.4	6.3
C: 100mM, u_p^{on}(5')/1Hz	0	0	0	0	56.6	11.3	32.1	0	9.2
D: 100mM, u_p^{on}(40s)/1Hz/w	0	0	1.6	27.7	70.7	0	0	48.9	18.1
H: 10mM, u_p^{on}(40s)/1Hz	0	0	20.8	27.1	52.0	0	0	21.3	7.5
E: 100mM, u_p^{on}(5')/0.5Hz	0	0	0	0	55.6	4.0	40.4	12.5	15.9
F: 100mM, u_p^{on}(40s)/0.5Hz	0	0	2.9	4.5	87.7	0	5.0	29.1	13.2
I: 10mM, u_p^{on}(40s)/0.5Hz	0	0	19.9	20.6	59.5	0	0	28.9	3.9

Table 7.3.1. Fit parameters (%) of the FIOPs of *T. elongatus* thylakoids measured before (control samples) and after 10 min of incubation with 10 mM (*G, H, I*) and 100 mM (*A - F*) hydrazine. All conditions are described in the legends to Figure 7.3.7. In case of 'w' – sample was span down and washed before the measurement. Calculations were done based on the extended Kok-model, which takes S_{-i} states (i = 1, 2…5) and their interaction with Y_D into account. The percentage of Y_D was obtained by fixing the first order rate constants of the S_3 (0.54 s^{-1}) and S_2 (0.6 s^{-1}) decay obtained from the lifetime measurements at 20°C (described in Chapter 3). In control sample at 2 Hz all parameters presented in Table were freely varied. Obtained values were fixed in control samples at 1Hz and 0.5 Hz and only Y_D parameter was varied. Fit quality (FQ) was slightly improved by this approach, compared to 2 Hz – sample.

The S states distribution for the FIOPs presented in Figure 7.3.7 is listed in Table 7.3.1. These data show that in samples *A*, *C* and *E*, the ratio S_{-3}/S_{-5} (correlated to Y_7/Y_9 in Figure 7.3.7) decreases from 3.75 at 2 Hz to 1.76 at 1Hz and 1.37 at 0.5 Hz. This shows that processes (i) and (ii) suggested above indeed need to be considered. Therefore, the changes in the S_{-3} - S_{-5} states and Y_D^{red} populations were monitored for all FIOPs presented in Figure 7.3.7. Table 7.3.1 shows that the comparatively high population in S_{-3} state at 2 Hz (76%) is reduced to ~57% at 1 Hz and 0.5 Hz, while population of S_{-5} state increases from 22% at 2 Hz to 32% at 1 Hz and 40% at 0.5 Hz. Simultaneously, the percentage of Y_D^{red} reduces from ~50% at 2 Hz to 0% at 1 Hz and 12.5% a 0.5 Hz. Based on this observations it can be proposed, that Y_D^{red} reduces the S states during the dark times between the flashes (see also control FIOPs in Table 7.3.1). Moreover, the increase of the S_{-5} state with lower flash frequency supports the idea that either the formation of this redox state is flash - time – dependent (compare samples *A* and *E*) via a reduction of e.g. S_2 by remaining free hydrazine or its observation is limited by a slow $S_{-5} \rightarrow S_{-4}$ transition.

However, although the only difference between samples *E* and *F* is a polarization time of 5 minutes vs. 40 s, the FIOPs of these samples are quite different. Therefore, not only the flash-time-dependence, but also the polarization time has a significant influence on the observed S_{-5} population.

One other reason for the effect of the polarization current maybe the formation of peroxide (or other species), which may be formed during polarization and react either in the dark ($S_{-3} \rightarrow S_{-5}$) or during the flash train (e.g. $S_{-2} \rightarrow S_0$) with the OEC. The former would lead to a true S_{-5} state population, while the latter reaction would create an artificial "S_{-5}" population. Both effects may be enhanced compared to the control, when extrinsic polypeptides are lost during hydrazine treatment.

The flash frequency dependence of the S_{-5} state indicates that a two-electron back reaction in the dark-times of the flash train may occur only in case of 5 min polarization (samples *A*, *C*, *E*), which favours back reactions of the S_2 state with peroxide. In contrast, only very small differences are seen in betain buffer between washed and unwashed samples (compare *D* (1 Hz) and *F* (0.5 Hz)), which indicates that back reactions in the flash train with hydrazine are negligible under these conditions.

At 10 min incubation with 10 mM hydrazine in 0.5 mM betaine buffer, the steady state oxygen yield is nearly equal to that obtained in presence of 50 mM $CaCl_2$ (60 – 70%), while at 10 min incubation with 100 mM hydrazine in betaine buffer, the steady state shows 30 - 40% of oxygen activity. 5 min polarization at 0.5 Hz strongly reduces the steady state oxygen yield to about 10% of the control pattern.

7.3.4 Effect of $MnCl_2$ on the stability of the OEC under hydrazine treatment

Several questions are addressed to this study: (1) are additional Mn ions in incubation medium able to prevent the destruction of the Mn_4O_xCa complex during hydrazine - induced redox changes in OEC? (2) What is the best approach to fit the lowest S_{-i} states under these conditions?

Figure 7.3.8 **A** presents normalized FIOPs of *T. elongatus* thylakoids incubated for 20 min with 20 mM hydrazine in presence (filled symbols) or absence (open symbols) of 10 mM $MnCl_2$ in the medium. Fit analysis of these patterns show that the FIOP obtained without Mn in the buffer has 77% of the S_{-3} state and ~40% of Y_D^{red}, while the FIOP obtained in the presence of $MnCl_2$ has ~60% centers in S_{-3} state, 22% in S_{-5} and 100% of Y_D^{red}.

This result shows that a higher S_{-5} state population can be observed in *T. elongatus* thylakoids in the presence of additional Mn ions, possibly via the stabilization of the S_{-4} and S_{-5} states. Correspondingly, the activity of OEC is expected to be higher in this case, which is confirmed by the data shown in Figure 7.3.8 **B**. Particularly, the steady state oxygen yield in presence of $MnCl_2$ (Figure 7.3.7 **B)** is almost identical in the control and samples after incubation with 20 mM hydrazine for up to 60 min. Based on these findings, it can be concluded that the presence of the additional Mn ions in incubation medium can prevent hydrazine-induced destruction of the OEC to a large extend.

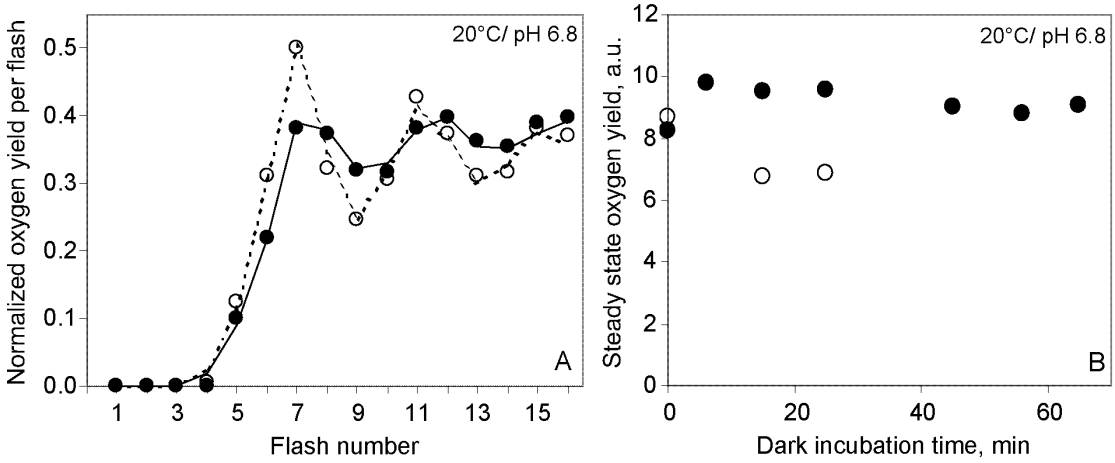

Figure 7.3.8. **A**: Normalized oxygen yield per flash as a function of flash number in FIOPs of *T. elongatus* thylakoids incubated for 20 min on ice with 20 mM hydrazine; **B**: steady state photosynthesis in *T. elongatus* thylakoids as a function of dark incubation time on ice with 20 mM hydrazine. MMCH buffer (open circles) or MMCH buffer with 10 mM $MnCl_2$ (filled circles) were used as a flow and incubation buffers and for hydrazine stock solutions (pH 6.8 / 4°C). FIOPs were measured after 5 min of the sedimentation time on the Joliot electrode (20°C) and polarized (–750 mV) 40 s before measurements. The steady state oxygen yield was calculated as average of the 9^{th} to 16^{th} flashes.

To find a reasonable answer on the second question, the different fit approaches were used to study the S_{-i} states population and possible effect of Y_D on the calculated populations (Figure 7.3.9). Initially the miss and double hit probabilities obtained from the "control" FIOP (i.e. laser-preflashed and dark-adapted FIOP obtained before hydrazine incubation, see also part 7.2 of this Chapter) were fixed during calculation of the S_{-i} states. In fit **A** (Figure 7.3.9 **A**) the Y_D population was additionally fixed to 11% that was also obtained from the "control" FIOP (for details see Table 3.3.2).

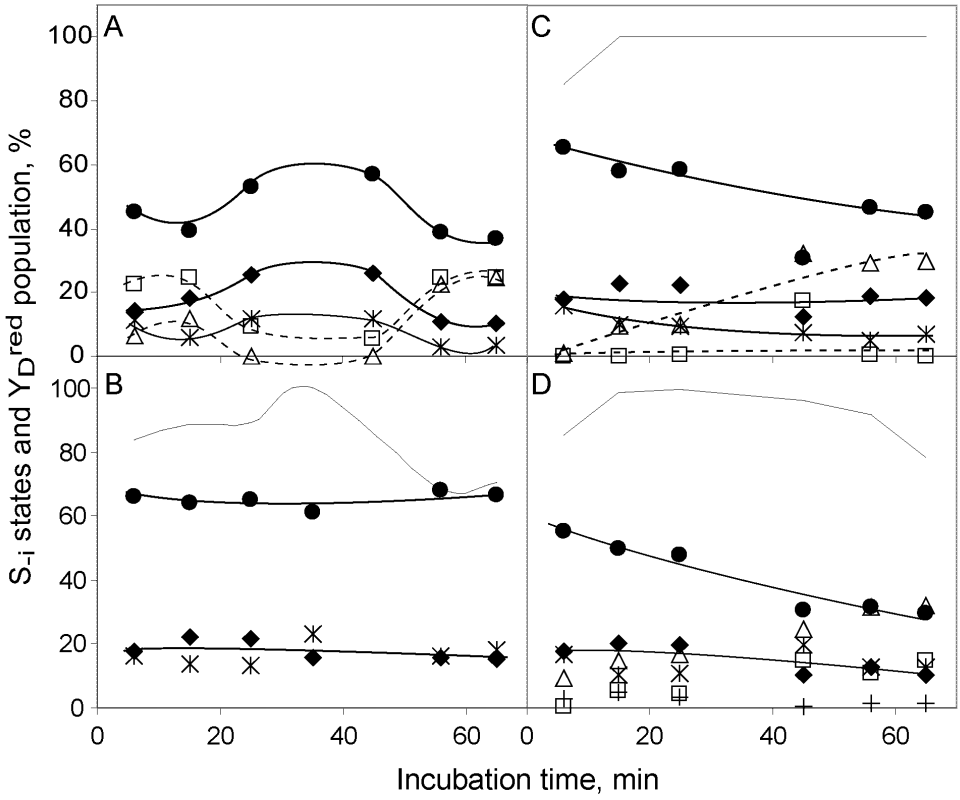

Figure 7.3.9. Different fit approaches of the FIOPS of *T. elongatus* thylakoids as a function of the dark incubation time with 20 mM hydrazine. The MMCH buffer (pH 6.8 / 4°C) with 10 mM $MnCl_2$ was used as a flow and incubation buffer and for hydrazine stock solutions. FIOPs were measured after 5 min of sedimentation time on the Joliot electrode (20°C) and were polarized (–750 mV) 40 s before measurements. In **A**, **B** and **C** the miss (8%) and double hit (6%) probabilities were fixed to those obtained from the control FIOP. In **D** – the double hit probability was varied. In fit **A** and in control FIOP (not shown in figure) the Y_D^{red} percentage was fixed to 11% (explained in the text to Table 3.3.2 / Chapter 3). The S_{-1} (stars), S_{-2} (open triangles), S_{-3} (filled circles), S_{-4} (open squares) and S_{-5} (filled diamonds) were free parameters. In fit **B** only S_{-1}, S_{-3}, S_{-5} states and Y_D^{red} (gray line) were varied. In fit **C** Y_D^{red} and all S_{-i} states were varied, while in fit **D** the double hit probability (plusses) was additionally varied. The average fit errors were determined to be: fit **A**: $298 \cdot 10^{-6}$; fit **B**: $292 \cdot 10^{-6}$ fit **C**: $75 \cdot 10^{-6}$ and fit **D**: $53 \cdot 10^{-6}$.

Varying the damping parameter, which is known to change under hydrazine treatment and S_{-i} states, the fits were obtained for different incubation times. These lead to monitor systematic and spontaneous changes, which can be revealed in different fit approaches.

Although Figure 7.3.9 **A** shows two-electron transition in the S_{-i} states (particularly, an increase in S_{-1}, S_{-3} and S_{-5} states is accompanied by a decrease of the S_{-2} and S_{-4} states), it looks unlikely that simultaneous increase or decrease in S_{-1}, S_{-3} and S_{-5} (or in S_{-2} and S_{-4}) populations can take place. This gives the idea that the redox state of Y_D may change during incubation with hydrazine. Thus, the percentage of Y_D^{red} is varied in all other fit approaches.

Figure 7.3.9 **B** represents a simple "two-electron-shift" approach, in which only S_{-1}, S_{-3} and S_{-5} states and Y_D^{red} are free parameters. Although about 70% of the S_{-3} state and nearly 20% of the S_{-5} state were obtained by this approach, these numbers do hardly change with incubation time, which seems unlikely. Additionally, the Y_D^{red} parameter displays a maximum at intermediate incubation times. Based on these observations, it can be suggested that the S_{-2} and S_{-4} states cannot be completely excluded from the calculation of the hydrazine-induced two electron shifts of the S_1 redox states of the OEC ($S_1 \rightarrow S_{-1} \rightarrow S_{-3} \rightarrow S_{-5}$). One possible explanation for that can be back reactions of the S_{-i} states with one-electron abstractor Y_D^{ox}. This can be checked by varying all S_{-i} states and Y_D^{red} in the fit. The resulting S states and Y_D populations are depicted in Figure 7.3.9 **C**. Indeed, this figure shows that the S_{-3} state (~65% at 5 min of incubation) decreases with longer dark incubation time (~45% at 65 min), while population of the S_{-2} state increases with the same time course. However, Y_D is already fully reduced at ~ 15 min incubation and stays reduced during the remaining incubation time. This observation suggest that the S_{-3} may be oxidized to S_{-2} state also by other electron acceptors. The population of the S_{-5} state varies only slightly in this fit approach and has a value of about 20% at 10 - 20 min of incubation with 20 mM hydrazine. This value is consistent in all fits presented in Figure 7.3.9. Additionally, this value is also in line with that in Table 7.3.1 **A**, where data were obtained for a sample incubated for 10 min with 100 mM hydrazine and 2 Hz in the presence of betain in medium. A similar value of 25% for the S_{-5} state is obtained in the presence of $CaCl_2$ and with 30 mM hydrazine at the incubation time of 10 - 20 min and 2 Hz (Figure 7.3.6). If one takes into account that (i) without any "protectors" of the oxygen evolving activity only 12% were calculated for the S_{-5} state (Figure 7.3.3) and (ii) the maximal population of the S_{-5} state (40%) was obtained under the low flash frequency (0.5 Hz, Table 7.3.1 E), it can be proposed that combination of those two factors, i.e. low flash frequency and oxygen activity stabilizers, are necessary to increase population of the unstable S_{-5} state.

7.3.5 Effect of the double hit probability (β) on calculation of the S_{-i} states population obtained in the presence of $MnCl_2$ in the medium

To examine whether the β parameter influences the amount of the S_{-5} state that is calculated in the fits, this parameter was additionally varied in the fit approach **D** (Figure 7.3.9 **D**, plusses). In this fit the S_{-3} state decreases slightly more, compared to fit **C**, in expense of the S_{-2} and S_{-4} populations. The β parameter varies at different incubation time with an apparent maximum at 15 min. Interestingly, the S_{-5} population changes in a similar way as the β parameter. To further analyze this question one FIOP was chosen, in which the β parameter was fixed to the values from 0 to 10%, while all other parameters described in fit approach **C** were varied. The resulting S states and Y_D^{red} populations and the values for the fit error are depicted in Figure 7.3.10.

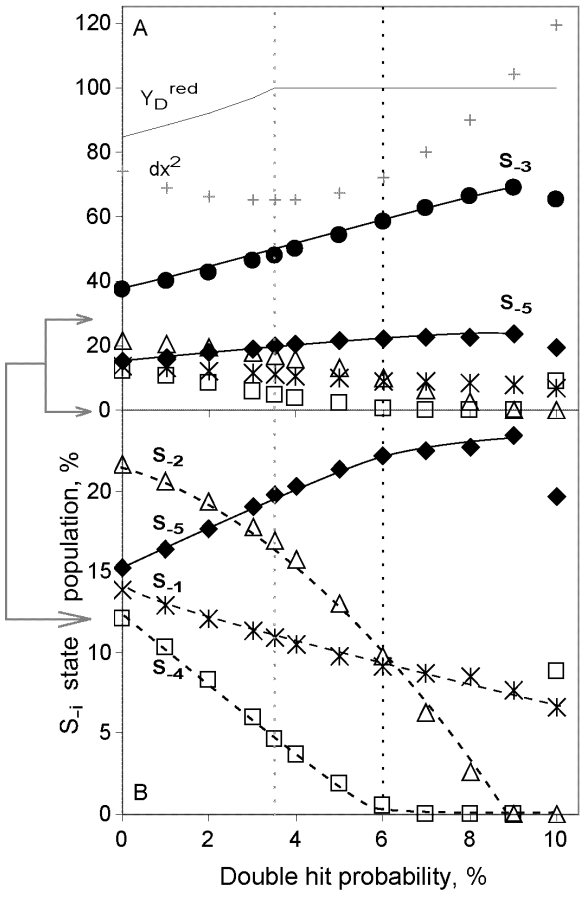

Figure 7.3.10. Numeric analysis of the S state population in *T. elongatus* thylakoids as a function of the double hit probability. The sample incubated for 20 min with 20 mM hydrazine in MMCH buffer with 10 mM $MnCl_2$ was chosen for analysis (Figure 7.3.8 **A**). In this fit approach the value of the miss probability was fixed from the control to 8%. The β parameter, Y_D^{red} (gray unbroken line) and S_{-i} states (S_{-1} – stars, S_{-2} – open triangles, S_{-3} – filled circles, S_{-4} – open squares and S_{-5} – filled diamonds) were varied. For a sake of clarity, values of the fit error (dx_i^2), determined as a difference of the squares of the measured and calculated oxygen yield, are presented without multiplying factor (10^{-6}). Figure 7.3.10 **B** presents only S_{-1}, S_{-2}, S_{-4} and S_{-5} states. The black and gray vertical dotted lines refer, correspondingly, to the fits C and D in Figure 7.3.9.

This figure shows that all values for the S_{-i} states populations are dependent on the value of the double hit probability. Particularly, an increase of the β parameter from 0% to 9% results in an increase of the S_{-3} and S_{-5} states from 40% to 70% and from 15% to 25%, respectively. Simultaneously, all other S_{-i} states decay with different percentages. The fit error ($dx_i^2(\cdot 10^{-6})$) calculated for each fit (Figure 7.3.10 A, plusses) shows a significant increase for $\beta > 6\%$. Based on these results, it can be concluded that the effect of the β parameter on the calculated S_{-4} and S_{-5} states appears to be rather small. Especially the S_{-5} state needs to be included at all reasonable β values for a good fit quality.

Numeric analysis of the different samples (Figure 7.3.9) has concluded that Y_D^{ox} is reduced during a hydrazine treatment under these conditions. On other hand, it has been shown that Y_D^{ox} can also oxidize the S_{-1} and S_{-2} states [182], while Y_D^{red} is reducing S_2 and S_3. Therefore, including all S_{-i} states and Y_D^{red} population in the fit (fit approach **C**) appears to be the most reasonable approach for calculation of the S_i states population after hydrazine treatment. For this reason, all FIOPs presented in this chapter were calculated using the fit approach **C**.

7.3.6 Analysis of the S_{-i} states using laser flash excitation

All FIOPs described above were obtained using a xenon flash excitation (see Chapter 2 for description). In this project, a Nd:YAG laser was used as an alternative source for flash excitation. This was done to exclude double hits, as this parameter depends mainly on the flash profile. Additionally, calculation of FIOPs without β parameter was expected either to prove or to decline the simulations of the S states dependence on the double hits analyzed in Figure 7.3.10.

FIOPs enriched with different S states are shown in Figure 7.3.11. In this Figure, sample *A* represents FIOPs of the preflashed and dark-adapted thylakoids, which have 81% of the PS II centers in the S_1 state. This is a control FIOP, which was best fit with a miss parameter of 9.5 % and a double hit parameter of 0.0 % (Figure 7.3.11 *A*). Indeed, the oxygen yield on the second flash, which would correspond to the double hits, is absent. Additionally, the control FIOP revealed 0% of the reduced tyrosine D. In sample *B* thylakoids were incubated for 10 min on ice with 30 mM hydrazine. The obtained FIOP shows that 65% of the PS II centers are in the S_{-3} state and 12% in S_{-5} state (Table 7.3.2, fit 2). These data are in line with Figure 7.3.3, where a similar population for the S_{-3} and S_{-5} states was obtained after 10 min incubation with 100 mM hydrazine but xenon flash excitation was used. To check the stability of the obtained S states, sample *B* was diluted (1:10), washed 3 times

and resuspended to the initial volume (Sample *E*). As expected, the S_{-5} state completely disappeared, but the S_{-3} state was quite stable (48% S_{-3} state population remained after washing, Table 7.3.2 *E*).

To obtain the S_{-2} and S_{-4} states, sample *A* was triple preflashed and reduced with 50 mM hydrazine (10 min on ice). The FIOP of the resulting sample *C* is shown in Figure 3.7.11 *C*. Analysis of the FIOP *C* has shown the first maximum on the S_{-2} state (42%) and, additionally, about 20% of the S_{-4} state (Table 7.3.2, fit 4). After one washing step applied to this sample an increase in the S_{-2} population (58%) and a decrease in S_{-4} (6.7%) are observed (Sample *D*). In contrast to the S_{-5} state, which was observed so far only in samples that were not washed to remove hydrazine after incubation (Figure 7.3.11 *B* and fits 2 and 4 of the Table 7.3.2), the S_{-4} state can be still observed (to a lesser extent) after one washing step, which decreases the N_2H_4 concentration from 50 mM to approx. 0.5 mM (Figure 7.3.11 *C* and fits 4 and 6, Table 7.3.2). Additionally, this can be also observed in Figure 7.3.3, where a xenon flash excitation is used. However, after extensive washing (3 times) the S_{-4} state is also lost, but the S_{-3} and higher states (if present) are not affected (not shown). This could be a consequence of the expected instability of the S_{-4} and S_{-5} states.

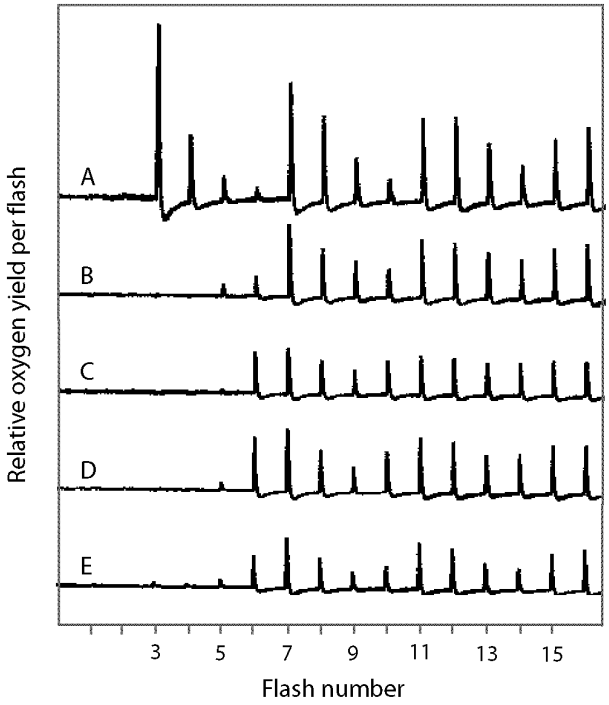

Figure 7.3.11. FIOPs of the *T. elongatus* thylakoids without (*A*) and after various hydrazine treatments (*B* - *E*). *Sample A*: control; *Sample B*: 10 min incubation of sample *A* with 30 mM N_2H_4 on ice (+ 5 min on electrode). *Sample C* was enriched in S_0 by 3 flashes and then incubated 10 min with 50 mM N_2H_4 on ice. *Sample D*: same as C, but washed once. *Sample E*: as B, but washed 3 times. The traces shown were obtained from the original data through subtraction of flash artefact and oxygen uptake traces. The MMCH buffer (pH 6.8 / 4°C) was used as flow and incubation buffer and for hydrazine stock solutions. FIOPs were measured with a flash frequency of 1 Hz after 5 min of the sedimentation time on the Joliot electrode (20°C). Polarization (–750 mV) was switched on 40 s before measurements.

It should be noted that the obtained miss and double hit parameters are almost unaffected by hydrazine incubation (data not shown). This may be related to the quite small changes in Y_D^{red} in samples *B*, *C* and *E*, compared to the control FIOP (Table 7.3.2, fits 0, 2, 4 and 7). In fits 1, 3 and 5 of Table 7.3.2 the S_{-4} and S_{-5} states were excluded from the fit approach **C**. However, the fit qualities in these fits are significantly worse than in those obtained by variation of all S_{-i} states. This comparison shows that the S_{-4} and S_{-5} states are required for acceptable fits of the FIOPs obtained after hydrazine incubation.

Sample	Fit	S_2	S_1	S_0	S_{-1}	S_{-2}	S_{-3}	S_{-4}	S_{-5}	Y_D^{red}	FQ (10^{-6})
A	0	2.3	81.2	7.1	9.4	-	-	-	-	0	25
B	1	-	-	-	16.9	13.0	70.1	-	-	30	47.2
	2	-	-	-	11.1	11.0	65.5	-	12.4	16	8.5
C	3	-	-	-	18.2	47.4	34.6	-	-	61.8	103
	4	-	-	-	5.7	41.8	27.4	19.5	5.7	3.4	29.5
D	5	-	-	1.4	11.9	57.1	29.6	-	-	56.7	10.9
	6	-	-	-	10.3	58.0	25.0	6.7	0.0	56.1	3.5
E	7	-	5.5	3.3	7.9	35.1	48.2	0.0	0.0	3.5	33

Table 7.3.2. Different fits of FIOPs presented in Figure 7.3.10. All fits were calculated based on the fit approach C (Figure 7.3.10). In Fits 1, 3 and 5 the S_{-4} and S_{-5} states were excluded. The fit quality (FQ) was calculated as sum(dx_i^2)/(data points - free parameters). The oxygen yields of the first 16 flashes were included in the fits. Fixed parameters: misses 10.0 % (free for A; 9.6 %), double hits 0.0 %, other S states 0.0 %.

As discussed before, one other explanations for the high oxygen yields in the 8th and 9th flashes can be involvement of back reactions of the S_2 and S_3 states with N_2H_4 or Y_D within the flash train. However, if back reactions with N_2H_4 were involved, then the difference in S_{-4} state population would be expected to be larger between patterns C and D. In contrast, back reactions with Y_D should not be affected at all by washing steps; thus S_{-4} would not be expected to disappear after 3 washing steps.

7.3.7 Effect of EDC on the stabilization of the thylakoid membrane and BBY fragments under hydrazine treatment

One possible reason for the deactivation of the OEC after hydrazine incubation can be related to the release of the extrinsic proteins. To check this possibility, the protein analysis of PS II was done in thylakoids from *T. elongatus* and spinach and, additionally, in spinach

PS II membrane fragments (BBY). The hydrazine – induced release of the extrinsic proteins was studied with SDS-Urea-PAGE and MALDI-TOF mass spectrometry. Loss of extrinsic proteins was observed with SDS-Urea-PAGE in the supernatant of samples incubated for 5 min with 5 mM hydrazine (data not shown). This explains the 30-50% lost of the oxygen evolving activity in spinach and *T. elongatus* thylakoids at this incubation time (Figure 3.3.4 – 3.3.5). The loss of the oxygen activity in BBY fragments found to be even more pronounced under these conditions (data not shown). Further increase of the hydrazine concentration continues to assist the release of the extrinsic proteins into the lumen. In Figure 7.3.12, lane 3 shows a significant amount of the 33, 24 and 18 kDa in the supernatant of the BBY fragments incubated for 5 min with 30 mM hydrazine. The protein composition of the resuspended pellets does not show any indication for the 24 kDa and 18 kDa but a tiny band for the 33 kDa. This may correlate with the remaining oxygen activity of about 20% under these conditions (Figure 7.3.12, lane 2).

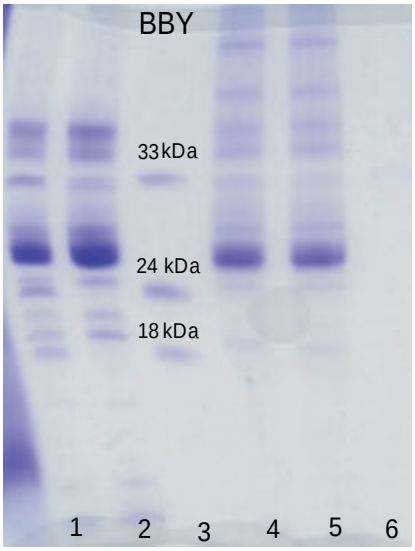

Figure 7.3.12. Protein analysis of the BBY fragments by SDS-Urea-PAGE:

Sample 1: Control (1 mM); *Sample 2*: As sample 1, but incubated for 5 min with 30 mM hydrazine, centrifuged and resuspended to initial volume; *Sample 3*: Supernatant of the sample 2; *Sample 4*: Sample 1 was incubated for 10 min with 0.5% EDC, then washed two times and resuspended in SMCH buffer {0.4 M Sucrose / 0.01 M $MgCl_2$ / 0.02 M $CaCl_2$ / 0.05 M HEPES/NaOH (pH 6.8/4°C)}; *Sample 5*: Sample 4 incubated for 5 min with 30 mM hydrazine, centrifuged and resuspended to initial volume; *Sample 6:* Supernatant of the sample 5. The 12% (resolving gel) and 4% (stacking gel) AA : BisAA (50:1.33) with 6 M Urea were used. Experimental details are given in Chapter 2 (2.2.4 - 2.2.5, 2.3).

To prevent hydrazine-induced release of the extrinsic proteins, a zero-length crosslinker, 1-ethyl-3-(3-demethylaminopropyl)carbodiimide (EDC) was used, which is known to couple these proteins with the 47 kDa subunit of PS II [191]. Indeed, two additional bands around 60 kDa and 80 kDa are formed, while, at the same time, the 18 kDa, 24 kDa, a few more low molecular weight protein subunits and a significant part of the 33 kDa disappear in BBY fragments incubated for 10 min with 0.5% EDC (compare lanes 4 and 1 of Figure 7.3.12). Hydrazine treatment of such a crosslinked sample does not result in any changes in the protein composition (compare lanes 4 and 5). Correspondingly, there are no proteins were detected in the supernatant obtained after washing of this sample (lane 6).

Another possibility to check the stability of the extrinsic proteins in PS II is to wash out extrinsic subunits with high concentration of salts in incubation medium [189, 191]. Particularly, to release the 24 kDa and 18 kDa proteins the photosynthetic samples were incubated for 30 min with buffer containing 1 M NaCl [189]. After centrifugation, the supernatant was dialyzed at 4°C overnight. To release all extrinsic proteins the same procedure was done, but a buffer with 2.6 mM Urea/200 mM NaCl was used [190]. The obtained supernatant was concentrated and studied with SDS-Urea-PAGE (data not shown) and MALDI-TOF mass spectrometry (Figure 7.3.13 *A* and *B*).

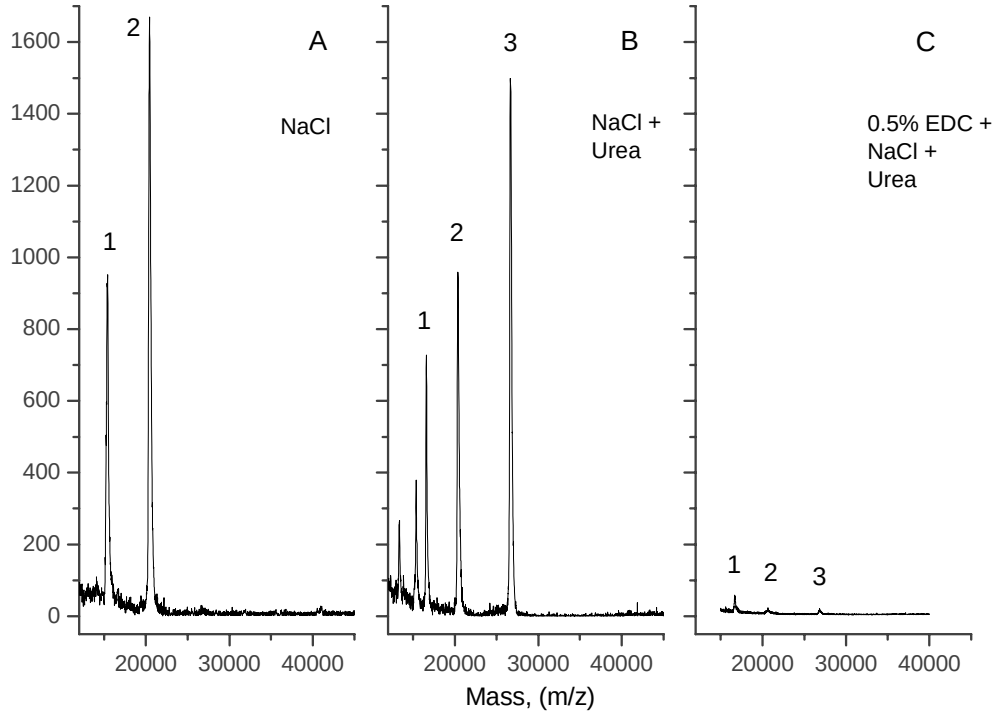

Figure 7.3.13. Protein composition of BBY fragments as measured with MALDI-TOF mass spectrometry. *Sample A*: was incubated for 20 min on ice with buffer containing 1 M NaCl and 25 mM MES (pH 6.5), spun down (8 000 g / 20 min / 4°C). The supernatant was dialyzed against 10 mM TRIS / 10 mM NaCl (pH 7.2) at 4°C overnight and afterwards concentrated. *Sample B*: the procedure is the same, but buffer with 2.6 M Urea / 200 mM NaCl / 25 mM MES was used for incubation. *Sample C*: as sample B, but prior to salt treatment was incubated for 10 min with 0.5% EDC and washed two times. The peaks 1, 2 and 3 are 18, 24 and 33 kDa, respectively. Measurement details are given in Chapter 2.7.3.

The peaks 1, 2 and 3 relate to the 18 kDa, 24 kDa and 33 kDa proteins. Figure 7.3.13 *C* shows results of the same experiment as in case *B*, bur the samples were first incubated with 0.5% EDC. This figure shows that crosslinking of PS II with 0.5 % EDC prevents the release of the extrinsic proteins in presence of high salt concentrations.

Similar results were obtained with thylakoids from spinach and *T. elongatus* (data not shown). However, FIOPs of the samples with crosslinked extrinsic proteins did not reveal expected high oxygen activity after hydrazine incubation. Quite similar FIOPs can be obtained before and after incubation of the samples with 0.5% EDC. However, after washing step and following hydrazine treatment, the oxygen activity significantly decreases (data not shown).

7.4 Discussion

The aim of this study was to investigate a two-electron shift in the S states of the OEC of *T. elongatus* thylakoids induced by the exogenous donor hydrazine. There are only a few studies on (i) hydroxylamine – induced reduction of the OEC from spinach [108, 118, 245, 248] and from *S. elongatus* [247, 252] (S_{-1} and/or S_{-2} states); (ii) hydrazine – induced reduction of the spinach OEC down to the S_{-3} state [119]. In spinach thylakoids, it was shown that hydrazine reacts predominantly as a two-electron reductant with the OEC, i.e. $S_1 \rightarrow S_{-1} \rightarrow S_{-3}$ ($\rightarrow S_{-5}$) or $S_0 \rightarrow S_{-2}$ ($\rightarrow S_{-4}$) [119]. In this study, *T. elongatus* thylakoids were used because they retain higher oxygen evolution activity during incubation with high (30-100 mM) hydrazine concentrations. Only six years ago it has been finally shown that the lowest S state of spinach OEC is the S_{-3} state with its first maximum of oxygen yield on the 7^{th} flash, which is a clear indication of the two electron shift from S_1 state via S_{-1} to S_{-3} state in FIOPs. The further shift to the S_{-5} state, which in FIOP would show as a first maximum of oxygen yield on the 9^{th} flash, has not yet been achieved because of the loss of the oxygen activity at too high hydrazine concentrations. On other hand, up to now the FIOPs are the most direct method to see if the reduction of the Mn_4O_xCa complex is possible down to $Mn(II)_4$, while the lowest paramagnetic S state found so far to be S_{-2} (Chapter 8, [116, 161]).

7.4.1 S_{-3} state

The data presented in this work provide direct evidence for the existence of the dark-stable S_{-3} state in *T. elongatus*. These data are in line with those reported for the S_{-3} state in spinach thylakoids [119]. Moreover, formation of the S_{-3} state in this study is significantly faster (5-10 min of incubation) compared to the previously published work (~ 1h) [119]. Additionally, inclusion of the Y_D parameter into the fit analysis leads to determine a percentage of the Y_D before and after formation of the S_{-3} state and to judge its effect on the S state deconvolution. It was found that Y_D does not influence the fit results showing the existence of the S_{-3} state.

The studies on the S_{-3} state presented in this Chapter are in line with the two earlier characteristics of this state [119]. It was discussed that the manganese ions of the PS II centers that remain active in oxygen evolution are still in their binding site and centers that

are inactivated are not easily photoactivated during the flash sequence. Taking into account proposal that the reduction of the OEC leads to Mn(II) ions that are released from their original binding sites (possibly, due to the loss of the μ-oxo bridges of the dimers [181]) but remain bound to the protein matrix. In this case, the restoration of the OEC could occur with a quantum yield significantly higher than that in the normal photoactivation process and a FIOP that is formally described by a higher miss parameter than that of the normal OEC turnover could arise.

The evidences for the high stability of the S_{-3} state given in this Chapter (Figures 7.3.3, 7.3.9 – 7.3.11) negate the previously proposed inactivation of PS II in the presence of hydrazine or hydroxylamine due to the instability of the S_{-3} state [245]. This proposal was based on the fact that Mn(II), which can be expected to be formed during S_{-3} formation, has a lower ligand field stabilization energy and is therefore expected to be less tightly bound by the OEC. In addition the results presented in this Chapter and in [119] show that inactivation of the oxygen evolution appears to occur largely independent of the redox state of the OEC and may be rate limited by reactions of hydrazine with the protein matrix (Figure 7.3.12) and/or other cofactors of PS II. Exceptions appear to be the S_{-4} and, especially, S_{-5} states, which are significantly less stable.

7.4.2 S_{-4} and S_{-5} states

This study shows that the addition of various known stabilizers of the oxygen evolving activity slows the inhibition of PS II by hydrazine and allows to observe higher S_{-4} and S_{-5} states populations. From the stabilizers tested in this study, $CaCl_2$ at concentrations of 20 mM to 50 mM and especially $MnCl_2$ (10 mM) were very effective. In the latter case essentially no loss of the oxygen evolving activity was observed after incubation with 20 mM hydrazine for 20 min.

In contrast, glycinebetaine did not effectively stabilize the oxygen activity of PS II in presence of hydrazine. Interestingly, under normal measuring conditions essentially no S_{-5} state was observed in presence of 0.5 M glycinebetaine. Similarly, crosslinking of the extrinsic proteins to PS II did not prevent inhibition.

One concern about the observed S_{-5} state populations is that they may be fit artefacts. Therefore, in this Chapter several different ways of fitting were explored. Especially the effects of various assumed β parameters and various degrees of reduction of Y_D were explored. In all tested cases, however, clearly better fits were obtained when S_{-5} state was included when fitting the relevant patterns after hydrazine incubation. Consequently, the S_{-}

$_4$ and S_{-5} states do not appear to be fit artefacts. Nevertheless, same concerns still remain to be disproved before the existence of the S_{-4} and S_{-5} states can be regarded as proven. The may concern is that the S_{-5} state appears almost simultaneously with the S_{-3} state (Figure 7.3.6). This finding is consistent with the earlier results on spinach thylakoids [119]. A second concern is that the S_{-5} state disappears after washing the sample with hydrazine free buffer. Therefore, the possibility exists that the S_{-5} state is not real, but arises from the interaction of NH_2NH_2 with the OEC during the flash train, e.g. via a fast reduction of the S_2 to S_0 state in the dark time between flashes.

On other hand, these findings do not role out the formation of the real S_{-4} and S_{-5} states, since e.g. some S_{-4} state remains after one washing step (Figure 7.3.3 and Table 7.3.2) and the lability of the S_{-5} state would not be very surprising if this state indeed corresponds to $Mn_4(II_4)$. Furthermore, the time course of the S_{-5} state formation may be explained by assuming that PS II preferentially deactivates in the S_{-4} and S_{-5} states.

It should be also mentioned that the stability of the S_{-3} state also toward washing with hydrazine free buffer as demonstrated in this study, argues against proposals that this state is already $Mn_4(II_4)$.

The outlined uncertainties can only be resolved if higher S_{-5} state populations are achieved. The most pronouncing strategy arises from the finding in this study that 10 mM $MnCl_2$ in the medium almost entirely prevents the inactivation of PS II during reduction with hydrazine down to S_{-3} state. This is probably due to the reduction of the driving force for the release of Mn_2^+ from PS II under these conditions.

Photoactivation experiments [156] have also identified HCO_3^- as being essential for the first steps of photoactivation. Therefore, bicarbonate can be also proposed as a possible “protector” of the OEC in our studies.

CHAPTER 8

Nitric Oxide Induced Formation of the S_{-2} state in the OEC of PS II from *Thermosynechococcus elongatus*

8.1 Introduction

In spinach PS II membranes the reduction of the Mn_4O_xCa complex with $NO^{\bullet}$ at -30°C leads to the formation of an intense EPR multiline signal, which was recently assigned to the S_{-2} state [179]. The S_{-2} EPR multiline signal can be very well simulated by a magnetically isolated Mn_2(II, III) dimer of spin S = 1/2 [161]. For unknown reasons the other two Mn ions of the OEC do not contribute to this signal, but based on the above assignment for the S_1 state the redox states of the whole cluster should be Mn_4(II, III, III, III) in the S_{-2} state.

In light of the emerging details about the structure of PS II in the thermophilic cyanobacterium *T. elongatus* based on X-ray crystallography [25, 26, 261] and the lack of crystallographic data about the otherwise better studied PS II from higher plants [20, 164, 262, 263] it is interesting to compare the structure and function of the two systems in detail. In this regard EPR measurements can play an important role because magnetic couplings are sensitive to changes in the structure and ligands of the OEC. The S_0, S_2 and S_3 state EPR signals have been detected in samples from both organisms and show only minor differences [199, 200, 264]. This is in agreement with structural information from EXAFS measurements on the S_1 and S_2 states [201]. Similarly, kinetic studies on the temperature dependence of the individual S state oxidations led to the conclusion that the reaction coordinates are very similar in cyanobacteria and plants [197]. In terms of EPR spectroscopy a notable exception is the g = 4.1 signal of the S_2 state. Despite intense efforts this EPR signal has not been detected in *T. elongatus* samples [205].

In this study the reactivity of $NO^{\bullet}$ with the OEC in spinach and *T. elongatus* samples was analyzed employing flash-induced oxygen evolution measurements and cw-EPR spectroscopy. Based on the presented data and results from the literature the close overall similarities of the OEC in cyanobacteria and higher plants are discussed together with possible structures of the Mn_4O_xCa complex in the S_{-2} state.

8.2 Experiments and analysis

8.2.1 Sample preparation

For NO• incubation all samples were transferred into the SNMM buffer (0.4 M Sucrose, 15 mM NaCl, 5 mM $MgCl_2$, 40 mM MES, pH 6.5). The final chlorophyll concentrations were 4-5 mg/ml, 0.8 mg/ml and 5-6 mg/ml for *T. elongatus* PS IIcc, *T. elongatus* thylakoids and spinach PS II membranes, respectively. To test the effect of cryoprotectants on NO• reduction the sucrose in SNMM buffer was substituted by either 25% Glycerol or by 400 mM Mannitol. In case of D_2O samples, SNMM buffer was prepared with D_2O (99.9 %, euriso-top) and the samples were washed twice with D_2O buffer, then incubated for 3 hours on ice and finally washed once more in D_2O buffer.

NO• treatment was carried out anaerobically in dim green light at 0°C in 4 mm EPR quartz tubes by slowly bubbling NO• through the samples. This procedure took about 1 min and the final NO• concentrations in the samples was estimated based on the known solubility of NO• in water (3 mM at 0°C) to be 0.2 mM and 0.6 mM for *T. elongatus* and spinach, respectively. The EPR tubes were then immediately sealed and transferred into liquid nitrogen. This was followed by an overnight incubation in a freezer at -30°C (± 2°C).

EPR

CW EPR spectra were recorded at liquid helium temperatures on a Bruker ESP 300E instrument fitted with a liquid helium cryostat (Oxford ESR 9) and a standard Bruker TE102 cavity.

FIOPs

FIOPs of *T. elongatus* thylakoids and PS II membranes were obtained in the absence of exogenous electron acceptors with a home-build Joliot type electrode [113, 196] at 20°C (details are given in Chapter 2.7.2 - 2.7.3). Saturating flashes at 2 Hz frequency were provided by a Xenon flash lamp (EG&G, model PS 302, light pack FY-604). For the oxygen measurements the NO•-treated samples were transferred, in the dark, from liquid nitrogen to ice temperatures. To remove NO• from the samples the space in the EPR tubes above the samples was carefully flushed with nitrogen while the sample was still frozen. After thawing was complete the samples were then slowly bubbled with 1 ml nitrogen using a syringe and finally transferred into Eppendorf reaction vials. They were kept

anaerobically on ice until shortly before the oxygen measurements, for which they were diluted in SNMM buffer to Chl concentrations of 0.2 mg/ml and 1 mg/ml for *T. elongatus* thylakoids and spinach PS II membranes, respectively.

8.2.2 Data analysis

8.2.2.1 Extensions to the Kok model to account for a possible direct electron donation of Y_D-NO to $P680^+$

To simulate the effects of direct Y_D-NO oxidation by $P680^+$ on flash-induced oxygen yield patterns, the initial Y_D-NO population, $[Y_D\text{-NO}]_0$, and the miss probability for its oxidation by $P680^+$, $\alpha_{YD\text{-NO}}$, were introduced as additional free parameters. The miss probability results from the relative rates by which Y_Z and Y_D-NO are able to reduce $P680^+$ after single flash excitation at room temperature and from the Q_A^- concentration prior to flash excitation. For simplicity it is assumed that $\alpha_{YD\text{-NO}}$ is S state independent. Because in a given PS II center Y_D-NO can be oxidized only once within a flash train, the absolute Y_D-NO fraction that is oxidized per flash, $\gamma_{YD\text{-NO}}(n)$, declines with flash number, n, during the flash train according to:

$$\gamma_{YD\text{-NO}}(n) = (1 - \alpha_{YD\text{-NO}}) \cdot [Y_D\text{-NO}]_{n-1}$$

where $[Y_D\text{-NO}]_{n-1} = [Y_D\text{-NO}]_{n-2} - \gamma_{YD\text{-NO}}(n-1)$ is the fraction of Y_D-NO present in PS II before the n-th flash. It is furthermore assumed that in the fraction of centers $(1 - \gamma_{YD\text{-NO}}(n))$ in which the OEC is oxidized the miss and double hit probabilities are the same as in the control. Since the oxidation of Y_D-NO leads to a miss for the OEC, the now flash number dependent miss parameter can be calculated to be:

$$\alpha\,(n) = \alpha\,(1 - \gamma_{YD\text{-NO}}(n)) + \gamma_{YD\text{-NO}}(n).$$

Similarly it follows that the double hit, β, and single hit, γ, probabilities of the OEC are:

$$\beta(n) = \beta\,(1 - \gamma_{YD\text{-NO}}(n))$$

$$\gamma(n) = (1 - \alpha - \beta)\,(1 - \gamma_{YD\text{-NO}}(n)).$$

8.2.2.2 Extensions to the Kok model to account for possible reductions of the S_2 and S_3 states by Y_D-NO during the flash train

Fast reductions of the S_2 and S_3 states by Y_D-NO were implemented into the extended Kok model described in Chapter 2.7.2 - 2.7.3 by splitting the initial S state populations into a fraction A, where the nitroso tyrosine had been formed, and a fraction B = 1-A, in which

back reactions do not take place during the flash train. Once the Y_D-NO centers of fraction A reach the S_2 or S_3 state they were allowed to convert from fraction A into fraction B according to:

$$d[S_2(A)]/dt = - k_{21} \bullet [\, S_2(A)]$$

$$d[S_3(A)]/dt = - k_{32} \bullet [\, S_3(A)]$$

$$d[S_1(B)]/dt = k_{21} \bullet [\, S_2(A)]$$

$$d[S_2(B)]/dt = k_{32} \bullet [\, S_3(A)].$$

8.3 Results

8.3.1 EPR

Figure 8.3.1 **A** shows an EPR difference spectrum ($NO^{\bullet}$ incubated state minus initial dark-adapted S_1 state) obtained from monomeric PS IIcc of *T. elongatus* after incubation with $NO^{\bullet}$ at - 30°C over night. Because of the frailness of the *T. elongatus* PS II core samples in the presence of $NO^{\bullet}$ the spectra shown were obtained prior to $NO^{\bullet}$ removal (see part 8.2 of this chapter). Therefore they also contain the free $NO^{\bullet}$ EPR signal which is centered at g = 2 (see e.g. [265]). For clarity of presentation most of this signal has been cut out, but the initial rise of the baseline on the high field side is still caused by $NO^{\bullet}$.

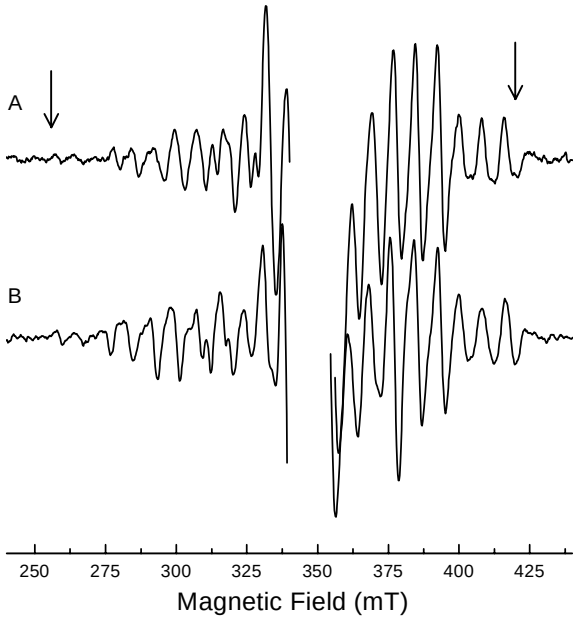

Figure 8.3.1. Comparison of S_{-2} EPR multiline signals (after subtraction of the S_1 dark stable spectrum) of *T. elongatus* monomeric core complexes (A) and spinach PS II membranes (B). The arrows indicate the spectral width of the complete spectrum, which is identical in both cases. The central part of the spectra, which is distorted by the signal of free $NO^{\bullet}$ was removed for clarity. EPR conditions: T = 8.5 K; microwave frequency 9.64 GHz; microwave power 31 mW; modulation amplitude 20 Gpp [116].

For comparison the S_{-2} EPR signal from spinach PS II membranes is shown in Figure 8.3.1 B. This signal was obtained under virtually identical conditions. The overall resemblance of the two EPR signals, namely a similar number of hyperfine peaks and the same spectral width (see arrows), suggests that the new $NO^{\bullet}$ induced EPR signal in *T. elongatus* PS IIcc also originates from the S_{-2} state. This assignment is further substantiated by flash-induced oxygen evolution patterns presented below.

In our initial trials we used glycerol instead of sucrose as cryoprotectant in the buffer, because the PS IIcc are more stable in such a buffer. In such samples $NO^{\bullet}$ incubation did not generate a multiline signal, although parallel flash-induced oxygen evolution measurements on thylakoids showed that the samples were reduced also under these conditions (data not shown, but similar to those presented below). Similarly, our tests showed that the addition of alcohols (methanol, ethanol) affects primarily the EPR multiline signal amplitude and not the S_{-2} state formation. In contrast, when mannitol was used, neither an EPR multiline signal nor a reduction was found.

Because of the excellent signal-to-noise ratio obtained for the S_{-2} state samples in sucrose buffer a detailed comparison of the two EPR spectra is possible. Such an inspection (Figure 8.3.2, traces **A** and **B**) reveals that the hyperfine structures of the two S_{-2} state EPR signals are somewhat different on the low field side. In contrast, most peaks on the high field side do line up. These differences have been consistently observed with several different PS IIcc samples. Thus, the spinach and the *T. elongatus* S_{-2} EPR multiline spectra are very similar, but not identical. For an accurate quantification of the observed differences measurements at other EPR frequencies and/or Mn ENDOR spectroscopy are required. This is beyond the scope of the current study.

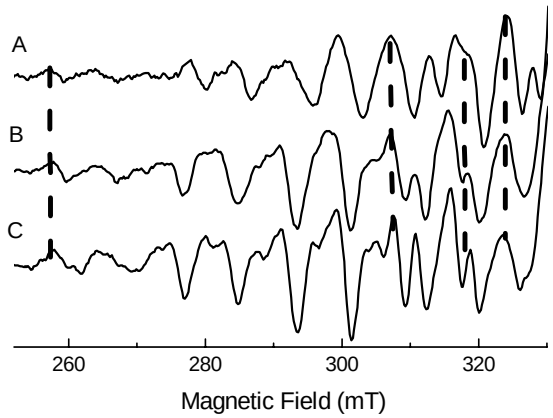

Figure 8.3.2. Comparison of the low field part of the S_{-2} EPR multiline signal: (A) *T. elongatus* monomeric core particles, (B) spinach PS II membranes (H_2O) and (C) spinach PS II membranes (D_2O). Experimental conditions as in Figure 8.3.1 [116].

To test the effect of proton hyperfine coupling on the structure of the S_{-2} state EPR signal, this signal was generated in a spinach sample suspended in D_2O buffer. The comparison of the EPR traces B and C in Figure 8.3.2 shows that the hyperfine structure in the D_2O sample is better resolved than in the H_2O sample which results from line narrowing. The hyperfine peak positions remain, however, unchanged.

The question has been raised, whether there is a magnetic interaction between the two PS II units in a dimeric PS IIcc that influences the EPR signals of the Mn_4O_xCa complex [200]. To test this interesting hypothesis for the case of the S_{-2} EPR multiline signal we have generated the S_{-2} state also in a dimeric PS IIcc isolated from *T. elongatus.* An S_{-2} EPR multiline signal identical to that of the monomers was found (data not shown). In case of the S_{-2} state this makes a magnetic interaction of the two OECs or of cytochrome C_{550} or b_{559} from monomer *a* with the OEC in monomer *b* in a dimeric PS IIcc unlikely. This result is in agreement with the distances between these components that can be obtained from the PS II crystal structure (Table 8.3.1). The distance between cytochrome C_{550} and the OEC within a monomer is about three times shorter than that of a OEC to the cytochrome C_{550} of the attached monomer.

Cofactors	Approximate distance (Å)
Mn_4(a)-Mn_4(b)	80
Mn_4(a) - Cyt C_{550}(a)	30
Mn_4(a) - Cyt C_{550}(b)	105
Mn_4(a) - Cyt b_{559}(a)	55
Mn_4(a) - Cyt b_{559}(b)	110

Table 8.3.1. Approximate center-to-center distances between different cofactors of the dimeric PS IIcc from *T. elongatus.* The numbers given are based on the 3.8 Å crystal structure [25]. The labels *a* and *b* refer to the two PS II monomers of a dimeric PS IIcc.

In addition to the reduction of the Mn_4O_xCa complex, which leads to the S_{-2} state EPR multiline signal, $NO^{\bullet}$ also binds to the non-heme iron on the acceptor side of PS II. This reversible binding of $NO^{\bullet}$ to high spin Fe^{2+} (S = 2) gives rise to a S = 3/2 state [265]. Following short $NO^{\bullet}$ incubation a g = 4 EPR signal from Fe(II)-NO is formed. Under our experimental conditions this signal is indistinguishable in spinach and *T. elongatus* (data not shown).

8.3.2 Flash-induced oxygen evolution

Flash-induced oxygen evolution patterns can provide insight into the reaction pathways of exogenous reductants of the OEC, since they allow the analysis of the S state composition of the samples after various incubation times and/or after treatment with different reductant

concentrations [179, 182]. To avoid side reactions $NO^{\bullet}$ was removed from the samples prior to the polarographic measurements presented below (see part 8.2 for details).

The FIOP of Figure 8.3.3 **a** is typical for PS II membrane fragments in absence of exogenous electron donors (see for example [208]). The first maximum of oxygen evolution occurs after the 3rd flash, which indicates a high S_1 state population in the dark-adapted sample prior to flash illumination. At higher flash numbers the oxygen yield decreases because the natural plastoquinone acceptor pool becomes reduced and thereby stable charge separation is prevented. Figure 8.3.3 **b** shows that $NO^{\bullet}$ incubation leads to a clear shift of the first maximum into the 6th flash.

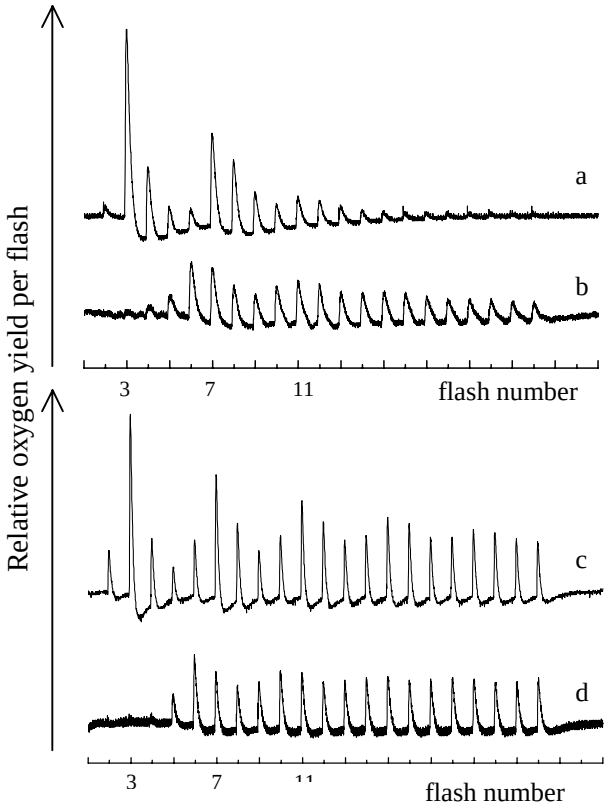

Figure 8.3.3. Flash-induced oxygen evolution patterns of spinach PS II membranes (a, b) and *T. elongatus* thylakoids (c, d) at 20°C and pH 6.5. **a** and **c** were obtained with untreated control samples, while traces **b** and **d** were obtained after incubation of the PS II samples with $NO^{\bullet}$ at - 30°C over night (b, d). In the latter cases $NO^{\bullet}$ was removed prior to the polarographic measurements (for details see part 8.2 of this chapter). The flash frequency was 2 Hz. No exogenous electron acceptors were added.

This measurement was obtained with an aliquot of a spinach PS II membrane sample that displayed an intense $NO^{\bullet}$-induced EPR multiline signal. The observed shift shows that $NO^{\bullet}$ has reduced a large number of PS II centers into the S_{-2} state that contains three additional electrons compared to the dark-stable S_1 state. For spinach PS II membranes this finding confirms similar results from a recent study [179]. The higher steady state oxygen yields observed after $NO^{\bullet}$ incubation of the PS II membranes (Figure 8.3.3 **b**) are indicative for the inactivation of part of the PS II complexes. The reason for this is that in absence of

exogenous electron acceptors the loss of some centers increases the number of available plastoquinone molecules for the PS II complexes that remain capable of oxygen evolution and share a common acceptor pool with the inactivated center(s) within a thylakoid membrane fragment. This effect has been previously observed using inhibitors like DCMU [239]. Because (i) no free Mn is observed in EPR measurements prior to the oxygen measurements and (ii) the S_{-2} state EPR signal has a very high intensity, this inactivation most likely occurs during the sample handling required to remove $NO^{\bullet}$ before the oxygen measurements (see part 8.2 for details).

Since exogenous electron acceptors cannot be used in the Joliot-type oxygen electrode set up and PS IIcc are largely devoid of the natural quinones, it was hard to obtain analogous data for *T. elongatus* PS IIcc. To prove that in *T. elongatus* samples the S_{-2} state can also be populated by $NO^{\bullet}$ incubation, data using *T. elongatus* thylakoids are provided (Figure 8.3.3 **c**, 8.3.3 **d**). Clearly, very similar flash-induced oxygen oscillation patterns to those shown above for spinach PS II membranes were obtained. The significantly higher steady state oxygen yields in *T. elongatus* thylakoids, which are not species related, but due to the larger plastoquinone pool in thylakoids compared to PS II membranes, allow a detailed analysis of these patterns in the framework of an extended Kok model (see Chapter 2). Fits C1 to C3 in Table 8.3.2 give normalized S state populations and the miss (α) and double hit (β) probabilities calculated for the *T. elongatus* thylakoid control measurement (Figure 8.3.3 **c**). Assuming 100 % S_1 state population, a reasonable fit was achieved with α = 11.3 % and β = 7.1 %. A significant improvement in fit quality is obtained when some S_2, S_0 and S_{-1} state populations are also allowed (fit C2). The small S_2 state population is due to incomplete dark-adaptation after the preflash treatment employed to oxidize most of Y_D through back reactions with the S_2 state. No further improvement in fit quality resulted when the S_{-2}, S_{-3}, S_{-4} and/or S_{-5} states were also included as free parameters (fit C3).

Based on EPR spectroscopy the lowest S state reached by $NO^{\bullet}$ incubation is the S_{-2} state. Therefore, a fit of the pattern 3d (see fit NO1) was attempted by only varying the S_1, S_0, S_{-1} and S_{-2} state populations and keeping the miss and double hit probabilities fixed to the values found for the control in fit C2. While this type of fit approach gives excellent results with samples reduced by moderate concentrations of hydrazine or hydroxylamine [182], it obviously fails to fit the data presented in Figure 8.3.3 **d**. If, in addition, the miss parameter is varied (fit NO2) a significantly better, but still insufficient fit quality can be achieved with a very high miss factor of about 18 %. It is therefore worthwhile to consider the possibility that additional donors are formed during $NO^{\bullet}$ incubation.

	Unknown donors															
fit	S_2 (%)	S_1 (%)	S_0 (%)	S_{-1} (%)	**S_{-2} (%)**	S_{-3} (%)	'S_{-4}' (%)	'S_{-5}' (%)	Y_D-NO (%)	$\alpha_{YD\text{-}NO}$ (%)	k_{21} s^{-1}	k_{32} s^{-1}	α (%)	β (%)	d	FQ x 10^{-6}
C1	-	100[f]	-	-	-	-	-	-	-	-	-	-	11.3	7.1	99.9	19
C2	**7.2**	**77.8**	**9.2**	**5.8**	-	-	-	-	-	-	-	-	**8.7**	**4.9**	**99.0**	**1.7**
C3	7.4	75.0	9.5	5.7	**0.0**	0.0	0.0	2.4	-	-	-	-	8.4	4.7	98.7	3
NO1	-	7.5	12.7	5.4	74.4	-	-	-	-	-	-	-	8.7[f]	4.9[f]	100[f]	248
NO2	-	1.0	0.2	15.3	83.6	-	-	-	-	-	-	-	18.1	4.9[f]	100[f]	34
NO3	-	0.4	0.0	26.0	**73.7**	-	-	-	87	76	-	-	8.7[f]	4.9[f]	99.7	36
NO4	-	0.0	6.7	23.0	**70.3**	-	-	-	53	-	14	14	8.7[f]	4.9[f]	100	68
NO5	-	1.1	0.0	8.1	**49.7**	19.7	20.2	1.2	-	-	-	-	8.7[f]	4.9[f]	99.2	8

Table 8.3.2. Fits of oxygen oscillation patterns shown in Figure 8.3.3
The extended Kok model described in Chapter 2.7.2 - 2.7.3 and the extensions outlined in the text and in the data analysis of part 8.2 were used to fit the oxygen oscillation patterns of dark-adapted *T. elongatus* control thylakoids (fits C1-C3 and Figure 8.3.3 **c**) and of the $NO^{\bullet}$ reduced thylakoids (fits NO1-NO5 and Figure 8.3.3 **d**) under different conditions (see text). Parameters: $S_2,\ldots,S_{-5}$, normalized S state populations of the OEC (currently only preliminary evidence for the S_{-4} and S_{-5} states exist [120]); Y_D-NO, nitroso tyrosine D which may act as an additional donor to $P680^+$ or the S_2 and S_3 states; $\alpha_{YD\text{-}NO}$, miss factor for proposed $P680^+$ reduction by Y_D-NO; k_{21} and k_{32}, rate constants for possible reductions of the S_2 and S_3 states by Y_D-NO (in fit NO4 only the lower limit is given); α, miss probability; β, double hit probability; d, damping parameter; fq, fit quality (data analysis of part 8.2). The first 16 flash-induced oxygen yields of each oscillation pattern have been analyzed. Other symbols (-) parameter was excluded from fit (fixed to zero); f, parameters were fixed to the value given in the table.

It was found recently [266] that $NO^{\bullet}$ can slowly ($t_{1/2}$ = 20 h at – 30°C) react with Y_D^{ox} and form the EPR silent nitroso-tyrosine (Y_D-NO). It is expected that Y_D-NO is a much more efficient electron donor then Y_D itself [266]. Therefore, Y_D-NO formation might be able to explain the increased miss parameter of fit NO2 by either direct electron donation to $P680^+$ or by rapid back reactions of the S_2 and S_3 states during the dark-times between the flashes. To further analyze these two possibilities the Kok model described in Chapter 2 was further extended to account for one additional donor (Y_D-NO) that can be oxidized only once within a flash train at the expense of the OEC. Fit NO3 shows that a similar fit quality to fit NO2 can be achieved if the initial Y_D-NO population is about 85 % and the miss probability $\alpha_{YD\text{-}NO}$ is about 75 %. However, based on the reported halftime of about 20 h at –30°C for Y_D-NO formation [266], this value for initial Y_D-NO population is significantly higher than one would expect to generate by an over night incubation with $NO^{\bullet}$. It is therefore worthwhile to also consider back reactions of S_2 and S_3 with Y_D-NO during the dark times of t_d = 0.5 s between the flashes. This was implemented into the extended Kok

model described in Materials and Methods by splitting the initial S state populations into a fraction A, where the nitroso tyrosine had been formed, and a fraction B = 1-A, in which back reactions do not take place during the flash train. Fit NO4 represents the best fit achieved when in addition to the S_1, .., S_{-2} states only the fraction of Y_D-NO centers (fraction A) and the two rate constants k_{21} and k_{32} were varied. The fit quality is lower by a factor of two compared to fits NO2 and NO3. It therefore appears that Y_D-NO formation alone is unable to fully explain the observed shifts in Figure 8.3.3 **d**.

As additional 'unknown' donors S states below the level of the S_{-2} state may be considered. Recent studies using hydrazine or hydroxylamine as reductants have provided clear evidence that reduced PS II samples can attain a fairly stable S_{-3} state [119]. In addition, first indications for the S_{-4} and S_{-5} states have been presented [120]. The S_{-5} state would represent the lowest possible oxidation state of the OEC (i.e. $Mn(II_4)$) if (i) the oxidation states of the S_1 state are Mn_4(III, III, IV, IV) as commonly assumed [47, 159, 174, 267]; see however [262] and (ii) only Mn-centered reductions take place. Although at present no EPR based evidence exist that states below the S_{-2} state can be generated by $NO^{\bullet}$ treatment at – 30°C, we are not aware of any principle reasons why $NO^{\bullet}$ should not be able to act in a similar way as other reductants and form small fractions of states below S_{-2}. In fact, the case of di-Mn-catalase from *Thermus thermophilus* shows that $NO^{\bullet}$ can reduce Mn ions down to Mn(II)Mn(II) level [268]. This possibility has been analyzed in fit NO5, in which the S_1, …, S_{-5} state populations were varied, but the miss and double hit probabilities were fixed to the control values. This fit approach gave an excellent fit quality, which is comparable to fit C2 of the control.

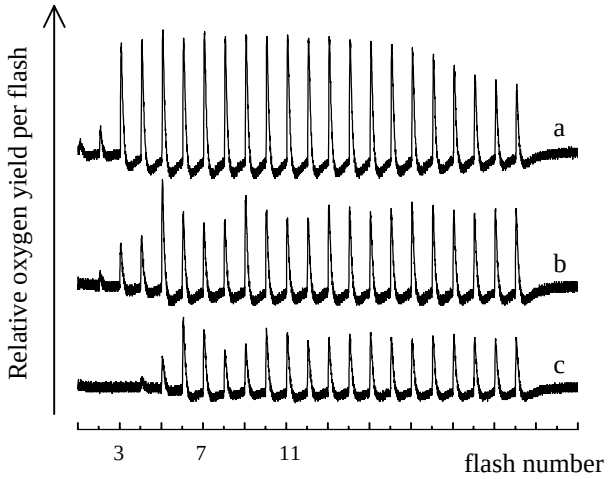

Figure 8.3.4. Flash-induced oxygen evolution patterns of *T. elongatus* thylakoids at 20°C and pH 6.5 after incubation of PS II samples with $NO^{\bullet}$ on ice for various times: a, 20 min; b, 1 h; c, 4 h. The flash frequency was 2 Hz. $NO^{\bullet}$ was removed before the polarographic measurements. No exogenous electron donors were added.

It is intriguing that the S_{-2} EPR signal is only observed when the $NO^{\bullet}$ reduction is performed at about - 30°C. Furthermore, when a sample displaying the S_{-2} EPR multiline signal is warmed to 0°C and is then quickly frozen to liquid nitrogen temperatures without a short incubation at - 30°C, then the S_{-2} EPR multiline signal is lost [266]. To test whether the incubation of the OEC with $NO^{\bullet}$ at ice temperature nevertheless also leads to the formation of the S_{-2} state and to learn more about the reduction mechanism, we incubated *T. elongatus* thylakoids with $NO^{\bullet}$ for various times on ice. Then the $NO^{\bullet}$ was removed and flash-induced oxygen evolution patterns were measured. The data in Figure 8.3.4 reveal that also at ice temperatures a reduction of the Mn_4O_xCa complex in one-electron steps of the type $S_1 \rightarrow S_0 \rightarrow S_{-1} \rightarrow S_{-2}$ ($\rightarrow S_{-3}$) takes place. This can be seen by the stepwise shift of the 1st maximum of oxygen evolution from the 3rd through the 4th and 5th flashes to the 6th flash. Interestingly, although the 4th flash undoubtedly increases transiently at short incubation times (Figure 8.3.4 **a**), no circumstances were found where it was clearly the maximum. This indicates that, similar to the reduction of the OEC with hydroxylamine [182], the S_0 state reacts slightly faster with $NO^{\bullet}$ than the S_1 state (see also [178]).

8.4 Discussion

8.4.1 Flash-induced oxygen evolution

A simple qualitative inspection of the flash-induced oxygen evolution patterns obtained in this study reveals that the OEC is reduced by $NO^{\bullet}$ at -30°C (Figure 8.3.3 **a**, 8.3.3 **b**) to states below S_0. The occurrence of the first maximum of oxygen evolution in the sixth flash suggests that most centers are in the S_{-2} state. In case of spinach PS II membranes the oxygen flash measurement could be performed on a sample that was first measured by EPR and displayed an intense $NO^{\bullet}$-induced multiline signal. These results confirm therefore the earlier assignment of the $NO^{\bullet}$-induced multiline signal from spinach samples to the S_{-2} state [179].

Because no exogenous electron acceptors can be used during the polarographic measurements, such a direct comparison between EPR and polarographic measurements proved impossible for the case of PS IIcc from *T. elongatus*. However, the new $NO^{\bullet}$-induced EPR signal in these *T. elongatus* samples can also be assigned to the S_{-2} state based on (i) the great similarity of the S_{-2} EPR spectrum of the spinach sample (Figures 8.3.1 and 8.3.2, see below) and (ii) the shift of the first maximum to the sixth flash in flash-induced oxygen yield patterns obtained from *T. elongatus* thylakoids after $NO^{\bullet}$ incubation under similar conditions (Figure 8.3.3 **d**).

The large plastoquinone pool of thylakoids allows a detailed analysis of the NO-induced flash patterns within extended Kok models (see Table 8.3.2). Since many different effects may contribute to the observed shifts of the flash-induced oxygen yields to higher flash numbers, different fit approaches have been applied. These consider effects like (i) a direct electron donation from Y_D-NO to $P680^+$, (ii) electron donation from Y_D-NO to S_2 and S_3 and (iii) the population of S states below the level of the S_{-2} state. With the current data it is impossible to decide which of the fits NO3, NO4 or NO5 is closest to reality. Probably all three effects contribute to the observed patterns. Nevertheless, the fits clearly show that 50 – 75 % of the PS II centers are in the S_{-2} state after NO-incubation at –30°C over night. This demonstrates that $NO^{\bullet}$ can also convert the OEC of *T. elongatus* into the S_{-2} state and supports thereby the assignment of the new EPR signal to this state. However, clearly a mixture of states is present in our samples with additional contributions from the S_{-1} state and, possibly, also from states below S_{-2}. Further studies are required to support the latter result.

8.4.2 EPR

Like the S_2 state of the 'normal' Kok cycle, the reduced S_{-2} state gives rise to a strong EPR signal, which provides valuable information about the electronic structure of the manganese cluster. The conditions for obtaining the S_{-2} EPR multiline signal are more critical than those require observing the S_2 state EPR multiline signal. Incubation temperatures different from - 30°C (under our conditions approx. ± 5°C), the use of different cryoprotectants (*vide supra*) or the addition of alcohols [178, 179, 266] all prevent the observation of this signal, although in many cases the formation of the S_{-2} state takes place as deduced from oxygen flash yield measurements [179] and this study). For example reduction at 0°C (Figure 8.3.4) does not lead to the EPR 'active' S_{-2} state (data not shown). The reasons for this specific temperature dependence of the magnetic properties of the Mn_4O_xCa complex are not yet understood.

The fact that the delicate S_{-2} state EPR signal can be generated in *T. elongatus* under virtually identical conditions as in spinach samples provides further evidence for the overall similarity of the OEC in plants and cyanobacteria [178, 179, 266]. The small but reproducible differences observed in the hyperfine structure between the S_{-2} EPR multiline signal from spinach and *T. elongatus* PS IIcc are, however, indicative of minor structural differences in the coordination geometry and/or the ligands of the Mn_4O_xCa complex.

Although the OEC contains four Mn ions, spectral simulations of the S_{-2} state EPR multiline signal from spinach PS II membranes showed that this signal can be ascribed to a magnetically isolated Mn_2(II, III) dimer [161]. This result for the S_{-2} state may be rationalized within a Mn_4O_xCa complex by a magnetic coupling of the four Mn ions to the limit of two uncoupled dimers [262]. The reasons why the four Mn ions do not interact magnetically in a similar way as for example in the S_2 state, where a coupling between all four Mn ions is assumed (for review see [263], are not understood. Protonation or loss of μ-oxo bridges during the reduction of the Mn_4O_xCa complex are possible explanations (see also [161, 269].

To better understand how incubation at - 30°C leads to a magnetic isolation of the $NO^{\bullet}$ induced Mn_2(II, III) dimer within the tetranuclear OEC, it would be very helpful to identify the two out of the four Mn ions that give rise to the observed EPR multiline signal. Based on the overall spectral similarity, it can be concluded that the same Mn_2(II, III) dimer gives rise to the S_{-2} EPR multiline signal in both spinach and *T. elongatus* samples. In the following we can therefore combine structural information obtained by EXAFS and EPR

spectroscopy with spinach PS II and those gathered from crystallography on *T. elongatus* samples.

Interestingly, the simulation parameters of the S_{-2} EPR multiline signals are very similar to those of the EPR signal of di-manganese catalase in the Mn_2(II, III) form [161, 162]. This may indicate a structural resemblance of the active center of Mn catalase in redox state Mn_2(II, III) and the dimeric building block of the OEC that gives rise to the S_{-2} EPR signal. The crystal structure of Mn catalase in *Thermus thermophilus* shows that the Mn-Mn distances are 3.18 Å in the Mn_2(II, II) form and 3.14 Å in the Mn_2(III, III) form and that in the fully reduced form the two Mn ions are bridged by one hydroxide, one water and one carboxylate. This bridging motif of the Mn_2(II, II) is similar to suggested bridging ligands of the 3.3 Å Mn-Mn distance in the OEC [159].

Additional information about the two Mn ions of the Mn_4O_xCa complex that give rise to the S_{-2} EPR multiline signal comes from the orientation dependence of this signal. A study with partially oriented spinach samples suggested that the Mn-(μ-oxo)-Mn plane makes an angle of about 20° (±10°) with the membrane plane [269]. This can be compared to Mn-Mn vectors determined by EXAFS spectroscopy. Based on new data for the Mn-Ca(Sr) vector [270] the orientation dependence of the 3.3 Å peak in Mn EXAFS could be deconvoluted into the Mn-Ca and Mn-Mn vectors at 3.4 Å and 3.3 Å, respectively [164]. This deconvolution results in an angle of about 28° for the 3.3 Å Mn-Mn vector relative to the membrane plane. Based on these results we propose that the Mn_2(II, III) dimer of the S_{-2} state might be assigned to the two Mn ions which form the 3.3 Å vector determined by EXAFS spectroscopy of PS II in the physiological S states.

From the 3.8 Å PS II crystal structure [25] the four shortest Mn-Mn vectors can be estimated to lie approximately 0°, 25°, 25° and 60° off the membrane plane. At 3.8 Å resolution it is not possible to discern exact Mn-Mn distances from the X-ray structure, but the four distances are all around 3 Å. Therefore, they probably correspond to the three 2.7 Å Mn-Mn distances and the one 3.3 Å Mn-Mn distance deduced from EXAFS spectroscopy in the S_0 state [166]. The crystallographic data show that there are two Mn-Mn vectors in the OEC with a similar angle to that determined by EPR for the Mn-Mn pair giving rise to the S_{-2} state multiline and to that obtained from EXAFS for the 3.3 Å Mn-Mn vector. Therefore, a definitive assignment of the 3.3 Å Mn-Mn vector and, thereby, a possible identification of the two Mn ions forming the S_{-2} multiline is not possible at present. Alternatively, as suggested previously [269], the one 2.7 Å Mn-Mn distances of the OEC that has an appropriate angle for the S_{-2} state EPR signal might become elongated to about 3.0 Å to 3.3 Å during the reduction process. A further discussion has to await a

higher resolution crystal structure of PS II, EXAFS studies of the S_{-2} state and detailed EPR studies on synthetic Mn_2(II, III) complexes with different bridging motifs.

In conclusion, it is shown that the S_{-2} state EPR signal can be generated in cyanobacteria in a similar way as in plants. Its signal magnitude and simple hyperfine structure makes it ideal for an inter species comparison and may allow the application of advanced EPR techniques in future.

APPENDIX

Table 1. The percentages of the fast or slow phases, A; rate constants (k, s^{-1}) and half-times ($t_{1/2}$, s) for the S states reduction in Y_D^{red} thylakoids from **spinach** resuspended in MMCH buffer (400 mM Mannitol, 10 mM $MgCl_2$, 20 mM $CaCl_2$ and 50 mM HEPES/NaOH) either at **pH 6.8**, **pD 6.8** or **pD 7.6**.

pH 6.8	**$S_2 \rightarrow S_1$**					
	Slow phase			**Fast phase**		
T,°C	k_{21}, s^{-1}	$t_{1/2}$, s	A, %	k_{21}, s^{-1}	$t_{1/2}$, s	A, %
10	0.0049	141	57	0.0515	13.4	43
15	0.0107	65	65	0.0978	7.1	35
20	0.0214	32	75	0.1994	3.5	25
25	0.0299	23	75	0.4198	1.7	25
30	0.0520	13	85	0.8342	0.8	15
pH 6.8	**$S_3 \rightarrow S_2$**					
T,°C	k_{32}, s^{-1}	$t_{1/2}$, s	A, %	k_{32}, s^{-1}	$t_{1/2}$, s	A, %
10	0.0050	140	67	0.0670	10.4	33
15	0.0090	76	70	0.1201	5.8	30
20	0.0163	42	70	0.2482	2.8	30
25	0.0263	26	71	0.3840	1.8	29
30	0.0481	14	71	0.6910	1	29

pD 6.8	**$S_2 \rightarrow S_1$**					
	Slow phase			**Fast phase**		
T,°C	k_{21}, s^{-1}	$t_{1/2}$, s	A, %	k_{21}, s^{-1}	$t_{1/2}$, s	A, %
10	0.0039	176	79	0.0351	19.7	21
15	0.0059	118	71	0.0534	13	29
20	0.0116	60	77	0.1094	6.3	23
25	0.0256	27	81	0.1921	3.6	19
30	0.0445	16	74	0.4097	1.6	16
pD 6.8	**$S_3 \rightarrow S_2$**					
T,°C	k_{32}, s^{-1}	$t_{1/2}$, s	A, %	k_{32}, s^{-1}	$t_{1/2}$, s	A, %
10	0.0076	91	77	0.0650	10.7	23
15	0.01088	64	79	0.1070	6.5	21
20	0.01965	35	79	0.1894	3.7	21
25	0.0330	21	78	0.3635	1.9	22
30	0.0644	11	82	0.6265	1.1	17

pD 7.6	$S_2Y_D \rightarrow S_1Y_D^{ox}$					
	Slow phase			**Fast phase**		
T,°C	k_{21}, s^{-1}	$t_{1/2}$, s	A, %	k_{21}, s^{-1}	$t_{1/2}$, s	A, %
5	0.0046	140	92	0.0149	46.6	8
10	0.0060	115	75	0.0395	17.6	25
15	0.0092	75	7.3	0.0483	14.3	27
20	0.0151	46	75	0.0871	8	25
25	0.0260	27	75	0.1581	4.4	25
30	0.0587	12	88	0.3791	1.8	12
35	0.0781	9	80	0.5389	1.3	20
pD 7.6	$S_3Y_D \rightarrow S_2Y_D^{ox}$					
T,°C	k_{32}, s^{-1}	$t_{1/2}$, s	A, %	k_{32}, s^{-1}	$t_{1/2}$, s	A, %
5	0.0039	177	93	0.0243	28.5	7
10	0.0058	119	86	0.0463	15	14
15	0.0101	69	90	0.0606	11.4	10
20	0.0115	60	77	0.0985	7	23
25	0.0197	35	76	0.1829	3.8	24
30	0.0362	19	81	0.2792	2.5	19
35	0.0602	12	80	0.4529	1.5	20

Table 2. The percentages of the fast or slow phases, A; rate constants (k, s^{-1}) and half-times ($t_{1/2}$, s) for the S states reduction in Y_D^{ox} (slow phase) and Y_D^{red} (fast phase) thylakoids from ***Thermosynechococcus elongatus*** resuspended in MMCH buffer (400 mM Mannitol, 10 mM $MgCl_2$, 20 mM $CaCl_2$ and 50 mM HEPES/NaOH) at **pH 6.8**.

pH 6.8	$S_2Q_B^{-/2-} \rightarrow S_1Q_B^{(-)}$			$S_2Y_D \rightarrow S_1Y_D^{ox}$		
	Slow phase			**Fast phase**		
T,°C	k_{21}, s^{-1}	$t_{1/2}$, s	A, %	k_{21}, s^{-1}	$t_{1/2}$, s	A, %
3.5	0.0003	2097	83	0.1120	6.2	93
10	0.0005	1506	83	0.2045	3.4	86
15				0.2824	2.5	80
20	0.0013	549	89	0.5945	1.2	55
25				0.9187	0.8	66
30	0.0023	298	86	1.5020	0.5	64
38	0.0058	120	73	2.5776	0.3	55
pH 6.8	$S_3Q_B^{-/2-} \rightarrow S_2Q_B^{(-)}$			$S_3Y_D \rightarrow S_2Y_D^{ox}$		
T,°C	k_{32}, s^{-1}	$t_{1/2}$, s	A, %	k_{32}, s^{-1}	$t_{1/2}$, s	A, %
3.5				0.0971	7.1	78
10	0.0002	2926	91	0.2416	2.9	83
15				0.3280	2.1	75
20	0.0006	1141	84	0.5366	1.3	74
25				0.8812	0.8	70
30	0.0031	221	88			
38	0.0129	54	82			

Table 3. The values of the rate constants (k, s^{-1}) and half-times ($t_{1/2}$, s) for the S_0 state dark reduction by Y_D^{ox} in thylakoids from ***Thermosynechococcus elongatus*** resuspended in MMCH buffer (400 mM Mannitol, 10 mM $MgCl_2$, 20 mM $CaCl_2$ and 50 mM HEPES/NaOH) at **pH 6.8**.

pH 6.8	$S_0Y_D^{ox} \rightarrow S_1Y_D$	
T,°C	k_{01}, s^{-1}	$t_{1/2}$, s
10	0.00008	8580
15	0.00010	7270
20	0.00016	4340
25	0.00014	4910
30	0.00018	3920

Table 4. The percentages of the fast phase, A; rate constants (k, s^{-1}) and half-times ($t_{1/2}$, s) for the S states reduction in Y_D^{red} (fast phase) thylakoids from ***Thermosynechococcus elongatus*** resuspended in MMCH buffer (400 mM Mannitol, 10 mM $MgCl_2$, 20 mM $CaCl_2$ and 50 mM HEPES/NaOH) either at **pD 6.8** or **pD 7.6**. The rate constants for the slow phase presented in Table 2 were used in calculation of the fast phases presented below. This approach was used as to separate fast and slow phases found to be difficult due to high percentage of Y_D^{red} in these samples.

	Fast phase		
pD 6.8	**$S_2Y_D^{red} \rightarrow S_1Y_D^{ox}$**		
T,°C	k_{21}, s^{-1}	$t_{1/2}$, s	A, %
10	0.0148	46.7	84
15	0.0366	18.9	83
20	0.0670	10.4	83
25	0.1648	4.2	83
30	0.2264	3.1	81
pD 6.8	**$S_3Y_D^{red} \rightarrow S_2Y_D^{ox}$**		
T,°C	k_{32}, s^{-1}	$t_{1/2}$, s	A, %
10	0.0183	37.8	81
15	0.0485	14.3	83
20	0.0727	9.5	92
25	0.1761	3.9	91
30	0.2586	2.7	92
	Fast phase		
pD 7.6	**$S_2Y_D^{red} \rightarrow S_1Y_D^{ox}$**		
T,°C	k_{21}, s^{-1}	$t_{1/2}$, s	A, %
10	0.0768	9	86
15	0.1157	6	91
20	0.1917	3.6	88
25	0.3695	1.9	91
30	0.6653	1	92
35	0.8684	0.8	89
pD 7.6	**$S_3Y_D^{red} \rightarrow S_2Y_D^{ox}$**		
T,°C	k_{32}, s^{-1}	$t_{1/2}$, s	A, %
10	0.0880	7.9	8.6
15	0.1129	6.1	94
20	0.2085	3.3	89
25	0.3998	1.7	91
30	0.7285	1	90
35	0.9079	0.8	90

BIBLIOGRAPHY

1. Brock, T. (1973) Evolutionary and ecological aspects of the cyanophytes in *The Biology of Cyanobacteria*, Eds: N.G. Carr and B.A. Whitton. *Blackwell Scientific*, Oxford 487-500.
2. Stanier, R.Y. and G. Cohenbazire (1977) Phototropic prokaryotes - cyanobacteria. *Annual Review of Microbiology* **31**: 225-274.
3. Stanier, R.Y. (1977) Position of cyanobacteria in world of phototrophs. *Carlsberg Research Communications* **42** (2): 77-98.
4. Fay, P. and C. Van Baalen (1987) The Cyanobacteria. *Elsevier*, Amsterdam.
5. Whitton, B.A. and M. Potts (2000) Ecology of cyanobacteria: their diversity in time and space. B.A. Whitton and M. Potts. *Kluw. Acad. Publ.*, London 1-3.
6. Schubert, W.D., O. Klukas, W. Saenger, H.T. Witt, P. Fromme and N. Krauss (1998) A common ancestor for oxygenic and anoxygenic photosynthetic systems: A comparison based on the structural model of PS I. *J. Mol. Biol.* **280** (2): 297-314.
7. Joyard, J. and R. Douce (1979) Chloroplast envelope is the site of galactolipid synthesis. *Plant Physiol.* **63** (5): 120-120.
8. Staehelin, L.A. and G.W.M. van der Staay (1996) Structure, composition, functional organization and dynamic properties of thylakoid membranes in *Oxygenic Photosynthesis: The Light Reactions*, Eds: D.R. Ort and C.F. Yocum. *Kluw. Acad. Publ.*, Dordrecht 11-30.
9. Wolfe, G. and J. Hoober (1996) Evolution of thylakoids structure in *Oxygenic Photosynthesis: The light reactions*, Eds: D. Ort and C. Yocum. *Kluw. Acad. Publ.*, Dordrecht 31-40.
10. Webb, M.S. and B.R. Green (1991) Biochemical and biophysical properties of thylakoid acyl lipids. *Biochim. Biophys. Acta* **1060** (2): 133-158.
11. Stern, K.R. (1997) Introductory plant biology. 7th Ed. *Wm. C. Brown Publ.*, Chicago.
12. Boffey, S.A. and R.M. Leech (1982) Chloroplast DNA levels and the control of chloroplast division in light-grown wheat leaves. *Plant Physiol.* **69** (6): 1387-1391.
13. Jagendorf, A.T. and A. Michaels (1990) Rough thylakoids - translation on photosynthetic membranes. *Plant Science* **71** (2): 137-145.

14. Somerville, C. and J. Browse (1991) Plant lipids - metabolism, mutants and membranes. *Science* **252** (5002): 80-87.

15. Lichtenthaler, H. (1968) Plastoglobuli and fine structure of plastids. *Endeavour* **27** (102): 144-149.

16. Dahlin, C. and H. Ryberg (1986) Accumulation of phytoene in plastoglobuli of San-9789 (norflurazon) - treated dark-grown wheat. *Physiol. Plant.* **68** (1): 39-45.

17. Barber, J. (2003) Homepage of J. Barber, Wolfson Laboratories, Department of Biological Sciences, Imperial College London. http://www.bio.ic.ac.uk/research/barber/photosystemII.html.

18. Rappaport, F., M. Guergova-Kuras, P.J. Nixon, B.A. Diner and J. Lavergne (2002) Kinetics and pathways of charge recombination in PS II. *Biochemistry* **41** (26): 8518-8527.

19. Renger, G. (1992) Energy transfer and trapping in Photosystem II in *Topics in Photosynthesis, The Photosystems: Structure, Function and Molecular Biology*, Eds: J. Barber. *Elsevier*, Amsterdam pp. 45–99.

20. Renger, G. (2001) Photosynthetic water oxidation to molecular oxygen: apparatus and mechanism. *Biochim. Biophys. Acta* **1503** (1-2): 210-228.

21. Bernarding, J., H.J. Eckert, H.J. Eichler, A. Napiwotzki and G. Renger (1994) Kinetic studies on the stabilization of the primary radical pair $P680^+$ $Pheo^-$ in different PS II preparations from higher plants. *Photochem. Photobiol.* **59** (5): 566-573.

22. Lavergne, J. and P. Joliot (1996) Dissipation in bioenergetic electron transfer chains. *Photosynth. Res.* **48** (1-2): 127-138.

23. Robinson, H.H. and A.R. Crofts (1983) Kinetics of the oxidation reduction reactions of the PS II quinone acceptor complex, and the pathway for deactivation. *FEBS Lett.* **153** (1): 221-226.

24. Nakamura, Y., T. Kaneko, S. Sato, M. Ikeuchi, H. Katoh, S. Sasamoto, A. Watanabe, M. Iriguchi, K. Kawashima, T. Kimura, Y. Kishida, C. Kiyokawa, M. Kohara, M. Matsumoto, A. Matsuno, N. Nakazaki, S. Shimpo, M. Sugimoto, C. Takeuchi, M. Yamada and S. Tabata (2002) Complete genome structure of the thermophilic cyanobacterium *Thermosynechococcus elongatus* BP-1. *DNA Research* **9** (4): 123-130.

25. Zouni, A., H.T. Witt, J. Kern, P. Fromme, N. Krauß, W. Saenger and P. Orth (2001) Crystal structure of PS II from *Synechococcus elongatus* at 3.8 Å resolution. *Nature* **409** (6821): 739-743.

26. Fromme, P., J. Kern, B. Loll, J. Biesiadka, W. Saenger, H.T. Witt, N. Krauss and A. Zouni (2002) Functional implications on the mechanism of the function of PS II including water oxidation based on the structure of PS II. *Philos. T. Roy. Soc. B* **357** (1426): 1337-1344.

27. Kamiya, N. and J.R. Shen (2003) Crystal structure of oxygen-evolving PS II from *Thermosynechococcus vulcanus* at 3.7-angstrom resolution. *Proc. Natl. Acad. Sci. USA* **100** (1): 98-103.

28. Hankamer, B., J. Nield, D. Zheleva, E.J. Boekema, S. Jansson and J. Barber (1997) Isolation and biochemical characterisation of monomeric and dimeric PS II complexes from spinach and their relevance to the organisation of PS II in vivo. *Eur J Biochem.* **243** (1-2): 422-9.

29. Hankamer, B., E. Morris, J. Nield, C. Gerle and J. Barber (2001) Three-dimensional structure of the PS II core dimer of higher plants determined by electron microscopy. *J. Struct. Biol.* **135** (3): 262-269.

30. Hankamer, B., J. Barber and E.J. Boekema (1997) Structure and membrane organization of PS II from green plants. *Ann. Rev. Plant. Phys. Plant. Mol. Biol.* **48**: 641–672.

31. Hankamer, B., E. Morris, J. Nield, A. Carne and J. Barber (2001) Subunit positioning and transmembrane helix organization in the core dimer of PS II. *FEBS Lett.* **504** (3): 142-151.

32. Barber, J. and J. Nield (2002) Organization of transmembrane helices in PS II: comparison of plants and cyanobacteria. *Philos. T. Roy. Soc. B* **357** (1426): 1329-1335.

33. Deisenhofer, J., O. Epp, K. Miki, R. Huber and H. Michel (1985) Structure of the Protein Subunits in the Photosynthetic Reaction center of *Rhodopseudomonas viridis* at 3 Å resolution. *Nature* **318**: 618-624.

34. Chang, C.-H., O. El-Kabbani, D. Tiede, J. Norris and M. Schiffer (1991) Structure of the Membrane-Bound Protein Photosynthetic Reaction center from *Rhodobacter sphaeroides*. *Biochemistry* **30**: 5352-5360.

35. Allen, J.P., G. Feher, T.O. Yeates, H. Komiya and D.C. Rees (1987) Structure of the reaction renter from *Rhodobacter spaeroides* R-26: The protein subunits. *Proc. Natl. Acad. Sci. USA* **84**: 6162-6166.

36. Trebst, A. (1986) The Topology of the Plastoquinone and Hebicide Binding Peptides of PS II in the Thylakoid Membrane. *Z. Naturforsch.* **41c**: 240-245.

37. Svensson, B., I. Vass and S. Styring (1991) Sequence Analysis of the D1 and D2 Reaction center Proteins of PS II. *Z. Naturforsch.* **46c**: 765-776.

38. Akabori, K., H. Tsukamoto, J. Tsukihara, T. Nagatsuka, O. Motokawa and Y. Toyoshima (1988) Disintegration and reconstitution of PS II reaction center core complex 1. Preparation and characterization of 3 different types of subcomplex. *Biochim. Biophys. Acta* **932** (3): 345-357.

39. Nanba, O. and K. Satoh (1987) Isolation of a PS II Reaction center Consisting of D-1 and D-2 Polypeptides and Cytochrome b-559. *Proc. Natl. Acad. Sci. USA* **84** (1): 109-112.

40. Satoh, K., Y. Kashino and H. Koike (1993) Electron-Transport from Q_A to Thymoquinone in a *Synechococcus* Oxygen-Evolving PS II Preparation - Role of Q_B and Binding-Affinity of Thymoquinone to the Q_B Site. *Z. Naturforsch. C* **48** (3-4): 174-178.

41. Cramer, W.A., S.M. Theng and W.R. Widger (1986) On the structure and function of Cytochrome b-559. *Photosynth. Res.* **10**: 393-403.

42. Zouni, A., R. Jordan, E. Schlodder, P. Fromme and H.T. Witt (2000) First PS II crystals capable of water oxidation. *Biochim. Biophys. Acta* **1457** (3): 103-105.

43. Bricker, T. (1990) The structure and function of CPa-1 and CPa-2 in PS II. *Photosynth. Res.* **24**: 1-13.

44. Bricker, T.M. and D.F. Ghanotakis (1996) Introduction to oxygen evolution and the Oxygen-Evolving Complex in *Oxygenic Photosynthesis: The Light Reactions*, Eds: D.R. Ort and C.F. Yocum. *Kluwer*, Dordrecht 113-136.

45. Harrer, R., R. Bassi, M.G. Testi and C. Schafer (1998) Nearest-neighbor analysis of a PS II complex from *Marchantia polymorpha* L. (liverwort), which contains Reaction center and Antenna proteins. *Eur. J. Biochem.* **255** (1): 196-205.

46. Ishikawa, Y., E. Nakatani, T. Henmi, A. Ferjani, Y. Harada, N. Tamura and Y. Yamamoto (1999) Turnover of the aggregates and cross-linked products of the D1 protein generated by acceptor-side photoinhibition of PS II. *Biochim. Biophys. Acta* **1413** (3): 147-158.

47. Debus, R.J. (1992) The manganese and calcium ions of photosynthetic oxygen evolution. *Biochim. Biophys. Acta* **1102**: 269-352.

48. Green, B.R. and D.G. Durnford (1996) The Chl - carotenoid proteins of oxygenic photosynthesis. *Annual Review of Plant Physiology and Plant Molecular Biology* **47**: 685-714.

49. Pichersky, E., R. Subramaniam, M.J. White, J. Reid, R. Aebersold and B.R. Green (1991) Chl a/b binding (Cab) polypeptides of Cp29, the internal Chl a/b complex of PS II - characterization of the tomato gene encoding the 26 kDa (type-I) polypeptide and evidence for a 2nd Cp29 polypeptide. *Molecular & General Genetics* **227** (2): 277-284.

50. Green, B.R., E. Pichersky and K. Kloppstech (1991) Chl a/b binding proteins - an extended family. *Trends Biochem. Sci.* **16** (5): 181-186.

51. Green, B.R. and E. Pichersky (1994) Hypothesis for the evolution of 3-helix Chl a/b and Chl a/c light-harvesting antenna proteins from 2-helix and 4-helix ancestors. *Photosynth. Res.* **39** (2): 149-162.

52. Horton, P., A.V. Ruban and R.G. Walters (1996) Regulation of light harvesting in green plants. *Annual Review of Plant Physiology and Plant Molecular Biology* **47**: 655-684.

53. Jansson, S. (1994) The Light-Harvesting Chl a/b Binding-Proteins. *Biochim. Biophys. Acta* **1184** (1): 1-19.

54. Kuttkat, A., R. Grimm and H. Paulsen (1995) Light-harvesting Chl a/b - binding protein inserted into isolated thylakoids binds pigments and is assembled into trimeric light - harvesting complex. *Plant Physiol.* **109** (4): 1267-1276.

55. Paulsen, H. (1995) Chl a/b - binding proteins. *Photochem. Photobiol.* **62** (3): 367-382.

56. Hobe, S., R. Foster, J. Klingler and H. Paulsen (1995) N-proximal sequence motif in light-harvesting Chl a/b - binding protein is essential for the trimerization of light-harvesting Chl a/b complex. *Biochemistry* **34** (32): 10224-10228.

57. Kuhlbrandt, W., D.N. Wang and Y. Fujiyoshi (1994) Atomic model of plant light-harvesting complex by electron crystallography. *Nature* **367** (6464): 614-621.

58. Peter, G.F. and J.P. Thornber (1991) Biochemical composition and organization of higher plant PS II light-harvesting pigment proteins. *J. Biol. Chem.* **266** (25): 16745-16754.

59. Sidler, W. (1994) Pycobilisome and Phycobiliprotein Structures in *The Molecular Biology of Cyanobacteria*, Eds: D.A. Bryant. *Kluw.Acad.Publ.* 139-216.

60. Bassi, R., D. Sandona and R. Croce (1997) Novel aspects of Chl a/b binding proteins. *Physiol. Plant.* **100** (4): 769-779.

61. Glazer, A.N. (1994) Phycobiliproteins - a family of valuable, widely used fluorophores. *Journal of Applied Phycology* **6** (2): 105-112.

62. Pakrasi, H.B., J.G.K. Williams and C.J. Arntzen (1988) Targeted mutagenesis of the Psb E and Psb F genes blocks photosynthetic electron transport. Evidence for a functional-role of Cytochrome b-559 in PS II. *Embo Journal* **7** (2): 325-332.

63. Komenda, J. and J. Barber (1995) Comparison of Psb O and Psb H deletion mutants of *Synechocystis* Pcc-6803 indicates that degradation of D1 protein is regulated by the Q_B site and dependent on protein synthesis. *Biochemistry* **34** (29): 9625-9631.

64. Bergantino, E., A. Brunetta, A. Segalla, I. Szabo, D. Carbonera, E. Bordignon, F. Rigoni and G.M. Giacometti (2002) Structural and functional role of the Psb H protein in resistance to light stress in *Synechocystis* PCC 6803. *Functional Plant Biology* **29** (10): 1181-1187.

65. Ikeuchi M, Shukla VK, Pakrasi HB and I. Y (1995) Directed inactivation of the Psb I gene does not affect PS II in the cyanobacterium *Synechocystis* sp. PCC 6803. *Mol Gen Genet.* **249** (6): 622-8.

66. Lind, L.K., V.K. Shukla, K.J. Nyhus and H.B. Pakrasi (1993) Genetic and immunological analyses of the cyanobacterium *Synechocystis* sp Pcc-6803 show that the protein encoded by the Psb J gene regulates the number of PS II centers in thylakoid membranes. *J. Biol. Chem.* **268** (3): 1575-1579.

67. Regel, R.E., N.B. Ivleva, H. Zer, J. Meurer, S.V. Shestakov, R.G. Herrmann, H.B. Pakrasi and I. Ohad (2001) Deregulation of electron flow within PS II in the absence of the Psb J protein. *J. Biol. Chem.* **276** (44): 41473-41478.

68. Hager, M., M. Hermann, A. Biehler, A. Krieger-Liszkay and R. Bock (2002) Lack of the small plastid-encoded PsbJ polypeptide results in a defective water-splitting apparatus of PS II, reduced PS I levels, and hypersensitivity to light. *J. Biol. Chem.* **277** (16): 14031-14039.

69. Sugimoto, I. and Y. Takahashi (2003) Evidence that the Psb K polypeptide is associated with the PS II core antenna complex CP43. *J. Biol. Chem.* **278** (45): 45004-45010.

70. Hoshida, H., R. Sugiyama, Y. Nakano, T. Shiina and Y. Toyoshima (1997) Electron paramagnetic resonance and mutational analyses revealed the involvement of PS II L subunit in the oxidation step of Y_Z by $P680^+$ to form the $Y_Z^+P680Pheo^-$ state in PS II. *Biochemistry* **36** (40): 12053-12061.

71. Anbudurai, P.R. and H.B. Pakrasi (1993) Mutational analysis of the Psb l Protein of PS II in the cyanobacterium *Synechocystis* sp Pcc-6803. *Z. Naturforsch. C* **48** (3-4): 267-274.

72. Ozawa, S., T. Kobayashi, R. Sugiyama, H. Hoshida, T. Shiina and Y. Toyoshima (1997) Role of PS II - L protein (Psb L gene product) on the electron transfer in PS II complex .1. Over-production of wild-type and mutant versions of PS II - L protein and reconstitution into the PS II core complex. *Plant Mol. Biol.* **34** (1): 151-161.

73. Funk, C. (2000) Functional analysis of the Psb X protein by deletion of the corresponding gene in *Synechocystis* sp PCC 6803. *Plant Mol. Biol.* **44** (6): 815-827.

74. Kapazoglou, A., F. Sagliocco and L. Dure (1995) PS II - T, a new nuclear-encoded lumenal protein from PS II - targeting and processing in isolated-chloroplasts. *J. Biol. Chem.* **270** (20): 12197-12202.

75. Shen, J., M. Ikeuchi and Y. Inoue (1997) Analysis of the psb U gene encoding the 12-kDa extrinsic protein of PS II and studies on its role by deletion mutagenesis in *Synechocystis* sp. PCC 6803. *J Biol Chem.* **272** (28): 17821-6.

76. Shen, J., W. Vermaas and Y. Inoue (1995) The role of Cytochrome c-550 as studied through reverse genetics and mutant characterization in *Synechocystis* sp. PCC 6803. *J Biol Chem.* **270** (12): 6901-7.

77. Irrgang, K.D., L.X. Shi, C. Funk and W.P. Schroder (1995) A nuclear-encoded subunit of the PS II Reaction center. *J. Biol. Chem.* **270** (29): 17588-17593.

78. Mant, A. and C. Robinson (1998) An *Arabidopsis* cDNA encodes an apparent polyprotein of two non-identical thylakoid membrane proteins that are associated with PS II and homologous to algal *ycf 32* open reading frames. *FEBS Lett.* **423** (2): 183-188.

79. Gau, A.E., H.H. Thole, A. Sokolenko, L. Altschmied, R.G. Herrmann and E.K. Pistorius (1998) Psb Y, a novel manganese-binding, low-molecular-mass protein associated with PS II. *Molecular and General Genetics* **260** (1): 56-68.

80. Meetam, M., N. Keren, I. Ohad and H.B. Pakrasi (1999) The Psb Y protein is not essential for oxygenic photosynthesis in the cyanobacterium *Synechocystis* sp PCC 6803. *Plant Physiol.* **121** (4): 1267-1272.

81. Swiatek, M., R. Kuras, A. Sokolenko, D. Higgs, J. Olive, G. Cinque, B. Muller, L.A. Eichacker, D.B. Stern, R. Bassi, R.G. Herrmann and F.A. Wollman (2001) The chloroplast gene *ycf 9* encodes a PS II (PS II) core subunit, Psb Z, that participates in PS II supramolecular architecture. *Plant Cell* **13** (6): 1347-1367.

82. Eckardt, N.A. (2001) A role for Psb Z in the core complex of PS II. *Plant Cell* **13** (6): 1245-1248.

83. Thornber, J.P., G.F. Peter, D.T. Morishige, S. Gomez, S. Anandan, B.A. Welty, A. Lee, C. Kerfeld, T. Takeuchi and S. Preiss (1993) Light Harvesting in PS I and PS II. *Biochem. Soc. Trans.* **21** (1): 15-18.

84. Green, B.R., D.R. Shen, R. Aebersold and E. Pichersky (1992) Identification of the polypeptides of the major Light-Harvesting Complex of PS II (LHC II) with their genes in tomato. *FEBS Lett.* **305** (1): 18-22.

85. Shen, J.R. and Y. Inoue (1993) Binding and functional properties of 2 new extrinsic components, Cytochrome c-550 and a 12-kDa protein in cyanobacterial PS II. *Biochemistry* **32** (7): 1825-1832.

86. Pakrasi, H.B. (1995) Genetic analysis of the form and function of PS I and PS II. *Annu Rev Genet.* **29**: 755-76.

87. Schröder, W.P. and H.-E. Åkerlund (1986) H_2O_2 accessibility to the PS II donor side in protein-depleted inside-out thylakoids measured as flash induced oxygen production. *Biochim Biophys Acta* **848**: 359-363.

88. Berg, S.P. and M. Seibert (1987) Is functional manganese involved in hydrogen-peroxide-stimulated anomalous oxygen evolution in $CaCl_2$-washed PS II membranes? *Photosynth. Res.* **13**: 3-17.

89. Hillier, W. and T. Wydrzynski (1993) Increases in peroxide formation by the PS II oxygen evolving reactions upon removal of the extrinsic 16, 22 and 33 kDa proteins are reversed by $CaCl_2$ addition. *Photosynth. Res.* **38**: 417-424.

90. Burnap, R.L. and L.A. Sherman (1991) Deletion Mutagenesis in Synechocystis sp Pcc6803 Indicates That the Mn-Stabilizing Protein of PS II Is Not Essential for O2 Evolution. *Biochemistry* **30** (2): 440-446.

91. Mayes, S.R., K.M. Cook, S.J. Self, Z.H. Zhang and J. Barber (1991) Deletion of the gene encoding the PS II 33 kDa protein from *Synechocystis* sp Pcc-6803 does not inactivate water-splitting but increases vulnerability to photoinhibition. *Biochim. Biophys. Acta* **1060** (1): 1-12.

92. Philbrick, J.B., B.A. Diner and B.A. Zilinskas (1991) Construction and characterization of cyanobacterial mutants lacking the manganese-stabilizing polypeptide of PS II. *J. Biol. Chem.* **266** (20): 13370-13376.

93. Shen, J.R., R.L. Burnap and I. Y. (1995) An independent role of Cytochrome c-550 in cyanobacterial PS II as revealed by double-deletion mutagenesis of the Psb O and Psb V genes in *Synechocystis* sp. PCC 6803. *Biochemistry* **34** (39): 12661-8.

94. Kok, B., B. Forbush and M. McGloin (1970) Cooperation of charges in photosynthetic oxygen evolution. *Photochem. Photobiol.* **11**: 457-476.

95. Joliot, P., G. Barbieri and R. Chabaud (1969) Un nouveau modele des centres photochimiques du systeme II. *Photochem. Photobiol.* **10**: 309-329.

96. Vermaas, W.E.J., G. Renger and G. Dohnt (1984) The reduction of the oxygen evolving system in chloroplasts by thylakoid components. *Biochim. Biophys. Acta* **764** (2): 194-202.

97. Nugent, J.H.A., C. Demetriou and C.J. Lockett (1987) Electron donation in PS II. *Biochim. Biophys. Acta* **894** (3): 534-542.

98. Rutherford, A.W. and S. Styring (1987) EPR signal II in PS II: redox and paramagnetic interactions with the molecular oxygen evolving enzyme. *Cytochrome Syst.: Mol. Biol. Bioenerg., [Proc. UNESCO Int. Symp.]*: 541-7.

99. Vermaas, W.F.J., A.W. Rutherford and O. Hansson (1988) Site directed mutagenesis in PS II of the cyanobacterium *Synechocystis sp.* PCC 6803: donor D is a tyrosine residue in the D2 protein. *Proc. Natl. Acad. Sci. USA* **85** (22): 8477-81.

100. Isgandarova, S., G. Renger and J. Messinger (2003) Functional differences of PS II from *Synechococcus elongatus* and spinach characterized by Flash-Induced Oxygen evolution Patterns. *Biochemistry* **42**: 8929-8938.

101. Diner, B.A. (1977) Dependence of deactivation reactions of PS II on redox state of plastoquinone pool-a varied under anaerobic conditions. Equilibria on the acceptor side of PS II. *Biochim. Biophys. Acta* **460**: 247-258.

102. Rutherford, A.W., A.R. Crofts and Y. Inoue (1982) Thermoluminescence as a probe of PS II photochemistry. The origin of the flash-induced glow peaks. *Biochim. Biophys. Acta* **682** (3): 457-65.

103. Rutherford, A.W. and Y. Inoue (1984) Oscillation of delayed luminescence from PS II: recombination of $S_2Q_B^-$ and $S_3Q_B^-$. *FEBS Lett.* **165** (2): 163-70.

104. Styring, S. and A.W. Rutherford (1987) In the oxygen evolving complex of PS II the S_0 state is oxidized to the S_1 State by Y_D^+ (Signal II_{slow}). *Biochemistry* **26**: 2401-2405.

105. Vass, I., Z. Deak and E. Hideg (1990) Charge equilibrium between the water oxidizing complex and the electron donor tyrosine D in PS II. *Biochim. Biophys. Acta* **1017**: 63-69.

106. Vass, I., Z. Deak, C. Jegerschold and S. Styring (1990) The accessory electron donor tyrosine-D of PS II is slowly reduced in the dark during low temperature storage of isolated thylakoids. *Biochim. Biophys. Acta* **1018** (1): 41-46.

107. Vass, I. and S. Styring (1991) pH dependent charge equilibria between tyrosine-D and the S-states in PS II. Estimation of relative midpoint potentials. *Biochemistry* **30**: 830-839.

108. Messinger, J. and G. Renger (1993) Generation, oxidation by the oxidized form of the tyrosine of polypeptide D2, and possible electronic configuration of the redox States S_0, S_{-1} and S_{-2} of the water oxidase in isolated spinach thylakoids. *Biochemistry* **32** (36): 9379-9386.

109. Messinger, J. and G. Renger (1994) Analysis of pH-induced modifications of the period four oscillation of the flash-induced oxygen evolution reveal distinct structural changes of the PS II donor side at characteristic pH values. *Biochemistry* **33**: 10896-10905.

110. Forbush, B., B. Kok and M.P. McGloin (1971) Cooperation of charges in photosynthetic oxygen evolution. II. Damping of flash yield oscillation, deactivation. *Photochem. Photobiol.* **14** (3): 307-21.

111. Renger, G. and B. Hanssum (1988) Studies on the deconvolution of flash induced absorption changes into the difference spectra of individual redox steps within the water oxidizing enzyme system. *Photosynth. Res.* **16**: 243-259.

112. Shinkarev, V. and C.A. Wraight (1993) Oxygen evolution in photosynthesis: from unicycle to bicycle. *Proc. Natl. Acad. Sci. USA* **90**: 1834-1838.

113. Messinger, J. (1993), Untersuchungen über die reaktiven Eigenschaften der verschiedenen Redoxzustände der Wasseroxidase Höherer Pflanzen in *Fachbereich 6TU Berlin*, Berlin 229.

114. Jursinic, P. (1981) Investigation of double turnovers in PS II charge separation and oxygen evolution with excitation flashes of different duration. *Biochim. Biophys. Acta* **635**: 38 - 52.

115. Meunier, P.C., R.L. Burnap and L.A. Sherman (1996) Improved 5-step modeling of the PS II S-state mechanism in cyanobacteria. *Photosynth. Res.* **47**: 61-76.

116. Sarrou, J., S. Isgandarova, J. Kern, A. Zouni, G. Renger, W. Lubitz and J. Messinger (2003) Nitric Oxide induced formation of the S_{-2} state in the oxygen evolving complex of PS II from *Synechococcus elongatus*. *Biochemistry* **42** (4): 1016-1023.

117. Bader, K.P., P. Thibault and G.H. Schmid (1983) A study on oxygen evolution and on the S-state distribution in thylakoid preparations of the filamentous blue-green alga *Oscillatoria chalybea*. *Z. Naturforsch. C* **38** (9-10): 778-792.

118. Messinger, J., S. Pauly and H.T. Witt (1991) The flash pattern of photosynthetic oxygen evolution after treatment with low concentrations of hydroxylamine as a function of the previous S_1/S_0 ratio. Further evidence that NH_2OH reduces the water oxidizing complex in the dark. *Z. Naturforsch. C* **46** (11-12): 1033-1038.

119. Messinger, J., G. Seaton, T. Wydrzynski, U. Wacker and G. Renger (1997) S_{-3} state of the water oxidase in PS II. *Biochemistry* **36**: 6862-6873.

120. Messinger, J., J.H. Robblee, U. Bergmann, C. Fernandez, P. Glatzel, S. Isgandarova, B. Hanssum, G. Renger, S.P. Cramer, K. Sauer and V.K. Yachandra (Year) Manganese oxidation states in PS II. in *Proceedings of the 12th International Congress on Photosynthesis*. Collingwood, Australia *CSIRO Publishing* S10-019.

121. Renger, G. (1969) Reaction of Cccp in photosynthesis on an intermediate between Chl-A2 and water. *Naturwissenschaften* **56** (7): 370-&.

122. Debus, R.J., B.A. Barry, I. Sithole, G.T. Babcock and L. Mcintosh (1988) Directed mutagenesis indicates that the donor to $P680^+$ in PS II is tyrosine-161 of the D1 polypeptide. *Biochemistry* **27** (26): 9071-9074.

123. Hoganson, C.W. and G.T. Babcock (1997) A metalloradical mechanism for the generation of oxygen from water in photosynthesis. *Science* **277**: 1953-1956.

124. Hillier, W. and J. Messinger (2004) Photosynthetic water oxidation in *PS II: The water/plastoquinone oxido-reductase in photosynthesis*, Eds: T. Wydrzynski and K. Satoh. *Kluwer Publications*, Dordrecht, The Netherlands submitted.

125. Faller, P., A. Boussac, R.J. Debus, K. Brettel and A.W. Rutherford (2001) Tyrosyl radicals in PS II: the stable tyrosyl D and the catalytic tyrosyl Z. *J. Inorg. Biochem.* **86** (1): 214-214.

126. Faller, P., R.J. Debus, K. Brettel, M. Sugiura, A.W. Rutherford and A. Boussac (2001) Rapid formation of the stable tyrosyl radical in PS II. *Proc. Natl. Acad. Sci. USA* **98** (25): 14368-14373.

127. Diner, B.A. and F. Rappaport (2002) Structure, dynamics, and energetics of the primary photochemistry of PS II of oxygenic photosynthesis. *An. Rev. Plant. Biol.* **53**: 551-580.

128. Ananyev, G.A., I. Sakiyan, B.A. Diner and G.C. Dismukes (2002) A functional role for tyrosine-D in assembly of the inorganic core of the water oxidase complex of PS II and the kinetics of water oxidation. *Biochemistry* **41** (3): 974-980.

129. Yocum, C.F. (1992) The calcium and chloride requirements for photosynthetic water oxidation in *Manganese Redox Enzymes*, Eds: V.L. Pecoraro. *VCH Publishers*, New York 71-84.

130. Van Rensen, J.J.S., C. Xu and Govindjee (1999) Role of bicarbonate in PS II, the water-plastoquinone oxido-reductase of plant photosynthesis. *Physiol. Plant.* **105**: 585-592.

131. Ananyev, G.M., L. Zaltsman, C. Vasko and G.C. Dismukes (2001) The inorganic biochemistry of photosynthetic oxygen evolution/water oxidation. *Biochim. Biophys. Acta* **1503**: 52-68.

132. Shen, J.-R., K. Satoh and S. Katoh (1988) Calcium content of oxygen-evolving PS II preparations from higher plants. Effects of NaCl treatment. *Biochim. Biophys. Acta* **933**: 358-364.

133. Ono, T.-A. and Y. Inoue (1988) Discrete extraction of the Ca atom functional for O_2 evolution in higher plant PS II by a simple low pH treatment. *FEBS Lett.* **227** (2): 147-152.

134. Ghanotakis, D.F., G.T. Babcock and C.F. Yocum (1984) Calcium reconstitutes high rates of oxygen evolution in polypeptide depleted PS II preparations. *FEBS Lett.* **167** (1): 127-130.

135. Chen, C., J. Kazimir and G.M. Cheniae (1995) Calcium modulates the photoassembly of PS II Mn_4-cluster by preventing ligation of nonfunctional high-valency states of manganese. *Biochemistry* **34**: 13511-13526.

136. Ananyev, G.M. and G.C. Dismukes (1997) Calcium induces binding and formation of a spin-coupled dimanganese (II, II) center in the *apo*-water oxidation complex of PS II as precursor to the functional tetra-Mn/Ca cluster. *Biochemistry* **36**: 11342-11350.

137. Mei, R. and C.F. Yocum (1991) Calcium retards NH_2OH inhibition of O_2 evolution activity by stabilization of Mn^{2+} binding to PS II. *Biochemistry* **30** (31): 7836-7842.

138. Tso, J., M. Sivaraja and G.C. Dismukes (1991) Calcium limits substrate accessibility or reactivity at the manganese cluster in photosynthetic water oxidation. *Biochemistry* **30**: 4734-4739.

139. Tso, J., M. Sivaraja, J.S. Philo and G.C. Dismukes (1991) Ca^{2+} depletion from the photosynthetic water oxidizing complex reveals photooxidation of a protein residue. *Biochemistry* **30**: 4740-4747.

140. Yocum, C.F. (1991) Calcium activation of photosynthetic water oxidation. *Biochim. Biophys. Acta* **1059**: 1-15.

141. Rutherford, A.W. (1989) Photosystem II, the water splitting enzyme. *Trends Biochem. Sci.* **14** (6): 227-32.

142. Tommos, C. and G.T. Babcock (1998) Oxygen production in nature: a light-driven metalloradical enzyme process. *Acc. Chem. Res.* **31**: 18-25.

143. Hendry, G. and T. Wydrzynski (2003) O-18 isotope exchange measurements reveal that calcium is involved in the binding of one substrate-water molecule to the oxygen-evolving complex in PS II. *Biochemistry* **42** (20): 6209-6217.

144. Siegbahn, P.E.M. and R.H. Crabtree (1999) Manganese oxyl radical intermediates and O-O bond formation in photosynthetic oxygen evolution and a proposed role for the calcium cofactor in PS II. *J. Am. Chem. Soc.* **121** (1): 117-127.

145. Kelley, P.M. and S. Izawa (1978) The role of chloride ion in PS II: effects of chloride ion on PS II electron transport and hydroxylamine inhibition. *Biochim. Biophys. Acta* **502**: 198-210.

146. Critchley, C., I.C. Baianu, Govindjee and H.S. Gutowsky (1982) The role of chloride in O_2 evolution by thylakoids from salt tolerant higher plants. *Biochim. Biophys. Acta* **682** (3): 436-445.

147. Haddy, A., J.A. Hatchell, R.A. Kimel and R. Thomas (1999) Azide as a competitor of chloride in oxygen evolution by PS II. *Biochemistry* **38**: 6104-6110.

148. Wincencjusz, H., C.F. Yocum and H.J. van Gorkom (1998) S-state dependence of chloride binding affinities and exchange dynmaics in the intact and polypeptide-depleted O_2 evolving complex of PS II. *Biochemistry* **37**: 8595-8604.

149. Wincencjusz, H., C.F. Yocum and H.J. van Gorkom (1999) Activating anions that replace Cl^- in the O_2 evolving complex of PS II slow the kinetics of the terminal step in water oxidation and destabilize the S_2 and S_3 states. *Biochemistry* **38**: 3719-3725.

150. Homann, P.H. (1986) The relation between the chloride status of the photosynthetic water splitting complex and the inhibitory effectiveness of amines. *Photosynth. Res.* **10**: 497-503.

151. Wydrzynski, T., F. Baumgart, F. MacMillan and G. Renger (1990) Is there a direct chloride cofactor requirement in the oxygen evolving reactions of PS II? *Photosynth. Res.* **25**: 59-72.

152. Olesen, K. and L.-E. Andréasson (2003) The function of the chloride ion in photosynthetic oxygen evolution. *Biochemistry* **42** (7): 2025-2035.

153. Lindberg, K. and L.-E. Andréasson (1996) A one-site, two-state model for the binding of anions in PS II. *Biochemistry* **35** (45): 14259-14267.

154. Wydrzynski, T. and K. Sauer (1980) Periodic changes in the oxidation state of manganese in photosynthetic oxygen evolution upon illumination with flashes. *Biochim. Biophys. Acta* **589**: 56-70.

155. Messinger, J. (2000) Towards understanding the chemistry of photosynthetic oxygen evolution: dynamic structural changes, redox states and substrate water binding of the Mn cluster in PS II. *Biochim. Biophys. Acta* **1459**: 481-488.

156. Klimov, V.V. and S.V. Baranov (2001) Bicarbonate requirement for the water-oxidizing complex of PS II. *Biochim. Biophys. Acta* **1503** (1-2): 187-196.

157. Baranov, S.V., G.M. Ananyev, V.V. Klimov and G.C. Dismukes (2000) Bicarbonate accelerates assembly of the inorganic core of the water-oxidizing complex in manganese depleted PS II: a proposed biogeochemical role for atmospheric carbon dioxide in oxygenic photosynthesis. *Biochemistry* **39** (20): 6060 -6065.

158. Yachandra, V.K. (2002) Structure of the manganese complex in PS II: insights from x-ray spectroscopy. *Philos. T. Roy. Soc. B* **357**: 1347-1358.

159. Yachandra, V.K., K. Sauer and M.P. Klein (1996) Manganese cluster in photosynthesis: where plants oxidize water to dioxygen. *Chem. Rev.* **96**: 2927-2950.

160. Kusunoki, M., T. Takano, T. Ono, T. Noguchi, Y. Yamaguchi, H. Oyanagi and Y. Inoue (1995) Advanced EXAFS studies of the S_1 state Mn_4 cluster in plant PS II in *Photosynthesis: from Light to Biosphere*, Eds: P. Mathis. *Kluwer Academic Publishers*, Dordrecht, The Netherlands 251-254.

161. Sarrou, J., N. Ioannidis, Y. Deligiannakis and V. Petrouleas (1998) A Mn(II)-Mn(III) EPR signal arises from the interaction of NO with the S_1 state of the water oxidizing complex of PS II. *Biochemistry* **37**: 3581-3587.

162. Zheng, M., S.V. Khangulov, G.C. Dismukes and V.V. Barynin (1994) Electronic structure of dimanganese(II,III) and dimanganese(III,IV) complexes and dimanganese catalase enzyme: a general EPR spectral simulation approach. *Inorg. Chem.* **33** (2): 382-387.

163. Cinco, R.M., J.H. Robblee, A. Rompel, C. Fernandez, V.K. Yachandra, K. Sauer and M.P. Klein (1998) Strontium EXAFS reveals the proximity of calcium to the manganese cluster of oxygen evolving PS II. *J. Phys. Chem. B* **102** (42): 8248-8256.

164. Robblee, J.H., R.M. Cinco and V.K. Yachandra (2001) X-ray spectroscopy based structure of the Mn cluster and mechanism of photosynthetic oxygen evolution. *Biochim. Biophys. Acta* **1503** (1-2): 7-23.

165. Hasegawa, K., T.-A. Ono, Y. Inoue and M. Kusunoki (1999) How to evaluate the structure of the tetranuclear Mn cluster from magnetic and EXAFS data: case of the S_2 state Mn cluster in PS II. *Bull Chem Soc Jpn* **72** (5): 1013-1023.

166. Robblee, J.H., J. Messinger, R.M. Cinco, K.L. McFarlane, C. Fernandez, S.A. Pizarro, K. Sauer and V.K. Yachandra (2002) The Mn cluster in the S_0 State of the oxygen evolving complex of PS II studied by EXAFS spectroscopy: are there three di-μ-oxo-bridged Mn_2 moieties in the tetranuclear Mn complex? *J. Am. Chem. Soc.* **124** (25): 7459-7471.

167. Diner, B.A. (2001) Amino acid residues involved in the coordination and assembly of the manganese cluster of PS II. Proton-coupled electron transport of the redox active tyrosines and its relationship to water oxidation. *Biochim. Biophys. Acta* **1503** (1-2): 147-163.

168. Debus, R.J. (2001) Amino acid residues that modulate the properties of tyrosine Y_Z and the manganese cluster in the water oxidizing complex of PS II. *Biochim. Biophys. Acta* **1503** (1-2): 164-186.

169. DeRose, V.J., V.K. Yachandra, A.E. McDermott, R.D. Britt, K. Sauer and M.P. Klein (1991) Nitrogen ligation to manganese in the photosynthetic oxygen evolving complex: continuous-wave and pulsed EPR studies of PS II particles containing ^{14}N or ^{15}N. *Biochemistry* **30** (5): 1335-134.

170. Tang, X.-S. and B.A. Diner (1994) Biochemical and spectroscopic characterization of a new oxygen evolving PS II core complex from the cyanobacterium *Synechocystis* PCC 6803. *Biochemistry* **33** (15): 4594-4603.

171. Wydrzynski, T., W. Hillier and J. Messinger (1996) On the functional significance of substrate accessibility in the photosynthetic water oxidation mechanism. *Physiol. Plant.* **96**: 342-350.

172. Yachandra, V.K., V.J. DeRose, M.J. Latimer, I. Mukerji, K. Sauer and M.P. Klein (1993) Where plants make oxygen: a structural model for the photosynthetic oxygen evolving manganese cluster. *Science* **260**: 675-679.

173. Roelofs, T.A., W. Liang, M.J. Latimer, R.M. Cinco, A. Rompel, J.C. Andrews, K. Sauer, V.K. Yachandra and M.P. Klein (1996) Oxidation states of the manganese cluster during the flash-induced S-state cycle of the photosynthetic oxygen evolving complex. *Proc. Natl. Acad. Sci. USA* **93** (April 1996): 3335-3340.

174. Messinger, J., J.H. Robblee, U. Bergmann, C. Fernandez, P. Glatzel, H. Visser, R.M. Cinco, K.L. McFarlane, E. Bellacchio, S.A. Pizarro, S.P. Cramer, K. Sauer, M.P. Klein and V.K. Yachandra (2001) Absence of Mn centered oxidation in the S_2 to S_3 transition: implications for the mechanism of photosynthetic water oxidation. *J. Am. Chem. Soc.* **123**: 7804-7820.

175. Bergmann, U., M.M. Grush, C.R. Horne, P. DeMarois, J.E. Penner-Hahn, C.F. Yocum, D.W. Wright, C.E. Dubé, W.H. Armstrong, G. Christou, H.J. Eppley and S.P. Cramer (1998) Characterization of the Mn oxidation states in PS II by Kß X-ray fluorescence spectroscopy. *J. Phys. Chem. B* **102**: 8350-8352.

176. Peloquin, J.M., K.A. Campbell, D.W. Randall, M.A. Evanchik, V.L. Pecoraro, W.H. Armstrong and R.D. Britt (2000) ^{55}Mn ENDOR of the S_2-state multiline EPR signal of PS II: implications on the structure of the tetranuclear Mn cluster. *J. Am. Chem. Soc.* **122** (44): 10926-10942.

177. Zheng, M. and G.C. Dismukes (1996) Orbital configuration of the valence electrons, ligand field symmetry, and manganese oxidation states of the photosynthetic water oxidizing complex: analysis of the S_2 state multiline EPR signals. *Inorg. Chem.* **35**: 3307-3319.

178. Ioannidis, N., J. Sarrou, G. Schansker and V. Petrouleas (1998) NO reversibly reduces the water oxidizing complex of PS II through S_0 and S_1 to the state characterized by the Mn(II)-Mn(III) multiline EPR signal. *Biochemistry* **37** (47): 16445-16451.

179. Schansker, G., C. Goussias, V. Petrouleas and A.W. Rutherford (2002) Reduction of the Mn cluster of the water oxidizing enzyme by nitric oxide: formation of an S_{-2} State. *Biochemistry* **41**: 3057-3064.

180. Riggs, P.J., R. Mei, C.F. Yocum and J.E. Penner-Hahn (1992) Reduced derivatives of the manganese cluster in the photosynthetic oxygen evolving complex. *J. Am. Chem. Soc.* **114** (26): 10650-10651.

181. Riggs-Gelasco, P.J., R. Mei, C.F. Yocum and J.E. Penner-Hahn (1996) Reduced derivatives of the Mn cluster in the oxygen evolving complex of PS II: an EXAFS study. *J. Am. Chem. Soc.* **118** (10): 2387-2399.

182. Messinger, J., U. Wacker and G. Renger (1991) Unusual low reactivity of the water oxidase in the redox state S_3 toward exogenous reductants. Analysis of the NH_2OH and NH_2NH_2 induced modifications of flash induced oxygen evolution in isolated spinach thylakoids. *Biochemistry* **30**: 7852-7862.

183. Schatz, G.H. and H.T. Witt (1984) Extraction and characterisation of oxygen-evolving PS II complexes from a thermophilic cyanobacterium *Synechococcus* spec. *Photobiochem. Photobiophys.* **7**: 1-14.

184. Winget, G.D., S. Izawa and N.E. Good (1965) Stoichiometry of photophosphorylation. *Biochem Biophys Res Commun* **21** (5): 438-441.

185. Messinger, J., W. Hillier, M. Badger and T. Wydrzynski (1996) Heterogenety in substrate water binding to PS II. *Photosynthesis: from Light to Biosphere (P.Mathis, ed.)* **II**: 283-286.

186. Berthold, D.A., G.T. Babcock and C.F. Yocum (1981) A highly resolved, oxygen-evolving PS II preparation from spinach thylakoid membranes. *FEBS Lett.* **134**: 231-234.

187. Ono, T.-A. and Y. Inoue (1983) Mn-preserving extraction of 33-, 24- and 16-kDa Proteins from O_2-evolving PS II particles by divalent salt-washing. *FEBS Lett.* **164** (2): 255-260.

188. Zouni, A., C. Lüneberg, P. Fromme, W.D. Schubert, W. Saenger and H.T. Witt (1998) Characterization of single crystals of PS II from the thermophilic cyanobacterium *Synechococcus elongatus* in *Photosynthesis: Mechanisms and Effects*, Eds: G. Garab. *Kluwer Academic Publishers*, Dordrecht 925-928.

189. Miyao, M. and N. Murata (1983) Partial disintegration and reconsitution of the photosynthetic oxygen evolution system: Binding of the 24 kDa and 18 kDa polypeptides. *Biochim. Biophys. Acta* **725**: 87-93.

190. Miyao, M. and N. Murata (1983) Partial reconstitution of the photosynthetic oxygen evolution system by rebinding of the 33 kDa polypeptide. *FEBS Lett.* **164** (2): 375-378.

191. Enami, I., M. Kaneko, N. Kitamura, H. Koike, K. Sonoike, Y. Inoue and S. Katoh (1991) Total immobilization of the extrinsic 33 kDa protein in spinach PS II membrane preparations - protein stoichiometry and stabilization of oxygen evolution. *Biochim. Biophys. Acta* **1060** (2): 224-232.

192. Laemmli, U.K. (1970) Cleavage of structural proteins during assembly of head of Bacteriophage-T4. *Nature* **227** (5259): 680-&.

193. Porra, R.J., W.A. Thompson and P.E. Kriedemann (1989) Determination of accurate extinction coefficients and simultaneous equations for assaying Chl a and Chl b extracted with 4 different solvents - verification of the concentration of Chl standards by atomic absorption spectroscopy. *Biochim. Biophys. Acta* **975** (3): 384-394.

194. Glasoe, P.K. and F.A. Long (1960) Use of glass electrodes to measure acidities in deuterium oxide. *Journal of Physical Chemistry* **64** (1): 188-190.

195. Truesdale, G.A. and A.L. Downing (1954) Solubility of oxygen in water. *Nature* **173** (4417): 1236-1236.

196. Joliot, P. (1972) *Methods Enzymol.* **24**: 123-134.

197. Koike, H., B. Hanssum, Y. Inoue and G. Renger (1987) Temperature dependence of the S-state transitions in a thermophilic cyanobacterium *Synechococcus vulcanus* Copeland measured by absorption changes in the ultraviolet region. *Biochim. Biophys. Acta* **893**: 524-533.

198. Renger, G. and B. Hanssum (1992) Studies on the reaction coordinates of the water oxidase in PS II membrane fragments from spinach. *FEBS Lett.* **299**: 28-32.

199. Boussac, A., M. Sugiura, Y. Inoue and A.W. Rutherford (2000) EPR study of the oxygen evolving complex in His-tagged PS II from the cyanobacterium *Synechococcus elongatus*. *Biochemistry* **39** (45): 13788-13799.

200. Boussac, A., H. Kuhl, E. Ghibaudi, M. Rogner and A.W. Rutherford (1999) Detection of an electron paramagnetic resonance signal in the S_0 state of the manganese complex of PS II from *Synechococcus elongatus*. *Biochemistry* **38** (37): 11942-11948.

201. McDermott, A.E., V.K. Yachandra, R.D. Guiles, J.L. Cole, S.L. Dexheimer, R.D. Britt, K. Sauer and M.P. Klein (1988) Characterization of the manganese O_2-evolving complex and the iron-quinone acceptor complex in PS II from a thermophilic cyanobacterium by electron paramagnetic resonance and X-ray absorption spectroscopy. *Biochemistry* **27** (11): 4021-4031.

202. Govindjee, H. Koike and Y. Inoue (1985) Thermoluminescence and oxygen evolution from a thermophilic blue-green alga obtained after single-turnover light flashes. *Photochem. Photobiol.* **42** (5): 579-585.

203. Vass, I. and Y. Inoue (1992) Thermoluminescence in the study of PS II in *The Photosystems: Structure, Function and Molecular Biology*, Eds: J. Barber. *Elsevier Science Publishers* 259-294.

204. Pauly, S., E. Schlodder and H.T. Witt (1992) The influence of salts on charge separation ($P680^+Q_A^-$) and water oxidation of PS II complexes from thermophilic cyanobacteria - active and inactive conformational states of PS II. *Biochim. Biophys. Acta* **1099** (3): 203-210.

205. Boussac, A., H. Kuhl, S. Un, M. Rogner and A.W. Rutherford (1998) Effect of near-infrared light on the S_2-state of the manganese complex of PS II from *Synechococcus elongatus*. *Biochemistry* **37** (25): 8995-9000.

206. Shen, J.-R., M. Ikeuchi and Y. Inoue (1992) Stoichiometric association of extrinsic cytochrome c_{550} and 12 kDa protein with a highly purified oxygen evolving PS II core complex from *Synechococcus vulcanus*. *FEBS Lett.* **301** (2): 145-149.

207. Karge, M., K.D. Irrgang, S. Sellin, R. Feinaugle, B. Liu, H.J. Eckert, H.J. Eichler and G. Renger (1996) Effects of hydrogen deuterium exchange on photosynthetic water cleavage in PS II core complexes from spinach. *FEBS Lett.* **378** (2): 140-144.

208. Messinger, J., W.P. Schröder and G. Renger (1993) Structure-function relations in PS II. Effects of temperature and chaotropic agents on the period four oscillation of flash induced oxygen evolution. *Biochemistry* **32**: 7658-7668.

209. Seeliger, A.G., J. Kurreck and G. Renger (1997) Kinetics of S_2 and S_3 reduction by tyrosine Y_D and other endogenous donors as a function of temperature in spinach PS II membrane fragments with a reconstituted plastoquinone pool. *Biochemistry* **36**: 2459-2464.

210. Lavorel, J. (1976) Matrix analysis of the oxygen evolving system of photosynthesis. *J. Theor. Biol.* **57**: 171-185.

211. Christen, G., F. Reifarth and G. Renger (1998) On the origin of the 35 µs kinetics of $P680^{+\cdot}$ reduction in PS II with an intact water oxidising complex. *FEBS Lett.* **429** (1): 49-52.

212. de Wijn, R. and H.J. van Gorkom (2002) S-state dependence of the miss probability in PS II. *Photosynth. Res.* **72** (2): 217-222.

213. Schilstra, M.J., F. Rappaport, J.H.A. Nugent, C.J. Barnett and D.R. Klug (1998) Proton/hydrogen transfer affects the S-state dependent microsecond phases of $P680^+$ reduction during water splitting. *Biochemistry* **37** (11): 3974-3981.

214. Christen, G., A. Seeliger and G. Renger (1999) $P680^{+\cdot}$ reduction kinetics and redox transition probability of the water oxidizing complex as a function of pH and H/D isotope exchange in spinach thylakoids. *Biochemistry* **38** (19): 6082-6092.

215. Shinkarev, V.P. (1996) Binary oscillations in the Kok model of oxygen evolution in oxygenic photosynthesis. *Photosynth. Res.* **48**: 411-417.

216. Boerner, R.J., K.A. Bixby, A.P. Nguyen, G.H. Noren, R.J. Debus and B.A. Barry (1993) Removal of stable tyrosine radical D+ affects the structure or redox properties of tyrosine-Z in manganese-depleted PS II particles from *Synechocystis* 6803. *J. Biol. Chem.* **268** (3): 1817-1823.

217. Reifarth, F. and G. Renger (1998) Indirect evidence for structural changes coupled with $Q_B^{-\cdot}$ formation in PS II. *FEBS Lett.* **428** (3): 123-126.

218. Garbers, A., F. Reifarth, J. Kurreck, G. Renger and F. Parak (1998) Correlation between protein flexibility and electron transfer from $Q_A^{-\cdot}$ to Q_B in PSII membrane fragments from spinach. *Biochemistry* **37** (33): 11399-11404.

219. Christen, G. and G. Renger (1999) The role of hydrogen bonds for the multiphasic $P680^{+\cdot}$ reduction by Y_Z in PS II with intact oxygen evolution capacity. Analysis of kinetic H/D isotope exchange effects. *Biochemistry* **38** (7): 2068-2077.

220. Jeans, C., M.J. Schilstra, N. Ray, S. Husain, J. Minagawa, J.H.A. Nugent and D.R. Klug (2002) Replacement of tyrosine D with phenylalanine affects the normal proton transfer pathways for the reduction of $P680^+$ in oxygen-evolving PS II particles from *Chlamydomonas*. *Biochemistry* **41** (52): 15754-15761.

221. Delrieu, M.J. (1983) Evidence for unequal misses in oxygen flash yield sequence in photosynthesis. *Z. Naturforsch. C* **38** (3-4): 247-258.

222. Renger, G., T. Bittner and J. Messinger (1994) Structure-function relationships in photosynthetic water oxidation. *Biochem. Soc. Trans.* **22**: 318-322.

223. Renger, G., J. Messinger and U. Wacker (1992) pH induced structural changes of PS II affect the reaction properties of the water oxidase in *Research in Photosynthesis*, Eds: N. Murata. *Kluwer Academic Press*, Dordrecht, The Netherlands 329 - 332.

224. Eckert, H.J. and G. Renger (1988) Temperature dependence of $P680^+$ reduction in O_2 evolving PSII membrane fragments at different redox states S_i of the water oxidizing system. *FEBS Lett.* **236** (2): 425-431.

225. Roffey, R.A., D.M. Kramer, Govindjee and R.T. Sayre (1994) Lumenal side histidine mutations in the D1 protein of PS II affect donor side electron transfer in *Chlamydomonas reinhardtii*. *Biochim Biophys Acta* **1185** (3): 257-70.

226. Roffey RA, v.W.K., Sayre RT, Styring S. (1994) Spectroscopic characterization of tyrosine-Z in histidine 190 mutants of the D1 protein in PS II in *Chlamydomonas reinhardtii*. Implications for the structural model of the donor side of PSII. *J Biol Chem* **269** (7): 5115-21.

227. Chu, H.-A., A.P. Nguyen and R.J. Debus (1995) Amino acid residues that influence the binding of manganese or calcium to PS II .2. The carboxy-terminal domain of the D1 polypeptide. *Biochemistry* **34** (17): 5859-5882.

228. Mamedov F, S.R., Styring S. (1998) Involvement of histidine 190 on the D1 protein in electron/proton transfer reactions on the donor side of PS II. *Biochemistry* **37** (40): .

229. Berthomieu, C., R. Hienerwadel, A. Boussac, J. Breton and B.A. Diner (1998) Hydrogen bonding of redox-active tyrosine Z of PS II probed by FTIR difference spectroscopy. *Biochemistry* **37** (30): 10547-54.

230. Ruffle, S.V., D. Donellelly, T.L. Blundell and J.H.A. Nugent (1992) A three dimensional model of the PS II reaction center of *Pisum sativum*. *Photosynth. Res.* **34**: 287-300.

231. Svensson, B., C. Etchebest, P. Tuffery, P. vanKan, J. Smith and S. Styring (1996) A model for the PS II Reaction center core including the structure of the primary donor P680. *Biochemistry* **35** (46): 14486-14502.

232. Renger, G., G. Christen and A. Seeliger (1998) H/D isotope exchange effects and pH-dependence of reactions leading to photosynthetic water cleavage. *Photosynthesis: Mechanisms and Effects, (G.Garab ed.)* **II**: 1357-1362.

233. Diner BA, F.D., Randall DW, Britt RD. (1998) Hydrogen bonding, solvent exchange, and coupled proton and electron transfer in the oxidation and reduction of redox-active tyrosine Y(Z) in Mn-depleted core complexes of PS II. *Biochemistry.* **37** (51): 17931-43.

234. Krieger, A. and E. Weis (1993) The role of calcium in the pH-dependent control of PS II. *Photosynth. Res.* **37**: 117-130.

235. Meyer, B., E. Schlodder, J.P. Dekker and H.T. Witt (1989) O_2 evolution and Chl *a* $^{II+}$ ($P680^+$) nanosecond reduction kinetics in single flashes as a function of pH. *Biochim. Biophys. Acta* **974** (1): 36-43.

236. Chapman DJ, D.F.J., Davis K, Barber J. (1989) Effect of alkaline pH on photosynthetic water oxidation and the association of extrinsic proteins with PS II. *Biochem J.* **258** (2.): 357-362..

237. Bernat, G., F. Morvaridi, Y. Feyziyev and S. Styring (2002) pH dependence of the four individual transitions in the catalytic S-cycle during photosynthetic oxygen evolution. *Biochemistry* **41** (18): 5830-5843.

238. Kebekus, U., J. Messinger and G. Renger (1995) Structural changes in the water oxidizing complex monitored via the pH dependence of the reduction rate of redox state S_1 by hydrazine and hydroxylamine in isolated spinach thylakoids. *Biochemistry* **34**: 6175-6182.

239. Renger, G., J. Messinger and R. Fromme (1989) Tribromotoluquinone induced modifications of the oscillation pattern of oxygen evolution and of herbicide binding in thylakoids and PSII membrane-fragments from spinach. *Z. Naturforsch. C* **44** (5-6): 423-430.

240. Völker, M., H.-J. Eckert and G. Renger (1987) Effects of trypsin and bivalent cations on $P680^+$ reduction, fluorescence induction and oxygen evolution in PS II membrane fragments from spinach. *Biochim. Biophys. Acta* **890**: 66-76.

241. Lindberg, K., T. Vänngård and L.-E. Andréasson (1993) Studies of the slowly exchanging chloride in PS II of higher plants. *Photosynth. Res.* **38** (3): 401-408.

242. Plijter, J.J., A. Degroot, M.A. Vandijk and H.J. Vangorkom (1986) Destabilization by high pH of the S_1-state of the Oxygen-Evolving Complex in PS II particles. *FEBS Lett.* **195** (1-2): 313-318.

243. Bouges, B. (1971) Action de faibles concentrations d'hydroxylamine sur l'emission d'oxygene des algues chlorella et des chloroplastes d'epinards. *Biochim. Biophys. Acta* **936**: 228-235.

244. Guiles, R.D., V.K. Yachandra, A.E. McDermott, J.L. Cole, S.L. Dexheimer, R.D. Britt, K. Sauer and M.P. Klein (1990) The S_0 state of PS II induced by hydroxylamine: differences between the structure of the manganese complex in the S_0 and S_1 states determined by X-ray absorption spectroscopy. *Biochemistry* **29** (2): 486-496.

245. Beck, W. and G. Brudvig (1987) Reactions of hydroxylamine with the electron-donor side of PS II. *Biochemistry* **26**: 8285-8295.

246. Brudvig, G.W. and W.F. Beck (1992) Oxidation-reduction and ligand-substitution reactions of the Oxygen-Evolving Center of PS II in *Manganese Redox Enzymes*, Eds: V.L. Pecoraro. *VCH Publishers*, New York 119-140.

247. Kretschmann, H., S. Pauly and H.T. Witt (1991) Evidence for a chemical reaction of hydroxylamine with the photosynthetic water splitting enzyme S in the dark: possible states of manganese and water in the S-cycle. *Biochim. Biophys. Acta* **1059** (2): 208-214.

248. Beck, W.F. and G.W. Brudvig (1988) Resolution of the paradox of ammonia and hydroxylamine as substrate analogs for the water-oxidation reaction catalyzed by PS II. *J. Am. Chem. Soc.* **110** (5): 1517-1523.

249. Ono, T.-A., T. Noguchi, Y. Inoue, M. Kusunoki, T. Matsushita and H. Oyanagi (1992) X-ray detection of the period-four cycling of the manganese cluster in the photosynthetic water oxidizing enzyme. *Science* **258**: 1335-1337.

250. Lavergne, J. (1989) Difference spectra of the oxidized intermediates in the photosynthetic oxygen-evolving system. Evidence for a small S_0 - S_1 absorption change. *Photochem. Photobiol.* **50** (2): 235-241.

251. Rich, P.R. (1996) Electron transfer complexes coupled to ion translocation in *Protein Electron Transfer*, Eds: D.S. Bendall. *BIOS Scientific Publishers*, Oxford 217-248.

252. Kretschmann, H. and H.T. Witt (1993) Chemical reduction of the water splitting enzyme system of photosynthesis and its light-induced reoxidation characterized by optical and mass spectrometric measurements: a basis for the estimation of the states of the redox active manganese and of water in the quaternary oxygen evolving S-state cycle. *Biochim. Biophys. Acta* **1144**: 331-345.

253. Han, K.-C. and S. Katoh (1992) Number and Function of Ca^{2+} bound to oxygen-evolving core complexes in *Research in Photosynthesis*, Eds: N. Murata. *Kluwer Academic Publishers*, Netherlands II.6.365-II.6.368.

254. MacLachlan, D.J., J.H.A. Nugent, P.J. Bratt and M.C.W. Evans (1994) The effects of calcium depletion on the O_2-evolving complex in spinach PS II: the S_1^*, S_2^* and S_3^* states and the role of the 17 kDa and 23 kDa extrinsic polypeptides. *Biochim. Biophys. Acta* **1186**: 186-200.

255. Lockett, C.J., C. Demetriou, S.J. Bowden and J.H.A. Nugent (1990) Studies on calcium depletion of PS II by pH 8.3 treatment. *Biochim. Biophys. Acta* **1016**: 213-218.

256. Boussac, A. and A.W. Rutherford (1992) The involvement of Ca^{2+} in the Ca^{2+}-effect on PS II oxygen evolution. *Photosynth. Res.* **32**: 207-209.

257. Boussac, A., B. Maison-Peteri, C. Vernotte and A.-L. Etienne (1985) The charge accumulation mechanism in NaCl-washed and in Ca^{2+}-reactivated PS II particles. *Biochim. Biophys. Acta* **808**: 225-230.

258. Allakhverdiev, S.I., H. Hayashi, Y. Nishiyama, A.G. Ivanov, J.A. Aliev, V.V. Klimov, N. Murata and R. Carpentier (2003) Glycinebetaine protects the D1/D2/Cyt b559 complex of PS II against photo-induced and heat-induced inactivation. *J Plant Physiol.* **160** (1): 41-49.

259. Lee, C.B., H. Hayashi and B.Y. Moon (1997) Stabilization by glycinebetaine of photosynthetic oxygen evolution by thylakoid membranes from *Synechococcus* PCC7002. *Mol Cells* **7** (2): 296-299..

260. Murata, N., P.S. Mohanty, H. Hayashi and G.C. Papageorgiou (1992) Glycinebetaine stabilizes the association of extrinsic proteins with the photosynthetic oxygen-evolving complex. *FEBS Lett.* **296** (2): 187-189.

261. Zouni, A., J. Kern, L. B., P. Fromme, H.T. Witt, P. Orth, N. Krauß, W. Saenger and J. Biesiadka (Year) Biochemical characterization and crystal structure of water oxidizing PS II from *Synechococcus elongatus*. in *Proceedings of the 12th International Congress on Photosynthesis*. Brisbane *CSIRO Publishers, Collingwood, Australia* S05-003.

262. Carell, T.G., A.M. Tyryshkin and G.C. Dismukes (2002) An evaluation of structural models for the photosynthetic water oxidizing complex derived from spectroscopic and X-ray diffraction signatures. *J. Biol. Inorg. Chem.* **7**: 2-22.

263. Peloquin, J.M. and R.D. Britt (2001) EPR/ENDOR characterization of the physical and electronic structure of the OEC Mn cluster. *Biochim. Biophys. Acta* **1503** (1-2): 96-111.

264. McDermott, A.E., V.K. Yachandra, R.D. Guiles, R.D. Britt, S.L. Dexheimer, K. Sauer and M.P. Klein (1988) Low-potential iron-sulfur centers in PS I: an X-ray absorption spectroscopy study. *Biochemistry* **27** (11): 4013-20.

265. Petrouleas, V. and B.A. Diner (1990) Formation by NO of nitrosyl adducts of redox components of the PS II reaction center .1. NO binds to the acceptor side non-heme iron. *Biochim. Biophys. Acta* **1015** (1): 131-140.

266. Goussias, C., N. Ioannidis and V. Petrouleas (1997) Low-temperature interactions of NO with the S_1 and S_2 states of the water oxidizing complex of PS II. A novel Mn multiline EPR signal derived from the S_1 state. *Biochemistry* **36**: 9261-9266.

267. Britt, R.D. (1996) Oxygen Evolution in *Oxygenic Photosynthesis: The Light Reactions*, Eds: D.R. Ort and C.F. Yocum. *Kluw. Acad. Publ.*, Dordrecht 137-164.

268. Ioannidis, N., G. Schansker, V.V. Barynin and V. Petrouleas (2000) Interaction of nitric oxide with the oxygen evolving complex of PS II and Mn catalase. A comparative study. *J. Biol. Inorg. Chem.* **5** (3): 354-363.

269. Hanley, J., J. Sarrou and V. Petrouleas (2000) Orientation of the Mn(II)-Mn(III) dimer which results from the reduction of the Oxygen-Evolving Complex in PS II by NO: an Electron Paramagnetic Resonance study. *Biochemistry* **39**: 15441-15445.

270. Cinco, R.M., C. Fernandez, J. Messinger, J.H. Robblee, H. Visser, K.L. McFarlane, U. Bergmann, P. Glatzel, S.P. Cramer, K. Sauer, M.P. Klein and V.K. Yachandra (1998) Refined model of the oxidation states and the structures of the Mn/Ca/Cl

cluster of the Oxygen Evolving Complex of PS II in *Photosynthesis: Mechanisms and Effects*, Eds: G. Garab. *Kluw. Acad. Publ.*, Dordrecht, The Netherlands 1273-1278.

EPILOGUE

This thesis would not be written without help of several people whom I am very grateful for their help, responsiveness and friendship. Once I would like to play piano for all of you, because only in this way I will be able to fully express my gratitude.

First of all I would like to thank my mother for her love, understanding and support (obwohl sie ist nicht besonderes begeistert von meinem Klavierspiel). Anacan, sänin säbirin olmasaydi, män bu ishi bitirmäzdim. Sänä ona qörä dä öz çox saqolmi çadtirmag istäyiräm. Sän bu dünyada mänimçün än äziz adam olmusan vä qalacaqsan.

I am thankful to my "Doktorvater" Dr. Johannes Messinger for the opportunity to do research in Germany and for the interesting project I was involved in. It was a great experience to work in his group. I also would like to thank Johannes for his hospitality and support during my first months in Germany.

I would like to thank Prof. Gernot Renger for the opportunity to work in his laboratories in Berlin and to do measurements with the Joliot electrode. I am also grateful to Prof. Renger for the interesting and helpful discussions. Besides that, I will never forget his kindness and responsiveness to my difficulties.

I am grateful to Prof. Wolfang Lubitz for the possibility to complete my research in his group and continuous support in MPI.

Especially I would like to thank group of Dr. Athina Zouni for the cyanobacterial samples, which was of great importance for my research. I am thankful to Dörte DiFiore, Jan Kern and Prof. Petra Fromme for their help. I also would like to thank Athina for her friendship and "Unterstützung" and for our conversations in Biergarten of Tiergarten.

My Iosifina I thank for the light, which she brought with her and left in our hearts. I thank her also for involving me to the "NO-project", for the interesting results and "grande" publication.

I am thankful to Prof. P. Hildebrandt and to Prof. Dr. A. Grohmann for the interest in my work.

I am grateful to Prof. Gasanov for his advices and directions in the beginning of my scientific carrier.

My special thanks to Norbert Dickmann for the MALDI-TOF-MS measurements and Dr. Leonid Kulik for the help in design of figure.

I would like to thank all my friends, collaborators and the administration staff in MPI and MVL for their assistance and warm attitude during all these years.

To Jens Niklas I am grateful for his friendship and especially for his support during last months of my Ph.D. studies.

My special thanks to my friends Naila Daneshani, Aliya Kombarbaeva, Amaya Blanco-Rivero, Solmaz Arvani, Maria Andrea Mroginski, Taras Petrenko, Parvana Hajieva, Boris Epel, Mrignayani Kotecha, Aruna Goenka and Alexey Silakov for their friendship and support.

On the end, I would like to thank all other members of my family and especially Aref for their love and patience.

LEBENSLAUF

Name	Sabina Gaytaran gizi Isgandarova
Geburtsdatum	05.03.1975
Geburtsort	Baku, Aserbaidschan
Ausbildung	
1981 - 1991	Grund- und Oberschule № 247 in Baku
1991	Abitur
1992 - 1997	Studium der Biologie an der Bakuen Staatlichen Universität, Baku
Juni 1997	Diplom
Oktober 2000 – Dezember 2003	Anfertigung der vorliegenden Doktorarbeit
Arbeitsverhältnisse	
September 1997 – März 1998	Laboroberassistentin im Institut für Molekularbiologie und Biotechnologie, Baku
März 1998 – September 2000	Wissenschaftliche Mitarbeiterin im Biophysiklabor des Botanischen Instituts, Baku
Januar 1999 – September 1999	Lehrerin für Biologie und Interdisziplinäre Beziehungen am Europäischen Lyceum, Baku
Oktober 2000 – September 2002	Wissenschaftliche Mitarbeiterin im Max-Volmer Laboratorium (MVL) der TU-Berlin im DFG Projekt (Me 1629/2-2): “Mechanismus der photosynthetische Wasseroxidation“
Oktober 2002 – 15. Februar 2004	Stipendiatin im Max-Planck Institut (MPI) für Bioanorganische Chemie, Mülheim an der Ruhr